Light-Induced Energy and Charge Transfer Processes in Artificial Photosynthetic Systems

D I S S E R T A T I O N

zur Erlangung des akademischen Grades

Dr. rer. nat.
im Fach Physik

eingereicht an der
Mathematisch-Naturwissenschaftlichen Fakultät I
Humboldt-Universität zu Berlin

von
Dipl.-Phys. Raoul Merijn Menting

Präsident der Humboldt-Universität zu Berlin:
Prof. Dr. Jan-Hendrik Olbertz

Dekan der Mathematisch-Naturwissenschaftlichen Fakultät I:
Prof. Stefan Hecht, PhD

Gutachter:
1. Prof. Dr. Beate Röder
2. Prof. Dr. Oliver Benson
3. Prof. Dr. Christian Brückner

eingereicht am: 30.07.2012
Tag der mündlichen Prüfung: 16.11.2012

voor Ines en Noah

"On the arid lands there will spring up industrial colonies without smoke and without smokestacks; forests of glass tubes will extend over the plains and glass buildings will rise everywhere; inside of these will take place the photochemical processes that hitherto have been the guarded secret of the plants, but that will have been mastered by human industry which will know how to make them bear even more abundant fruit than nature, for nature is not in a hurry and mankind is" - Giacomo Ciamician (1912) [1].

Contents

1 Introduction

The sun is the most important energy source for life on earth. Within one hour more solar energy reaches our planet than the amount of energy that mankind consumes in one year. The quality of life on earth depends strongly on accessible energy sources. However, we are running out of fossil fuels. In order to meet our future energy needs it is therefore urgently necessary to develop devices that are able to collect and store the energy of the sun in a usable form.

One of the most important biological processes is photosynthesis. The genesis of the photosynthetic apparatus was an essential step forward in the evolution of life on earth. In the course of evolution bacteria and plants developed biological systems for the conversion of solar energy into chemical energy. As a result, every year global photosynthesis converts solar energy into biomass corresponding to approximately 50 times the annual human energy consumption [2]. For this reason, during the last few decades attempts have been made to mimic photosynthesis [3, 4, 5, 6, 7]. For the development of artificial photosynthetic systems it is essential to gain in-depth knowledge about the processes involved in natural photosynthesis. A schematic representation of the processes involved in photosynthesis is shown in figure 1.1.

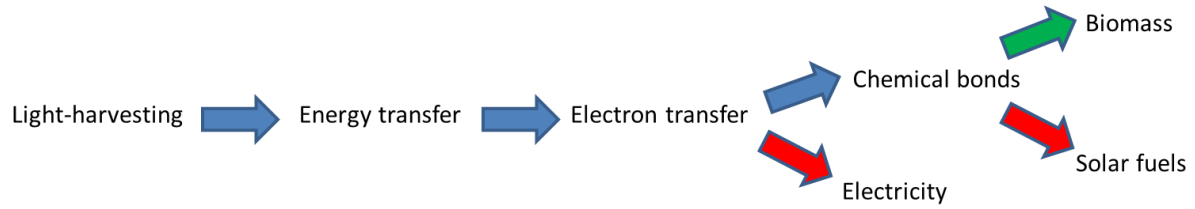

Figure 1.1: Schematic representation of the processes involved in photosynthesis. The blue arrows indicate processes that take place in both natural and artificial photosynthesis. The red and green arrows show processes that occur in artificial and natural photosynthesis, respectively.

The primary events in natural photosynthesis such as light-harvesting, charge separation and water splitting are highly efficient with almost unity quantum yields. However, due to the energy requirements of various life processes the overall energy conversion efficiency of plants is very low, approximately 1% [8]. The objective of artificial photosynthesis, however, is to maximize the total amount of energy that can be converted into electrical or chemical energy. For this reason, the rational design of artificial systems that mimic natural photosynthesis may be a promising way to achieve an increase in conversion efficiency [9].

In the present thesis, the primary events of photosynthesis presented in figure 1.1 are studied, i.e. light-harvesting, excitation energy transfer and photo-induced electron transfer. For this purpose different molecular arrays have been synthesized that can potentially serve in artificial photosynthetic systems.

Two different approaches have been employed to construct the molecular arrays, namely covalent and supramolecular chemistry. The first part of the work consists of studies on covalently linked molecular arrays, i.e. several triads and a pentad. Owing to their well-defined architectures, the covalently bound heteromers possess intriguing characteristics including very fast energy and electron transfer. The focus of the second part of the current work is set on the self-assembly of supramolecular complexes that consist of three different dyes. For the first time, it is shown that such supramolecular complexes can be formed. Moreover, it is demonstrated that they exhibit light-harvesting and charge separation properties, thereby mimicking the primary events of photosynthesis.

The thesis is subdivided into several chapters. The aim of the work is described in chapter 1 (section 1.1). In chapter 2, sections 2.1 and 2.2 introduce the concepts of natural and artificial photosynthesis, respectively. An example of artificial photosynthesis, the dye sensitized solar cell, is presented in section 2.3. Chapter 3 outlines relevant principles of photo-induced transfer processes, namely photo-induced electron transfer (section 3.1) and excitation energy transfer (section 3.2). Chapter 4 describes the experimentally used materials: section 4.1 introduces general properties of the molecules studied and section 4.2 provides information about the experimental setups. The results of steady-state and time-resolved measurements are structured in separate chapters according to the covalently bound and self-assembled systems, chapters 5 and 6, respectively. Finally, the summary and the German summary are presented in chapters 7 and 8, respectively.

1.1 Aim of the work

The aims of this work are development and photophysical investigations of novel self-assembled and covalently linked multicomponent artificial photosynthetic systems. In order to gain a comprehensive understanding of the photo-induced electron and energy transfer processes, thorough steady-state and time-resolved spectroscopic measurements have been carried out. Furthermore, a comparative study between the self-assembled and covalently-linked systems has been conducted.

The questions that arise may be divided into three groups, one pertaining to the covalently linked systems and two pertaining to the self-assembly systems. The first set of questions is devoted to the covalently linked systems:

- How do the constituent parts of the systems interact upon light excitation?
- Which kind of interaction is dominant under the used conditions?
- Which parameters can be tuned to optimize the system?
- What is the quantum efficiency of charge separation in the different systems?
- What is the lifetime of the charge-separated state?

The second group of issues addresses the formation of the supramolecular complexes:

- Is it possible to obtain controlled self-assembly between three different chromophores?
- What is the overall efficiency of the formation of a ternary supramolecular complex?
- Which strategies could be used to optimize the efficiency of complex formation?

After demonstrating the successful formation of supramolecular complexes, in a next step the photophysical parameters should be unravelled. Therefore, the third set of questions is related to the photophysical properties of the ternary supramolecular complexes:

- How does the complexation process influence the electronic properties of the constituent parts?
- Which function fulfils each individual molecular part within the supramolecular complex?
- Is it possible to control the photo-induced transfer processes in the self-assembled complexes?
- Is it possible to create synergistic effects with respect to light-harvesting and charge separation between the two binary complexes by merging them into a ternary complex?
- What are the quantum efficiencies of energy and electron transfer?
- Do any sequential electron and energy transfer processes take place?

2 Photosynthesis

2.1 Natural photosynthesis

At first, the primary events of natural photosynthesis occurring in photosystem II (PSII) of aerobic cyanobacteria are briefly described. The described mechanism bears resemblance to all photosynthetic apparatuses found in other organisms. Before the energy of the sunlight can be used, photosynthetic organisms need to gather the light energy. This is achieved by large light-harvesting complexes. In fact, 99% of the pigments employed in photosynthesis are responsible for the capture of light. One single light-harvesting complex II (LHCII) consists of around 200 chlorophylls (Chl) and 50 carotenoids (Car). The Chls exclusively collect photons and direct the absorbed energy to the so-called special pair at the reaction centre (figure 2.1). The Cars also serve as light-harvesters, but their major function is to protect the photosynthetic apparatus from damage, for the Cars can directly deexcite the triplet state of Chl.

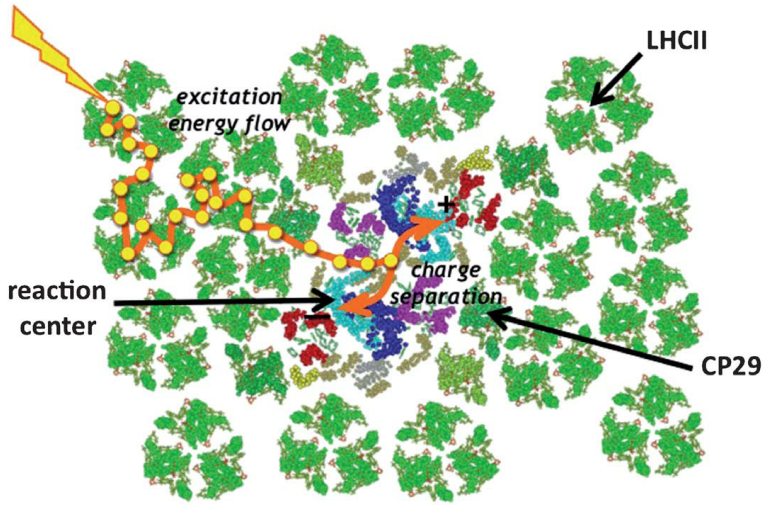

Figure 2.1: Light-harvesting in LHCII: the excitation energy migrates from the antennae to the reaction centre *via* a potential trajectory. Figure taken from [9].

In figure 2.2, the sequential electron transfer chain inside the reaction centre is shown. The special pair P_{D1}-P_{D2} serves as primary electron donor. When excited by light, either direct or indirect *via* energy transfer, P_{D1} donates an electron to the primary electron acceptor pheophytin (Pheo). As a result, the radical pair $P_{D1}^{\bullet+}$-$Pheo_{D1}^{\bullet-}$ is formed. The electron transfer from the excited P_{D1}^{*} to $Pheo_{D1}$ takes just a few picoseconds, thereby ensuring a high quantum yield. Subsequently, the electron is transferred to secondary and tertiary electron acceptors, i.e. quinones Q_A and Q_B. Each electron transfer step in the reaction centre occurs rapidly enough to compete with loss of energy by other pathways, because it possesses sufficient thermodynamic driving force, and the electronic coupling between initial and final

states is relatively strong. Stepwise recombination is slow, because the first step is endergonic [10]. Hence, the multi-step charge transfer precludes electron-hole recombination, while a long lived charge-separated state is generated. Eventually, Q_B is reduced to HQ_B. After absorption of a second photon, again electron transfer proceeds to HQ_B, which is further reduced to H_2Q_B. The latter is passed along a transport chain to photosystem I (PSI) (not shown). PSI absorbs a photon that further reduces the redox potential. In this way, sufficient energy is accumulated to drive the fixation of carbon dioxide. At the oxidative site, the $P_{D1}^{\bullet+}$ species oxidizes tyrosine (Tyr_Z). The oxidized Tyr_Z is in turn reduced by a manganese cluster. The latter extracts electrons from water which results in the oxidation of water. Detailed descriptions of the electron transfer processes involved in PSII are given in [11, 12, 13, 14].

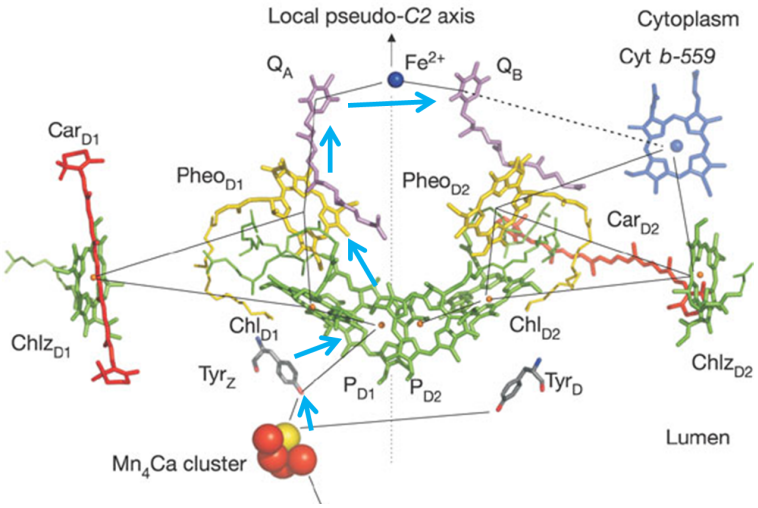

Figure 2.2: Redox-active cofactors and electron transfer chain (blue arrows) of the PSII of the cyanobacterium *Thermosynechococcus elongatus*. Figure modified from [12].

2.2 What is artificial photosynthesis?

"In the broadest sense, artificial photosynthesis means exploiting the physics and chemistry underlying natural photosynthesis to harvest solar energy for technological purposes." - Devens Gust (2012) [7].

In this sense, even photovoltaic solar cells based on inorganic semiconductors are artificial photosynthetic devices. However, in the literature "artificial photosynthesis" usually refers to systems in which the energy of light is converted into chemical or electric energy, thereby mimicking the primary steps of natural photosynthesis. As in their natural counterparts, artificial photosynthetic systems gather sunlight and separate charge. Unlike inorganic solar cells, the charge separation and light-harvesting functions are separated.

The earliest artificial model systems developed in the late 1970's and 1980's were molecular dyads that consisted of firstly a porphyrin and secondly a porphyrin, or a carotenoid or a quinone. The choice of pigments was predicated on the natural prevalence of the aforementioned dyes [5]. The porphyrin-porphyrin dyads were designed to mimic the reaction centre special pair. The porphyrin-carotenoid dyads

were employed to fill the absorbance region where chlorophylls do not absorb and to elucidate the role of the carotenoids in photo-protection from singlet oxygen damage [15, 16]. The porphyrin-quinone systems were constructed for the mimicry of electron transfer [17]. Meanwhile, a substantial number of conjugates have been studied extensively employing a large variety of dyes such as phthalocyanines, subphthalocyanines, porphyrins, carotenoids, fullerenes, ruthenium polypyridine complexes, perylenes, boron dipyrromethenes, and viologens [18, 19, 20, 21, 22, 23, 24, 25, 26, 27, 28].

2.3 Dye sensitized solar cell as example for artificial photosynthesis

An example of an artificial photosynthetic device is the dye sensitized solar cell (DSC). The systems described in this thesis were investigated for potential use in DSCs. Therefore, the aim of this section is to give a brief overview of the working principle of the DSC. Extended overviews about the DSC can be found in [29, 30, 31, 32, 33, 34, 35].

2.3.1 Working principle of the dye sensitized solar cell

The DSC consists essentially of five components, as can be seen from figure 2.3: a conducting glass, a mesoporous TiO_2 film, a dye, an electrolyte and a counter electrode (cathode).

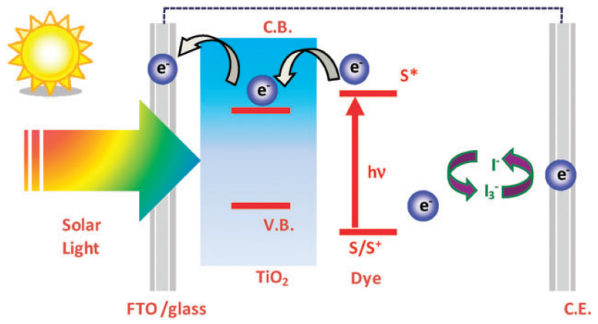

Figure 2.3: Working principle of a DSC. Figure from [36].

A transparent conductive oxide, for example fluorine-doped tin dioxide (FTO) or tin-doped indium oxide (ITO), is placed on top of the cell. Mesoscopic semiconductor nanoparticles are deposited on the transparent glass. The most used material is TiO_2 (anatase), while other wide-band-gap oxides such as ZnO and Nb_2O_5 have also been investigated [32]. A monolayer of photosensitizer is attached to the surface of semiconductor nanoparticles. Optical excitation of the sensitizer results in the injection of an electron into the conduction band of the oxide within which the electron diffuses to the conducting glass. That is, in the DSC the light-harvesting and charge generation from charge carrier transport are separated; the former is done by absorbance of the dye whereas the latter is controlled by the TiO_2 nanoparticles. The dye-covered nanoparticles are placed in contact with a redox electrolyte. The oxidized dye is reduced by an electron from the electrolyte, which usually is an organic solvent containing redox system such as the iodide/triiodide redox couple. The iodide is in turn regenerated by the reduction of triiodide at the counter electrode (C.E.). The circuit is now complete if an external load connects the

electrodes.

The first DSC was reported in the 1991 publication by O'Regan and Grätzel [37]. Herein, a ruthenium bispyridyl complex was used as sensitizer. Naturally, a broader spectral absorbance of the chromophore increases the efficiency of the DSC. The ideal sensitizer for a single-junction photovoltaic cell should absorb all light below a threshold wavelength of around 920 nm to compete with single junction semiconductor solar cells [30]. The dye must be linked to the semiconductor surface to achieve unity charge injection quantum yields Φ_{inj}. This is usually achieved by covalent linkage of the dye to anchoring groups such as -COOH, -H_2PO_3, -SO_3H. These groups are able to firmly graft the sensitizer to the semiconductor oxide surface. For a DSC device to be efficient, in addition to a rapid charge injection process, the quantum efficiency Φ_{inj} should be high. The latter is defined by

$$\Phi_{inj} = \frac{k_{inj}}{k_{inj} + k_1} \tag{2.1}$$

where k_{inj} is the charge injection rate and k_1 is the reciprocal lifetime of the first excited singlet state of the photosensitizer. That is, the electron injection should be much faster than the lifetime of the dye's first excited state. The latter lies between 20-60 ns for common Ru-complexes used in DSCs. Indeed, for many Ru-based systems charge injection occurs within femto- to picoseconds and it follows $\Phi_{inj} \approx 1$. After the rapid electron injection into the anastase, the oxidized dye should be quickly reduced by the electrolyte to regenerate the dye. In contrast to natural chlorophyll, which is continuously synthesized in the leaf, the dye in the DSC must satisfy high stability requirements to maintain performance in practical applications. It should have a redox turn-over number of at least 10^8 corresponding to a 20-year exposure to natural light. The best photovoltaic performances in terms of conversion yield and long-term stability have been achieved with polypyridyl complexes of ruthenium and osmium [29].

Probably the most pioneering idea of Grätzel was the use of a mesoporous film. Before the publication of his eminent paper in *Nature* in 1991 [37], it was believed that only smooth semiconductor surfaces could be employed in DSCs. The smooth surface is covered by one monolayer of dye. However, the light-harvesting efficiency for a monolayer of chromophores, even for phthalocyanines and porphyrins with very high extinction coefficients, is very poor due to the low optical density of solely one layer. For this reason, far less than 1% of the incoming radiation is absorbed. Attempts to harvest more light by using multilayers of dyes were not successful. Grätzel's idea was to use dyes linked to fractal TiO_2 with a large roughness in order to increase the surface area. Each TiO_2 nano-particle is coated with a monolayer of sensitizer formed by self-assembly from a staining solution. Typically, the increase of surface area by using TiO_2 nano-particles is about a factor of 1000. This led to a striking photon-to-current efficiency of 7.1% [37].

Since the light-harvesting and charge carrier transport functions are separated, another point of concern is that compact semiconductor films need to be n-doped to conduct electrons. As a consequence, there is energy transfer quenching of the excited sensitizer by the electrons in the semiconductor. On the other hand, when using an undoped mesoporous film, the light-induced electron injection from the adsorbed dye into the film renders the TiO_2 conductive [30]. In this way losses introduced by energy transfer quenching will be limited. To remain insulating, the band-gap of the semiconductor should be high with respect to the energy of the incoming light. The radiation of the sun at sea level starts at a lower wavelength of around 300 nm. However, only 5% of the solar energy distribution lies between 300-

400 nm. The band-gap of TiO_2 is 3.2 eV corresponding to a photon of 378 nm wavelength and fulfils the requirements.

Up to now, the highest efficiencies have been obtained by using TiO_2. TiO_2 possesses high stability in contrast to ZnO which dissolves under both acidic and basic conditions. Furthermore, TiO_2 is non-toxic and it is widely used as white pigment in paint, toothpaste and even food (E171) [34]. Therefore, it is expected that TiO_2 will remain the material of choice.

2.3.2 Advantages and disadvantages of dye sensitized solar cells

The DSCs possess some inherent advantages over the conventional silicon photovoltaic cells. Since the light-harvesting and charge separation functions are separated, both dye and mesoporous film can be tuned rationally to achieve optimal performance. As a result, the DSCs operate even under diffusive conditions such as cloudy skies and indirect sunlight. In contrast, in all other known photovoltaic devices including Si-cells both operations are performed simultaneously. When the intensity of incoming light is insufficient (diffusive light), the Si-cells suffer from an operation cut-out. This results from the fact that charge carrier mobility is low at these conditions and the electron-hole recombination becomes a major process. The demands on the purity of the semiconductor are high; solar grade Si should be 99.9999% pure [38]. This results in relatively high production costs and long energy payback times. Additionally, the DSC does not exhibit any inherent instability, in contrast to amorphous silicon. The latter undergoes photo-degradation due to the Staebler-Wronski effect [39]. As a consequence of which, the efficiency of an amorphous silicon solar sell drops during the first six months of operation. DSCs perform relatively better at higher temperatures than other solar cell technologies. Moreover, various design options are possible due to its flexibility, light weight and multi-colour options. Integration into different products opens up new commercial opportunities [34].

The major disadvantage of the DSC is the use of a liquid electrolyte. The electrolyte solution contains volatile organic compounds which are dangerous to human health. Despite the principally temperature independent performance, at low temperatures the cell might freeze which can lead to malfunction or cell-damage. At high temperatures, the liquid expands leading to problematic cell-sealing. First attempts have been made to replace the liquid electrolyte by a solid p-type semiconductor that interpenetrates the TiO_2 structure [34].

The choice of the dye remains a problem, too. The main photophysical drawbacks of the aforementioned ruthenium and osmium complexes, are the lack of absorption in the red region of the UV/Vis spectrum and the relatively low molar extinction coefficients [33]. Both ruthenium and osmium are highly toxic and carcinogenic. Moreover, ruthenium is exceedingly rare and is only the 74th most abundant metal on earth [40]. Osmium is the least abundant stable element in the earth's crust [41]. Therefore, the search for new chromophores that can replace the ruthenium and osmium based dyes is indispensable. The dyes investigated in this thesis could possibly meet the high demands.

3 Theoretical framework of relevant photo-induced transfer processes

This chapter introduces the theoretical framework of the transfer processes that are relevant for the analysis of the photophysical investigations carried out, namely photo-induced electron transfer (ET) and excitation energy transfer (EET).

3.1 Photo-induced electron transfer

A photo-induced electron transfer process can be written as:

$$D + A \xrightarrow{h\nu} D^* + A \xrightarrow{k_{ET}} D^+ + A^- \xrightarrow{k_{CR}} D + A \tag{3.1}$$

here D is the electron donor, A the electron acceptor, $h\nu$ the excitation energy, k_{ET} the rate of electron transfer and k_{CR} the charge recombination rate.

In this scheme, it is assumed that donor and acceptor are in close proximity. In the systems under investigation diffusion-controlled electron transfer reactions do not play a significant role. Besides excitation of the donor, as in equation 3.1, electron transfer may also be possible for excitation of the acceptor. The direction of the charge transfer depends on the redox-potential of the reacting agents.
The classical Marcus theory [42, 43] formulates the electron transfer as the transition from a reactant (R) state to a product state (P). The product state corresponds to the aforementioned $D^+ + A^-$. In order to describe the system a generalized reaction coordinate r is introduced, which includes the coordinates of all atoms involved. The potential energy surfaces of the reactant and product states are estimated to depend parabolically on the reaction coordinate. Moreover, the coordinates of the nuclei do not change during the electron transfer. In classical terms, the transfer occurs at fixed positions and momenta of the atoms and hence, the Franck-Condon principle is satisfied [43].

Figure 3.1 shows the potential energy surfaces of the reactant and product states in harmonic approximation. Accordingly, the charge transfer takes place at the intersection point of the two parabolas and the configuration at the intersection point is called the transition state. According to the analytical geometry of intersecting parabolas the free enthalpy of the reaction can be written as:

$$\Delta G^* = \frac{(\lambda - \Delta G_0)^2}{4\lambda} \tag{3.2}$$

With ΔG^* the free activation enthalpy, ΔG_0 the driving force and λ the reorganization enthalpy. The latter represents the change of free enthalpy that is required to distort the reactant state to reach the equilibrium of the product state without provoking electron transfer.

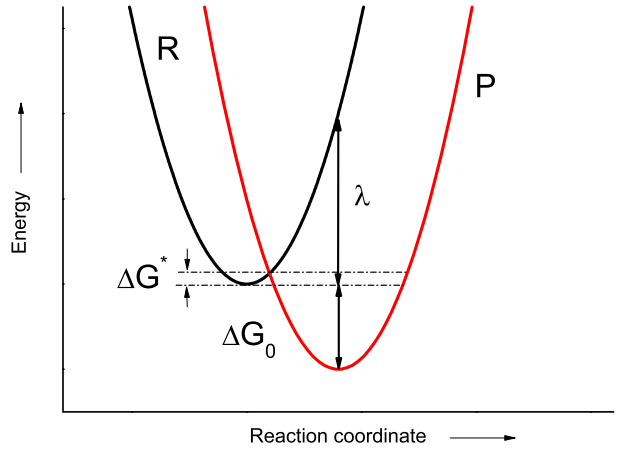

Figure 3.1: Potential energy surfaces of the reactant and product states in harmonic approximation versus a single reaction coordinate. ΔG_0 denotes the driving force, λ the reorganization energy and ΔG^* the free activation enthalpy.

The reorganization enthalpy λ is composed of inner reorganization λ_{in} and solvational λ_{out} components:

$$\lambda = \lambda_{in} + \lambda_{out} \tag{3.3}$$

The solvent-independent term λ_{in} arises from differences between the equilibrium configurations of the nuclei of the donor and acceptor product and reactant states. The values of λ_{in} are comparably small and vary between 0.1-0.3 eV [44, 45, 46].

The solvational component λ_{out} on the other hand consists of the reorganization enthalpy of the solvent and is the result of differences in orientation of the solvent molecules in the vicinity of the reactant and product. Using a spherical charge distribution of the transferred electron at the donor as well as the acceptor, λ_{out} is expressed in terms of the two ionic radii r_A and r_D, the centre-to-centre distance R of the reactants, the optical and static dielectric constants of the solvent, n^2 and ε_S, and the charge transferred from one reactant to the other [42]:

$$\lambda_{out} = \frac{e^2}{4\pi\varepsilon_0}\left(\frac{1}{2r_A} + \frac{1}{2r_D} - \frac{1}{R}\right)\left(\frac{1}{n^2} - \frac{1}{\varepsilon_S}\right) \tag{3.4}$$

The value λ_{out} varies from nearly zero for very non-polar solvents (for which $n^2 \approx \varepsilon_S$) to 1.0-1.5 eV for polar solvents [46]. The solvation shell consists of more molecules than the charge-separated species and accordingly, the reorganization enthalpy is larger. Therefore, λ_{out} is usually greater than λ_{in}.

The reaction rate in a double well potential is described classically according to an Arrhenius-type equation [47]:

$$k_{ET} = \kappa_{el}\nu_{nuc}\exp\left\{-\frac{\Delta G^*}{k_B T}\right\} \tag{3.5}$$

and with the assumptions made:

$$k_{ET} = \kappa_{el} \nu_{nuc} \exp\left\{ -\frac{(\lambda - \Delta G_0)^2}{4\lambda k_B T} \right\} \tag{3.6}$$

here κ_{el} is the electronic transmission coefficient, T the temperature, ν_{nuc} the transition frequency of the nuclei ($\approx 10^{13}$ s^{-1}) and k_B the Boltzmann constant. Classically, κ_{el} has unity value (adiabatic electron transfer), i.e. at the intersection point of the two parabolas electron transfer occurs on any account. Equation 3.6 is known as the classical Marcus equation.

In the case of non-adiabatic electron transfer $\kappa_{el} = 1$ is no longer given. For those systems a quantum mechanical description is necessary. The transfer coupling between the donor and the acceptor will be accounted for in lowest order of perturbation theory. In principle, the quantum mechanical description is based on the Golden Rule rate formula [48]:

$$k_{ET} = \frac{2\pi}{\hbar} \sum_{N,M} f(E_{DM}) |V_{DM,AN}|^2 \delta(E_{DM} - E_{AN}) \tag{3.7}$$

This formulation of the Golden Rule describes the coupling between the initial and final states. It is assumed that the ensemble stays in thermal equilibrium with some environment at temperature T; the term $f(E_{DM})$ is a quantum statistical thermal equilibrium distribution. If any dependence of the transfer integral $V_{DM,AN}$ on the vibrational coordinates (Condon-like approximation) is neglected, then the transfer integral consists of an electronic part V_{DA} and the Franck-Condon integral $\langle \chi_{DM} | \chi_{AN} \rangle$ [48]. The graphical interpretation of $V_{DM,AN}$ is the splitting between the diabatic reactant and product states. In case of small splitting (or perturbation), the transfer is called non-adiabatic electron transfer. Qualitatively the transfer process is described by tunnelling processes and the charge transfer probability is determined by the vibrational overlap between reactant and product states. Using classical treatment of the vibrational modes of the solvent and merging all high frequency modes of the reactant state to one mode, time-dependent perturbation theory yields the following equation:

$$k_{ET} = \frac{2\pi}{\hbar} \frac{|V_{DA}|^2}{\sqrt{4\pi k_B T \lambda}} \exp\left\{ -\frac{(\lambda - \Delta G_0)^2}{4\lambda k_B T} \right\} \tag{3.8}$$

Equation 3.8 is the so-called high-temperature limit of the semi-classical Marcus equation, it is equivalent to equation 3.6 and it links the non-adiabatic case to the adiabatic case [46, 48, 49]. The main advantage of using the Marcus formula is the capacity to represent a complex system consisting of many coordinates by a small number of macroscopic parameters, namely, the reorganization energy λ, the transfer coupling V_{DA} and the driving force ΔG_0 [48].

A closer inspection of the quadratic dependence in equation 3.8 reveals that a distinction can be made between four different cases with respect to the relation between ΔG_0 and λ. This is illustrated in figure 3.2.

As can be seen from figure 3.2 A, there is no driving force. From geometric considerations it follows that $\Delta G^* = \lambda/4$. The situation depicted in figure 3.2 B is usually obtained in the experiment; it represents a moderately exothermic reaction. If the parabola of the products is shifted towards lower free enthalpy, the rate k_{ET} becomes maximal for $\Delta G_0 = \lambda$, which is depicted in case C. Finally, in case D ΔG_0 is even

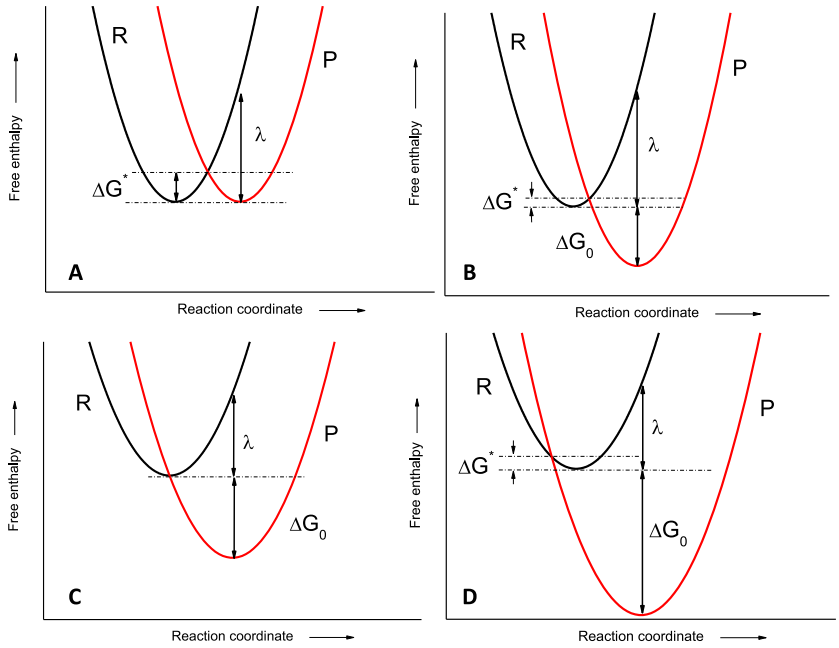

Figure 3.2: Reactant and product states of four special cases for non-adiabatic electron transfer reactions. ΔG_0 denotes the driving force, λ the reorganization energy and ΔG^* the free activation enthalpy.

greater than λ and the rate k_{ET} decreases with increasing ΔG_0. This region is the so-called Marcus inverted region and was originally predicted by R. Marcus in the mid 1950's. However, this inverted region could not be verified experimentally until 1984. In that year, Miller, Calcaterra and Closs provided the experimental evidence of the existence of the inverted region [50, 51].

Up to now, it is assumed that there is sufficient overlap of the electronic wave functions. V_{DA} is critically dependent on the extent of overlap of the reactant and product electronic wave functions. An approximation based on the tunnelling between two potential wells through a barrier of constant height over a distance R yields an exponential decay of the wave function overlap [49, 52, 53, 54]:

$$|V_{DA}(R)|^2 = |V_{DA,0}|^2 \exp\left(-\beta(R-R_0)\right) \tag{3.9}$$

The exponential coefficient β describes how well the electronic wave functions overlap and $V_{DA,0}$ is the coupling matrix for a donor-acceptor pair at van der Waals separation R_0. From this equation, it follows that electron donor and acceptor have to be in close proximity to facilitate electron transfer; the transfer rate falls rapidly with increasing distance [51].

Equation 3.8 describes the ET reaction occurring from the donor to the acceptor. The rate for back electron transfer k_{BET} is obtained by using Boltzmann statistics and the principle of detailed balance

[47, 48]:

$$\frac{k_{BET}}{k_{ET}} = \exp\left\{-\frac{\Delta G_0}{k_B T}\right\} \tag{3.10}$$

Note that back electron transfer does not mean charge recombination to the ground state, but a transition from the product to the reactant state.

In the experiment, k_{ET} can be obtained by fluorescence lifetime measurements:

$$k_{ET} = \frac{1}{\tau} - \frac{1}{\tau_0} \tag{3.11}$$

τ_0 is the fluorescence lifetime of the electron donor (acceptor) in absence of the electron acceptor (donor) and τ is the fluorescence lifetime of the electron donor (acceptor) taking into account the transfer process. It is noted that this formula is valid if other fluorescence quenching processes such as excitation energy transfer, do not take place.
ΔG_0 can be calculated from experimental data by means of the Rehm-Weller equation [55, 56, 57]:

$$\begin{aligned}\Delta G_0^{A/D} = e\left(E_{1/2}^{ox}\left(D/D^+\right) - E_{1/2}^{red}\left(A/A^-\right)\right) - E_{0,0}^{A/D} - \frac{e^2}{4\pi\varepsilon_0\varepsilon_S R} \\ - \frac{e^2}{8\pi\varepsilon_0}\left[\frac{1}{r_D} + \frac{1}{r_A}\right]\left[\frac{1}{\varepsilon_{ref}} - \frac{1}{\varepsilon_S}\right]\end{aligned} \tag{3.12}$$

Here $G_0^{A/D}$ is the free enthalpy of charge separation with selective excitation of the electron donor D or electron acceptor A, $E_{1/2}^{ox}$ is the half-wave oxidation potential of the electron donor and $E_{1/2}^{red}$ is the half-wave reduction potential of the electron acceptor, $E_{0,0}^{A/D}$ is the energy of the $S_1 \leftarrow S_0$ transition of the acceptor A or donor D and R is the distance between the electron donor and acceptor. An additional term accounts for the different dielectric constant ε_{ref} for the solvent used for the electrochemical studies compared to that for the spectroscopic measurements. In this thesis, the solvent used for electrochemical studies is DMF with a dielectric constant of 38.3. It also accounts for the effective radii of the cation r_D and the anion r_A radicals. As usual, ε_0 is the vacuum permittivity and e is the charge of the transferred electron. It is noted that the third and the fourth term in equation 3.12 can be neglected for solvents with high polarity. Table 1 (appendix) summarizes the dielectric constants ε_S of the solvents used.

3.2 Excitation energy transfer

Excitation energy transfer can be described by the following scheme:

$$D + A \xrightarrow{h\nu} D^* + A \xrightarrow{k_{EET}} D + A^* \tag{3.13}$$

The excitation energy donor is labelled D and the excitation energy acceptor A, the excitation energy transfer rate is described by k_{EET}. The donor is excited by a photon of sufficient energy, $h\nu$, and then, the excitation energy is transferred to the acceptor which results in the excited acceptor and the donor in its ground state. In this scheme, diffusion-controlled energy transfer is not taken into account, i.e. it is assumed that donor and acceptor are already in close proximity.
Firstly, a distinction is drawn between trivial and non-trivial energy transfer, namely radiative and non-radiative energy transfer. In the case of trivial energy transfer, the excited donor emits a photon, which is absorbed by the acceptor. The donor and acceptor moieties do not interact with each other; the lifetime of the first excited singlet state of the donor is not affected by the transfer process. The distance r and the orientation of both molecules determine the probability p of this process $p = p(r^{-2})$. Compared to the energy transfer processes listed below, this decrease is slow; in diluted solutions it can become the dominant energy transfer mechanism.

For the non-radiative case, a differentiation in coupling strength is made [48, 58]: strong, intermediate and weak coupling. The first two cases are outlined briefly, whereas the case of weak coupling energy transfer will be discussed in more detail for it is the key energy transfer process in this work.

The strong coupling is described by means of dipole-dipole interactions. In the following, a brief summary of the formal treatment on molecular excitons by Michael Kasha is given [59]. It is assumed that the interchromophoric overlap of electronic wave functions is small. Then, it is possible to apply first order perturbation theory to compute the wave functions and energies of the donor-acceptor pair. The donor and acceptor are denoted as D and A, respectively, and the Hamiltonian reads:

$$\hat{H} = \hat{H}_A + \hat{H}_D + \hat{V}_{DA} \tag{3.14}$$

The perturbation term $\hat{V}_{DA}$ accounts for the Coulomb interaction between the nuclei and electrons of acceptor A and donor D:

$$\hat{V}_{DA} = -\sum_{i,j} \frac{e^2}{\boldsymbol{R}_{Ai} - \boldsymbol{r}_{Dj}} - \sum_{i,j} \frac{e^2}{\boldsymbol{R}_{Di} - \boldsymbol{r}_{Aj}} + \sum_{i,j} \frac{e^2}{\boldsymbol{r}_{Ai} - \boldsymbol{r}_{Dj}} + \sum_{i,j} \frac{e^2}{\boldsymbol{R}_{Ai} - \boldsymbol{R}_{Dj}} \tag{3.15}$$

where $\boldsymbol{R}_{Ai}$ are the coordinates of the nuclei and $\boldsymbol{r}_{Ai}$ denote the coordinates of the electrons of the acceptor A. The donor coordinates of the nuclei and electrons are represented by $\boldsymbol{R}_{Di}$ and $\boldsymbol{r}_{Di}$, respectively. The last term in equation 3.15 represents the repulsion of the nuclei and the third term in equation 3.15 takes into account the Coulomb repulsion of the electrons. The first two contributions describe the attraction between acceptor nuclei and donor electrons and *vice versa*. The ground state (G) wave function of the dimer is given by the product of the ground states of molecules D and A:

$$|\Psi_G\rangle = |\psi_A\rangle\,|\psi_D\rangle \tag{3.16}$$

Using the Hamiltonian $\hat{H}$, the energy E_G can be obtained by solving the time-independent Schrödinger

equation:

$$\hat{H}\,|\Psi_G\rangle = E_G\,|\Psi_G\rangle \tag{3.17}$$

and it follows

$$E_G = E_A + E_D + \langle\Psi_A\Psi_D|\,\hat{V}_{DA}\,|\Psi_A\Psi_D\rangle \tag{3.18}$$

The last term represents the van der Waals interaction energy (energy lowering) between the ground states of molecules A and D, and E_A and E_D are the ground state energies of the isolated molecules A and D.

The excited state (E) dimer wave-functions may be written as

$$|\Psi_E\rangle = c_1\,|\psi_A^*\rangle\,|\psi_D\rangle + c_2\,|\psi_A\rangle\,|\psi_D^*\rangle \tag{3.19}$$

where $|\psi_A^*\rangle$ and $|\psi_D^*\rangle$ represent excited state wave functions for a particular excited state and c_i are coefficients to be determined. By solving the Schrödinger equation, the wave functions and related energies take the form

$$\left|\Psi_E^{1,2}\right\rangle = \frac{1}{\sqrt{2}}\left\{|\psi_A^*\rangle\,|\psi_D\rangle \pm |\psi_A\rangle\,|\psi_D^*\rangle\right\} \tag{3.20}$$

$$E_E^{1,2} = E_D^* + E_A + \langle\Psi_A\Psi_D^*|\,\hat{V}_{DA}\,|\Psi_A\Psi_D^*\rangle \pm \langle\Psi_A\Psi_D^*|\,\hat{V}_{DA}\,|\Psi_A^*\Psi_D\rangle \tag{3.21}$$

The last term in equation 3.21 is the exciton splitting term, which will be called ε. In the point-dipole point-dipole approximation, ε becomes

$$\varepsilon = \left[\frac{\boldsymbol{\mu}_A\boldsymbol{\mu}_D}{r^3} - \frac{3(\boldsymbol{\mu}_D\boldsymbol{r})(\boldsymbol{\mu}_A\boldsymbol{r})}{r^5}\right] \tag{3.22}$$

$\boldsymbol{\mu}_A$ and $\boldsymbol{\mu}_D$ are the transition dipole moments of molecule A and D, and $\boldsymbol{r}$ is the position vector of dipole A referred to dipole D as origin. The third term in equation 3.21 is analogous to the corresponding term in equation 3.18 and characterizes the energy lowering caused by the van der Waals interaction between an excited molecule and a ground state molecule.

The exciton splitting in the strong-coupling case has consequences for the electronic absorption spectra of the dimer. The UV/Vis absorption bands may be split and shifted to the blue or red, which depends on the orientation between the dipoles according to equation 3.22.

The energy transfer time τ_{EET} between the donor and acceptor moieties is faster than the vibrational relaxation time τ_{vib} into the ground state i.e. (k_{EET}>10^{14} s^{-1}). The excitation energy is localized neither at the donor's nor at the acceptor's site and the exciton is able to move freely through the aggregate as a quantum mechanical wave packet. The phase relations between excited state wave functions of different molecules are fixed [48].

The regime of intermediate coupling describes the case that the energy transfer rate depends quadratically on the Franck-Condon integral and the dipole-dipole interaction, accordingly $\tau_{EET} \approx \tau_{vib}$. The transfer rate lies between 10^{11} s^{-1} up to 10^{13} s^{-1}. The excitation energy is localized at the energy donor's site and is transferred subsequently to the acceptor moiety. These are called localized excitons. For both strong and intermediate coupling regimes, the energy transfer probability p is described by $p = p(r^{-3})$

[60].

The weak coupling regime differs fundamentally from the excitonic interactions mentioned above. In this case, the relaxation time τ_{vib} of the nuclei is faster than the energy transfer time τ_{EET}. The rate k_{EET} is smaller than 10^{11} s^{-1} The transfer proceeds *via* deexcitation of the donor and simultaneous excitation of the acceptor. That means, the excitation energy hops from the energy donor's to the acceptor's site. The theory of EET in the weak coupling regime was firstly described by Förster in the 1940's [61, 62, 63]. In [48] an elegant derivation of the energy transfer rate k_{EET} is given, which is briefly summarized below.

The transfer is described in first order of perturbation theory. The Golden Rule of quantum mechanics is applied to obtain the general transfer rate:

$$\begin{aligned} k_{EET} = \frac{2\pi}{\hbar} \sum_{\mu,\nu} \sum_{N,M} f_{De} f_{Ag} \times |\langle \Psi_{De}, \Psi_{Ag} | V_{DA} | \Psi_{Ae}, \Psi_{Dg} \rangle|^2 \\ \times \delta \left(E_{De} + E_{Ag} - E_{Ae} - E_{Dg} \right) \end{aligned} \tag{3.23}$$

Where f_{De} and f_{Ag} are distribution functions that describe the initial vibrational equilibria, e and g represent excited and ground states, respectively. Each parameter in equation 3.23 depends on vibrational coordinates and the summation takes into account all vibrational modes of the donor/acceptor in the excited (μ, M) and ground state (ν, N). The dipole-dipole interaction term V_{DA} has already been discussed in the previous section, *cf.* equation 3.15. We assume that the transfer integral V_{DA} does not depend on the vibrational coordinates (Condon approximation). Furthermore, the interaction matrix V_{DA} consists of two contributions, namely the Coulomb interaction and the exchange interaction. The latter is called Dexter mechanism[64]. Energy transfer *via* the exchange mechanism is efficient if the electronic wave functions show sufficient spatial overlap. In the following, distances greater than 10 Å will be considered, thereby neglecting the exchange term. Using these assumptions, the following equation is obtained:

$$\langle \Psi_{De}, \Psi_{Ag} | V_{DA} | \Psi_{Ae}, \Psi_{Dg} \rangle = V_{DA} \langle \chi_{De} | \chi_{Dg} \rangle \langle \chi_{Ag} | \chi_{Ae} \rangle \tag{3.24}$$

As can be seen it strongly depends on the Franck-Condon overlap integrals $\langle \chi_{De} | \chi_{Dg} \rangle$ and $\langle \chi_{Ag} | \chi_{Ae} \rangle$.

The δ-function in equation 3.23 can be separated into two parts:

$$\begin{aligned} \delta \left(E_{De} + E_{Ag} - E_{Ae} - E_{Dg} \right) = \hbar \int d\omega \delta \left(E_{De} + E_{Ag} - \hbar\omega \right) \\ \times \delta \left(\hbar\omega - E_{Ae} - E_{Dg} \right) \end{aligned} \tag{3.25}$$

The first δ-function in the integrand accounts for the emission of the donor with energy $\hbar\omega$ that excites the acceptor. The definitions of the donor emission coefficient $I_D(\omega)$ and the acceptor absorption coefficient $\varepsilon_A(\omega)$ are

$$I_D(\omega) = \frac{4\hbar\omega^3}{3c^3} |\boldsymbol{\mu}_D|^2 \sum_{\mu,\nu} f_{De} |\langle \chi_{De} | \chi_{Dg} \rangle|^2 \delta \left(E_{De} - E_{Dg} - \hbar\omega \right) \tag{3.26}$$

$$\varepsilon_A(\omega) = \frac{4\pi^2 \omega n_{mol}}{3c} |\boldsymbol{\mu}_A|^2 \sum_{N,M} f_{Ag} |\langle \chi_{Ag} | \chi_{Ae} \rangle|^2 \delta (E_{Ag} - E_{Ae} + \hbar\omega) \tag{3.27}$$

Here n_{mol} is the volume density of molecules in the sample volume. Combining the previous equations, a quantitative treatment leads to the following expression [63]:

$$R_0^6 = \frac{9000 \ln(10) \kappa^2 \Phi_{fl}}{128 \pi^5 n^4 N_A} \int \frac{I_D(\tilde{\nu}) \varepsilon_A(\tilde{\nu})}{\tilde{\nu}^4} d\tilde{\nu} \tag{3.28}$$

N_A is Avogadro's number, Φ_{fl} is the fluorescence quantum yield of the donor in the absence of an acceptor, n is the refractive index of the medium, $\tilde{\nu}$ is the wavenumber in [cm^{-1}], and $\varepsilon_A(\tilde{\nu})$ is the extinction coefficient of the acceptor at $\tilde{\nu}$ in [mol^{-1} cm^{-1}].

In equation 3.28, $I_D(\tilde{\nu})$ is the fluorescence intensity of the donor whose integral has unity value,

$$1 = \int I_D(\tilde{\nu}) d\tilde{\nu} \tag{3.29}$$

The term κ^2 is a factor that accounts for the relative orientation in space of the transition dipole moments of acceptor and donor and is given by:

$$\kappa^2 = (\cos\theta_T - 3\cos\theta_D \cos\theta_A)^2 \tag{3.30}$$

where θ_T is the angle between the emission transition dipole of the donor and the transition absorption dipole of the acceptor, θ_D and θ_A are the angles between these dipoles and the vector joining the donor and the acceptor (see figure 3.3). Depending on the relative orientation of the donor and acceptor, the orientation factor can range from 0 to 4. However, the exact determination of κ^2 is not trivial and is beyond the scope of this thesis. Instead, the value of κ^2 is assumed to be 2/3, which corresponds to dynamic random averaging of free rotating donor and acceptor chromophores in solution [65].

Equation 3.28 describes the dependence of R_0 on the optical properties of the donor and acceptor and R_0 is called the Förster distance [62]. The latter is defined by the distance at which EET is 50% efficient. The rate of the energy transfer depends on R_0 [63]:

$$k_{EET} = \frac{1}{\tau_0} \left(\frac{R_0}{R} \right)^6 \tag{3.31}$$

Where R is the distance between donor and acceptor, τ_0 is the fluorescence lifetime of the donor in absence of the acceptor and R_0 is the Förster radius. The efficiency of this transfer E_{EET} may be calculated using

$$E_{EET} = 1 - \frac{\tau}{\tau_0} \tag{3.32}$$

τ_0 and τ are the fluorescence lifetimes of the donor in absence and in presence of an acceptor, respectively.

The Förster rate can be determined from experimental data by measuring the emission spectrum of the donor and the absorption spectrum of the acceptor. With regard to the condition of spectral overlap the

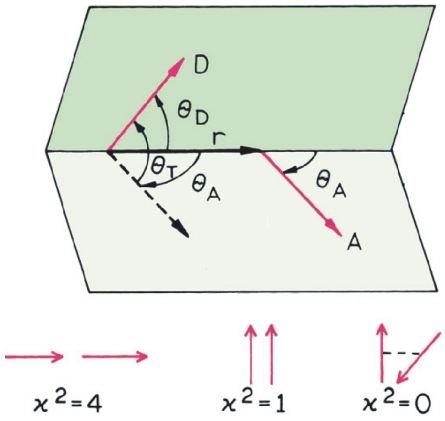

Figure 3.3: Orientation factor κ^2, figure adapted from [65].

energy transfer is often called fluorescence resonance energy transfer (FRET). This may appear similar to the reabsorption of the sensitizer fluorescence by the acceptor. It is emphasized that the mechanism of non-trivial EET is of completely different nature; the transfer takes place *before* the donor fluoresces.

For randomly distributed donors and acceptors, the fluorescence intensity of the donor is given by [65]:

$$I_D = I_{0,D} \exp\left\{-\frac{t}{\tau_0} - 2\frac{A}{A_0}\sqrt{\frac{t}{\tau_0}}\right\} \tag{3.33}$$

where A is the acceptor concentration in [M] and the term A_0 is called the critical concentration. The latter represents the acceptor concentration that results in 76% energy transfer [65]. This expression is valid for an orientation factor of $\kappa^2 = 2/3$, that is, rapid rotational diffusion, but without translational diffusion and homotransfer during the lifetime of the donor's first excited state. If R_0 is given in [Å], the value of A_0 is given by

$$A_0 = \frac{447}{R_0^3} \tag{3.34}$$

This reveals an important feature between unlinked donors and acceptors, which is that the acceptor concentration needs to be rather high to facilitate FRET. The high acceptor concentration results in high optical densities and inner filter effects complicate the interpretation. On the other hand, FRET can relatively easily be observed in molecular donor-acceptor dyads.

4 Experimental

4.1 General properties of the molecular building blocks employed in the artificial photosynthetic systems

The covalently bound and self-assembled systems are composed of different dyes. In this section, basic photophysical properties of the molecular building blocks, which are phthalocyanines, subphthalocyanines, porphyrins and boron dipyrromethenes are discussed. The aforementioned chromophores are attractive candidates to mimic the natural events of photosynthesis, since they are characterized by their high absorbance in the UV/Vis spectral region, high fluorescence quantum yields, reasonably long first excited singlet state lifetime and high chemical stability. Moreover, they are known for their comparatively easily tuneable electrochemical and photophysical properties, so that one can optimize them for each desired system.

4.1.1 Porphyrins and phthalocyanines

Porphyrins (Pors) and phthalocyanines (Pcs) are both members of the tetrapyrrole dye class. The chemical core of cyclic tetrapyrroles consists of four pyrrolic rings, which are covalently linked in macrocyclic form *via* methin-bridges. The basic structure of cyclic tetrapyrroles is called porphin, see figure 4.1. Additional benzene rings can be bound at the β-positions of the porphin core; as a result, tetrabenzo-porphyrin is obtained. A formal substitution of the carbon atoms of the methin-bridges at the *meso*-position by nitrogen atoms yields the tetra-aza-porphyrin. The unification of tetra-aza-porphyrin and tetra-benzo-porphyrin yields tetra-aza-tetra-benzo-porphyrin, which is called phthalocyanine (Pc). The first Pc was synthesized in 1907 by Braun and Tcherniac [66].

Cyclic tetrapyrroles play an important role in plants and animals due to their extended π-electron systems. Photosynthesis and respiration would be impossible without cyclic tetrapyrroles. However, natural tetrapyrroles are not sufficiently photo-stable with respect to technical application, e.g. chlorophylls react with mild chemical reagents. On the contrary, artificial tetrapyrroles, with Pcs as well-known representatives, show similar optical properties as chlorophyll, but possess a much higher intrinsic chemical and photophysical stability.

Pors exhibit a very rich chemistry due to feasible functionalization at either the β-pyrrolic- or *meso*-positions. The chemistry of Pcs is limited by the lack of solubility and synthetic methods that would allow selective functionalization of the unsubstituted macrocycle [36]. On the other hand, over 70 different metals can be incorporated into the Pc-core (MePc). Furthermore, moieties can be linked at the periphery of the Pc. Electronic and photophysical properties can be tuned rationally by modification of the Pc, which is a condition for use in artificial photosynthesis [22].

The electronic structure of tetrapyrroles is explained well by the four orbital model, which was established by Gouterman et al. at around 1960 [67, 68, 69, 70]. Most properties of Pors and Pcs can

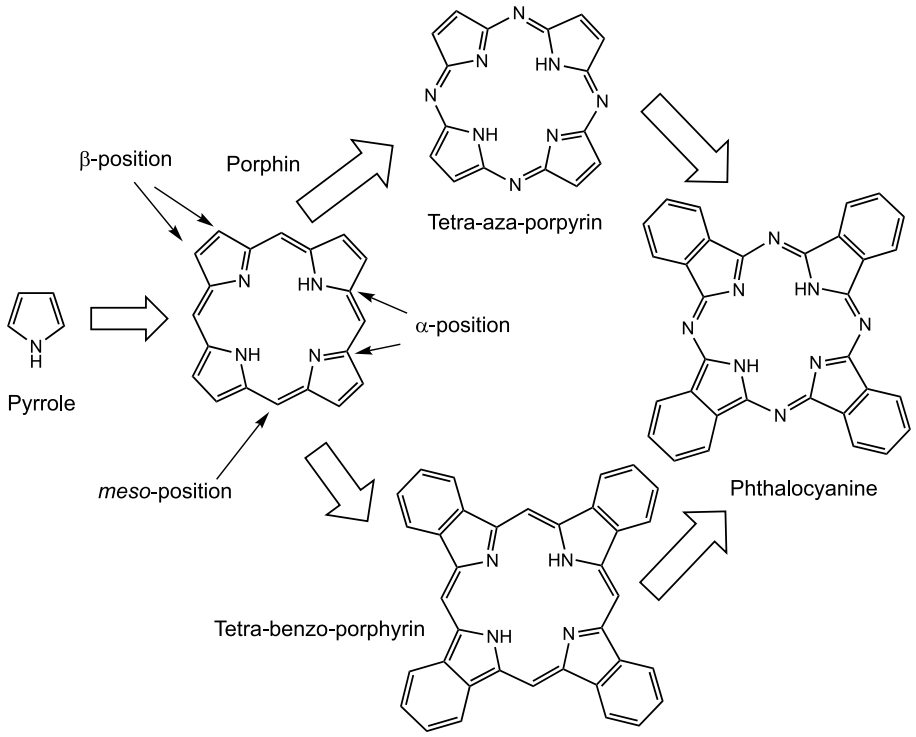

Figure 4.1: Structural resemblance of porphyrins and phthalocyanines.

be explained by the model reasonably, e.g. the relative transition energies are determined by the central metal and the substituents. Both Pors and Pcs possess two-dimensional conjugated 18-π-electron systems. The UV/Vis absorption bands are mainly π-π^*-transitions and they can be divided in B- and Q-bands corresponding to upper and lower transitions and according to the nomenclature introduced in [71]. By means of selection rules the allowed B-bands and the formally forbidden Q-bands of Pors are explained. For Pors the HOMOs lie very close, they are practically degenerated. As a consequence of this accidental degeneracy the B- and Q-transitions keep their allowed and accordingly forbidden character. For Pcs the additional aza- and benzo-linkages provoke a perturbation of the orbital energies and cause a larger energetic distance between these HOMOs. A direct consequence of this is that the previously forbidden Q-transition gains significant intensity from the allowed B-transition. As a result the Q-band dominates the UV/Vis absorption spectrum at around 700 nm. A detailed description of the symmetry of molecular orbitals, the energetic positions and the origin of the π-π^*-transitions can be found in [72].

Pcs strongly absorb in the region 650-750 nm with extinction coefficients as large as 2×10^5 M^{-1} cm^{-1}, consequently they are deeply coloured blue/green. Additionally, they show B-band absorption at 300-350 nm, however the B-transition has less intensity. On the contrary, Pors show intense B-band absorption at around 400-450 nm (the so-called Soret-band) with even larger extinction coefficients of around 5×10^5 M^{-1} cm^{-1}. Moreover, metal free Pors show four Q-bands with much lower extinction, i.e. ε=10^4 M^{-1} cm^{-1}, in the spectral 500-650 nm region. That means Pors and Pcs show complementary absorption profiles and a combination of both dyes covers a broad spectrum that ranges from 300-700 nm [73, 74, 75, 76, 77].

In addition to their ability to collect light, both Pors and Pcs are attractive sensitizers for DSCs due to their appropriate redox properties with respect to the conduction band of TiO_2 and the redox potential of the iodine electrolyte [36]. Due to its broader available chemical modifications the number of Pors that have been tested in Grätzel cells is significantly greater than that of Pcs, despite the lower light-harvesting efficiency of Pors limiting the performance of Por-based DSCs. Recently, Grätzel et al. reported a Por-sensitized solar cell with an efficiency exceeding the 12% benchmark [38]. This cell is the actual efficiency record holder of DSCs. Due to the tendency of Pcs to aggregate, Pc-based DSCs show relatively poor performance with an actual power conversion efficiency of up to 3.5% [78].

In the present work, the key feature of all systems is the use of a silicon (IV) phthalocyanine (SiPc). The use of a silicon central atom has some intrinsic advantages. Firstly, a covalent linkage enables axial substitution at both sides of the SiPc. The preparation and modification of SiPc by manipulation of the axial substituents is relatively straightforward [79]. Secondly, an important characteristic of axially substituted SiPcs is the lack of aggregation, which is a serious problem for most planar Pcs. As a result, SiPcs exhibit much better solubility and possess improved photophysical properties with respect to non-axially substituted Pcs. For this reason, SiPcs attracted increasing interest in the last few years [15, 22, 73, 74, 79, 80, 81, 82, 83, 84, 85, 86, 87, 88, 89]. In the present work, SiPc serves as electron acceptor in addition to its light-harvesting function. A feature of the $SiPc^{\bullet -}$ radical anion is its absorption bands at 580 and 620 nm [15, 75, 76, 77, 90, 91, 92]. Throughout the course of the present work, we will often encounter the 580 nm absorption band.

4.1.2 Bodipys

A very promising class of chromophores are boron dipyrromethenes, in literature often abbreviated to Bodipys. They constitute a dipyrromethene complexed with a disubstituted boron atom, typically a BF_2. The first Bodipy was discovered by Treibs and Kreuzer in 1968 [93]. However, its potential was not realized until the late 1980's. A large variety of different Bodipys has been synthesized and employed since then. The core of a Bodipy is shown in figure 4.2. It should be noted that the IUPAC numbering system of Bodipy dyes differs from that of dipyrrins, which may cause confusion. However, the α-, β- and *meso*-labelling are the same for both systems.

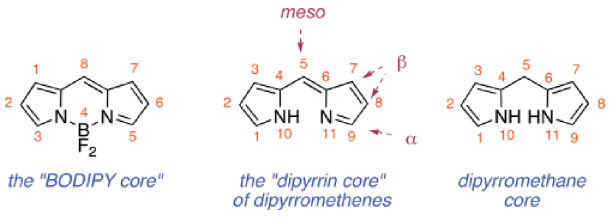

Figure 4.2: The Bodipy core [94] with the IUPAC numbering system.

An important feature of Bodipy dyes is their moderate-large extinction coefficients in the order of 0.4-1.0×10^5 M^{-1} cm^{-1}; the UV/Vis absorption bands are sharp and tuneable in the 500-800 nm region. The absorption- and emission spectra do not change significantly when dissolved in various solvents [94]. The absorption and emission properties of Bodipys can be tuned rationally by chemical modification of

the Bodipy core [95]. In figure 4.3 the spectral tuning of Bodipy fluorescence is outlined.

Other characteristics of Bodipys are excellent thermal and photochemical stability, high fluorescence quantum yields, good solubility in many organic solvents and chemical robustness. The fluorescence quantum yields do not depend on the solvent and Bodipys show little or no tendency to aggregate [94, 95, 96, 97].

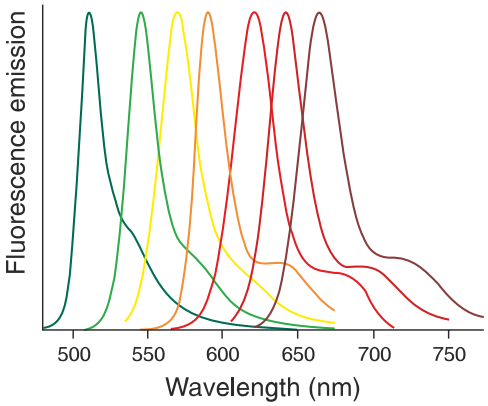

Figure 4.3: Fluorescence spectra of some selected Bodipys. Figure taken from [98].

The energy of the triplet state for a basic Bodipy lies around 1.6 eV, which is much lower than the first excited singlet state of around 2.5 eV (unmodified Bodipys absorb at around 500 nm). This is accompanied by a slow rate of intersystem crossing (ISC) $S_1 \rightarrow T_1$ (approx. 10^6 s^{-1}) and accordingly, the quantum yield of ISC, Φ_{ISC}, is usually very small [99]. As a result, the singlet oxygen generation is very low, too, thereby keeping photo-degeneration small. If desired, enhanced population of the triplet state can be achieved through the inner heavy-atom effect, for example the covalent linkage of two iodine atoms at positions two and six as reported in [96].

Bodipy-based molecular systems showing excitation energy transfer have been well-documented [24]. In contrast, electron transfer reactions which involve Bodipys have been studied only recently [100, 101]. In general, Bodipys possess ampholytic character, i.e. its redox potentials E_{ox} and E_{red} are similar [96]. For this reason, they can be employed either as an electron donor or an electron acceptor. Despite their attractive properties, up to now only a few examples are known from literature where Bodipys have been investigated for their use in DSCs. The first use of Bodipys in DSCs was reported in 2005 by Hattori et al. [102]. Herein it was shown that the radical anion Bodipy$^{\bullet -}$ absorbs light of a wavelength of 580 nm, whereas the radical cation Bodipy$^{\bullet +}$ shows absorption at 513 nm. This is confirmed by the results presented in [103]. The latest application of Bodipy in DSCs can be found in [104], where a modest overall efficiency of 2.46% was reported. In [105] Bodipys have been employed in bulk heterojunction solar cells.

4.1.3 Subphthalocyanines

Subphthalocyanines, abbreviated to SubPcs, are the lowest homologues of phthalocyanines. The molecular structure is presented in figure 4.4. The discovery of SubPcs was made in 1972 by Meller and Ossko [106] as they were trying to obtain boron Pc. Although many attempts have been made to change

the boron atom up to now, only SubPcs with a central boron atom have been synthesized. SubPcs possess some unusual electrical and optical properties. Their 14 π-electron core is cone-shaped as determined by X-ray crystallography [107], see figure 4.5. The cone-shaped molecular structure of SubPcs prevents them from aggregation.

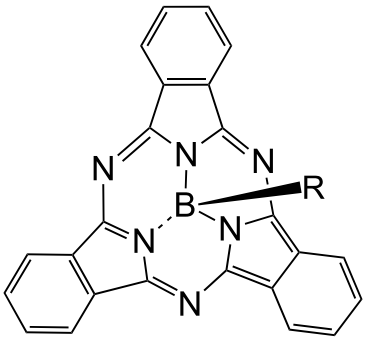

Figure 4.4: Subphthalocyanine core.

Because SubPcs are constrained homologues of phthalocyanines, their Q- and B-Bands in the UV/Vis absorption spectra are shifted to the blue. Typically, SubPcs absorb in the 550-650 nm region with extinction coefficients in the order of $\sim 5 \times 10^4$ M^{-1} cm^{-1}. Due to their rigid non-planar core SubPcs show small Stokes-shifts and low reorganization energies [108].

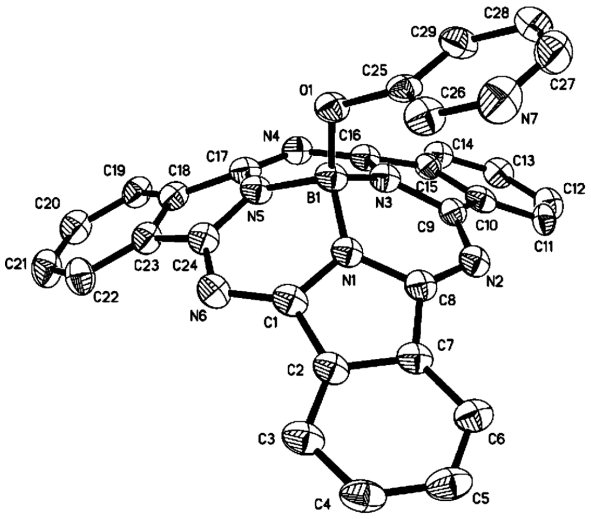

Figure 4.5: Molecular structure of a SubPc obtained from X-ray diffraction studies. The non-planarity of SubPc can be clearly seen. Figure taken from [109].

The energy gap between first excited singlet and triplet states of SubPcs (0.3-0.4 eV) is significantly smaller than that of Pcs (0.5-0.7 eV). Therefore, non-radiative deactivation of the first excited singlet state due to ISC is more efficient for SubPcs than for Pcs. The triplet and singlet oxygen quantum yields

are quite large, with values around 0.60 and 0.55, respectively.

Complementary to high ISC quantum yields are modest fluorescence quantum yields. Typical fluorescence quantum yields of 0.25 are about one-half the values observed for Pcs. The corresponding fluorescence lifetimes are around τ_{fl}=3 ns which is also about two times faster than the typical lifetime of the first excited singlet state of metal-free Pcs ($\sim$6 ns) [110]. SubPcs are shown to be very promising molecular building blocks for the construction of multicomponent photo-active arrays. Several molecular hetero dyads consisting of a SubPc and another dye have been reported, e.g. SubPc-fullerene [108], SubPc-(osmium(II) tris(2,2'-bipyridine)) [111], SubPc-Bodipy [112], SubPc-ferrocenyl [113] and SubPc-Pc [114] which exhibit efficient excitation energy or electron transfer processes, either from the SubPc to the anchoring moiety or *vice versa*. For studying electron transfer processes it is useful to know the absorption of the charged species: the radical anion $SubPc^{\bullet -}$ shows broad absorption with a maximum at 490 nm [115] whereas the radical cation $SubPc^{\bullet +}$ absorbs light at 620 nm [116].

4.1.4 Cyclodextrins

Cyclodextrins (CDs) are rings made of D-glucopyranose ($C_6H_{10}O_5$) units. Cyclodextrins were firstly discovered by Villiers in 1891 [117]. The nomenclature of CDs is determined by the number of glucose units: α-, β,- and γ-CDs consist of six, seven and eight glucose units, respectively, see figure 4.6. For steric reasons, rings that consist of less than six glucose moieties do not exist. On the other hand, δ-, ε- up to μ-CDs have been described in literature, corresponding to rings with 9 up to 17 glucose units. The larger CDs are not regular cylinder-shaped structures anymore: they are collapsed and their real cavity is even smaller than that of γ-CD [118].

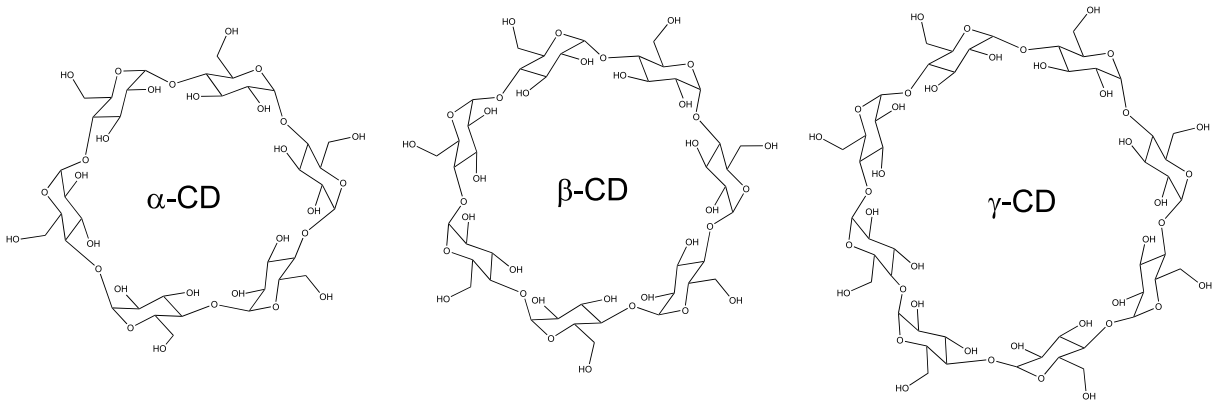

Figure 4.6: Structural formulae of α-, β- and γ-cyclodextrins.

In solution, CDs are able to form stable complexes with organic molecules and they are attractive building blocks for the construction of supramolecular architectures [119]. The relatively hydrophilic exterior and hydrophobic interior of the CD nano-cavities make them suitable hosts for hydrophobic guests. The principal interactions involved in complexation are believed to be van der Waals and hydrophobic interactions. Hydrogen bonding and steric effects may also play minor roles [120]. Furthermore, the size of the guest with respect to that of the cavity plays an important role in the stability of the system. The minimum internal diameters of the three different CDs are summarized in table 4.1. Guests thicker

than d_{min} are not able to penetrate the ring; however, they can sometimes form sandwich-like complexes with CDs.

Table 4.1: Minimum internal diameters d_{min} of CDs [121].

Cyclodextrin	$\boldsymbol{d_{min}}$ **[Å]**
α-CD	4.4
β-CD	5.8
γ-CD	7.4

The stoichiometry of the formed complex depends both on the CD and the guest molecule. Often 1:1 ratios are obtained but some studies have shown the formation of higher stoichiometries (1:2, 2:1 and 2:2) or even the formation of nanotubes where a large number of CD cavities is involved [122].

In aqueous solution a CD can serve as host for a tetrasulfonated tetraphenyl porphyrin (TPPS, see figure 4.8). The complexation of β-CDs and TPPS has been well documented. The formation of 2:1 inclusion complexes between heptakis(2,6-di-*O*-methyl)-β-CD and TPPS was firstly reported by Manka and Lawrence [123]. For TPPS, the tendency towards self-aggregation is known. As shown by Ribo et al. native β- and γ-CDs can dissociate the aggregates of TPPS in aqueous medium [124].

A tri-methylated form of β-CD is called heptakis(2,3,6-tri-*O*-methyl)-β-CD (TMe-β-CD) and the structural formula of TMe-β-CD is shown in figure 4.7.

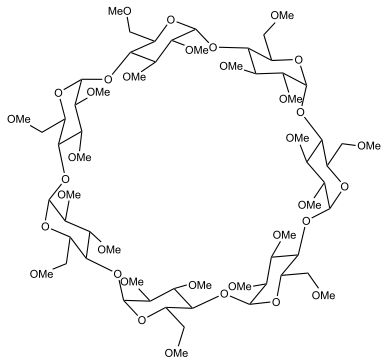

Figure 4.7: Structural formula of heptakis(2,3,6-tri-*O*-methyl)β-cyclodextrin.

As reported by Kano et al. [125] TMe-β-CD provides more favourable conditions for self-assembly with TPPS than β-CD. Kano et al. established a model that describes the self-assembly process between porphyrins and TMe-β-CDs:

- The positively polarized rim and interior of the TMe-β-CD pull the anionic guest molecules inside of the nano-cavity, thereby acting as a barrier for penetration of a cationic guest. Therefore, the cavity of TMe-β-CD is favourable for loading anionic porphyrin guests. Cationic porphyrins show much smaller association constants upon complexation with TMe-β-CD.

- TMe-β-CD has a strong tendency to include the aryl groups of TPPS. Two TMe-β-CDs cover the centre of the porphyrin, thereby providing a microscopically non-polar environment and hence, a 2:1 CD:TPPS association stoichiometry is obtained, see figure 4.8.

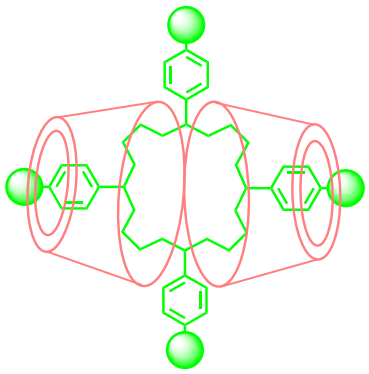

Figure 4.8: The 2:1 association stoichiometry between TPPS and TMe-β-CD.

In the following, for simplicity we will refer to TMe-β-CD as CD.

4.2 Experimental setups

The experimental methods used for the photophysical investigations are well established in the photobiophysics group and are presented in this section. The methods include steady-state UV/Vis absorption, steady-state fluorescence, time-resolved fluorescence and transient absorption spectroscopy in the ps time domain.

4.2.1 Steady-state absorption

UV/Vis absorption spectra were recorded using a commercial spectrophotometer Shimadzu UV-2501 PC. The combination of a deuterium and a halogen lamp enables the recording of UV/Vis spectra in a range from 200-1100 nm. The spectral bandwidth is 2 nm and the error of the optical density is ± 0.005, provided that the OD is lower than 1.5. The wavelength measurement error lies within 0.5 nm. The absorption spectra of the compounds were taken twice: before and after experiments to check photobleaching or decomposition. It was observed that all compounds are stable under used excitation conditions.

4.2.2 Steady-state fluorescence

Steady-state fluorescence experiments have been carried out using a combination of a cw-Xenon lamp (XBO 150) and a monochromator (Lot-Oriel, bandwidth 10 nm) for excitation and a polychromator with a cooled CCD matrix as detection unit (Lot-Oriel, Intaspec IV). The fluorescence quantum yields were calculated according to the following equation [126, 127, 128]:

$$\Phi_{fl}^{x} = \Phi_{fl}^{ref} \frac{OD_{ref}(\lambda_{ex})}{OD_{x}(\lambda_{ex})} \frac{I_x}{I_{ref}} \frac{n_x^2}{n_{ref}^2} \tag{4.1}$$

where Φ_{fl}^{x}, Φ_{fl}^{ref}, I_x, I_{ref}, $OD_x(\lambda_{ex})$ and $OD_{ref}(\lambda_{ex})$ are the fluorescence quantum yield, the integrated fluorescence intensity, and the optical density at the excitation wavelength, λ_{ex}, of a sample and a reference substance, respectively, n_x and n_{ref} are the refractive indices of the solvents used for the sample and the reference compounds. For the determination of fluorescence quantum yields, the following dye solutions have been used as references: rhodamine 6G in ethanol ($\Phi_{fl} = 0.95$ [129, 130]), rhodamine 110 in ethanol ($\Phi_{fl} = 0.94$ [131]), tetraphenylporphyrin in DMF (H_2TPP, $\Phi_{fl} = 0.11$ [132]), BDP in toluene ($\Phi_{fl} = 0.55$ [92]), MSBDP in toluene ($\Phi_{fl} = 0.78$ [92]) and SiPc in toluene ($\Phi_{fl} = 0.60$ [92]). Repeated measurements showed that fluorescence quantum yields could be determined with an accuracy of $\pm$ 5%, although with a minimum error of $\pm$ 0.005. Fluorescence excitation spectra were recorded by scanning the excitation wavelength and monitoring the signal at a fixed wavelength region.

In order to minimize reabsorption, in all fluorescence experiments (including steady-state fluorescence, excitation spectra, time-resolved fluorescence) the *OD* of the samples was held below a value of 0.1 at the maximum of the absorption band of lowest energy.

4.2.3 Time-correlated single photon counting

Fluorescence lifetimes were measured by time-correlated single photon counting technique, commonly abbreviated to TCSPC. The latter in combination with scanning of the detection wavelength was used

to acquire decay associated fluorescence (DAF) spectra [133]. The experimental setup was previously described in detail in [134] and is shown in figure 4.9. A frequency doubled, linearly polarized pulse of a Nd:VO_4 laser (Cougar, Time Bandwidth Products) with a wavelength of 532 nm, a pulse width of 12 ps, and a repetition rate of 60 MHz was employed. Utilizing the 532 nm laser to synchronously pump a DCM dye laser (Model 599, Coherent), excitation wavelengths between 615-670 nm could be selected. For excitation of the samples at 400 nm the frequency doubled pulses of a Ti:sapphire laser (Coherent Mira 900, FWHM 160 fs, a repetition rate of 76 MHz) were used. In order to avoid the pile-up effect, the light intensity was held low to ensure that at most one molecule is excited per 100 pulses [135]. Fluorescence was detected under the 'magic' angle [65] relative to excitation with a thermoelectrically cooled micro channel plate (R3809-01, Hamamatsu). The instrument response function was 42 ps, as measured at an excitation wavelength with Ludox. For DAF spectra, decay times and time shift were linked through all measurements of one scan sampled every 2-4 nm.

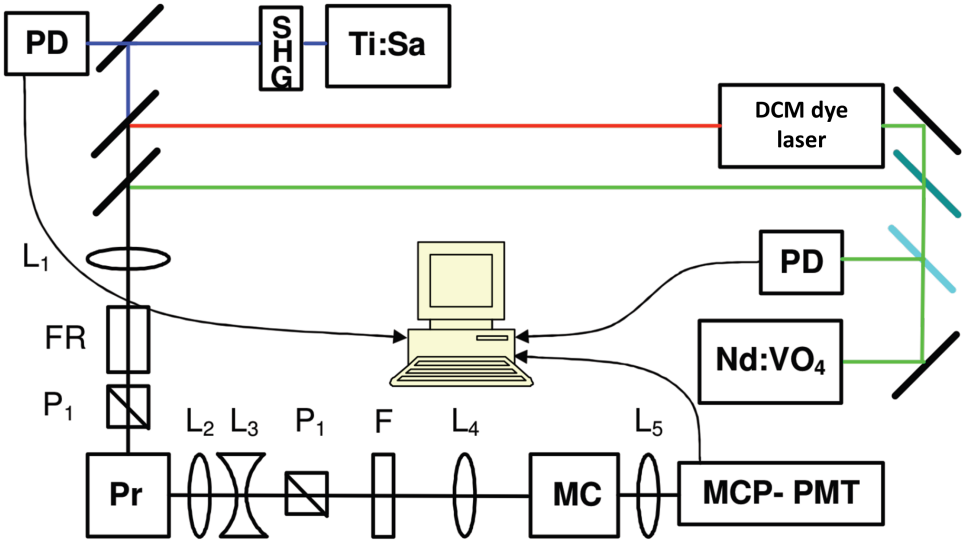

Figure 4.9: TCSPC setup with Pr: sample, L_{1-5}: lens, FR: Fresnel rhomb, MC: multi-channel plate, F: filter, P: polarizer, SHG: second harmonic generator, Ti:Sa: titan-sapphire laser, Nd:VO_4: green laser, PD: photodiode. Figure adapted from [134].

4.2.4 Transient absorption spectroscopy

A powerful tool to follow population dynamics of non-luminescent states is transient absorption spectroscopy in the picosecond time domain (ps-TAS). In this thesis, charge-separated states and triplet states are of interest, both of them can be examined with ps-TAS.

Principle of transient absorption spectroscopy

Transient absorption spectroscopy is a typical pump-probe experiment. First, the sample is selectively excited with monochromatic light of a short, intense laser pulse. Subsequently, the sample is probed with a white light continuum at a well-defined delay time after excitation (see figure 4.10).

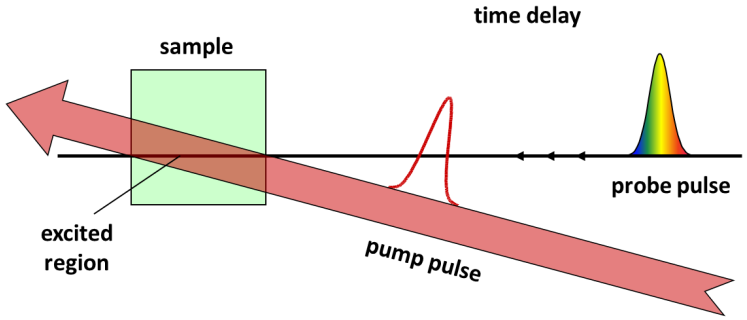

Figure 4.10: Principle of a pump-probe experiment: after a well-defined delay the transmission of the excited sample is measured. Figure adapted from [136].

The measurand of TAS is the change in OD of the sample as a function of the delay time between pump- and probe pulse according to the following equation:

$$\Delta OD(\lambda,t) = OD^*(\lambda,t) - OD(\lambda) = -\log\frac{T^*(\lambda,t)}{T(\lambda)} \tag{4.2}$$

Here ΔOD is the change in optical density, OD^* and T^* the optical density and transmission of the excited sample at delay time t, OD and T the optical density and transmission of the sample that resides in the ground-state, respectively.

The interpretation of the ΔOD-spectra is much more delicate than the ground-state absorption spectra. After excitation of the sample, the molecules will be in different excited states. However, some of the molecules remain in the ground state, which results in a spectral overlap of the absorption bands of the corresponding states. Competing deactivation channels complicate the interpretation of the ΔOD signal. Even if the assumption is made that directly after excitation the molecules reside either in the first excited singlet state or in the ground state, the ΔOD-signal is composed of the following three transients (see figure 4.11): the reduced ground state absorption of the remaining molecules in the ground state, the induced absorption of excited molecules and stimulated emission from the S_1-state [136, 137].

Compared to the unexcited ensemble, the reduced population of the ground state induces bleaching of the ground state absorption, which is expressed by a negative ΔOD signal. The stimulated emission provokes a spectrally dependent amplification of the probe pulse and thus gives a negative signal to the ΔOD spectrum. The absorption of the molecules that reside in excited states causes a positive ΔOD

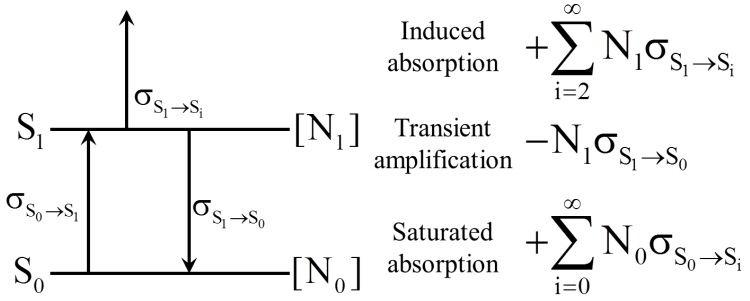

Figure 4.11: Three transients in a two-level system. Figure adapted from [136].

signal due to transitions to higher excited states. Using the Beer-Lambert law, the OD^* consists of the following contributions [136, 137] (*cf.* figure 4.11):

$$OD^*(\lambda,t) = \frac{l}{10}\left\{\sum_{i=1}^{\infty} N_0(t)\,\sigma_{S_0(\rightarrow)S_i}(\lambda) + \sum_{i=2}^{\infty} N_1(t)\,\sigma_{S_1(\rightarrow)S_i}(\lambda) - N_1(t)\,\sigma_{S_1(\rightarrow)S_0}(\lambda)\right\} \tag{4.3}$$

With N_i concentration of the molecules in state i, σ (in cm^2) absorption cross section of the corresponding transition. With equation 4.2, it follows for $\Delta OD(\lambda,t)$:

$$\Delta OD(\lambda,t) = \frac{l}{\ln 10} N_1(t)\left\{\sum_{i=2}^{\infty} \sigma_{S_1(\rightarrow)S_i}(\lambda) - \sum_{i=1}^{\infty} \sigma_{S_0(\rightarrow)S_i}(\lambda) - \sigma_{S_1(\rightarrow)S_0}(\lambda)\right\} \tag{4.4}$$

The spectrally dependent cross sections are merged to cross sections of the separate transients:

$$\Delta OD(\lambda,t) = \frac{l}{\ln 10} N_1(t)\left(\sigma_{ia}(\lambda) - \sigma_{se}(\lambda) - \sigma_{ga}(\lambda)\right) \tag{4.5}$$

With σ_{ia} absorption cross section of the excited state, σ_{se} luminescence cross section of the transient amplification, σ_{ga} absorption cross section of the ground state. In general, more states have to be taken into consideration, for instance a triplet state or a charge-separated state. Hence, equation 4.4 is expanded to:

$$\Delta OD(\lambda,t) = \frac{l}{\ln 10}\sum_{j=1}^{\infty} N_j(t)\left\{\sum_{i=j+1}^{\infty} \sigma_{S_j(\rightarrow)S_i}(\lambda) - \sum_{i=1}^{\infty} \sigma_{S_0(\rightarrow)S_i}(\lambda) - \sigma_{S_j(\rightarrow)S_0}(\lambda)\right\} \tag{4.6}$$

The N_j can represent both singlet and triplet states in due consideration that there will be no stimulated emission from the T_1- or charge-separated states.

The data obtained with ps-TAS are analysed by means of the compensation method [136, 137]. In this way, lifetimes of excited states and intersystem crossing quantum yields Φ_{ISC} can be determined.

Experimental setup

The experimental ps-TAS setup is shown in figure 4.12 and has been previously described in [136].

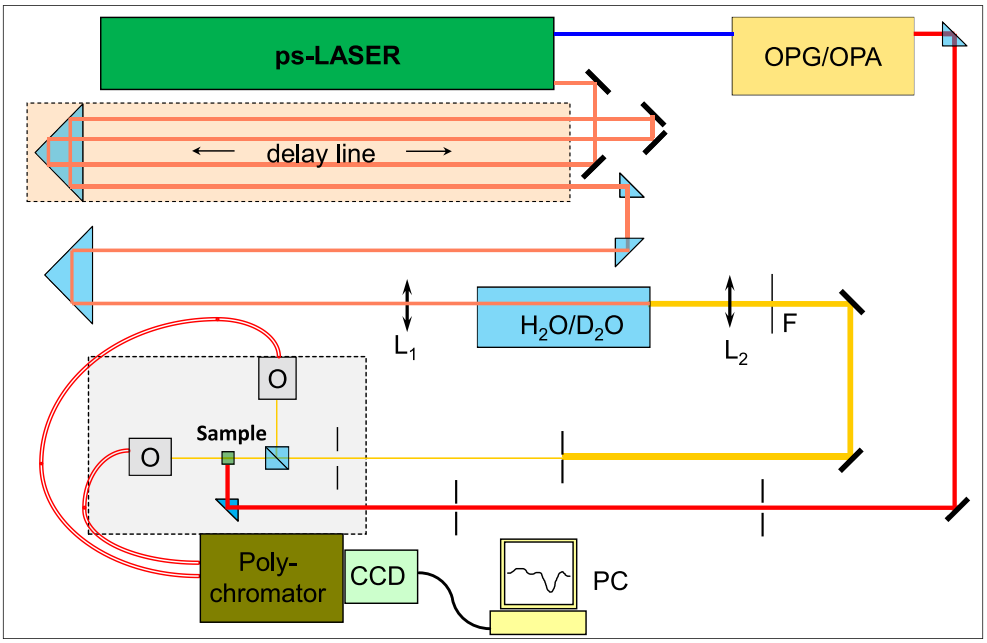

Figure 4.12: ps-TAS setup with L: lens, F: filter, O: fibre optic, CCD: CCD-matrix. Figure taken from [138].

The pump pulse is generated in an optical parametrical generator (OPG/OPA, Ekspla PG 401/SH), which in turn is pumped by the third harmonic of a Nd^{3+}:YAG laser (PL 2143A, Ekspla, 355 nm) with a pulse width of 25 ps. The OPG/OPA system generates light which is tuneable in the 200-2300 nm spectral range. The pump pulse is focussed by a cylindrical lens to obtain a 5 mm $\times$ 2 mm excited area on a 5 mm quartz cell which contains the sample. A white probe pulse is generated in a H_2O/D_2O-mixture by the fundamental wave of the Nd^{3+}:YAG laser (1064 nm). In order to minimize heating and the formation of bubbles, the mixture is circulated through the cell. The generated continuum possesses a large fraction of infrared light from the fundamental wave; moreover the light is divergent due to the non-linear optical processes involved. Therefore, the light is focussed with lens L_2, hereafter the infrared part is removed by an edge filter F. The continuum fluctuates strongly from pulse to pulse, for this reason, it is split to get a reference spectrum. Before passing through the sample, the white light is polarized at the magic angle [65] with respect to the pump beam in order to minimize time-dependent anisotropy effects. Both the beam transmitted through the sample and the reference beam are focussed into optical fibres and are recorded simultaneously at different traces on a CCD-matrix (LOT-Oriel, Intaspec IV).

The time domain of interest lies in the order of magnitude of the first excited singlet states, which are a few ns. The delay time between pump and probe pulse should be adjustable on a ps-time scale. In order to achieve such short delay times, a mechanical delay line is used that adjusts the optical path length of the probe pulse. The mechanical delay line enables measurements of ΔOD signals up to 15 ns after excitation. The accuracy of the mechanical delay line corresponds to 5 ps.

To maximize the signal-to-noise-ratio a large OD is necessary. On the other hand, reabsorption and

aggregation should be minimized. Therefore, the *OD* of all samples was set to 1.0 in the absorption band of lowest energy. Moreover, a filter was used to adjust the intensity of the pump beam in order to keep the change of population below 30%. Otherwise, measurements at the magic angle cannot avoid time-dependent anisotropy effects [139].

5 Photo-induced processes in the covalently bound systems

The construction of functional structures from molecular building blocks has drawn a lot of attention during the last decades. Due to their well-defined structures and robustness, covalently bound molecular systems provide a powerful tool to study energy and electron transfer processes in artificial photosynthesis. As outlined in chapter 4.1, phthalocyanines (Pcs) and boron dipyrromethenes (Bodipys) are good candidates to mimic the primary events of photosynthesis due to their high extinction coefficients, high fluorescence quantum yields and high chemical stability. Moreover, Bodipys and Pcs are known for their comparatively easily tuneable electronic properties making them adaptable for any given system. For this reason, a substantial number of conjugates of these chromophores have been studied extensively in combination with other dyes as porphyrins, ferrocenes, carotenes, fullerenes, ruthenium polypyridine complexes, perylenes, and viologens. This led to a large variety of covalently bound photosynthetic model compounds [15, 22, 73, 74, 79, 80, 81, 82, 83, 84, 85, 86, 87, 88, 89, 102, 104, 140, 141, 142, 143, 144, 145, 146].

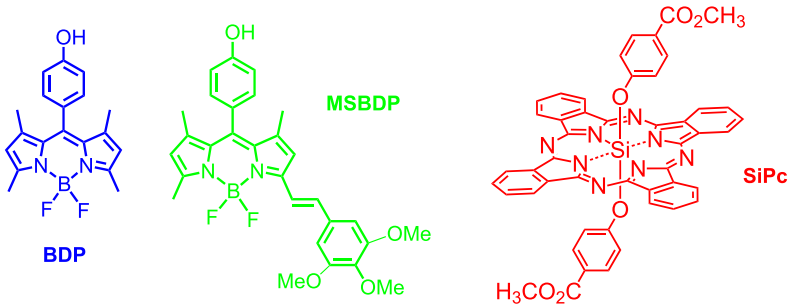

Figure 5.1: Structural formulae of BDP (blue), MSBDP (green) and SiPc (red).

However, despite the favourable characteristics of both chromophores a combination of Pcs and Bodipys still remains rare. Only a few conjugates have been reported in literature [92, 147, 148]. For this reason, in the present work a combination of two different Bodipys and a central SiPc as building blocks has been employed to construct several triads and a pentad. The compounds were synthesized in the group of Prof. Dr. Dennis K.P. Ng (Chinese University of Hong Kong).

The monomeric compounds are shown in figure 5.1. The Bodipys BDP and MSBDP were prepared according to the procedures in [112, 149] and they were axially linked to the commercially available SiPc dichloride to construct the SiPc$(BDP)_2$ and SiPc$(MSBDP)_2$ triads [148], which are shown in figure 5.2. The photophysical characterization of the SiPc$(BDP)_2$ and SiPc$(MSBDP)_2$ triads was outlined in detail in [92, 148, 150]. Herein, it was shown that ET and EET processes occur from the photo-excited Bodipy moieties to the SiPc-part of the triads. Both triads were studied in toluene and DMF and it was

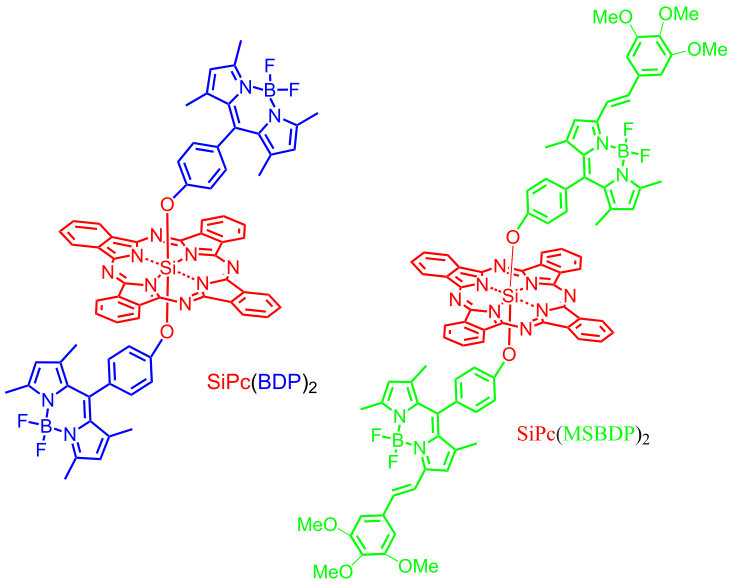

Figure 5.2: Structural formulae of the reference triads $SiPc(BDP)_2$ and $SiPc(MSBDP)_2$. For clarity, the monomeric moieties are coloured blue (BDP), green (MSBDP) and red (SiPc).

shown that the polarity of the solvent exerts great influence on the electron and energy transfer processes involved. Both triads feature strong UV/Vis absorbance along a large part of the sunlight spectrum. However, as can be seen from figure 4 (appendix) the absorption profiles of both triads exhibit spectral gaps, either in the region 520-600 nm ($SiPc(BDP)_2$) or in the region 400-520 nm ($SiPc(MSBDP)_2$). As BDP, MSBDP and SiPc absorb at complementary spectral regions, these chromophores were combined to compose a triad BDP-SiPc-MSBDP and a pentad $SiPc(BDP\text{-}MSBDP)_2$ for optimal light-harvesting. Both dyes exhibit *de facto* continuous UV/Vis absorbance that spans from 300 to 700 nm. The triad will be presented in the next section (chapter 5.1), whereas the pentad is described in detail in section 5.2.

5.1 The BDP-SiPc-MSBDP triad

The BDP and MSBDP moieties were linked on each side of the SiPc unit to construct the BDP-SiPc-MSBDP triad, the structural formula of which is shown in figure 5.3. For the photophysical investigations, the SiPc(BDP)$_2$ and SiPc(MSBDP)$_2$ triads serve as references. In the reference triads the ET and EET processes proceed from the Bodipys to the SiPc moiety. For BDP-SiPc-MSBDP, it is therefore expected that the peripheral Bodipys lead the excitation energy to the SiPc core. Arrived here, electron transfer from a Bodipy to SiPc may occur.

The polarity of the solvent strongly affects the probability of ET between the constituent parts [92, 148]. Therefore, thorough spectroscopic investigations in as many as five different solvents with different polarity for the triad as well as its reference triads SiPc(BDP)$_2$ and SiPc(MSBDP)$_2$ and the monomers BDP, MSBDP and SiPc were carried out. All triads as well as the monomeric compounds were dissolved in toluene, xylene, chloroform, tetrahydrofuran (THF) and *N*,*N*-dimethylformamide (DMF).

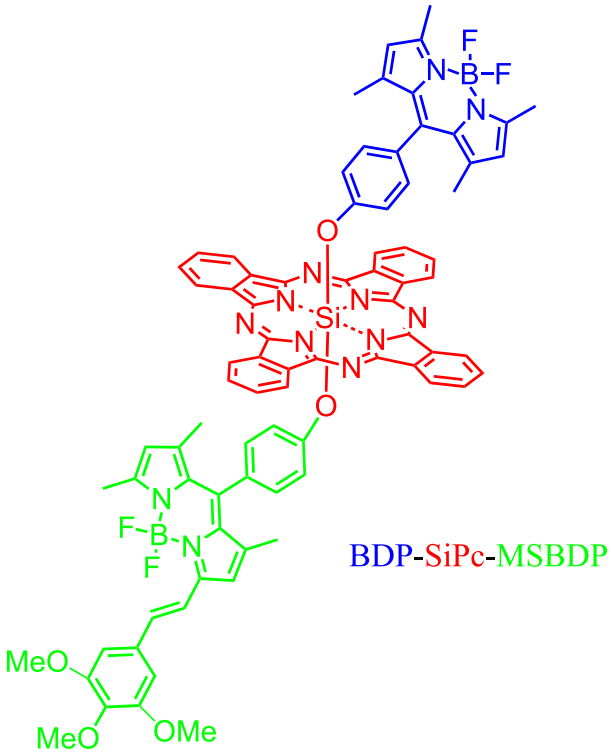

Figure 5.3: Structural formula of the BDP-SiPc-MSBDP triad. For clarity, the monomeric moieties are coloured blue (BDP), green (MSBDP) and red (SiPc).

5.1.1 Steady-state characterization of the triad

The UV/Vis absorption spectra of BDP-SiPc-MSBDP and its monomeric reference compounds dissolved in toluene are shown in figure 5.4a.

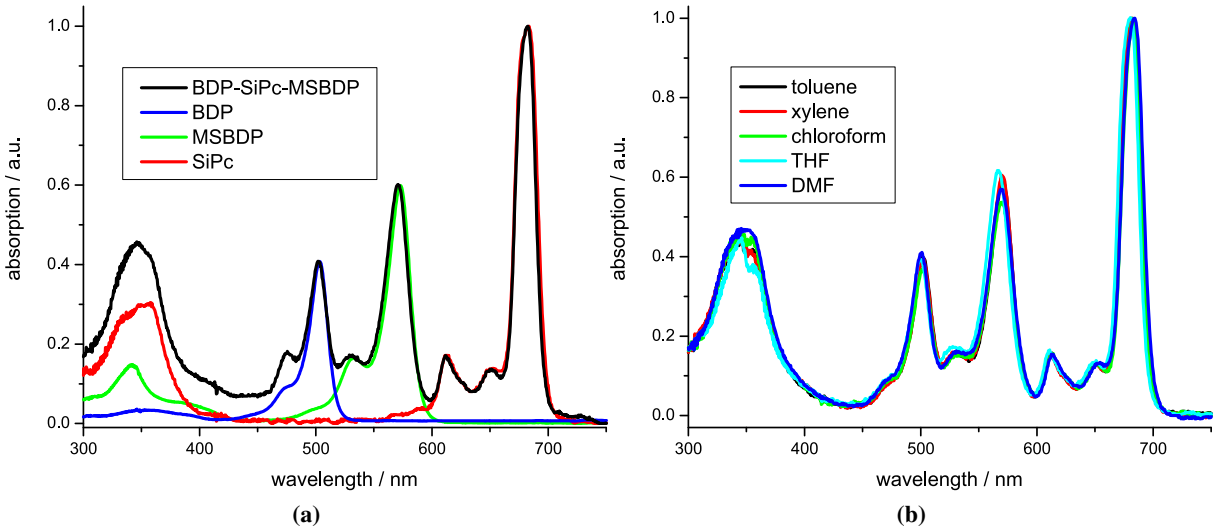

Figure 5.4: UV/Vis absorption spectra of the BDP-SiPc-MSBDP triad and its monomeric references SiPc, BDP and MSBDP dissolved in toluene (a) and the corresponding spectra of the triad dissolved in toluene, xylene, chloroform, THF and DMF (b).

In toluene the monomers BDP, MSBDP and SiPc show strong absorbance at 503 nm, 572.5 nm and 683 nm, respectively. As can be seen from figure 5.4a, the absorption spectrum of BDP-SiPc-MSBDP is a superposition of the absorption bands of monomeric BDP, MSBDP and SiPc. Small spectral shifts (within 50-80 cm^{-1}) of the absorption maxima of the triad compared to the positions of monomeric compounds were observed. Due to the comparably small spectral shifts and due to the unchanged shapes of the absorption bands compared to its monomeric reference compounds, the moieties within the triad are considered as electronically decoupled in their ground states. The absorption spectra of the triad BDP-SiPc-MSBDP dissolved in xylene, chloroform, THF and DMF are similar to the absorption spectra of those dissolved in toluene and are shown in figure 5.4. The corresponding absorption maxima are listed in table 5.1. The UV/Vis absorption spectra of the $SiPc(BDP)_2$ and $SiPc(MSBDP)_2$ triads are shown in figure 4 (appendix).

Table 5.1: Absorption and fluorescence maxima of highest intensity of the triad BDP-SiPc-MSBDP and its references dissolved in toluene, xylene, chloroform, THF and DMF.

Compound	**Solvent**	λ_{abs} **[nm]**	λ_{fl} **[nm]**		
			λ_{ex}**=470 nm**	λ_{ex}**=532 nm**	λ_{ex}**=615 nm**
BDP	toluene	503	512	-	-
	xylene	503	512	-	-
	chloroform	502	510	-	-
	THF	500	508	-	-
	DMF	500	510	-	-
MSBDP	toluene	572.5	-	583	-
	xylene	572.5	-	583	-
	chloroform	570.5	-	581	-
	THF	567	-	577	-
	DMF	567	-	580	-
SiPc	toluene	683	-	-	689
	xylene	683	-	-	689
	chloroform	683	-	-	687
	THF	681	-	-	686
	DMF	683	-	-	689
$SiPc(BDP)_2$	toluene	502[a] 682.5[c]	N.d. [a] 687[c]	-	687[c]
	xylene	502[a] 682.5[c]	N.d[a] 687[c]	-	687[c]
	chloroform	501[a] 683[c]	N.d. [a] 687[c]	-	687[c]
	THF	500[a] 681[c]	509[a] 685[c]	-	685[c]
	DMF	500[a] 683[c]	510[a] 689[c]	-	689[c]

Continued on next page

Table 5.1: Absorption and fluorescence maxima of highest intensity of the triad BDP-SiPc-MSBDP and its references dissolved in toluene, xylene, chloroform, THF and DMF.

Compound	Solvent	λ_{abs} [nm]	λ_{fl} [nm]		
			λ_{ex}=470 nm	λ_{ex}=532 nm	λ_{ex}=615 nm
$SiPc(MSBDP)_2$	toluene	570[b] 683[c]	-	588[b] 686[c]	686[c]
	xylene	570[b] 683[c]	-	590[b] 687[c]	687[c]
	chloroform	568[b] 683[c]	-	584[b] 686[c]	686[c]
	THF	566[b] 681[c]	-	583[b] 686[c]	686[c]
	DMF	567[b] 683[c]	-	580[b] 689[c]	689[c]
Triad	toluene	502[a] 570[b] 681.5[c]	512[a] 588[b] 687[c]	586[b] 687[c]	687[c]
	xylene	502[a] 570[b] 681.5[c]	513[a] 589[b] 687[c]	587[b] 687[c]	687[c]
	chloroform	501.5[a] 569[b] 682.5[c]	509[a] N.d[b] 687[c]	582[b] 687[c]	687[c]
	THF	500[a] 567[b] 680.5[c]	509[a] N.d[b] 684[c]	579[b] 686[c]	684[c]
	DMF	500[a] 569[b] 684[c]	509[a] 582[b] 689[c]	582[b] 688[c]	688[c]

[a] BDP-part
[b] MSBDP-part
[c] SiPc-part

The absorption bands of the BDP, MSBDP and SiPc moieties of the BDP-SiPc-MSBDP triad are spectrally well separated (see figure 5.4a). For this reason, it was possible to record steady-state fluorescence spectra of BDP-SiPc-MSBDP upon photo-selective excitation of its parts. The fluorescence spectra of the triad dissolved in toluene are shown in figure 5.5. By way of example the emission spectra of the reference triads dissolved in non-polar xylene and polar THF are shown in figure 5 (appendix).

In toluene the emission maxima of the monomeric reference compounds BDP, MSBDP and SiPc are located at 512 nm, 583 nm and 689 nm, respectively. As can be seen from figure 5.5 and table 5.1, for all excitation wavelengths only minor changes occur with respect to the shape and position of the fluorescence bands of BDP-SiPc-MSBDP compared to that of BDP, MSBDP and SiPc. Moreover, the

shape and position of the fluorescence bands of BDP-SiPc-MSBDP do not differ significantly when the triad is dissolved in other solvents. The calculated fluorescence quantum yields of all compounds dissolved in toluene, xylene, chloroform, THF and DMF are summarized in table 5.2.

Table 5.2: Fluorescence quantum yields of the triad and its references dissolved in different solvents.

Compound	**Solvent**	Φ_{fl}		
		BDP-part excitation	**MSBDP-part excitation**	**SiPc-part excitation**
BDP	toluene	0.55	-	-
	xylene	0.59	-	-
	chloroform	0.54	-	-
	THF	0.50	-	-
	DMF	0.32	-	-
MSBDP	toluene	-	0.78	-
	xylene	-	0.83	-
	chloroform	-	0.77	-
	THF	-	0.79	-
	DMF	-	0.48	-
SiPc	toluene	-	-	0.60
	xylene	-	-	0.64
	chloroform	-	-	0.58
	THF	-	-	0.58
	DMF	-	-	0.47
$SiPc(BDP)_2$	toluene	<0.001[a] 0.35[c]	-	0.60[c]
	xylene	<0.001[a] 0.29[c]	-	0.58[c]
	chloroform	<0.001[a] 0.27[c]	-	0.52[c]
	THF	0.002[a] 0.021[c]	-	0.053[c]
	DMF	0.005[a] 0.006[c]	-	0.016[c]

Continued on next page

Table 5.2: Fluorescence quantum yields of the triad and its references dissolved in different solvents.

Compound	Solvent	Φ_{fl}		
		BDP-part excitation	**MSBDP-part excitation**	**SiPc-part excitation**
$SiPc(MSBDP)_2$	toluene	-	0.003[b] 0.002[c]	0.003[c]
	xylene	-	0.036[b] 0.018[c]	0.034[c]
	chloroform	-	0.020[b] 0.003[c]	0.006[c]
	THF	-	0.016[b] 0.002[c]	0.002[c]
	DMF	-	0.004[b] 0.003[c]	0.012[c]
BDP-SiPc-MSBDP	toluene	<0.001[a] <0.001[b] 0.013[c]	0.004[b] 0.017[c]	0.023[c]
	xylene	<0.001[a] <0.001[b] 0.018[c]	0.003[b] 0.012[c]	0.035[c]
	chloroform	<0.001[a] <0.001[b] 0.010[c]	0.003[b] 0.007[c]	0.020[c]
	THF	0.002[a] <0.001[b] 0.004[c]	0.004[b] 0.001[c]	0.009[c]
	DMF	<0.001[a] <0.001[b] 0.002[c]	0.002[b] 0.001[c]	0.006[c]

[a] BDP-part emission
[b] MSBDP-part emission
[c] SiPc-part emission

Upon excitation of the SiPc moiety, for the reference compound $SiPc(MSBDP)_2$ small fluorescence quantum yields in the order of $\sim$0.01 are obtained, independent of the solvent used. Reference triad $SiPc(BDP)_2$ shows different behaviour: it exhibits a high fluorescence quantum yield of around 0.60 when dissolved in non-polar toluene, xylene and chloroform. This quantum yield is similar to that of monomeric SiPc. A dramatic decrease in fluorescence intensity is observed when $SiPc(BDP)_2$ is dissolved in polar solvents such as THF and DMF: Φ_{fl}(THF)=0.053 and Φ_{fl}(DMF)=0.016. For the

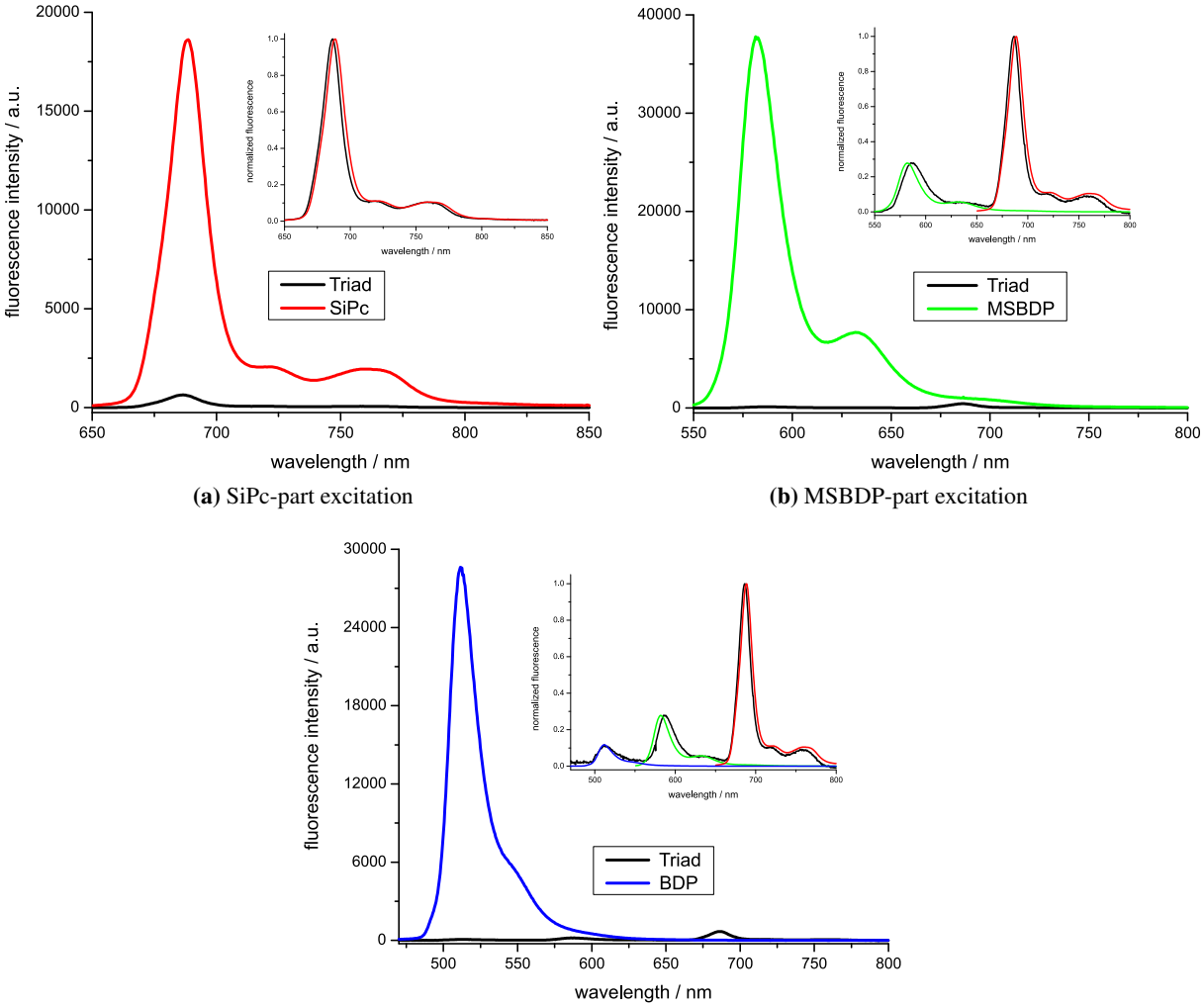

(a) SiPc-part excitation

(b) MSBDP-part excitation

(c) BDP-part excitation

Figure 5.5: Steady-state fluorescence spectra of BDP-SiPc-MSBDP dissolved in toluene upon excitation of its parts. In the insets normalized spectra are shown for comparison.

BDP-SiPc-MSBDP triad regardless of which solvent was used, the quantum yield of SiPc-part emission is strongly reduced and its value amounts to ∼0.02.

Upon selective excitation of the MSBDP-part of SiPc(MSBDP)$_2$, fluorescence of SiPc-part is observed showing that energy transfer from the photo-excited MSBDP* to the SiPc moiety in its ground state takes place. The fluorescence quantum yields of both MSBDP- and SiPc-part emission are strongly reduced compared to the values of the references MSBDP and SiPc. Independent of the solvent, Φ_{fl}(MSBDP-part) is approximately 0.02, whereas Φ_{fl}(SiPc-part) does depend on the polarity of the solvent and its value varies from 0.036 (xylene) down to 0.001 (DMF). BDP-SiPc-MSBDP shows the same qualitative behaviour as SiPc(MSBDP)$_2$, i.e. strong quenching of the MSBDP-part fluorescence and weak emission of SiPc. The MSBDP-part fluorescence quantum yield is approx. 0.003, while Φ_{fl}(SiPc) is 0.017 in

toluene and its value decreases to 0.001 in DMF.

Following excitation of the BDP moiety, the BDP-part fluorescence of the SiPc(BDP)$_2$ triad is strongly quenched, its fluorescence quantum yields do not exceed 0.005. At the same time, SiPc-part emission is observed, indicating that EET takes place from the initially excited BDP to SiPc. The intensity of the SiPc-part fluorescence of SiPc(BDP)$_2$ depends on the polarity of the solvent and remains comparably high with Φ_{fl} ~0.30 for non-polar solvents (toluene, xylene and chloroform). In polar solvents (THF and DMF) the fluorescence intensity decreases dramatically with Φ_{fl}=0.021 in THF and Φ_{fl}=0.006 in DMF. It is noted that in non-polar solvents the SiPc-part fluorescence intensity is weaker when SiPc moiety is excited indirectly *via* energy transfer from the BDP-part (Φ_{fl}=0.30) than when excited directly (Φ_{fl} ~0.60). Apparently, there is an additional way of BDP's first excited singlet state depopulation. After BDP-part excitation of the triad BDP-SiPc-MSBDP, practically no BDP-part fluorescence is observed, Φ_{fl}(BDP-part)<0.001. Moreover, excitation of the BDP-part results in fluorescence of both MSBDP- and SiPc-part. Besides EET from BDP to SiPc, this suggests that energy is transferred to MSBDP as well. The fluorescence quantum yields of MSBDP and SiPc emission are small with Φ_{fl}(MSBDP-part)<0.001 in all solvents and Φ_{fl}(SiPc-part)~0.01 for non-polar solvents and Φ_{fl}(SiPc-part)~0.003 for polar solvents.

From the results presented above combined with the findings presented in [92, 148, 150]*, the following preliminary conclusions can be drawn:*

- Appearance of SiPc fluorescence with selective excitation of BDP- (or MSBDP-) part of the triad is an indicator of EET from the photo-excited energy donor BDP (or MSBDP) to the energy acceptor SiPc in its ground state. In addition, the fluorescence of MSBDP after excitation of BDP indicates that energy is transferred from BDP to MSBDP, too.
- The SiPc-part fluorescence of the triad is strongly quenched compared to monomeric SiPc. This means that an additional process competes with fluorescence. Based on the results in [92, 148, 150], it is postulated that charge transfer is responsible for the efficient fluorescence quenching of BDP-SiPc-MSBDP.
- The fluorescence quantum yield of SiPc-emission is lower when SiPc is excited indirectly (*via* EET) compared to direct excitation. Besides EET, a charge transfer plays a role in the depopulation of the first excited singlet state of the Bodipy-part of the triad.

5.1.2 Excited-state dynamics of the triad

As a complement to the steady-state assays, time-resolved fluorescence and absorption experiments have been carried out to shed more light onto the electron and energy transfer processes.

Time-resolved fluorescence

In toluene the fluorescence of BDP, MSBDP and SiPc decays mono-exponentially, with lifetimes of 3.08, 3.44 and 5.26 ns, respectively (see table 5.3). Variation of the solvent exerts minor influence on the fluorescence lifetimes of monomeric MSBDP and SiPc. For BDP, the first excited singlet state decays approximately two times faster in DMF (τ_{fl}= 1.69ns) than in other solvents (τ_{fl}~3 ns).

The fluorescence lifetimes of the triads were examined using three different excitation wavelengths - 400, 532 and 620 nm, corresponding to selective excitation of the BDP-, MSBDP- and SiPc-part, respectively. It turned out that the fluorescence lifetimes of the BDP and MSBDP parts of the triads lie below the 10 ps detection limit of the setup. Therefore, the analysis of the time-resolved fluorescence of the three triads is carried out only for SiPc-part emission. The discussion starts with the analysis of the time-resolved fluorescence of the SiPc(BDP)$_2$ and SiPc(MSBDP)$_2$ triads.

Table 5.3: Fluorescence lifetimes of BDP-SiPc-MSBDP and its references dissolved in toluene, xylene, chloroform, THF and DMF.

Compound	**Solvent**	τ_{fl} **±0.02 [ns], A [%]**		
		BDP-part excitation	**MSBDP-part excitation**	**SiPc-part excitation**
BDP	toluene	3.08	-	-
	xylene	3.30	-	-
	chloroform	3.34	-	-
	THF	3.05	-	-
	DMF	1.69	-	-
MSBDP	toluene	-	3.44	-
	xylene	-	3.45	-
	chloroform	-	3.70	-
	THF	-	3.63	-
	DMF	-	3.55	-

Continued on next page

Table 5.3: Fluorescence lifetimes of BDP-SiPc-MSBDP and its references dissolved in toluene, xylene, chloroform, THF and DMF.

Compound	Solvent	τ_{fl} ±0.02 [ns], A [%]		
		BDP-part excitation	**MSBDP-part excitation**	**SiPc-part excitation**
SiPc	toluene	-	-	5.09
	xylene	-	-	5.08
	chloroform	-	-	5.48
	THF	-	-	5.47
	DMF	-	-	5.35
$SiPc(BDP)_2$	toluene	5.20	-	5.20
	xylene	5.22	-	5.24
	chloroform	5.54	-	5.59
	THF	0.668	-	0.668
	DMF	0.296	-	0.323
$SiPc(MSBDP)_2$	toluene	-	0.017, 88 2.86, 12	0.018, 87 2.78, 13
	xylene	-	0.026, 78 3.23, 22	0.025, 84 3.17, 16
	chloroform	-	0.043	0.038
	THF	-	0.021	0.017
	DMF	-	0.025	0.029
BDP-SiPc-MSBDP	toluene	0.032, 90 2.36, 10	0.021, 90 2.78, 10	0.021, 88 2.88, 12
	xylene	0.037, 91 2.74, 9	0.026, 88 3.02, 12	0.026, 87 3.53, 13
	chloroform	0.044	0.038	0.035
	THF	0.027	0.023	0.023
	DMF	0.032	0.028	0.027

Remark: for the triads τ_{fl} corresponds to SiPc-part fluorescence. Fluorescence lifetimes with amplitudes <2% are considered as impurities and are not taken into account.

Upon both BDP- and SiPc-part excitation the SiPc-part fluorescence decay of the triad $SiPc(BDP)_2$ occurs mono-exponentially. In solvents with comparably low dielectric constants (toluene, xylene and chloroform), the fluorescence lifetimes of the SiPc moiety of $SiPc(BDP)_2$ are similar to that of monomeric SiPc, τ_{fl} ∼5 ns. In contrast, when $SiPc(BDP)_2$ is dissolved in polar solvents such as THF and

DMF, the fluorescence decays faster with τ_{fl}=0.68 ns and τ_{fl}=0.30 ns, respectively. This correlates well with the relatively high SiPc-part fluorescence quantum yields in non-polar solvents of around 0.60 and on the other hand the low fluorescence quantum yields in polar THF and DMF of Φ_{fl}=0.053 and Φ_{fl}=0.016. As outlined below (page 55), the fluorescence quenching is due to electron transfer from BDP to SiPc.

Irrespective of the initially excited moiety of SiPc(MSBDP)$_2$, the fluorescence decay of the SiPc-part occurs mono-exponentially in chloroform, THF and DMF with fast decay times of 40 ps, 20 ps and 30 ps, respectively. Efficient electron transfer from MSBDP to SiPc is responsible for the reduction of the SiPc-part lifetime from 5 ns down to 20 ps.

In toluene and xylene the emission decay of SiPc(MSBDP)$_2$ shows a more complicated behaviour. In figure 5.6 the DAF spectra of the SiPc-part fluorescence of SiPc(MSBDP)$_2$ in toluene are shown following SiPc- and MSBDP-part excitation.

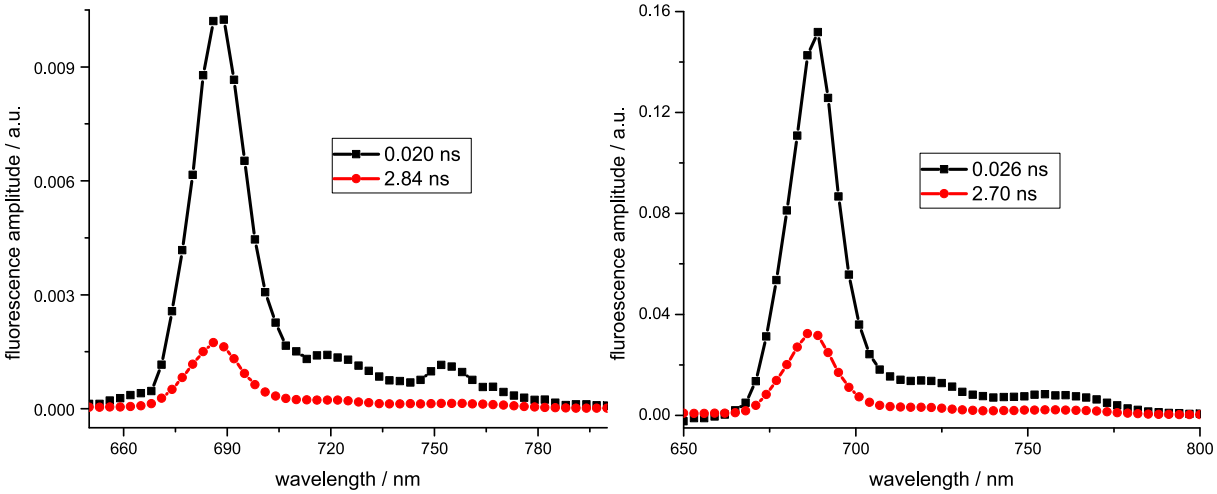

(a) SiPc-part excitation **(b)** MSBDP-part excitation

Figure 5.6: DAF spectra of SiPc(MSBDP)$_2$ dissolved in toluene upon excitation of its parts.

The SiPc-part fluorescence decay of SiPc(MSBDP)$_2$ has been properly fit with a bi-exponential function. Besides a fast decay time of around 20 ps that was also revealed in other solvents, an additional lifetime of around 3 ns emerges (red curve in figure 5.6) whose relative amplitude is approximately 0.15. The shape and position of this DAF spectrum is identical to that of the fast fluorescence component and stems from the SiPc moiety.

As found for the reference triads, the SiPc-part fluorescence of BDP-SiPc-MSBDP turns out to be independent of the initially excited moiety. The fate of the excited SiPc-part of BDP-SiPc-MSBDP bears resemblance to the emission decay of SiPc(MSBDP)$_2$. In chloroform, THF and DMF fast deactivation of the SiPc first excited singlet state is expressed by a decay time of around 20-40 ps. On the contrary, in toluene and xylene a bi-exponential function was required to fit the experimental data. The corresponding DAF spectra of BDP-SiPc-MSBDP dissolved in toluene are shown in figure 5.7. Besides the fast decay

time of around 25 ps, a comparably long lifetime of around 3 ns appears with relative amplitude of approximately 0.10. The shape and position of the DAF spectra resemble the steady-state emission spectra of SiPc.

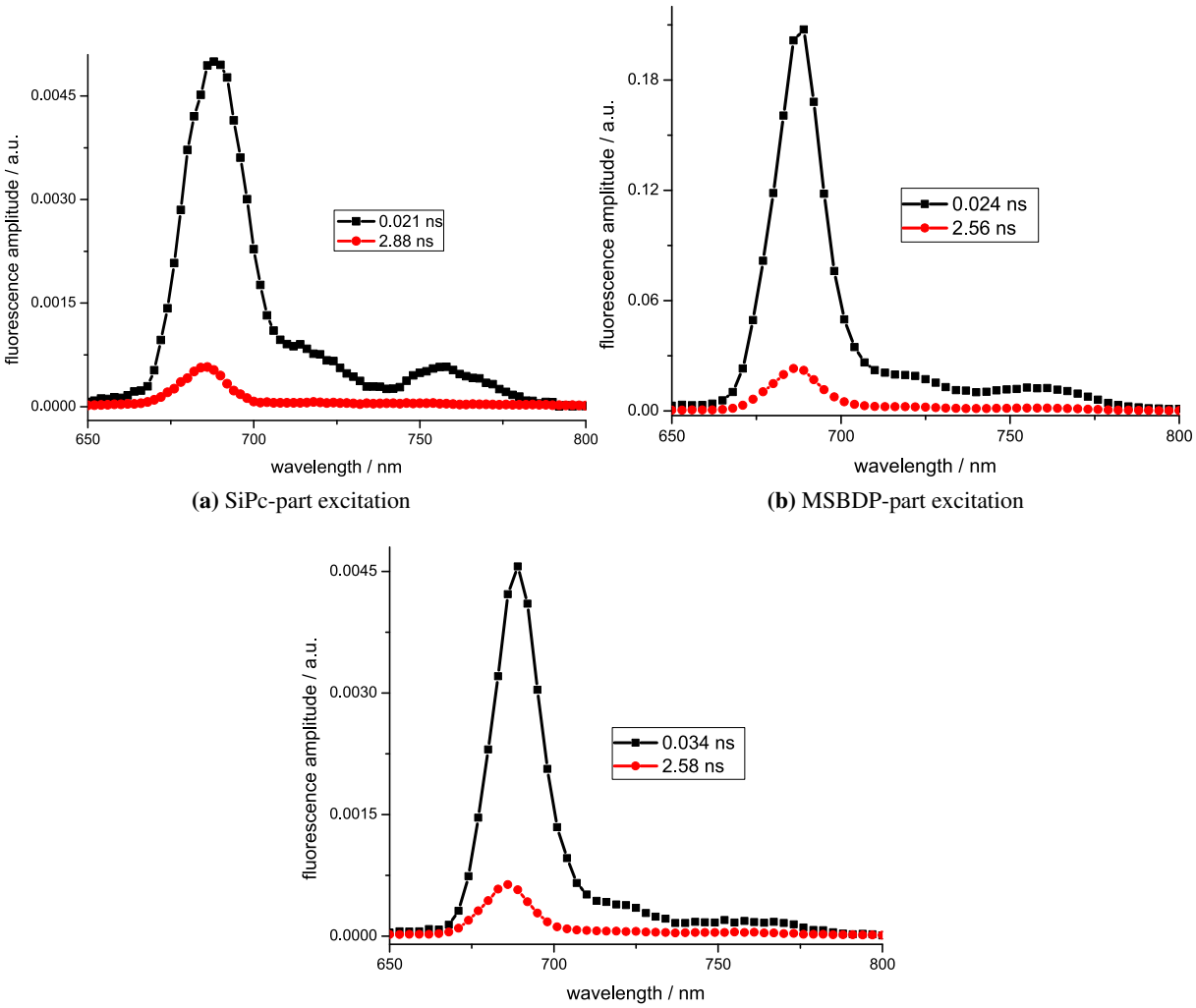

(a) SiPc-part excitation

(b) MSBDP-part excitation

(c) BDP-part excitation

Figure 5.7: DAF spectra of the BDP-SiPc-MSBDP triad dissolved in toluene upon excitation of its parts.

Transient absorption

To gather additional evidence of non-fluorescent intermediates such as charge-separated states, transient absorption spectra were recorded. As expected, the recovery of the ground state population of the monomeric BDP, MSBDP and SiPc occurs mono-exponentially with characteristic times that are consistent with their corresponding fluorescence lifetimes. As expected, the triplet formation of the Bodipy monomers is negligible, whereas for SiPc the intersystem crossing quantum yield Φ_{ISC} was found to be 0.32 in toluene and 0.34 in DMF.

The transient absorption spectra and the SiPc ground state bleaching signal of the triad SiPc(BDP)$_2$ dissolved in THF and chloroform upon excitation of the SiPc moiety are shown in figure 5.8.

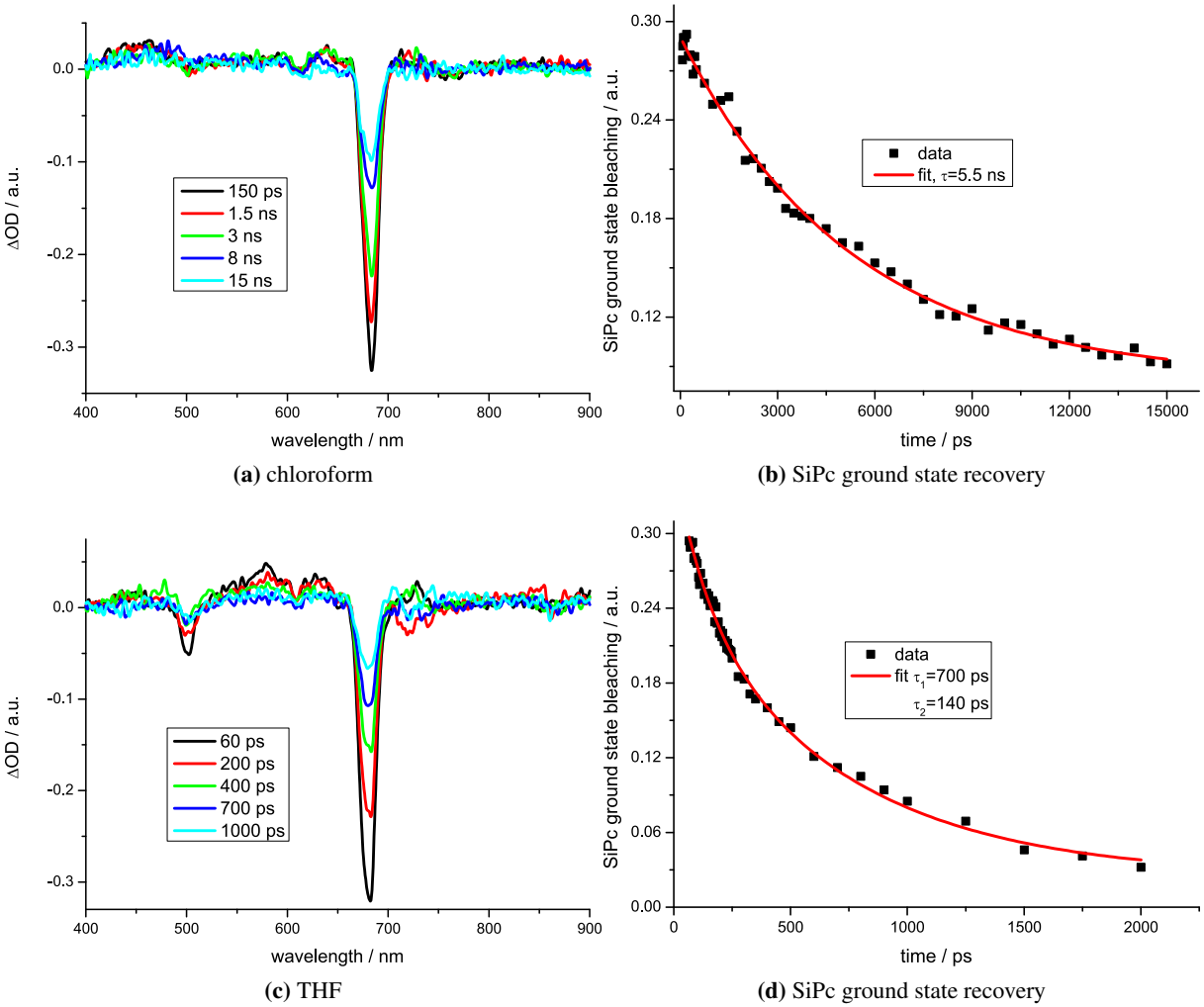

(a) chloroform

(b) SiPc ground state recovery

(c) THF

(d) SiPc ground state recovery

Figure 5.8: ΔOD spectra of SiPc(BDP)$_2$ dissolved in chloroform (a) and THF (c) upon excitation of SiPc at different delay times and SiPc ground state bleaching signals in chloroform (b) and THF (d).

Upon excitation of SiPc(BDP)$_2$ at 615 nm, the TA spectra show strong bleaching signals around

680 nm which is due to SiPc ground state depletion. In polar THF, a negative transient absorption signal at around 500 nm is observed, which originates from BDP ground state bleaching apparent from its position and shape. In addition, a transient signature appears at around 580 nm which is readily assigned to the absorption of the radical anion $SiPc^{\bullet -}$. In DMF a transient feature at 518 nm is observed, which could be assigned to the absorption of the $BDP^{\bullet +}$ radical cation. In chloroform neither induced absorption nor BDP ground state bleaching were observed in the TA spectra. The SiPc recovery times in toluene and chloroform are similar to the fluorescence lifetimes of around 5.5 ns.

Following BDP-part excitation at 480 nm, bleaching signals of both SiPc and BDP ground states were observed regardless of which solvent was used. The recovery time of the BDP-part ground state absorption was found to be much longer than the fluorescence lifetime (τ_{fl}<10 ps) and could be identified with the lifetime of the charge-separated state. The kinetic parameters are summarized in table 5.4 and they vary from 4.5 ns in toluene, 4.4 ns in chloroform, 140 ps in THF to 40 ps in DMF. In THF the decay of the SiPc ground state bleaching obeys bi-exponential kinetics with decay times of 140 ps and 700 ps. The amplitude of the latter is twice as large as the amplitude of the former. The decay times could be separated into a fluorescence part (700 ps) and a charge recombination part (140 ps), since the SiPc-part fluorescence decays with 700 ps in THF. In non-polar chloroform and toluene the quantum yields of triplet state formation of both 0.32 are comparable with that of monomeric SiPc, whereas in polar THF and DMF the values of Φ_T are 0.05 and 0 respectively, see table 5.4.

In figure 5.9 the TA spectra and SiPc ground state recovery of $SiPc(MSBDP)_2$ dissolved in chloroform and THF are shown.

For all excitation wavelengths and in all solvents it was found that the TA spectra of the $SiPc(MSBDP)_2$ triad exhibit two striking bleach features, namely strong SiPc ground state depletion with a minimum at 680 nm and MSBDP ground state bleaching at around 570 nm. In between these two bands positive transient absorption predominates the spectra. The effects underline the formation of a charge-separated state $MSBDP^{\bullet +}$-$SiPc^{\bullet -}$ as was reported in [92, 151]. The recovery of the SiPc and MSBDP ground state depletion occurs mono-exponentially. The former process is strongly solvent-dependent and the calculated recovery time differs from the corresponding SiPc-part fluorescence lifetime. It can therefore be associated with the lifetime of the charge-separated state. The repopulation of the SiPc ground state occurs with lifetimes of 1.7 ns, 1.5 ns, 0.40 ns, 90 ps and 30 ps in toluene, xylene, chloroform, THF and DMF, respectively. In toluene, xylene and chloroform remaining SiPc ground state depletion is seen even at 15 ns. This can be ascribed to population of the first excited triplet state $^3SiPc^*$. In toluene and xylene the quantum yields of triplet state population were found to be 0.32 and they are the same as for monomeric SiPc; in chloroform its value of 0.075 is somewhat reduced. In polar THF and DMF, the formation of the triplet state is negligible. The values of Φ_T are summarized in table 5.4.

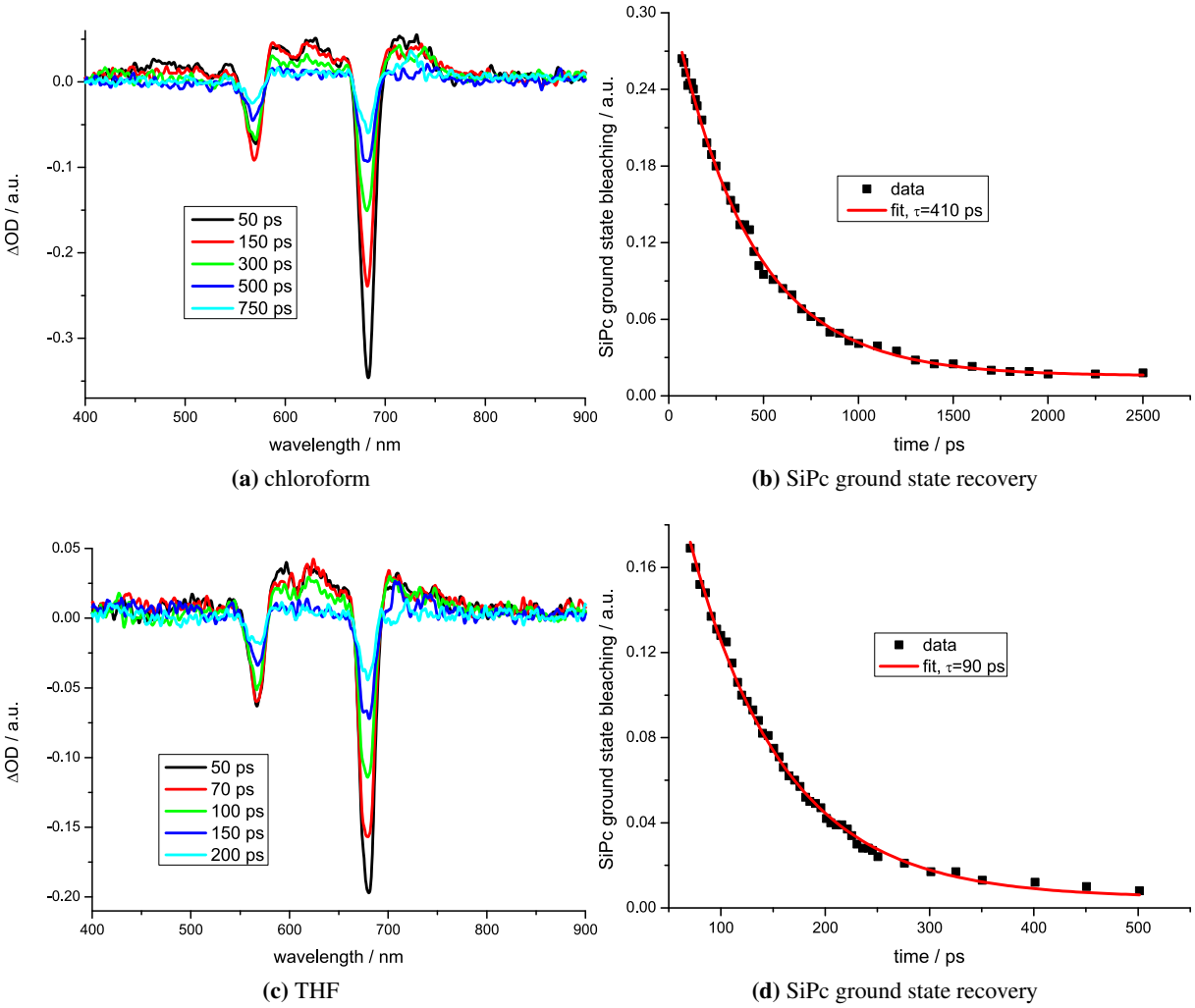

(a) chloroform **(b)** SiPc ground state recovery

(c) THF **(d)** SiPc ground state recovery

Figure 5.9: ΔOD spectra of SiPc(MSBDP)$_2$ dissolved in chloroform (a) and THF (c) upon excitation of SiPc at different delay times and SiPc ground state bleaching signals in chloroform (b) and THF (d).

The TA spectra of the BDP-SiPc-MSBDP triad exhibit similar features as those of the reference triad SiPc(MSBDP)$_2$. The spectral features and kinetics of the TA spectra are independent of the excitation wavelength. In figure 5.10 TA spectra of BDP-SiPc-MSBDP dissolved in toluene and THF upon selective excitation of the MSBDP moiety are shown at different delay times. The recovery of the SiPc ground state population in toluene and THF is also shown in figure 5.10. By way of example the transient absorption spectra of the triad dissolved in xylene and chloroform upon excitation of the BDP- and SiPc-part, are presented in figure 6 (appendix) and are similar to those at excitation of MSBDP. The recovery times of the SiPc ground state are listed in table 5.4.

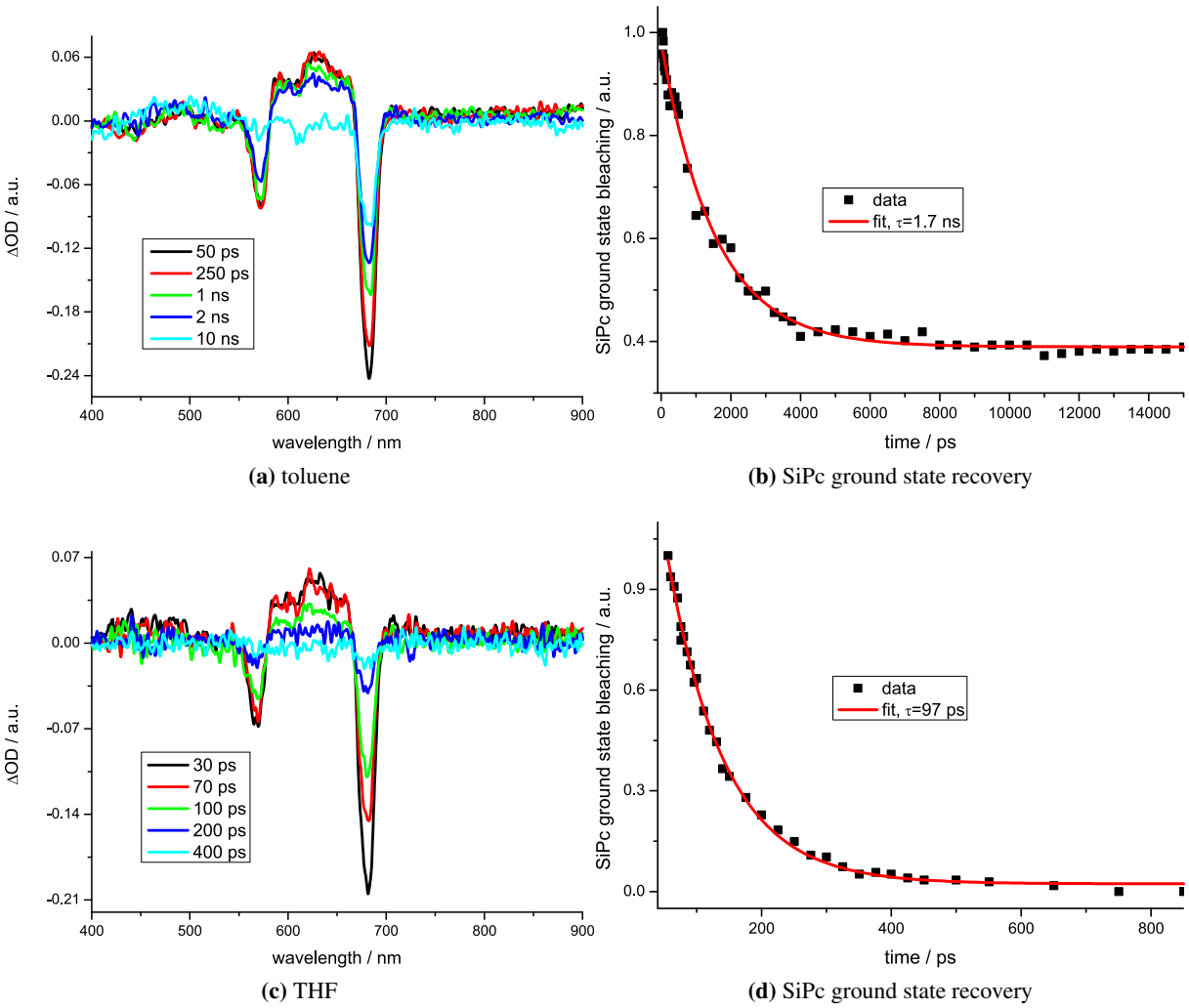

(a) toluene **(b)** SiPc ground state recovery

(c) THF **(d)** SiPc ground state recovery

Figure 5.10: ΔOD spectra of BDP-SiPc-MSBDP dissolved in toluene (a) and THF (c) upon excitation of MSBDP at different delay times and SiPc ground state bleaching signals in toluene (b) and THF (d).

Independent on the used excitation wavelength, two sets of transient absorption minima (at 570 and 680 nm, respectively) that resemble the ground state absorption of MSBDP and SiPc moieties were observed. In between these negative features the ΔOD spectra exhibit pronounced induced absorption. The SiPc ground state population recovers mono-exponentially with 1.7 ns, 1.7 ns, 0.34 ns, 100 ps and 30 ps in toluene, xylene, chloroform, THF and DMF, respectively. These recovery times differ greatly from the fluorescence lifetimes of around 20-40 ps. Obviously, the energy is accumulated in the charge-separated state. It is noted that the spectra lack any trace of BDP-part transients. It seems that the BDP moiety is not involved in the formation of the charge-separated state.

A bleach at 680 nm belonging to the SiPc-part ground state depletion is observed in toluene, xylene and chloroform for all excitation wavelengths and even at delay times in the order of 15 ns. In these non-polar solvents, a transition from the charge-separated state to the first excited triplet state CS→T_1 takes place.

The corresponding quantum yields are listed in table 5.4. In toluene and xylene the quantum yield of triplet state formation was found to be 0.37 and 0.38 and the values are somewhat greater than Φ_T=0.32 of monomeric SiPc. In chloroform the value of Φ_T is reduced to 0.07. The triplet state formation quantum yields vanish in polar THF (0.01) and DMF (0).

Table 5.4: Charge-separated state lifetime, τ_{CR}, and quantum yield of triplet state population, Φ_T, of the triads dissolved in toluene, xylene, chloroform, THF and DMF.

Compound	**Solvent**	τ_{CR} **[ns]**	$\Phi_T \pm$ **0.03**
$SiPc(BDP)_2$	toluene	4.5 ± 0.2	0.32
	chloroform	4.7 ± 0.2	0.32
	THF	0.14 ± 0.01	0.05
	DMF	0.040 ± 0.01	0
$SiPc(MSBDP)_2$	toluene	1.7 ± 0.1	0.32
	xylene	1.5 ± 0.1	0.32
	chloroform	0.41 ± 0.03	0.075
	THF	0.090 ± 0.01	0.02
	DMF	0.030 ± 0.01	0
BDP-SiPc-MSBDP	toluene	1.7 ± 0.1	0.37
	xylene	1.7 ± 0.1	0.38
	chloroform	0.34 ± 0.03	0.07
	THF	0.10 ± 0.01	0.01
	DMF	0.030 ± 0.01	0

5.1.3 Discussion of the triad's photo-induced processes

The absorption and fluorescence spectra of BDP-SiPc-MSBDP are well described by a superposition of the individual components in both polar and non-polar solvents. The shapes of all spectra are only slightly altered. Moreover, the spectral shifts are comparably small. For this reason, it is assumed that the molecular parts BDP, MSBDP and SiPc of the triad are electronically decoupled in their ground states as well as in their first excited states. It follows that the molecular parts can be described independent of each other. Due to the edge-to-face linkage the polarity of the solvent has only minor influence on the molecular geometry of the triad. Thus, it is expected that a good comparison can be drawn between the dyes dissolved in different solvents.

In line with the results presented by Menting in [151], two different interactions between the Bodipys and the SiPc are taken into account, namely EET and ET. Firstly, EET is discussed.

Excitation energy transfer

In steady-state fluorescence experiments SiPc-part fluorescence following excitation of the BDP- or MSBDP-part is observed. In addition, also MSBDP-part fluorescence occurs after excitation of the BDP moiety. Hence, EET is expected to be responsible for the observed behaviour. The separation between BDP/MSBDP and SiPc is approximately 6 Å, the distance between BDP and MSBDP moieties in BDP-SiPc-MSBDP was estimated to be 15 Å [150]. The separation of 6 Å is relatively short; however, the covalent edge-to-face linkage prevents close contact between the molecules within the triad, allowing them to orient almost in an orthogonal manner. It follows that the probability of an exchange energy transfer is likely to be small. Moreover, a broad spectral overlap between the emission of the Bodipys and the absorption of SiPc exists, which is required for the FRET mechanism. Thus, FRET is assumed to be the dominant EET process in further considerations.

In order to estimate the efficiency of FRET, the Förster radii R_0, the rate of FRET k_{FRET} and the FRET efficiency E_{FRET} have been calculated using equations 3.28, 3.31 and 3.32, respectively, and are summarized in table 5.5. Since absorption and fluorescence spectra do not change significantly upon variation of the solvent, the Förster radii are independent on the solvent. The Förster radii are much greater than the centre-to-centre distance between the chromophores. Hence, EET occurs efficiently for all donor-acceptor combinations listed in table 5.5.

Table 5.5: Förster radii R_0, FRET rates k_{FRET} and FRET efficiencies E_{FRET} that are relevant for the triad BDP-SiPc-MSBDP.

Donor-acceptor	$\boldsymbol{R_0}$ **[Å]**	$\boldsymbol{k_{FRET}} \times \mathbf{10^{11}}$ **[s^{-1}]**	$\boldsymbol{E_{FRET}}$
BDP-MSBDP	52	5.7	0.999
BDP-SiPc	33	9.1	0.999
MSBDP-SiPc	65	47	0.999

At this point it should be mentioned that for the derivation of equation 3.31, only dipole-dipole interaction is taken into account [48, 63]. Hence, the calculation of R_0 with equation 3.31 is valid only when the distance R between the moieties is much greater than the dimension of the chromophores. Ob-

viously, this condition is not fulfilled: the radii of the π-systems of BDP, MSBDP and SiPc are 3 Å, 3 Å and 4.6 Å, respectively, and the distance between BDP/MSBDP and SiPc was estimated to be 6 Å. Moreover, at small values of R the rates k_{FRET} are sensitive to small deviations of R. The rates k_{FRET} in table 5.5 are therefore rough estimations and yet they underline that energy transfer will proceed with high probability.

Charge transfer

As shown above, an induced absorption band at 580 nm appears in the TA spectra of the triads in picosecond TAS experiments. This band can be assigned to the absorption of the $SiPc^{\bullet -}$ anion. Furthermore, it was reported in [92, 148, 150] that for both reference triads $SiPc(BDP)_2$ and $SiPc(MSBDP)_2$ photo-induced charge transfer plays a dominant role in the depopulation of excited states. For both reference triads, the electron is transferred from the Bodipy moieties to SiPc. In order to prove the possibility of photo-induced charge transfer for BDP-SiPc-MSBDP, the free enthalpy of charge separation was calculated for all solvents using the Rehm-Weller approach. For the triads the following parameters were used: R(BDP-SiPc)=6 Å, R(MSBDP-SiPc)=6 Å, r(BDP)=3 Å, r(MSBDP)=4 Å, r(SiPc)=4.6 Å. The redox potentials are taken from table 2 (appendix) and the energies of the first excited states were calculated from the absorption maxima (table 5.1). The calculated values of ΔG_0 are listed in table 5.6.

Table 5.6: Driving force ΔG_0 for different electron donor-acceptor combinations calculated with equation 3.12. $E_{0,0}$ denotes the first excited singlet state energy of the initially excited moiety (Bodipy or SiPc).

Solvent	$\Delta G_0 \pm 0.05$ [eV] $BDP^{\bullet +}$-$SiPc^{\bullet -}$		$\Delta G_0 \pm 0.05$ [eV] $MSBDP^{\bullet +}$-$SiPc^{\bullet -}$	
	$E^D_{0,0}$(BDP)	$E^A_{0,0}$(SiPc)	$E^D_{0,0}$(MSBDP)	$E^A_{0,0}$(SiPc)
Toluene	-0.28	0.36	-0.40	-0.05
Xylene	-0.28	0.36	-0.40	-0.05
Chloroform	-0.61	0.03	-0.60	-0.25
THF	-0.73	-0.09	-0.67	-0.32
DMF	-0.89	-0.25	-0.77	-0.42

The blue-coloured values in table 5.6 indicate that charge transfer is thermodynamically favourable, whereas the red ones indicate that charge transfer is not a feasible process.

According to table 5.6, electron transfer from the initially excited BDP to SiPc is a feasible process in the $SiPc(BDP)_2$ triad, regardless of which solvent is used. In the TA spectra this is expressed by the transient signature of the $SiPc^{\bullet -}$ radical anion at 580 nm, as well as the SiPc and BDP ground state depletion. ET and EET processes from the BDP-part to the SiPc moiety compete with each other resulting in vanishing BDP-part fluorescence quantum yields. Therefore, the quantum efficiency of charge separation Φ_{CS} can be calculated using $\Phi_{CS} = 1 - \Phi_{fl}/\Phi^0_{fl}$, where Φ_{fl} and Φ^0_{fl} are the fluorescence quantum yields of the SiPc-part with and without charge separation. For non-polar solvents the charge separation occurs with moderate efficiency: Φ_{CS}(toluene)=0.42, Φ_{CS}(xylene)=0.50 and Φ_{CS}(chloroform)=0.48, whereas

for more polar THF and DMF, charge transfer proceeds more efficiently and the values of Φ_{CS} are calculated to 0.96 and 0.99, respectively.

On the other hand, upon excitation of SiPc charge transfer takes place solely for ε_S>5.2, as can be derived by means of equation 3.12. As a result, in xylene, toluene and chloroform electron transfer is not feasible, Φ_{CS}=0, whereas in THF with ε_S=7.5 and in DMF with ε_S=38.3 electron transfer is switched on with quantum yields of Φ_{CS}(THF)=0.91 and Φ_{CS}(DMF)=0.97. The sudden drop of fluorescence intensities in polar solvents is a direct consequence of enabling the charge transfer. The decrease in SiPc-part fluorescence is accompanied by the decrease of fluorescence decay times of 5 ns in non-polar solvents to 0.7 ns in THF and 0.3 ns in DMF. The lifetime of the charge-separated state was estimated to be 4.5 ns (toluene), 4.8 ns (chloroform), 140 ps (THF) and 40 ps (DMF).

With regard to SiPc(MSBDP)$_2$, solving the Rehm-Weller equation yields negative values of ΔG_0 for all solvents, independent of the initially excited moieties (table 5.6). Following excitation of the SiPc-part, very efficient hole transfer from SiPc to MSBDP leads to the strong quenching of the SiPc-part fluorescence accompanied by the fast emission kinetics of the SiPc moiety. The SiPc transient with a sharp minimum at 680 nm and the concomitant MSBDP bleach feature at 570 nm underline the successful formation of the MSBDP$^{\bullet+}$-SiPc$^{\bullet-}$-MSBDP charge-separated state. Upon excitation of the MSBDP-part EET from the initially excited MSBDP-part to the SiPc moiety in its ground state competes with ET from MSBDP to SiPc. EET results in the population of the first excited singlet state of SiPc, subsequently hole transfer occurs from SiPc to MSBDP. As a result, in both cases (SiPc- or MSBDP-part excitation) the charge-separated state is generated. The efficiency of charge separation is more or less solvent independent with a value of Φ_{CS}=0.99. In TA experiments, the recovery of the SiPc ground state is associated with charge recombination. The lifetime of the charge-separated states is determined to 1.7 ns (toluene), 1.5 ns (xylene), 400 ps (chloroform), 90 ps (THF) and 30 ps (DMF).

For the BDP-SiPc-MSBDP triad, principally both charge separated species BDP$^{\bullet+}$-SiPc$^{\bullet-}$-MSBDP and BDP-SiPc$^{\bullet-}$-MSBDP$^{\bullet+}$ could be formed according to the values of ΔG_0 in table 5.6. The driving force is, however, greater for the generation of BDP-SiPc$^{\bullet-}$-MSBDP$^{\bullet+}$. The quantum yield of the formation of the latter is therefore expected to be larger, unless the ET reaction takes place in the Marcus inverted region. In this case, the generation of BDP$^{\bullet+}$-SiPc$^{\bullet-}$-MSBDP is more favourable.

Despite the negative values of the driving force ΔG_0 for the formation of BDP$^{\bullet+}$-SiPc$^{\bullet-}$-MSBDP, the transient absorption spectra do not reveal any BDP-part ground state depletion. In contrast, for SiPc(BDP)$_2$ BDP-part bleaching signals are clearly distinguishable due to the generation of BDP$^{\bullet+}$-SiPc$^{\bullet-}$-BDP. That means that if the charge-separated state BDP$^{\bullet+}$-SiPc$^{\bullet-}$-MSBDP was generated, BDP-bleaching signals around 500 nm would be discernible in the TA spectra. Thus, BDP does not play a role in charge separation.

On the other hand, it was observed in the TA spectra that both MSBDP and SiPc ground states are depleted, independent of the initially excited moiety and solvent used. Bleaching of both ground states can be readily associated with the appearance of the charge-separated state BDP-SiPc$^{\bullet-}$-MSBDP$^{\bullet+}$. The fluorescence of the SiPc-part of BDP-SiPc-MSBDP is strongly quenched and the fluorescence lifetime is short, irrespective of the solvent used. The charge separation takes place efficiently with nearly unity quantum yields; the efficiency of charge separation was calculated to be 0.96 in toluene up to 0.99 in DMF. The lifetime of the charge-separated state BDP-SiPc$^{\bullet-}$-MSBDP$^{\bullet+}$ was determined to be 1.7 ns

(toluene and xylene), 0.34 ns (chloroform) 0.10 ns (THF) and 30 ps (DMF). It is worth noting that these values are very similar to the lifetimes of the charge-separated state of the SiPc(MSBDP)$_2$ triad dissolved in the corresponding solvents.

Delayed fluorescence

From table 5.6 it is remarkable that the energetic difference between the charge-separated state SiPc$^{\bullet-}$-MSBDP$^{\bullet+}$ and the excited state SiPc* is only 0.05 eV in toluene and xylene. At this point, it is worth noting that the thermal energy at ambient room temperature is 0.025 eV. In addition, in toluene and xylene a comparably long decay time of around 3 ns was resolved in the DAF spectra of SiPc(MSBDP)$_2$ and BDP-SiPc-MSBDP. The 3 ns-lifetime could be assigned to thermally activated delayed fluorescence from the charge-separated state. The depicted process is shown in a simplified Jablonski-diagram in figure 5.11.

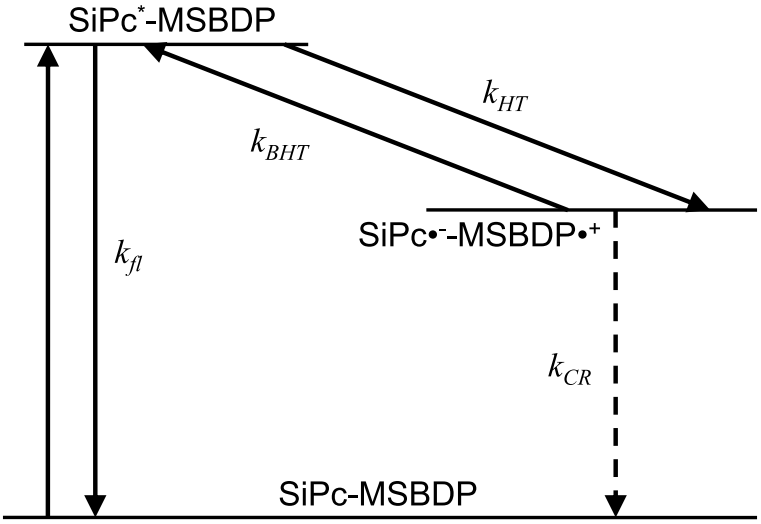

Figure 5.11: Delayed fluorescence in SiPc(MSBDP)$_2$ and BDP-SiPc-MSBDP dissolved in xylene and toluene. Note that two hole transfer channels k_{HT} exist for SiPc(MSBDP)$_2$, as two identical MSBDPs can act as a donor.

Delayed fluorescence from the charge-separated state is only possible for a small energy gap between the charge-separated state and the first excited state of SiPc. This is expressed by a small driving force ΔG_0. Equation 3.10 describes the back electron transfer from the charge-separated state to the first excited singlet state of a chromophore. For hole transfer, the same equation can be applied if the indices ET and BET are changed to HT and BHT, and accordingly

$$\frac{k_{BHT}}{k_{HT}} = \exp\left\{-\frac{\Delta G_0}{k_B T}\right\} \tag{5.1}$$

The maximum value of ΔG_0 can be estimated for which back-hole transfer becomes thermodynamically favourable. The maximum value ΔG_0 at which delayed fluorescence is feasible, is arbitrarily set to 4×0.025 eV=0.10 eV. Since the driving force is a function of the dielectric constant of the solvent,

ΔG_0=$\Delta G_0(\varepsilon_S)$, the dielectric constant ε_S of the solvent can be tuned in order to control delayed fluorescence. With equation 5.1 it follows that the threshold for delayed fluorescence lies at ε_S=2.8, below this value delayed fluorescence is thermodynamically favourable. In toluene and xylene the dielectric constant has a value of ε_S=2.4 and ΔG_0 is 0.05 eV. Due to the small gap between first excited singlet state and charge-separated state, the charge-separated state SiPc$^{\bullet-}$-MSBDP$^{\bullet+}$ is activated thermally back to the first excited singlet state ^{1}SiPc*. The energy will fluctuate between these two states, until the system either fluoresces or returns to the ground state *via* charge recombination. This matches with the bi-exponential fluorescence decay of BDP-SiPc-MSBDP and SiPc(MSBDP)$_2$ when dissolved in toluene and xylene. Furthermore, it explains the somewhat higher SiPc-part fluorescence quantum yields of SiPc(MSBDP)$_2$ and BDP-SiPc-MSBDP dissolved in xylene and toluene. On the other hand, the energetic gap between the SiPc-singlet state and the charge-separated state is 0.25 eV in chloroform (ε_S=4.8), which is too large to overcome thermally. Thus, delayed fluorescence is inhibited in chloroform and solvents with higher polarities such as THF and DMF. This correlates well with the experimental findings.

The kinetic equations for the three-level system in figure 5.11 can be solved explicitly as shown in [75, 150, 152, 153]. Given the normalized fluorescence intensity $I(t)$ by

$$I(t) = a_1 \exp\{-k_1 t\} + (1-a_1)\exp\{-k_2 t\} \tag{5.2}$$

The amplitudes a_1, $1-a_1$ and rates k_i in this equation are obtained experimentally from the DAF spectra. Furthermore, one can express the experimentally determined rates k_i by the following set of equations:

$$\begin{aligned} k_1 &= \frac{(X+Y)}{2} + \frac{1}{2}\sqrt{(X-Y)^2 + 4k_{HT}k_{BHT}} \\ k_2 &= \frac{(X+Y)}{2} - \frac{1}{2}\sqrt{(X-Y)^2 + 4k_{HT}k_{BHT}} \\ a_1 &= \frac{X-k_2}{k_1-k_2} \\ X &= k_{fl} + k_{HT} \\ Y &= k_{CR} + k_{BHT} \end{aligned} \tag{5.3}$$

in these equations k_{HT} is the rate of the hole transfer, k_{BHT} the rate of the back hole transfer, k_{CR} the rate of charge recombination, $1/k_{fl}$ the fluorescence lifetime of SiPc in absence of MSBDP. The calculated rates k_{HT} and k_{BHT} are summarized in table 5.7.

The hole-transfer-to-back-hole-transfer ratio k_{HT}:k_{BHT} can be calculated with the values in table 5.7. This yields 1:7.3 and 1:7.5 for BDP-SiPc-MSBDP and SiPc(MSBDP)$_2$, respectively. On the other hand, using Boltzmann statistics (equation 5.1) with a driving force ΔG_0=0.05 eV, a ratio of 1:7.4 is obtained. The latter is in accord with the values obtained in the experiment.

Table 5.7: Rates of the three-level system in figure 5.11 for BDP-SiPc-MSBDP and SiPc(MSBDP)$_2$ dissolved in xylene.

Rate	$k \times 10^8$ [s^{-1}]	
	SiPc(MSBDP)$_2$	**BDP-SiPc-MSBDP**
k_{HT}	510	330
k_{BHT}	68	45
k_{CR}	6.7	5.9
$k_{fl,SiPc}$	2.0	2.0
k_1	590	390
k_2	3.6	3.1

5.1.4 Population of the triplet state

In non-polar solvents pronounced SiPc ground state depletion of the three triads can be observed at 15 ns delay after excitation, which is addressed to the population of the first excited triplet state ^{3}SiPc*. For phthalocyanines it is well-known that ISC $S_1 \rightarrow T_1$ occurs with quite high probability. In contrast, a feature of common Bodipys is the negligible probability of the T_1 state population *via* ISC. This is illustrated by the vanishing ground state bleaching signals of both BDP and MSBDP moieties after some ns. The triplet state energy of SiPc is about 1.26 eV [85, 86, 87, 88]. The energy of the charge-separated state depends on the polarity of the solvent and the electron donor-acceptor pair and varies from 2.18 eV (BDP$^{\bullet+}$-SiPc$^{\bullet-}$, toluene) to 1.39 eV (SiPc$^{\bullet-}$-MSBDP$^{\bullet+}$, DMF), *cf.* table 5.6. A transition from the charge-separated state to the triplet state ^{3}SiPc* is therefore energetically feasible for all combinations of solvents and molecules. However, the rapid charge recombination in polar solvents precludes an efficient transition from the charge-separated state to the T_1 state, which typically occurs on a time scale of a few nanoseconds [86]. Therefore, the values of the quantum yield of first excited triplet state population are negligibly small for all triads dissolved in THF and DMF, whereas in toluene and xylene the Φ_T quantum yields are in the same order of magnitude of Φ_{ISC}=0.32 of monomeric SiPc. In chloroform the situation is slightly different. The fluorescence lifetime and the lifetime of the charge-separated state of SiPc(BDP)$_2$ are in the order of 5 ns, which explains the comparably high ISC quantum yield of 0.32. It is emphasized that the population of the first excited triplet state occurs *via* two pathways: ISC from the first excited singlet state of the SiPc moiety and from the CS state. On the other hand, for BDP-SiPc-MSBDP and SiPc(MSBDP)$_2$ charge recombination takes place within 400 ps, thereby decreasing Φ_T. In fact, one can carry out some estimations in order to calculate the quantum yield of first excited triplet state formation:

$$\Phi_T(\text{chloroform}) = \Phi_T(\text{toluene}) \frac{\tau_{CR}(\text{chloroform})}{\tau_{CR}(\text{toluene})} \tag{5.4}$$

For the BDP-SiPc-MSBDP and SiPc(MSBDP)$_2$ triads dissolved in chloroform the calculated quantum yields are 0.076 and 0.077 which correlate well with the experimentally determined values of 0.070 and 0.075.

5.1.5 Conclusions

The BDP-SiPc-MSBDP triad turned out to be an excellent light-harvester with broad UV/Vis absorption ranging from 300 to 700 nm. The photophysical properties of BDP-SiPc-MSBDP are strongly affected by two different types of interactions between the Bodipy and Pc moieties; namely EET and ET. After excitation of any part of the triad, the energy is funnelled to the SiPc core. Arrived here, electron transfer from MSBDP to SiPc occurs with almost unity quantum yield. The charge-separated state is stabilized in non-polar toluene and xylene, its lifetime is 1.7 ns in both solvents. The lifetime of the CS state decreases as the polarity of the solvent increases and its value amounts to 400 ps in chloroform, 100 ps in THF and 30 ps in DMF. The energy gap between charge-separated state and first excited singlet state of the SiPc moiety is very small in toluene and xylene facilitating the back hole transfer process. The latter results in the appearance of thermally activated delayed fluorescence. In polar solvents the charge-separated state undergoes deactivation directly to the ground state, whereas in non-polar solvents charge recombination leads to the population of the SiPc first excited triplet state. The photophysical processes involved are summarized in a Jablonski-diagram, figure 5.12. As was shown, the characteristic transfer processes of $SiPc(MSBDP)_2$ and $SiPc(BDP)_2$, namely ET and EET, have been merged into one molecule. BDP-SiPc-MSBDP is superior to the aforementioned triads and the conjugate is therefore a potential candidate for use in artificial photosynthetic systems.

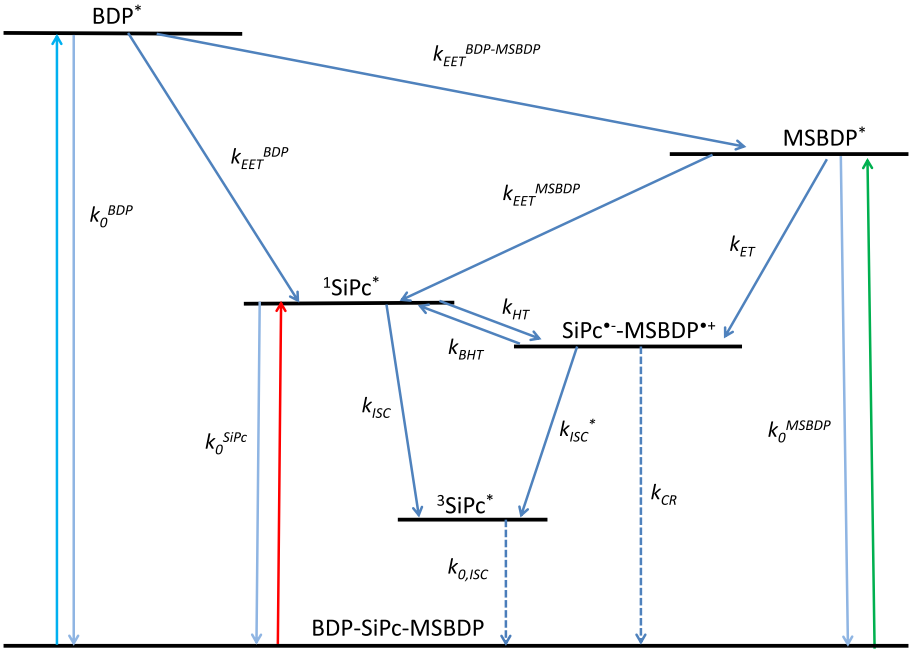

(a) Toluene, xylene, chloroform

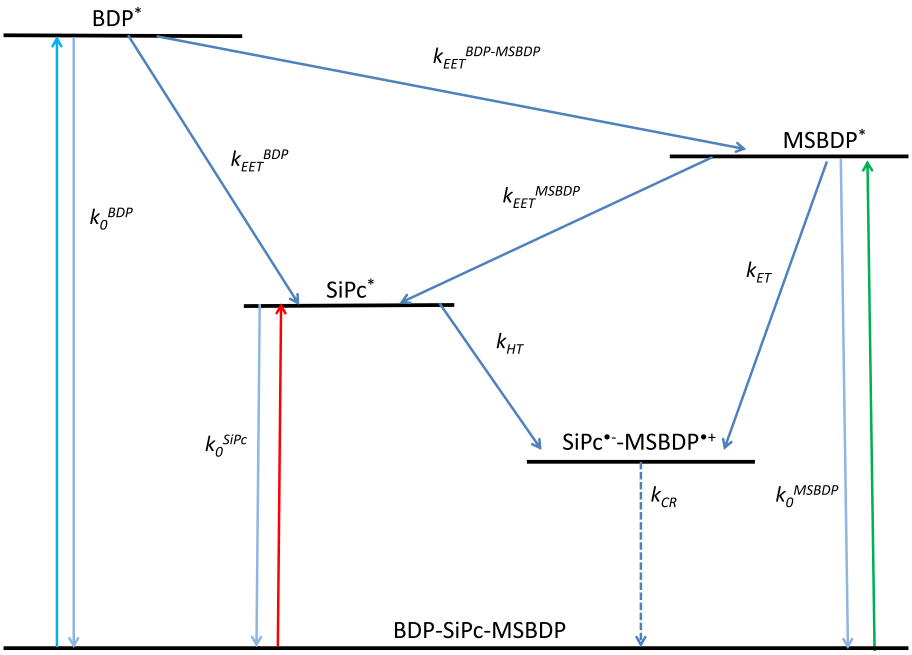

(b) THF, DMF

Figure 5.12: Jablonski diagram of BDP-SiPc-MSBDP dissolved in toluene, xylene, chloroform (a) and THF, DMF (b). Note that the rate k_{BHT} is negligible in chloroform.

5.2 The SiPc(BDP-MSBDP)$_2$ pentad

The SiPc(MSBDP)$_2$ triad was extended by two BDP units to compose a pentad. The molecular structure of the resulting conjugate is shown in figure 5.13. In the following, it will be denoted either as pentad or as SiPc(BDP-MSBDP)$_2$. The pentad has been designed to take advantage of the characteristics of its constituent parts. With respect to the triads presented in the previous section, it is expected that the pentad has much higher extinction in the regions where BDP and MSBDP absorb owing to the doubled BDP and MSBDP moieties.

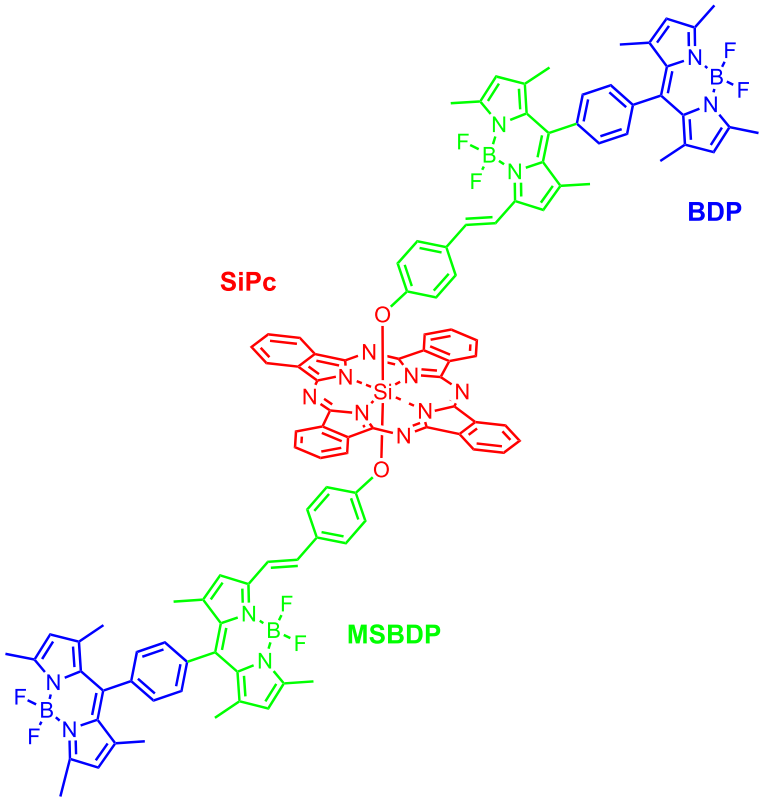

Figure 5.13: Structural formula of the pentad SiPc(BDP-MSBDP)$_2$.

As was illustrated for the Bodipy-SiPc triads, the absorbed energy is funnelled from the peripheral Bodipys to the central SiPc reaction centre. Arrived here, electron transfer now occurs from the Bodipy to the SiPc core. Obviously, for the pentad it is expected that the absorbed energy is directed to the SiPc-core, too. Here a charge-separated state could be generated, possibly *via* multi-step electron transfer from MSBDP to SiPc and subsequently from BDP to MSBDP, thereby mimicking the sequential charge transfer processes that occur in natural photosynthesis. The increase in distance between the charge-separated species should result in slower rates of charge recombination. A similar decrease in charge recombination has been reported by Martín-Gomis et al. for a SiPc-based pentad [87]. Due to the improved light-harvesting function and longer charge-separated state the pentad is expected to be superior to the triads discussed above. Interestingly, as will be shown, this is not the case.

Before studying the pentad, it is necessary to unravel the photophysical behaviour of its constituent parts. The pentad consists of a SiPc that is linked at both axial positions to a BDP-MSBDP dyad. The latter is composed of two Bodipy units, see figure 5.14. It is noted that the Bodipys in figure 5.14 differ slightly from BDP and MSBDP presented above (*cf.* figure 5.1), nevertheless, in the following they will also be denoted as BDP and MSBDP.

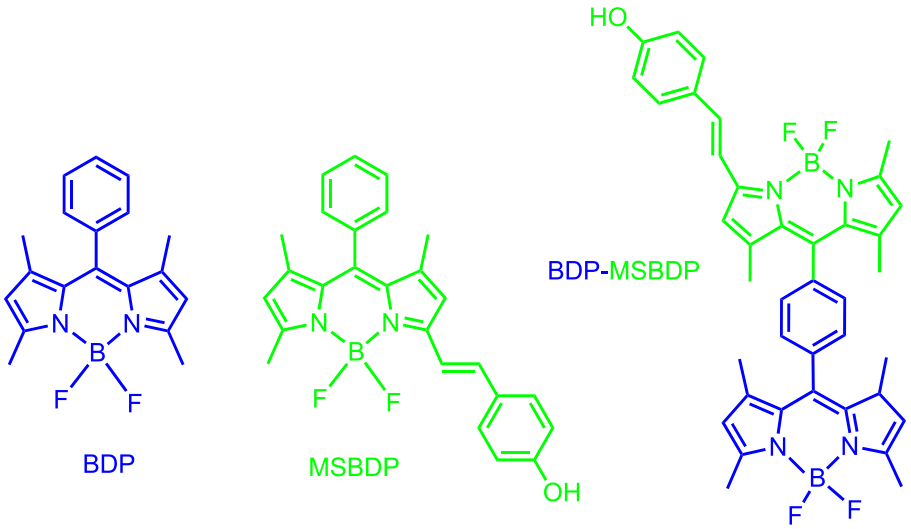

Figure 5.14: Structural formulae of BDP, MSBDP and the dyad BDP-MSBDP

In the next section, a detailed analysis of the photophysical parameters of the BDP-MSBDP dyad is presented. Subsequently, the photophysical behaviour of the pentad is outlined. As is shown, the presence of SiPc in the SiPc(BDP-MSBDP)$_2$ pentad dramatically alters the photophysical behaviour of the BDP-MSBDP dyad.

5.2.1 Photophysical parameters of the BDP-MSBDP dyad as constituent part of the pentad

The photophysical experiments have been carried out in four solvents with different polarity: toluene, chloroform, dichloromethane (DCM) and acetonitrile.

Steady-state characterization of the BDP-MSBDP dyad

In figure 5.15 the UV/Vis spectra of the dyad as well as the reference compounds dissolved in acetonitrile are shown. The corresponding spectra in toluene are shown in figure 7a (appendix).

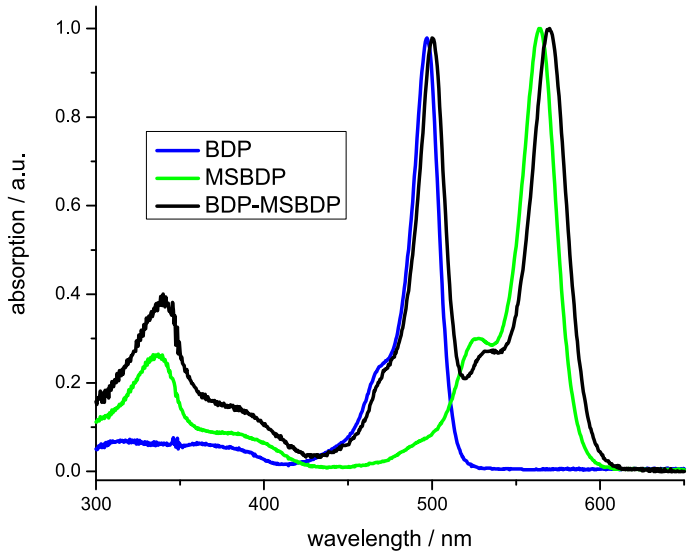

Figure 5.15: UV/Vis spectra of BDP, MSBDP and the BDP-MSBDP dyad dissolved in acetonitrile.

The absorption spectrum of the dyad is essentially the superposition of the absorption bands of the corresponding monomeric components and has three pronounced peaks: one with a maximum at 570 nm that belongs to MSBDP, another one at 500 nm that belongs to BDP, and the third band, located in the blue spectral region at around 350 nm, is a superposition of the S_2 and S_3 absorption bands of BDP and MSBDP [154]. The absorption maxima of highest intensity of the dyad as well as the reference compounds BDP and MSBDP in different solvents are given in table 5.8. Due to the small spectral shifts of the absorption bands of the dyad compared with those of the corresponding reference compounds, the BDP- and MSBDP-part of the dyad in the ground state are considered electronically decoupled.

Due to the fact that the absorption bands of the BDP- and MSBDP-part of the dyad are well separated, both the steady-state fluorescence spectra upon selective excitation of the BDP and MSBDP moieties were recorded, see figure 5.16. The calculated fluorescence quantum yields are summarized in table 5.9.

Upon excitation at 532 nm, where only the MSBDP moiety absorbs light, the fluorescence of the dyad shows a similar structure to that of the reference MSBDP (figure 5.16). The fluorescence intensity of the dyad decreases as the dielectric constant of the solvent increases: in toluene the fluorescence of the dyad is slightly quenched with Φ_{fl}=0.70, in DCM the value of Φ_{fl} is reduced to 0.35, whereas in acetonitrile

Table 5.8: Absorption and fluorescence maxima of highest intensity of BDP, MSBDP and the dyad in different solvents.

Compound	Solvent	λ_{abs} [nm]	λ_{fl} [nm]	
			BDP-part excitation	MSBDP-part excitation
BDP	toluene	503.5	512	-
	chloroform	503	511	-
	DCM	501	510	-
	acetonitrile	497	505	-
MSBDP	toluene	571.5	-	581
	chloroform	571	-	585
	DCM	566.5	-	578
	acetonitrile	564.5	-	580
Dyad	toluene	506[a] 578[b]	520[a] 588[b]	588[b]
	chloroform	506[a] 578[b]	520[a] 594[b]	594[b]
	DCM	505[a] 573.5[b]	514[a] 586[b]	586[b]
	acetonitrile	500[a] 570[b]	506[a] 585[b]	587[b]

[a] BDP-part
[b] MSBDP-part

the fluorescence quantum yield is only 0.023. These fluorescence quantum yields are lower than the fluorescence quantum yields of the reference MSBDP, whose values are in the order of 0.80. This means that an additional deactivation process depletes the first excited singlet state of the MSBDP moiety.

Upon excitation of the dyad at 470 nm, which corresponds to BDP-part absorption, the fluorescence of the BDP-part of the dyad is strongly reduced compared to the reference compound independent of the solvent. At the same time, a peak of MSBDP-part fluorescence with a maximum at 588 nm appears. The latter effect is an indicator of excitation energy transfer EET from the initially excited energy donor (BDP) to the energy acceptor (MSBDP) in its ground state. The fluorescence quantum yield of BDP emission does not exceed 0.007 (see table 5.8). In polar acetonitrile, the fluorescence quantum yield of MSBDP emission following BDP-part excitation amounts to 0.019, which is significantly lower than the corresponding value of the reference MSBDP, Φ_{fl}(MSBDP)=0.74. In contrast, in non-polar toluene a strong peak of the MSBDP-part fluorescence with a fluorescence quantum yield of 0.66 was detected. The intensity of MSBDP-part emission in DCM lies in between with a quantum yield of 0.22. It should be mentioned that the quantum yield of MSBDP-part fluorescence following BDP-part excitation is

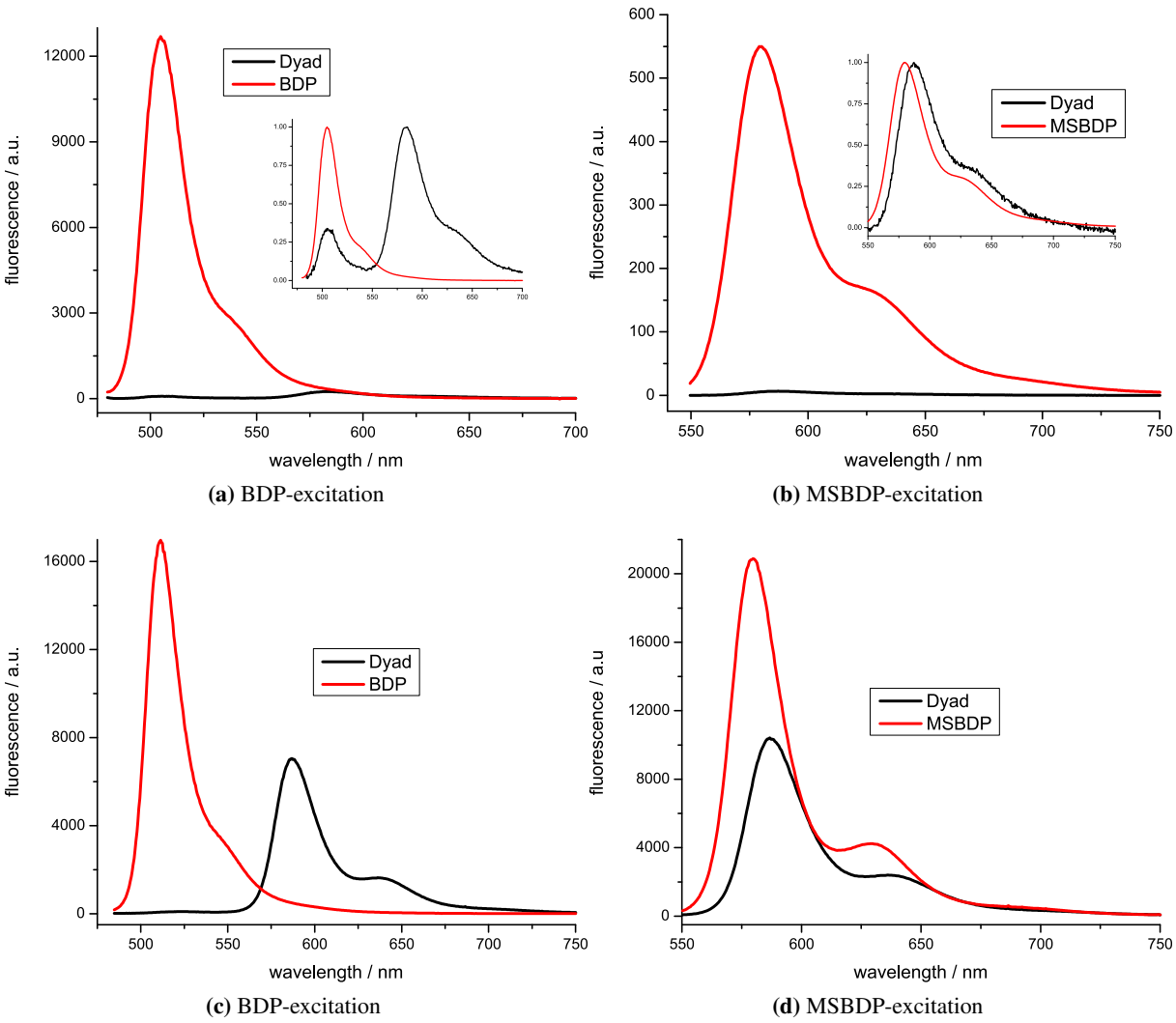

(a) BDP-excitation

(b) MSBDP-excitation

(c) BDP-excitation

(d) MSBDP-excitation

Figure 5.16: Steady-state fluorescence spectra of the dyad dissolved in acetonitrile (a,b) and toluene (c,d). The normalized spectra are shown in the insets.

lower compared to that measured upon direct excitation of the MSBDP moiety and this effect is solvent independent.

In figure 7b (appendix) the fluorescence excitation (registration at 588 nm) and the absorption spectra of the BDP-MSBDP dyad dissolved in toluene are shown. The excitation spectrum of the MSBDP-part fluorescence matches the absorption spectrum of the dyad well. The band of the excitation spectrum around 500 nm has an intensity of 94% compared to the BDP-absorption band, which underlines the efficient energy transfer from BDP to MSBDP. Similar results were obtained for BDP-MSBDP dissolved in acetonitrile.

From the steady-state experiments it is inferred that efficient EET is the dominant process for the

Table 5.9: Fluorescence quantum yields of BDP, MSBDP and the dyad in different solvents.

Compound	Solvent	Φ_{fl}	
		BDP-part excitation	**MSBDP-part excitation**
BDP	toluene	0.57	-
	chloroform	0.58	-
	DCM	0.49	-
	acetonitrile	0.46	-
MSBDP	toluene	-	0.78
	chloroform	-	0.85
	DCM	-	0.88
	acetonitrile	-	0.74
dyad	toluene	0.007[a] 0.66[b]	0.70[b]
	chloroform	0.004[a] 0.63[b]	0.78[b]
	DCM	0.002[a] 0.22[b]	0.35[b]
	acetonitrile	<0.001[a] 0.019[b]	0.023[b]

[a] BDP-part emission
[b] MSBDP-part emission

deactivation of the BDP S_1-state. A solvent dependent quenching of the MSBDP-part fluorescence implies that charge transfer is involved in the deactivation of the MSBDP first excited singlet state, too. Time-resolved measurements have been performed in order to, first, corroborate this assumption and, second, to reveal the nature of this charge separation.

Excited-state dynamics of the BDP-MSBDP dyad

The fluorescence decay of the reference compounds BDP and MSBDP was found to be mono-exponential with lifetimes of around 3.2 ns and 3.7 ns, respectively (see table 5.10). The fluorescence decay of the dyad was measured upon selective excitation of the BDP and MSBDP moieties. The DAF spectra of the dyad dissolved in toluene and acetonitrile upon BDP-part excitation are shown in figure 5.17, while the DAF spectra upon MSBDP-part excitation can be found in figure 7b (appendix).

Table 5.10: Fluorescence lifetimes of BDP, MSBDP and the BDP-MSBDP dyad in different solvents.

Compound	**Solvent**	$\tau_{fl} \pm 0.02$ **[ns]**	
		BDP-part excitation	**MBDSP-part excitation**
BDP	toluene	3.11	-
	chloroform	3.45	-
	DCM	3.32	-
	acetonitrile	3.03	-
MSBDP	toluene	-	3.46
	chloroform	-	3.75
	DCM	-	3.72
	acetonitrile	-	3.91
Dyad	toluene	<0.010[a] 3.86[b]	3.89[b]
	chloroform	<0.010[a] 3.76[b]	3.76[b]
	DCM	<0.010[a] 2.42[b]	2.33[b]
	acetonitrile	<0.010[a] 0.088[b]	0.092[b]

[a] BDP-emission
[b] MSBDP-emission

Upon excitation of the dyad at 400 nm (BDP-part excitation) in both toluene and acetonitrile only one DAF spectrum was resolved that resembled the steady-state fluorescence spectrum of monomeric MSBDP. No trace of BDP-part fluorescence was resolved; apparently, the quenching of the first excited singlet state of the BDP moiety is so effective that it was not possible to detect a reliable signal within the time resolution of the experimental setup.

In toluene the decay time of the DAF spectrum was estimated to be 3.76 $\pm$ 0.02 ns, which is similar to the lifetime of the reference MSBDP. In acetonitrile a decay time of 88 $\pm$ 10 ps is observed, which clearly indicates that an additional efficient pathway exists for the deactivation of the first excited singlet

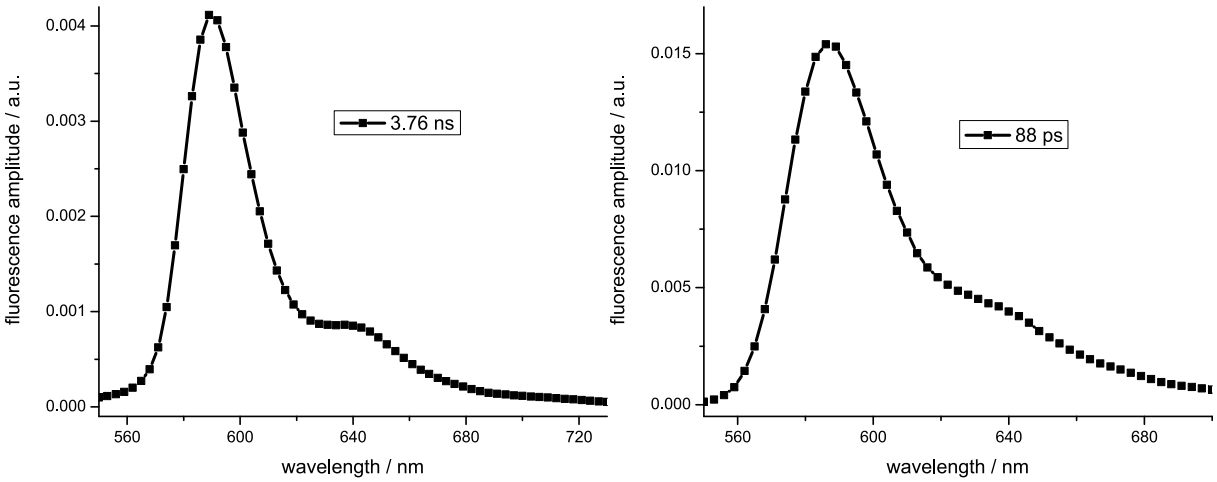

(a) Toluene **(b)** Acetonitrile

Figure 5.17: DAF spectra of the dyad dissolved in toluene and acetonitrile upon excitation of BDP at 400 nm.

state of the MSBDP moiety. The fast decay time correlates with the small fluorescence quantum yield found for the dyad dissolved in polar environment. In DCM the lifetime of the MSBDP moiety of 2.42 ns is also reduced compared to that of the reference MSBDP (3.72 ns). This is accompanied by the lower MSBDP-part fluorescence quantum yield. However, the decrease in fluorescence lifetime and quantum yield is not that strong as observed in acetonitrile.

Similar results have been obtained upon direct excitation of the MSBDP-part at 532 nm, see table 5.10.

In order to obtain information about the nature of the assumed charge-separated state, the transient absorption spectra of all compounds have been recorded. The decay of the ground state bleaching of all the reference compounds was found to be mono-exponential with characteristic times similar to their fluorescence decay times. The intersystem crossing $S_1 \rightarrow T_1$ quantum yields were estimated to be zero in all solvents for both BDP and MSBDP.

The transient absorption spectra of the dyad dissolved in acetonitrile and in toluene upon excitation of MSBDP are shown in figure 5.18.

In both solvents ground state bleaching of the MSBDP-part and broad induced absorption around 870 nm are seen. The latter is also observed for the monomeric MSBDP and can be ascribed to S_n induced absorption of the MSBDP moiety. Furthermore, a negative ΔOD signal with a minimum at 508 nm was observed, indicating depletion of the ground state absorption of the BDP moiety. At this point it is emphasized that EET from MSBDP to BDP is energetically unfavourable. In addition, a new induced absorption band at around 518 nm appears. Control experiments verified that none of the reference compounds BDP and MSBDP exhibits these features alone.

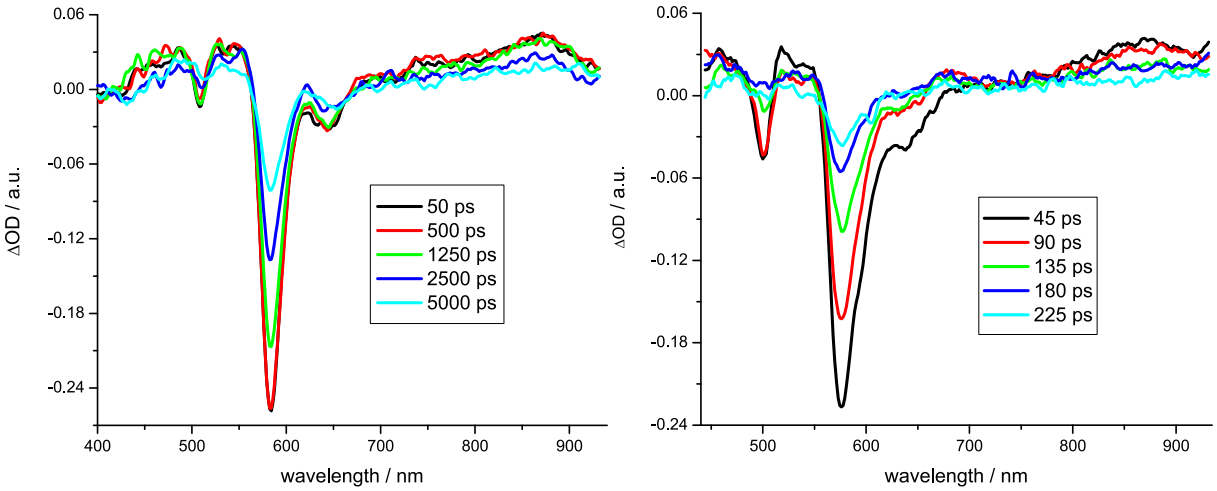

(a) Toluene **(b)** Acetonitrile

Figure 5.18: Transient absorption spectra of BDP-MSBDP dyad dissolved in toluene (a) and in acetonitrile (b) at different delay times after MSBDP-part excitation.

The TA spectra of the dyad upon BDP-part excitation are shown in figure 5.19. The same features as described above for the dyad upon MSBDP-part excitation have been observed: transient bleaching signals at 500 nm and 570 nm that belong to BDP and MSBDP parts and induced absorption bands at 518 nm and 870 nm.

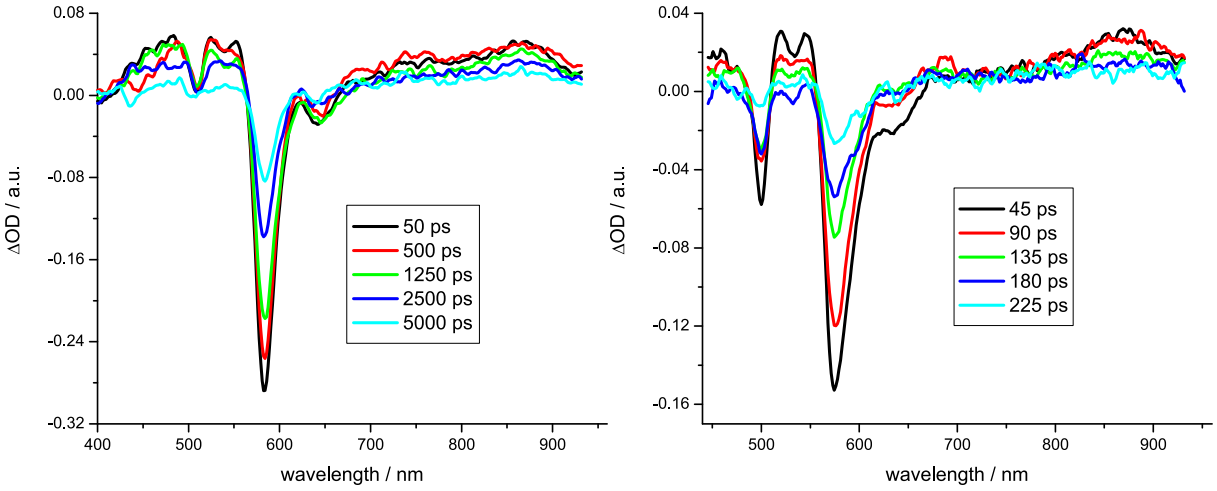

(a) Toluene **(b)** Acetonitrile

Figure 5.19: Transient absorption spectra of BDP-MSBDP dyad dissolved in toluene (a) and in acetonitrile (b) upon excitation of the BDP moiety at different delay times.

The characteristic ground state recovery times of the BDP and MSBDP moieties are summarized in

Table 5.11: Ground state recovery times τ_{rec} of the BDP and MSBDP moieties of the BDP-MSBDP dyad dissolved in toluene and acetonitrile.

Solvent, moiety	τ_{rec} [ns]
toluene, BDP	3.8 ± 0.2
toluene, MSBDP	3.8 ± 0.2
acetonitrile, BDP	0.11 ± 0.02
acetonitrile, MSBDP	0.11 ± 0.02

table 5.11. In acetonitrile the decay time of the ground state bleaching of the BDP moiety was found to be 110 ± 20 ps independent of the excitation wavelength. This time is much longer than the BDP-part fluorescence lifetime, which is faster than 10 ps (time resolution of the TCSPC setup). The recovery of the MSBDP-part ground state occurs with the same characteristic time of 110 ± 20 ps. It is worth to mention that the fluorescence lifetime of the MSBDP-part is somewhat shorter (∼90 ps).

In toluene the MSBDP-part ground state bleaching signal decays with a lifetime of 3.7 ± 0.2 ns after either BDP- or MSBDP-part excitation. This correlates well with the measured fluorescence lifetime of 3.76 ns. The recovery of the ground state population of the BDP moiety takes place with roughly the same lifetime: 4.0 ± 0.2 ns after direct excitation of the BDP moiety and 3.8 ± 0.2 ns after MSBDP-part excitation.

Discussion of the dyad's photo-induced processes

For clarity the discussion is focussed on the dyad dissolved in toluene and acetonitrile. The absorption and fluorescence spectra of the dyad are well described by a superposition of the spectra of the reference compounds in polar acetonitrile as well as in non-polar toluene as can be seen from figures 5.15 and 5.16. These observations indicate that despite close proximity in the dyad, there is no strong coupling between electronic systems of the BDP and MSBDP moieties neither in the ground state nor in the first excited state. To explain the results obtained, two different types of interaction between the BDP and MSBDP moieties were taken into consideration, namely EET and ET.

As can be seen from the excitation spectrum of the BDP-MSBDP dyad and by comparison of the fluorescence quantum yields, EET is mainly responsible for efficient depopulation of the BDP S_1-state. As a result, the decay time of the BDP-part fluorescence and the fluorescence rise time of the MSBDP-part were faster than the time resolution of the TCSPC setup, i.e. k_{EET}>10^{11} s^{-1}. Comparing the fluorescence quantum yield of the MSBDP moiety upon direct excitation with that upon BDP-part excitation, the efficiency of EET was calculated to be around 0.83 in acetonitrile and 0.94 in toluene. One would expect the EET to occur with a quantum yield of unity, as the rate is much greater than the fluorescence lifetime of the monomeric reference BDP, the rate of the latter being k_{fl}=3.3×10^8 s^{-1}. Due to the fact that the value of Φ_{EET} is less than one, an additional process that is responsible for the deactivation of the BDP S_1 state is expected to be involved.

In the transient absorption spectra, bleaching of the BDP ground state absorption after MSBDP-part

excitation indicates that energy is stored in an intermediate state. This state can be identified as a charge-separated state. In order to prove the possibility of ET, the free energy of charge separation was calculated using the Rehm-Weller approach, equation 3.12. It is noted that the calculated values are based on the electrochemical properties of BDP-OH and MSBDP-OH, see table 2. This approximation is valid when the redox data are similar. Indeed, in [102] a Bodipy similar in structure to BDP was reported which has basically the same redox properties as BDP. R, r_{BDP} and r_{MSBDP} are 6 Å, 3 Å and 4 Å, respectively [92]. The values of ΔG_0 are summarized in table 5.12.

Table 5.12: Driving force ΔG_0 for possible electron transfer reactions.

Transition	**$\Delta G_0 \pm 0.05$ [eV], toluene**	**$\Delta G_0 \pm 0.05$ [eV], acetonitrile**
BDP*-MSBDP$\rightarrow$BDP$^{\bullet-}$-MSBDP$^{\bullet+}$	0.28	-0.44
BDP-MSBDP* $\rightarrow$BDP$^{\bullet-}$-MSBDP$^{\bullet+}$	0.58	-0.14
MSBDP*-BDP$\rightarrow$MSBDP$^{\bullet-}$-BDP$^{\bullet+}$	0.59	-0.13
MSBDP-BDP* $\rightarrow$MSBDP$^{\bullet-}$-BDP$^{\bullet+}$	0.29	-0.43

As can be seen from table 5.12 only positive ΔG_0 values were calculated when the dyad is dissolved in toluene (this means that ET is not a thermodynamically favourable process), whereas for acetonitrile the values of ΔG_0 are negative. However, picosecond pump-probe experiments have clearly shown that ET occurs for the dyad dissolved in toluene. At this point it should be mentioned that for non-polar solvents, the influence of the radii of ions and the centre-to-centre distance of the electron donor and acceptor on the calculated value of ΔG_0 increases dramatically due to the small values of the dielectric constant. Since determination of R, r_D and r_A is quite error-prone, the values determined by equation 3.12 are just a very rough estimation. In acetonitrile negative values of ΔG_0 have been calculated for both the generation of BDP$^{\bullet-}$-MSBDP$^{\bullet+}$ and BDP$^{\bullet+}$-MSBDP$^{\bullet-}$ charge-separated states which can be ascribed to the ampholytic character of Bodipys and the similar redox properties of BDP and MSBDP [100]. Hence, from table 5.12 it is not clear, whether BDP$^{\bullet-}$-MSBDP$^{\bullet+}$ or BDP$^{\bullet+}$-MSBDP$^{\bullet-}$ is generated. Nevertheless, it was possible to reveal the nature of the charge-separated state by comparing transient absorption spectra with those found in literature. At this point, it is necessary to emphasize that both after BDP- and MSBDP-part excitation transient absorption at 518 nm was observed. In chapter 5.1 we became acquainted with Bodipy-SiPc triads, where two similar BDP or MSBDP molecules were covalently linked to the central silicon atom of a Pc moiety (SiPc). It was shown for both systems that after photo-excitation efficient charge separation occurs and in both triads the Bodipy moieties play the role of an electron donor and the SiPc moiety is reduced to SiPc$^{\bullet-}$.

It is worthwhile comparing the TA spectra of SiPc(BDP)$_2$ and SiPc(MSBDP)$_2$ with that of the BDP-MSBDP dyad. From figure 5.20, it can be seen that besides BDP-MSBDP, SiPc(BDP)$_2$ exhibits an induced absorption band at around 518 nm, too, whereas triad SiPc(MSBDP)$_2$ lacks this transient signature. The BDP moiety of the SiPc(BDP)$_2$ triad was oxidized after photo-excitation. This suggests that the BDP moiety of the BDP-MSBDP dyad is the electron donor, since SiPc(BDP)$_2$ and BDP-MSBDP have a transient absorption band at approx. 518 nm in common. This is corroborated by the absorption band at 513 nm of an electrochemically oxidized solution of a similar Bodipy with a trimethoxybenzene linked at the *meso*-position as reported by Hattori, Fukuzumi et al. [102].

The charge transfer probability Φ_{CS} can be calculated by comparing the fluorescence quantum yields

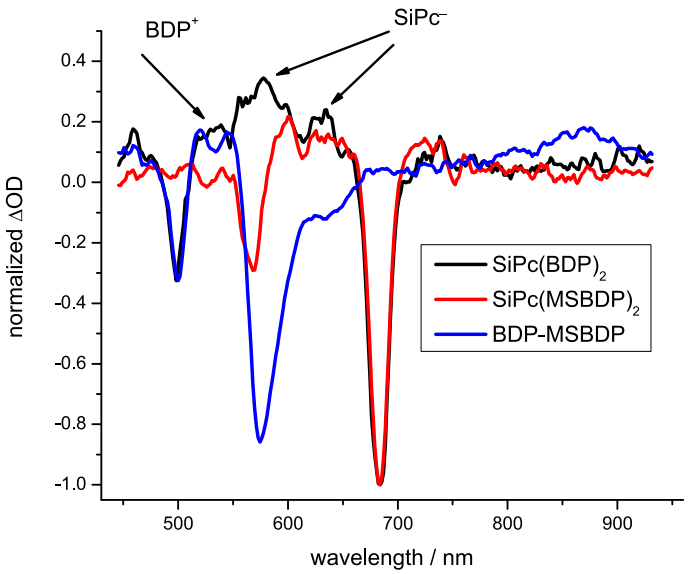

Figure 5.20: Transient absorption spectra of SiPc(BDP)$_2$, SiPc(MSBDP)$_2$ and BDP-MSBDP directly after excitation. Both triads are dissolved in DMF, the dyad is dissolved in acetonitrile.

of the monomeric MSBDP, Φ^0_{fl}, and the MSBDP-part of the dyad, Φ_{fl}, with $\Phi_{CS} = 1 - \Phi_{fl}/\Phi^0_{fl}$. The calculated quantum yield following BDP- and MSBDP-part excitation are listed in table 5.13.

Table 5.13: Quantum yields of charge separation of the dyad following selective excitation of BDP or MSBDP in different solvents.

Solvent	Φ_{CS}	
	BDP-part excitation	**MBDSP-part excitation**
toluene	0.15	0.10
chloroform	0.26	0.08
DCM	0.75	0.60
acetonitrile	0.98	0.97

Following MSBDP-part excitation in toluene hole transfer occurs from MSBDP to BDP and the calculated charge separation quantum yield is Φ_{CS}=0.10. Due to the rather low probability, the fluorescence behaviour is affected to a lesser extent. The calculated HT rate k_{HT}=3.0×10^7 s^{-1} is small compared to the fluorescence rate k_{fl}=2.7×10^8 s^{-1}.

Excitation of the BDP moiety results in a higher quantum yield, Φ_{CS}=0.15. Apparently, a direct electron transfer channel BDP*-MSBDP→BDP$^{\bullet+}$-MSBDP$^{\bullet-}$ exists next to the aforementioned energy transfer from the photo-excited BDP to MSBDP in its ground state. It was found by means of ps-TAS that independent of the excitation wavelength, the ground state recovery of the BDP moiety occurs with the lifetime of the S$_1$-state of the MSBDP-part. An explanation could be given, taking into account that

the charge recombination k_{CR} is fast compared to the MSBDP fluorescence lifetime. Hence, the kinetics of the BDP bleach follow the lifetime of the MSBDP excited state.

Increase of the polarity of the solvent leads to an increase of the charge separation probability. In DCM the corresponding quantum yield amounts to 0.60 (MSBDP-part excitation) and 0.75 (BDP-part excitation). In polar acetonitrile the formation of the charge-separated state is more favourable with quantum yields of almost unity, i.e. 0.97 and 0.98 for MSBDP- and BDP-part excitation, respectively. The hole transfer rate is calculated to be k_{HT}=1.1×10^{10} s^{-1}, which is 360 times faster than k_{HT} in toluene.

Conclusions

The UV/Vis absorption of the dyad covers a spectral region that ranges from 300 to 600 nm with high extinction. After absorption of light the energy is directed to the MSBDP moiety, subsequently the charge-separated BDP$^{\bullet+}$-MSBDP$^{\bullet-}$ state is generated. By comparing transient absorption spectra of reference triads SiPc(BDP)$_2$ and SiPc(MSBDP)$_2$ with those of the dyad, it was possible to reveal the nature of the charge-separated state. It was found that BDP acts as electron donor and MSBDP as electron acceptor. The probability of this charge transfer depends on the polarity of the solvent and the excitation wavelength. Upon BDP-part excitation the CS quantum yield values of 0.15, 0.26, 0.75 and 0.98 were calculated for solution in toluene, chloroform, DCM and acetonitrile, respectively, whereas the corresponding values of 0.10, 0.08, 0.60 and 0.97 were measured upon MSBDP-part excitation. In all solvents EET is the main transfer process that funnels the energy absorbed by the BDP-part to the MSBDP moiety. For this reason, the dyad can be used to effect an initial charge separation and as an energy antenna in the SiPc(BDP-MSBDP)$_2$ pentad. It can be potentially employed in other artificial photosynthetic systems, too. The electron and energy transfer processes that take place in the dyad are shown in figure 5.21; the energy levels of the dyad and transitions between them are presented in figure 5.22.

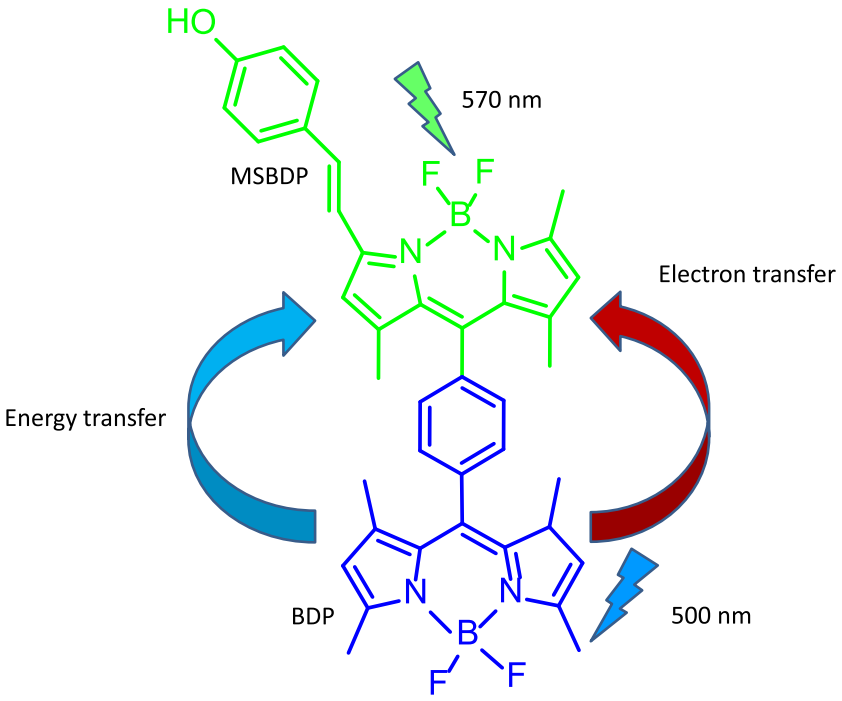

Figure 5.21: Transfer processes involved in the BDP-MSBDP dyad.

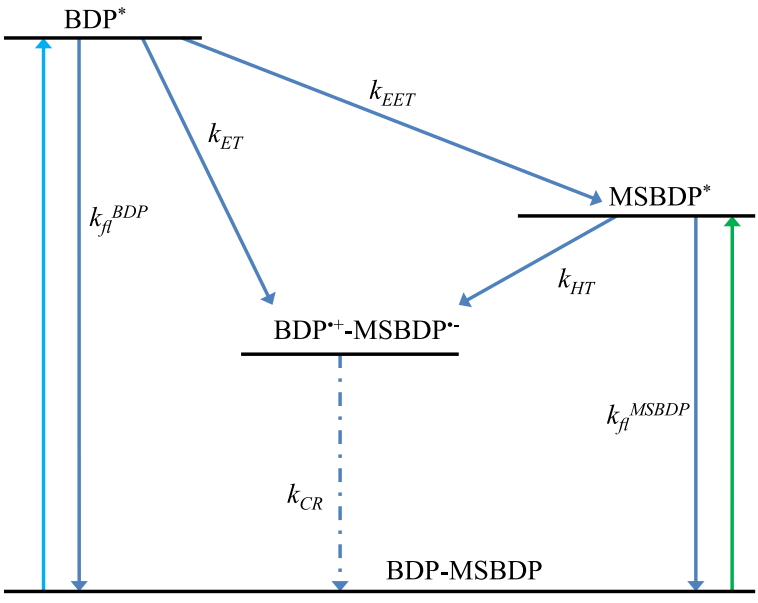

Figure 5.22: Scheme of energy levels ans transitions between them for the BDP-MSBDP dyad.

5.2.2 Steady-state characterization of the pentad

For the photophysical investigations, the pentad was dissolved in different solvents. However, the pentad's solubility was poor in dimethyl sulfoxide (DMSO), DMF, acetonitrile, THF, acetone, pyridine, ethanol, toluene, xylene and DCM. The only solvent that turned out to be suitable for all measurements was chloroform. For this reason, the pentad was dissolved in chloroform in all experiments performed.

Figure 5.23 shows the UV/Vis absorption spectra of the pentad and its monomeric references dissolved in chloroform.

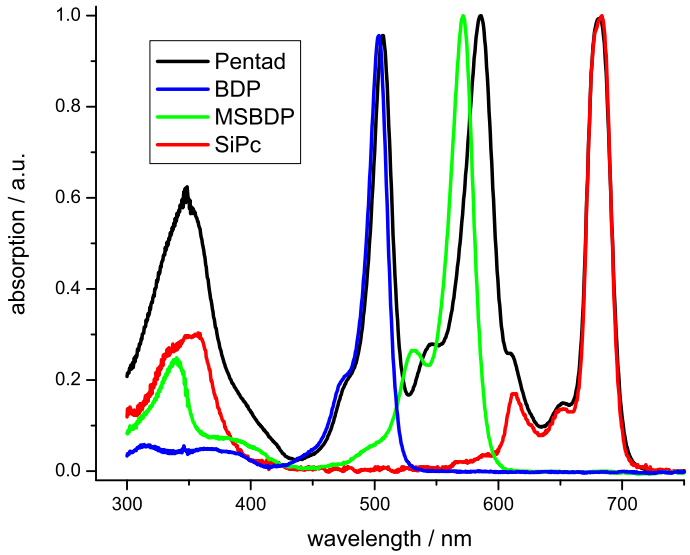

Figure 5.23: UV/Vis absorption spectra of the pentad and its monomeric references BDP, MSBDP and SiPc dissolved in chloroform.

The UV/Vis absorption spectrum of the pentad is well described by a superposition of the monomeric compounds BDP, MSBDP and SiPc. The absorption maxima of the BDP and MSBDP moieties of the pentad undergo bathochromic shifts of 120 cm^{-1} and 420 cm^{-1}, respectively. The absorption maximum of the SiPc moiety undergoes a hypsochromic shift of 22 cm^{-1}. The spectral positions of the corresponding absorption maxima of highest intensity are summarized in table 5.14. Due to the comparably small spectral shifts and due to the fact that the shapes of the absorption bands of the pentad are essentially the same as the monomeric references, one can consider the excited states of the molecular parts as electronically decoupled.

Since the absorption bands of BDP, MSBDP and SiPc are well-separated spectrally, steady-state fluorescence spectra of the pentad were recorded upon photo-selective excitation of its parts. The corresponding fluorescence spectra of the pentad and its references are shown in figure 5.24; and the emission peaks of highest intensity are summarized in table 5.14.

After selective excitation of the SiPc moiety of SiPc(BDP-MSBDP)$_2$ at 615 nm, strong quenching of fluorescence is observed compared to monomeric SiPc. In the normalized fluorescence spectrum (see inset in figure 5.24a) the fluorescence of the SiPc moiety of the pentad is 240 cm^{-1} shifted hypso-

Table 5.14: UV/Vis absorption maxima and fluorescence maxima of the pentad and its references dissolved in chloroform.

Compound	λ_{abs} [nm]	λ_{fl} [nm]		
		BDP-part excitation	**MSBDP-part excitation**	**SiPc-part excitation**
BDP	503	511	-	-
MSBDP	571	-	585	-
SiPc	683	-	-	687
Dyad	506[a] 578[b]	520[a] 594[b]	594[b]	-
SiPc(BDP)$_2$	501[a] 683[c]	N.d.[a] 687[c]	-	687[c]
SiPc(MSBDP)$_2$	568[b] 683[c]	-	584[b] 686[c]	686[c]
BDP-SiPc-MSBDP	501.5[a] 569[b] 682.5[c]	509[a] N.d.[b] 687[c]	582[b] 687[c]	687[c]
Pentad	506[a] 585[b] 682[c]	519[a] 594[b] 688[c,d]	594[b] 688[c,d]	688[c,d]

[a] BDP-part
[b] MSBDP-part
[c] SiPc-part
[d] from DAF spectra (*vide infra*)

chromically compared to the reference compound SiPc. In addition, the fluorescence maximum lies at 676 nm, which is even at smaller wavelength than the absorption maximum of 682 nm. This is probably caused by a small SiPc impurity. Beside the 676 nm peak of the impurity, DAF spectra reveal a clear fluorescence maximum at 688 nm (*vide infra*), which is associated with the SiPc-part fluorescence of the pentad. The fluorescence quantum yields could be corrected accordingly and the impurity corrected fluorescence quantum yield was calculated to be smaller than 0.001.

Excitation of the MSBDP-part of the pentad results in strong quenching of MSBDP fluorescence (figure 5.24b). Furthermore, weak SiPc-part fluorescence is observed, which is indicative of EET from the photo-excited MSBDP to the SiPc in its ground state. The MSBDP-part fluorescence quantum yield is 0.006, while the SiPc-part fluorescence quantum yield is even smaller with a value <0.001.

Excitation of the BDP moiety results in strong quenching of the BDP-part emission and appearance of weak fluorescence of MSBDP and SiPc moieties (figure 5.24c). Apparently, energy is transferred from the photo-excited BDP to MSBDP and SiPc in their ground states. The position and shape of the fluorescence of BDP and MSBDP parts resemble the fluorescence of the dyad BDP-MSBDP. However, regardless of which molecular part is initially excited, the fluorescence quantum yield of each molecular

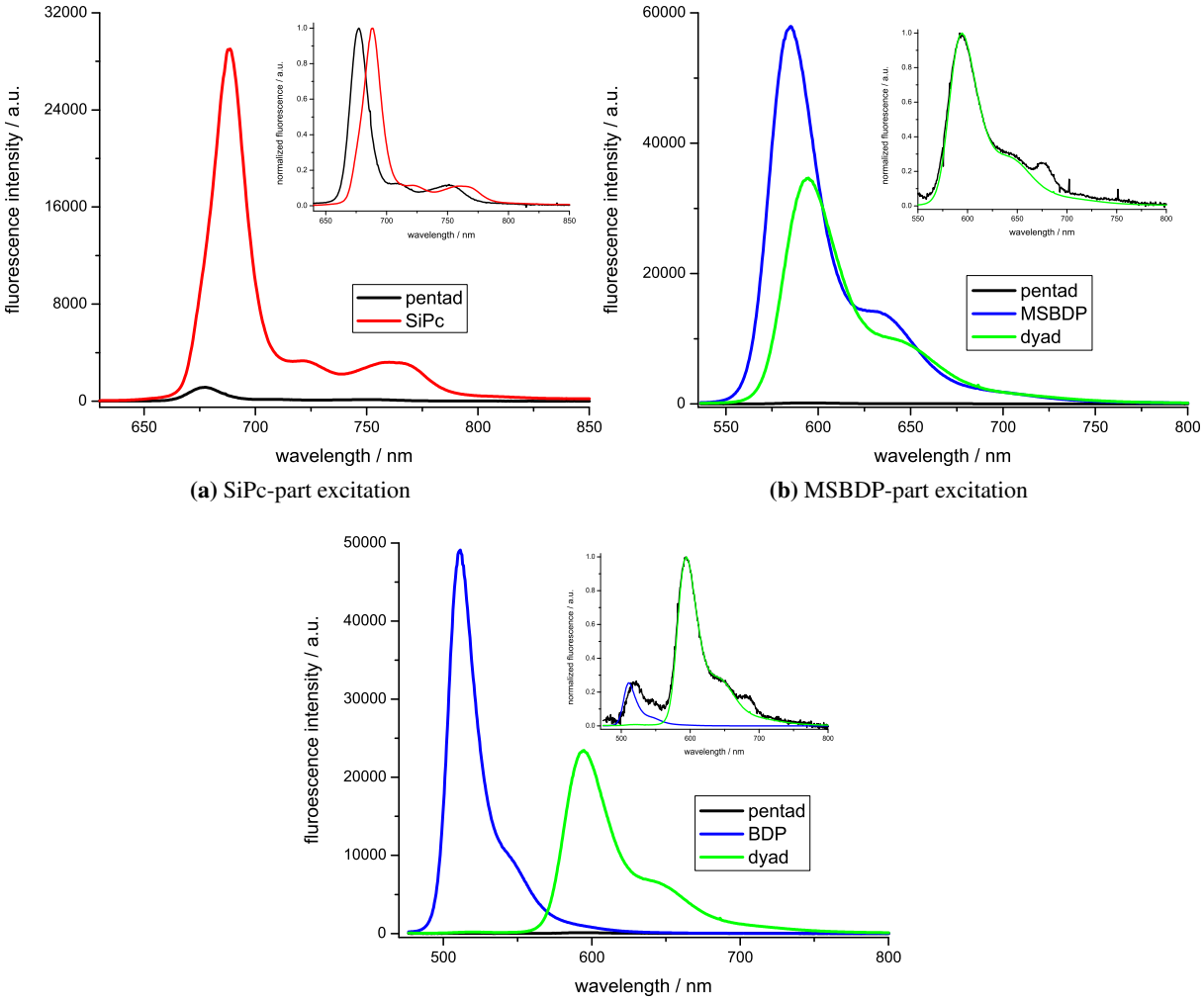

(a) SiPc-part excitation

(b) MSBDP-part excitation

(c) BDP-part excitation

Figure 5.24: Steady-state fluorescence spectra of the pentad and its references dissolved in chloroform upon excitation of its parts. In the insets normalized spectra are shown for comparison.

part does not exceed 0.007 and is in most cases even smaller than 0.001, see table 5.15. Obviously, conjugation of the dyad to SiPc results in strong quenching of fluorescence irrespective of which moiety is excited.

Table 5.15: Fluorescence quantum yields of the pentad and its references dissolved in chloroform.

Compound	Φ_{fl}		
	BDP-part excitation	**MSBDP-part excitation**	**SiPc-part excitation**
BDP	0.58	-	-
MSBDP	-	0.85	-
SiPc	-	-	0.58
Dyad	0.004[a] 0.63[b]	0.78[b]	-
SiPc(BDP)$_2$	<0.001[a] 0.27[c]	-	0.52[c]
SiPc(MSBDP)$_2$	-	0.020[b] 0.003c	0.006[c]
BDP-SiPc-MSBDP	<0.001[a] <0.001[b] 0.010[c]	0.003[b] 0.007[c]	0.020[c]
Pentad	<0.001[a] 0.004[b] <0.001[c]	0.006[b] <0.001[c]	<0.001[c]

[a] BDP-emission
[b] MSBDP-emission
[c] SiPc-emission

Combining the results obtained in the Triads and Dyad sections with the results of the pentad from steady-state experiments it is assumed that:

- Efficient EET occurs from the peripheral Bodipys to the central SiPc core.
- The pentad exhibits almost vanishing fluorescence properties when dissolved in chloroform. This is indicative of a high yield of charge separation, as was found for SiPc(MSBDP)$_2$ and BDP-SiPc-MSBDP.

Up to now, the nature of this charge-separated state is unclear. Based on experience gained in the previous chapters, it is assumed that SiPc is reduced and a Bodipy is oxidized. In order to clarify the situation, time-resolved measurements have been performed. Particularly with regard to pentad's low fluorescence quantum yields (<0.001), the emission decay times are expected to be extremely fast. The transient absorption experiments will elucidate the identity of the charge-separated species.

5.2.3 Excited-state dynamics of the pentad

Time-resolved fluorescence

The DAF spectra of the pentad dissolved in chloroform upon selective excitation of the SiPc-, MSBDP- and BDP-part are shown in figure 5.25. The resulting fluorescence lifetimes are summarized in table 5.16. For comparison the decay times of the references are listed in table 5.16, too.

Table 5.16: Fluorescence lifetimes of the pentad and its reference compounds dissolved in chloroform.

Compound	$\tau_{fl} \pm 0.020$ [ns]		
	BDP-part excitation	**MSBDP-part excitation**	**SiPc-part excitation**
BDP	3.45	-	-
MSBDP	-	3.75	-
SiPc	-	-	5.48
dyad	-[a] 3.86[b]	3.89[a]	-
$SiPc(BDP)_2$	-[a] 5.54[c]	-	5.59[c]
$SiPc(MSBDP)_2$	-	-[b] 0.043[c]	0.038[c]
BDP-SiPc-MSBDP	-[a] -[b] 0.044[c]	-[b] 0.038[c]	0.035[c]
pentad	-[a] 0.010[b,d] 0.010[c,d]	0.010[b,d] 0.010[c,d]	0.011[c,d]

[a] BDP-emission
[b] MSBDP-emission
[c] SiPc-emission
[d] at detection limit

Upon SiPc-part excitation of the pentad at 622 nm, two lifetimes are unravelled (figure 5.25a). The slow one has a lifetime of 4.46 ns, its amplitude is rather small and its maximum lies at 676 nm. The absorption maximum of the SiPc moiety of the pentad lies at 682 nm (see above). In addition, the lifetime of around 5 ns is typically for pristine SiPc. For this reason, this component could be assigned to a small SiPc impurity. Due to its relatively long fluorescence lifetime and high fluorescence quantum yield, the impurity dominates the steady-state fluorescence spectrum (*cf.* figure 5.24a). The fast component decays with 11 ps, its amplitude is much greater than the slow component and its maximum lies at

688 nm. It is likely that the fluorescence is even faster, because it basically follows the excitation pulse. Furthermore, a small, narrow peak at 766 nm is seen in the 11 ps DAF spectrum. The same peak is revealed for a cuvette filled with pristine chloroform, i.e. without dye. As further outlined below, the signal could be identified with Raman scattering. Upon excitation at 622 nm the 3019 cm^{-1} vibration mode of chloroform corresponds to a Raman signal at 766 nm [155].

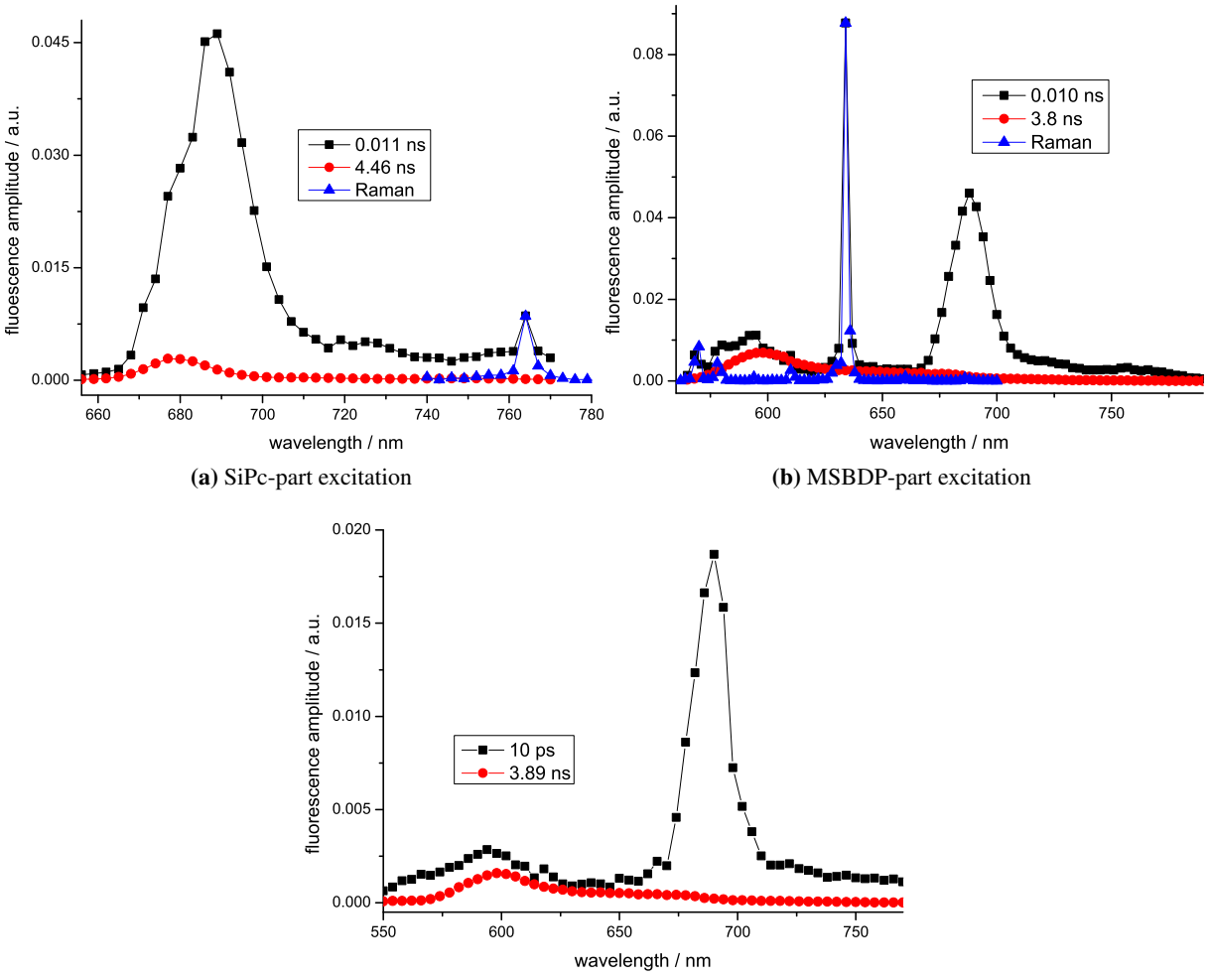

(a) SiPc-part excitation

(b) MSBDP-part excitation

(c) BDP-part excitation

Figure 5.25: DAF spectra of the pentad dissolved in chloroform upon excitation of its parts. The blue curves are signals obtained from cuvettes filled with pristine chloroform and represent Raman scattering signals.

Selective excitation of the MSBDP moiety at 532 nm results in a fast fluorescence lifetime of 10 ps and a slow decay time of 3.8 ns (figure 5.25b). The maximum of the latter is at 594 nm. According to its lifetime, peak position and shape, this component is assigned to a small impurity of BDP-MSBDP dyad (*cf.* table 5.14). The fast DAF spectrum exhibits three distinct maxima at 595, 688 and 634 nm. The peak at 595 nm corresponds to the fluorescence maximum of the MSBDP-part and the peak at 688 nm belongs to SiPc-part emission. The latter indicates that EET from MSBDP to SiPc takes place. A striking

feature in the 10 ps spectrum is the very narrow peak at 634 nm (FWHM=3 nm) that does not appear in steady-state fluorescence experiments. For verification, a cuvette filled with pristine chloroform was measured. The same peak with identical intensity and some other minor peaks which also appear in the DAF spectrum of the pentad were observed. Since these peaks were also resolved in pure chloroform, they are associated with Raman scattering. The intense peak at 634 nm is assigned to the 3019 cm^{-1} vibrational mode of chloroform and the small peak at 569 nm arises from the 1214 cm^{-1} mode [155]. Because scattering is instantaneous, this scattering follows the excitation pulse. Moreover, since the detection limit of the setup is around 10 ps, all processes faster than 10 ps are merged to one decay component of 10 ps. Apparently, the emission of SiPc and MSBDP units is of around 10 ps or even faster. For this reason, both the fluorescence of SiPc and MSBDP as well as the Raman scattering signal follows the excitation pulse.

Excitation at 400 nm (BDP-part excitation) results in a bi-exponential fluorescence decay: a fast decay time of 10 ps and a slow one of 3.89 ns were resolved (figure 5.25c). For the fast component, the maxima at 688 and 594 nm can be assigned to SiPc- and MSBDP-part fluorescence. Both are indicative of EET from the photo-excited BDP to the corresponding moieties. As discussed at MSBDP-part excitation, the TCSPC setup reaches its detection limit and the fluorescence components of SiPc and MSBDP are merged together into one spectrum with a lifetime that corresponds to the instrument response function. The 3.89 ns DAF spectrum can therefore be addressed to small amounts of BDP-MSBDP, according to its lifetime and peak-position. It is noted that the Raman scattering signal of the 3019 cm^{-1} vibrational mode of chloroform would peak at 455 nm, which is outside the measured range.

Transient absorption

Due to the very effective quenching of fluorescence observed in steady-state as well as time-resolved fluorescence experiments, it stands to reason that the absorbed energy is stored in charge-separated states. In order to investigate this charge separation and the ground state recovery of BDP-, MSBDP- and SiPc-part of the pentad, transient absorption spectra of the pentad have been recorded. In figure 5.26 the transient absorption spectra of the pentad are shown directly after selective excitation of its parts.

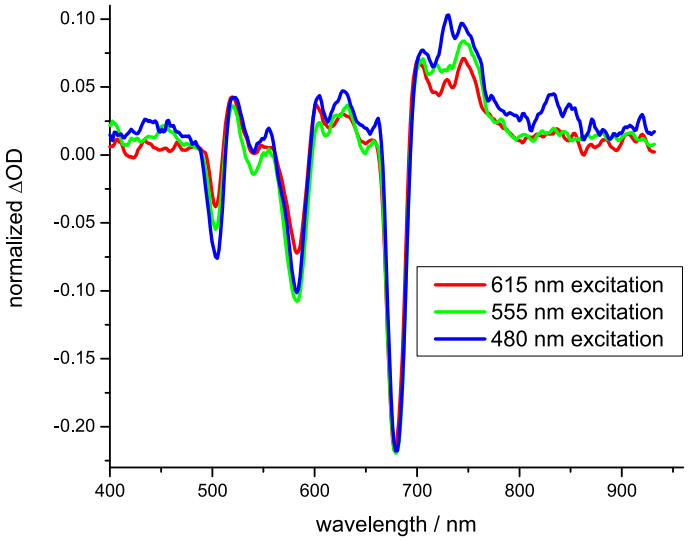

Figure 5.26: Transient absorption spectra of the pentad dissolved in chloroform directly after selective excitation of its parts BDP, MSBDP and SiPc.

As can be seen from figure 5.26, independent of the excitation wavelength used, negative ΔOD signals at around 500 nm, 570 nm and 680 nm appear. Owing to their shapes and spectral positions, the transients originate from BDP, MSBDP and SiPc parts, respectively. Interestingly, all three ground states are depleted, regardless of which moiety was initially excited. Here it is emphasized that EET from the initially excited SiPc* to the BDP- or MSBDP-part in the ground state is energetically unfavourable. The spectra exhibit transient absorption at 520 nm and 620 nm. Moreover, in each ΔOD spectrum a transient signature at 750 nm is observed. Control experiments verified that none of the reference compounds including the dyad BDP-MSBDP and the Bodipy-SiPc triads features this band.

In figure 5.27, transient absorption spectra of the pentad are shown at different delay times. The time evolution of the SiPc ground state recovery is shown in figure 5.27d. Irrespective of the initially excited moiety, the SiPc ground state recovers mono-exponentially with a characteristic time of 25 ps, which is the detection limit of the setup. The kinetics of the MSBDP and BDP bleach recoveries resembles that of SiPc. After 150 ps, all ground states are recovered, which implies that any transition to a triplet state is negligible. The TA spectra reveal isobestic points at 691, 595 and 511 nm, which are characteristic of a transition between two states [156].

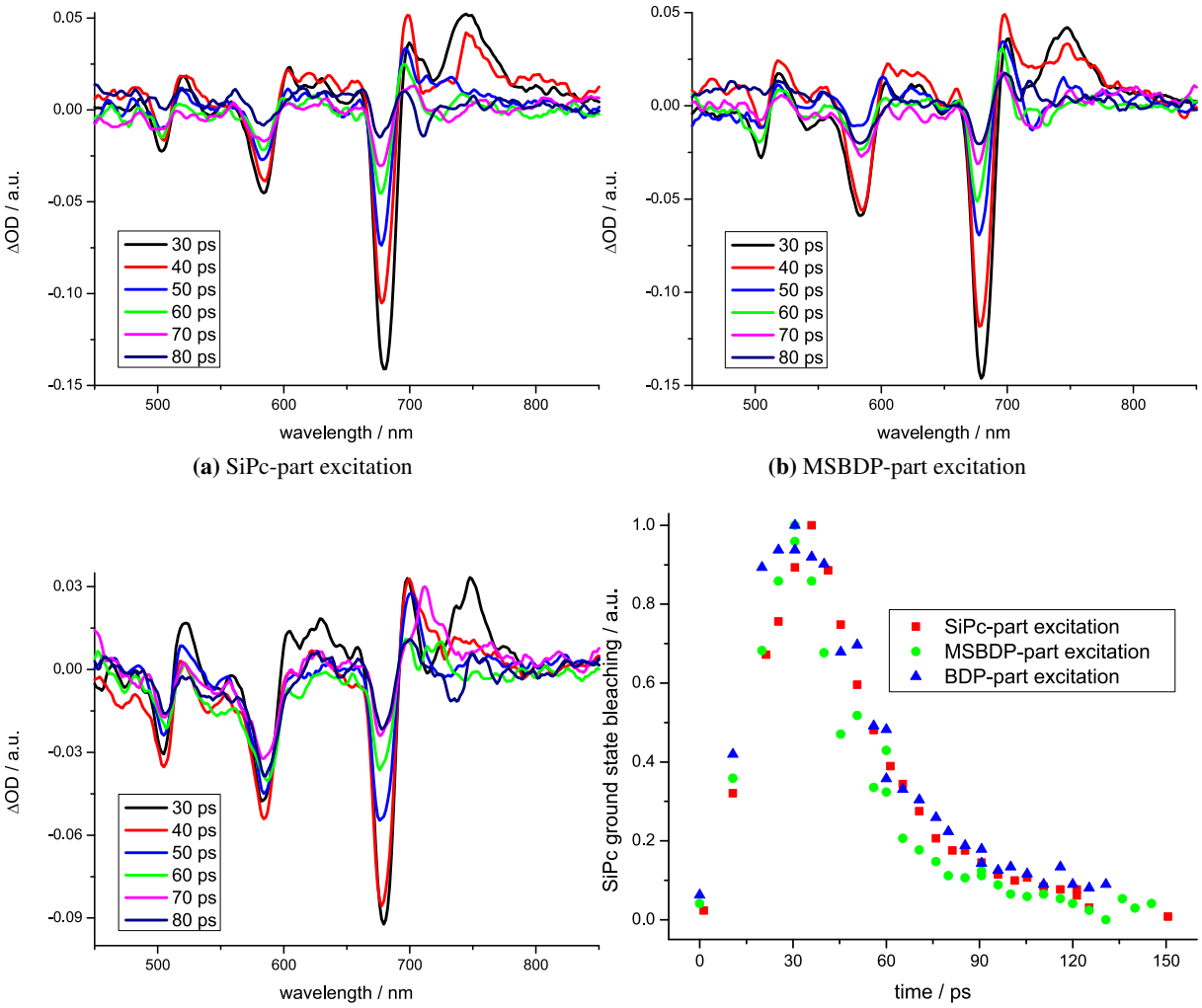

(a) SiPc-part excitation

(b) MSBDP-part excitation

(c) BDP-part excitation

(d) Ground state recovery of SiPc

Figure 5.27: Transient absorption spectra of the pentad dissolved in chloroform upon excitation of its parts at different delay times. In figure (d) the SiPc-part ground state recovery is shown.

5.2.4 Discussion of the pentad's photo-induced processes

The UV/Vis absorption and fluorescence spectra of the pentad are well described by a superposition of its monomeric references. That means that despite the short separation between Bodipy and SiPc parts, the Bodipy and SiPc moieties couple neither in the ground, nor in the first excited state. This is a consequence of the nature of the edge-to-face linkage, which prevents the chromophores from stacking. As described above, after photo-excitation of the Bodipy-SiPc triads and the BDP-MSBDP dyad, EET and ET play a dominant role in the deactivation of the first excited states. Hence, it is expected that both processes are involved in the pentad, too.

The molecular structure of the pentad is reminiscent of the triads. At the triad section it was pointed out that FRET is the dominant energy transfer process. It is therefore assumed that FRET is the dominant EET mechanism for the pentad, too. The spectral overlap between the donor's emission and acceptor's absorption is large. The calculated Förster radii of the various donor-acceptor combinations are similar to those of the triad: R_0(MSBDP→SiPc)=54 Å, R_0(BDP→MSBDP)=51 Å and R_0(BDP→SiPc)=33 Å. The separation distances between the single moieties are much smaller, supporting that EET takes place efficiently and rapidly. This is accompanied by the very fast fluorescence lifetimes and the strongly reduced fluorescence quantum yields of the donors and the absence of fluorescence rise times of the acceptors. As was shown above for the BDP-SiPc-MSBDP triad EET from BDP to MSBDP occurs. It is therefore reasonable to assume that EET in the pentad from BDP to SiPc may occur either *via* hopping from BDP to MSBDP to SiPc, BDP*-MSBDP-SiPc → BDP-MSBDP*-SiPc → BDP-MSBDP-SiPc*, or directly from BDP to SiPc according to BDP*-MSBDP-SiPc → BDP-MSBDP-SiPc*. The energy transfer processes from BDP to MSBDP, from BDP to SiPc and from MSBDP to SiPc are estimated to occur with rates greater than 1.0×10^{11} s^{-1} (time resolution of the TCSPC setup).

It was shown above that in the BDP-MSBDP dyad an electron is transferred from BDP to MSBDP, regardless of which constituent part of the dyad is initially excited. The probability of this charge transfer rises when the dielectric constant of the solvent increases. For non-polar chloroform the probability of ET is rather small resulting in relatively high fluorescence quantum yields. For the SiPc(MSBDP)$_2$ triad ET occurs from MSBDP to SiPc with a high yield even in non-polar chloroform. Both facts suggest that this charge transfer occurs in the pentad, too.

Since the photophysical behaviour of SiPc(BDP)$_2$, SiPc(MSBDP)$_2$ and BDP-MSBDP is elucidated very well, it is worthwhile comparing the TA spectra of these compounds to the TA spectrum of the pentad. In figure 5.28 the TA spectra of the pentad, SiPc(BDP)$_2$ and SiPc(MSBDP)$_2$ are shown.

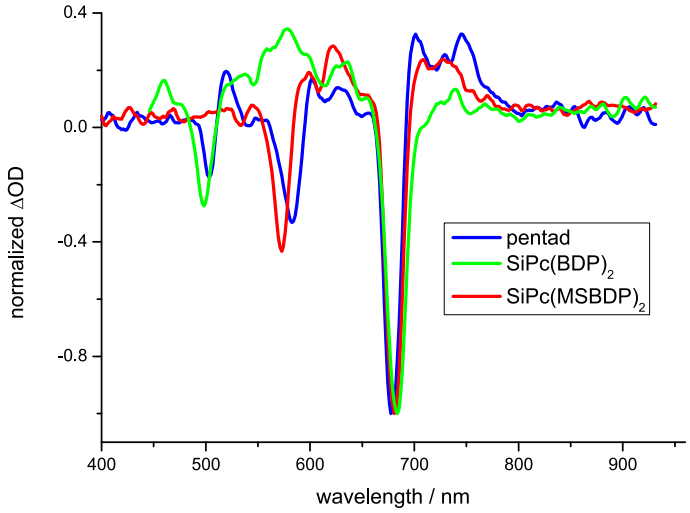

Figure 5.28: TA spectra of the pentad and triads directly after excitation.

The TA spectrum of the pentad exhibits the same features as those of the triads: transient absorption at 520 nm and 620 nm that can be addressed to the BDP$^{\bullet+}$ radical cation and the SiPc$^{\bullet-}$ radical anion,

respectively, and bleach signals of BDP, MSBDP and SiPc moieties. In figure 5.29a, the sum of the TA spectra of SiPc(BDP)$_2$ and SiPc(MSBDP)$_2$ is compared with the TA spectrum of the pentad. The SiPc-bleach of the sum of the triads is much more pronounced. When the TA spectra of SiPc(BDP)$_2$ and SiPc(MSBDP)$_2$ are added, two SiPc$^{\bullet-}$ anions are represented. Obviously, in the pentad only one SiPc$^{\bullet-}$ anion is generated. To account for the mismatch of the SiPc-bleach, in figure 5.29 the TA spectrum of SiPc$^{\bullet-}$ ranging from 550-710 nm was subtracted from the sum of the triads' TA spectra. Figure 5.29b shows a substantial overlap of TA spectra of the pentad and the triads. The red spectrum in figure 5.29b represents the transient absorption of BDP$^{\bullet+}$, MSBDP$^{\bullet+}$ and SiPc$^{\bullet-}$ moieties. This means that indeed, the ground states of BDP, MSBDP and SiPc moieties are depleted at the same time. This is corroborated by the recovery time of 25 ps found in TA experiments, with which the moieties synchronously repopulate their ground states. However, due to conservation of charge the generation of both BDP$^{\bullet+}$ and MSBDP$^{\bullet+}$ radical cations and only one SiPc$^{\bullet-}$ anion is not possible at the same time. For this reason, it is assumed that the positive hole is delocalized over the π-electron systems of BDP and MSBDP.

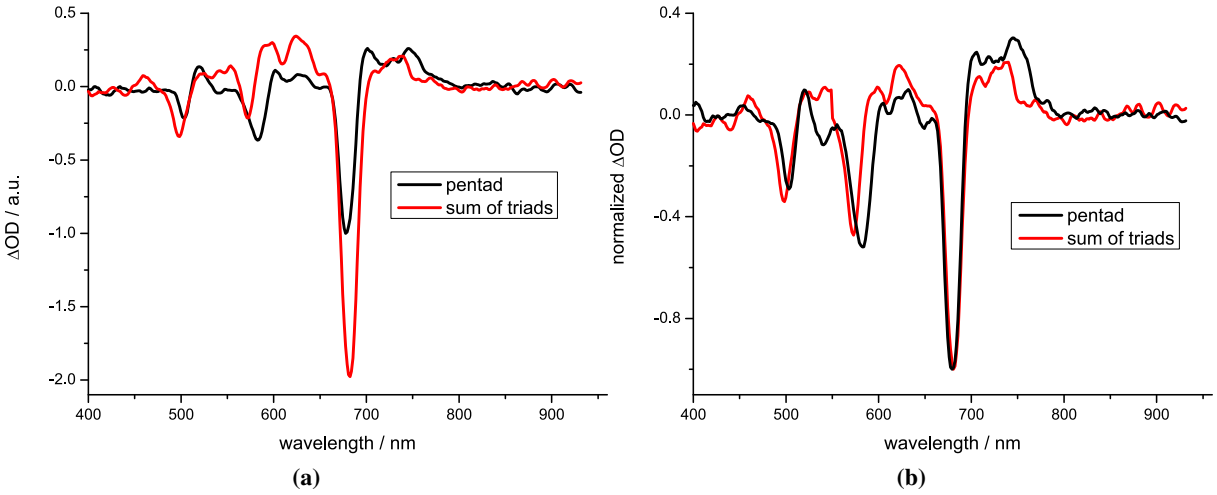

Figure 5.29: TA spectra of the pentad and the sum of TA spectra of SiPc(BDP)$_2$ and SiPc(MSBDP)$_2$ (a). To compensate for double SiPc absorption, the SiPc$^{\bullet-}$ anion spectrum ranging from 550-710 nm is subtracted from the sum of TA spectra of SiPc(BDP)$_2$ and SiPc(MSBDP)$_2$ (b) (see text for explanation).

The lifetime of the charge-separated state is very short compared to that of the SiPc(MSBDP)$_2$ triad. This can be explained by comparing the molecular structures of the molecules, *cf.* figures 5.2 and 5.13. On closer examination, the MSBDP moieties of the pentad and SiPc(MSBDP)$_2$ were linked differently to SiPc. The phenol group of MSBDP is not part of the π-system of MSBDP. In contrast, the styryl group extends the π-system of MSBDP, thereby shifting the UV/Vis absorption of MSBDP to the red, compared to BDP. For SiPc(MSBDP)$_2$ the phenol group links MSBDP to SiPc and it prevents close contact of the π-electron systems of MSBDP and SiPc. On the contrary, for SiPc(BDP-MSBDP)$_2$, the styryl moiety of MSBDP is covalently bound to SiPc. The distance between the π-electron systems of MSBDP and SiPc is much shorter than for SiPc(MSBDP)$_2$. This enhances the charge separation rate: for SiPc(MSBDP)$_2$ the hole transfer rate k_{HT} amounts to 2.3×10^{10} s^{-1}, whereas for the pentad $k_{HT} \geq 1.0 \times 10^{11}$ s^{-1}. On the other hand, the shorter distance increases the charge recombination rate. The latter is much faster for the

pentad, <25 ps compared to 410 ps for SiPc(MSBDP)$_2$ dissolved in chloroform. At this point it is noted that the transfer processes in the pentad could be more delicate and a full characterization of the pentad should be done by carrying out fluorescence and TAS experiments with femtosecond time resolution.

5.2.5 Conclusions

The pentad exhibits excellent UV/Vis absorption that spans from 300-700 nm. The SiPc(BDP-MSBDP)$_2$ pentad covers the same spectral region as the BDP-SiPc-MSBDP triad, but its UV/Vis absorption is much more pronounced due to the doubled BDP and MSBDP moieties. The absorbed light energy is directed from the peripheral BDP and MSBDP moieties to the SiPc centre. After excitation of any of its constituent parts, the (BDP-MSBDP)$^{\bullet+}$-SiPc$^{\bullet-}$-MSBDP-BDP charge-separated state is generated with unity quantum yield. The transfer processes are depicted in figure 5.30. Unfortunately, despite excellent absorption and unity charge separation quantum yields, charge recombination occurs too fast for practical purposes with a decay time that is shorter than 25 ps.

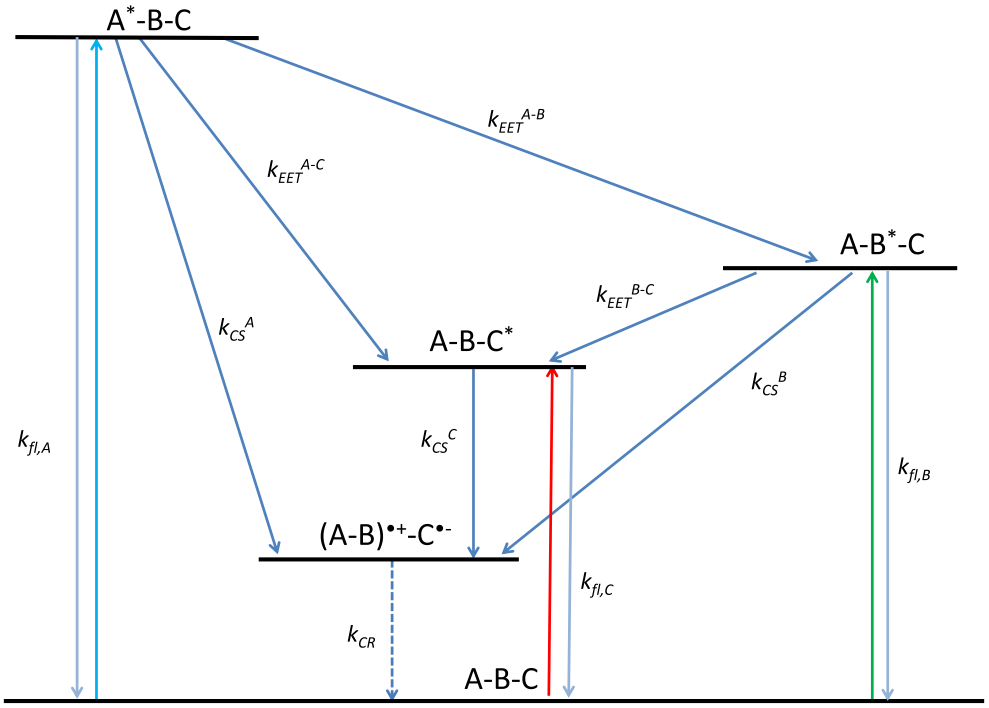

Figure 5.30: Jablonski diagram of the pentad SiPc(BDP-MSBDP)$_2$. A, B and C denote BDP, MSBDP and SiPc moieties, respectively.

The pentad was originally designed to improve the characteristics of the aforementioned triads, i.e. light-harvesting function and lifetime of charge-separated state. As shown above, the latter is too short for use in artificial photosynthesis. The pentad's deviant behaviour could be addressed to the nature of the covalent linkage between BDP-MSBDP and SiPc. Therefore, it is proposed that different types of linkers between BDP-MSBDP and SiPc should be tested to obtain a longer lifetime of the charge-separated state.

This trial and error method may yield nice results. On the other hand, it illustrates the restriction that is imposed on covalently linked systems, i.e. time-consuming syntheses. In addition, covalent syntheses become inefficient and costly as size and complexity of the systems grow. Naturally, it would be very convenient if the moieties could be exchanged with other subunits without having to resynthesize the system. This problem can be overcome if another approach is chosen, namely the self-assembly strategy. The latter is presented in the next chapter.

6 Photo-induced processes in the self-assembled systems

Owing to its facile assembling procedure and resemblance to nature, supramolecular chemistry represents a powerful means to build complex molecular systems from small building blocks. Based on this idea, various self-assembly approaches have been investigated for use in artificial photosynthesis such as metal coordination, hydrogen bonding and π-π stacking [157, 158, 159, 160, 161, 162, 163, 164, 165, 166, 167, 168, 169, 170]. In the present thesis, the self-assembly process between CD and TPPS in aqueous solution by means of hydrophobic interactions is employed to construct architectures consisting of multiple chromophores (*cf.* section 4.1.4).

The structural formulae of the molecular building blocks used for the construction of the self-assembled systems are shown in figure 6.1.

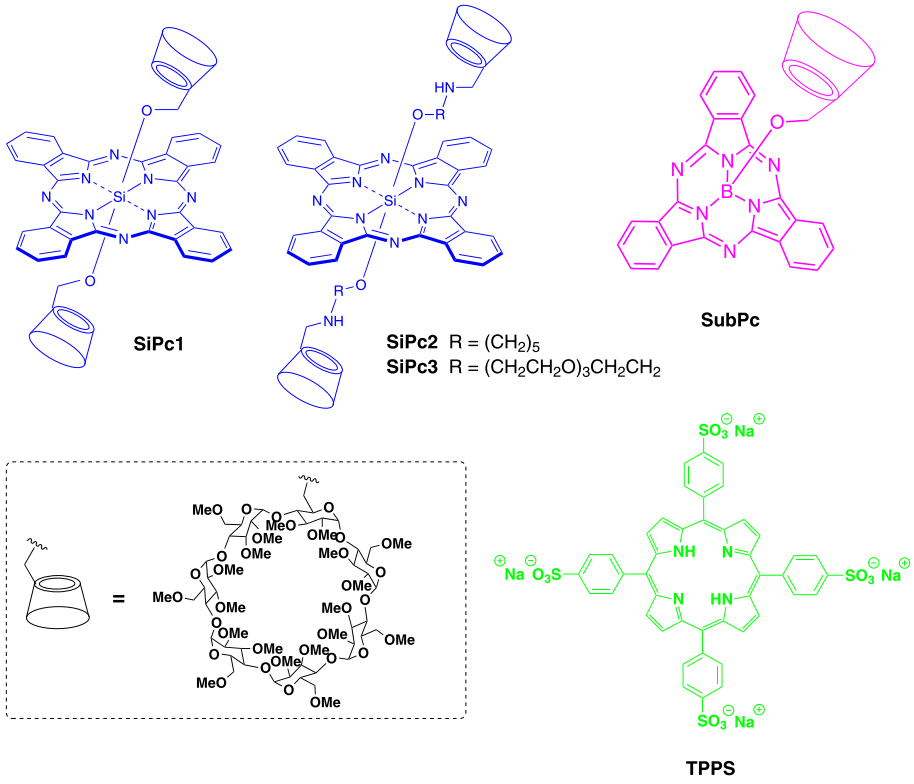

Figure 6.1: Structural formulae of SiPc1, SiPc2, SiPc3, SubPc and TPPS.

The compounds SiPc1, SiPc2, SiPc3 and SubPc were synthesized in the group of Prof. Dr. Dennis

K. P. Ng (Chinese University of Hong Kong) by typical substitution reactions of silicon(IV) phthalocyanine dichloride and boron(III) subphthalocyanine chloride with the corresponding hydroxy CDs according to procedures described in [171, 172, 173].

The photophysical properties of a self-assembled complex consisting of a CD-conjugated SubPc and a tetrasulfonated tetraphenyl porphyrin (TPPS) have been reported by Xu, Ermilov et al. [171]. Herein it was found that SubPc forms stable inclusion complexes with TPPS in aqueous solution. The chromophores associate in a 2:1 manner (SubPc-TPPS-SubPc) and the complex exhibits energy and electron transfer properties from the photo-excited SubPc moiety to the TPPS core.

On the other hand, Ermilov, Menting et al. reported host-guest complexes formed by TPPS and CD-conjugated SiPcs [77]. The SiPcs and TPPS moieties undergo complexation spontaneously in aqueous solution with high association constants and the molecules arrange in 1:1 pairs to TPPS-SiPc complexes. Depending on the spacer between CD and SiPc, electron and energy transfer processes take place in the supramolecular complexes.

The idea was to combine the aforementioned systems in order to generate synergistic effects. Firstly, especially an array of SubPc, Por and Pc shows great promise for the construction of artificial photosynthetic systems since they feature complementary absorption profiles: Pors show intense absorbance at around 410 nm, whereas SubPcs and Pcs exhibit strong absorbance at around 570 and 680 nm, respectively. For this reason, it is expected that a combination of these dyes will cover a broad spectrum of the UV and visible sun light, thereby maximizing the light-harvesting efficiency. Secondly, by using a three-component system it is assumed that a temporal stabilization of the charge-separated state can be achieved by two sequential rapid, short-range electron transfers.

Recently, Menting, Ermilov et al. have shown the formation of a host-guest-host supramolecular complex between SubPc, TPPS and SiPc [151]. It was shown that the three components form a complex spontaneously and very efficiently in aqueous solution. Furthermore, the complex exhibits light-harvesting properties: the light energy absorbed by the complex is funnelled to the SiPc moiety. As an extension of this work, in the present thesis detailed photophysical studies of this complex and a series of analogues in which the CD moieties are linked to the SiPc centre by different spacers are discussed. After light absorption two main transfer processes are involved, namely excitation energy transfer and photo-induced charge transfer. The spacer between CD and SiPc exerts great influence on the photophysical properties of the formed complexes. By altering this linker, it is possible to control the intramolecular photo-induced processes.

The synthesis of the combination of the aforementioned SubPc-TPPS and TPPS-SiPc systems is straightforward. To obtain the supramolecular complexes, the molecules were mixed in aqueous solution in a 1:1:1 equimolar ratio if not stated otherwise. In the following, the equimolar 1:1:1 mixtures consisting of SubPc, TPPS and SiPc chromophores are abbreviated to **1**, **2** and **3**, according to the SiPcs in figure 6.1.

6.1 Steady-state characterization of the self-assembled systems

6.1.1 UV/Vis absorption

The UV/Vis absorption spectra of **1**-**3** as well as the free references SubPc, TPPS and SiPcs in aqueous medium are shown in figure 6.2. The spectral positions of the corresponding absorption maxima of highest intensity are summarized in table 6.1.

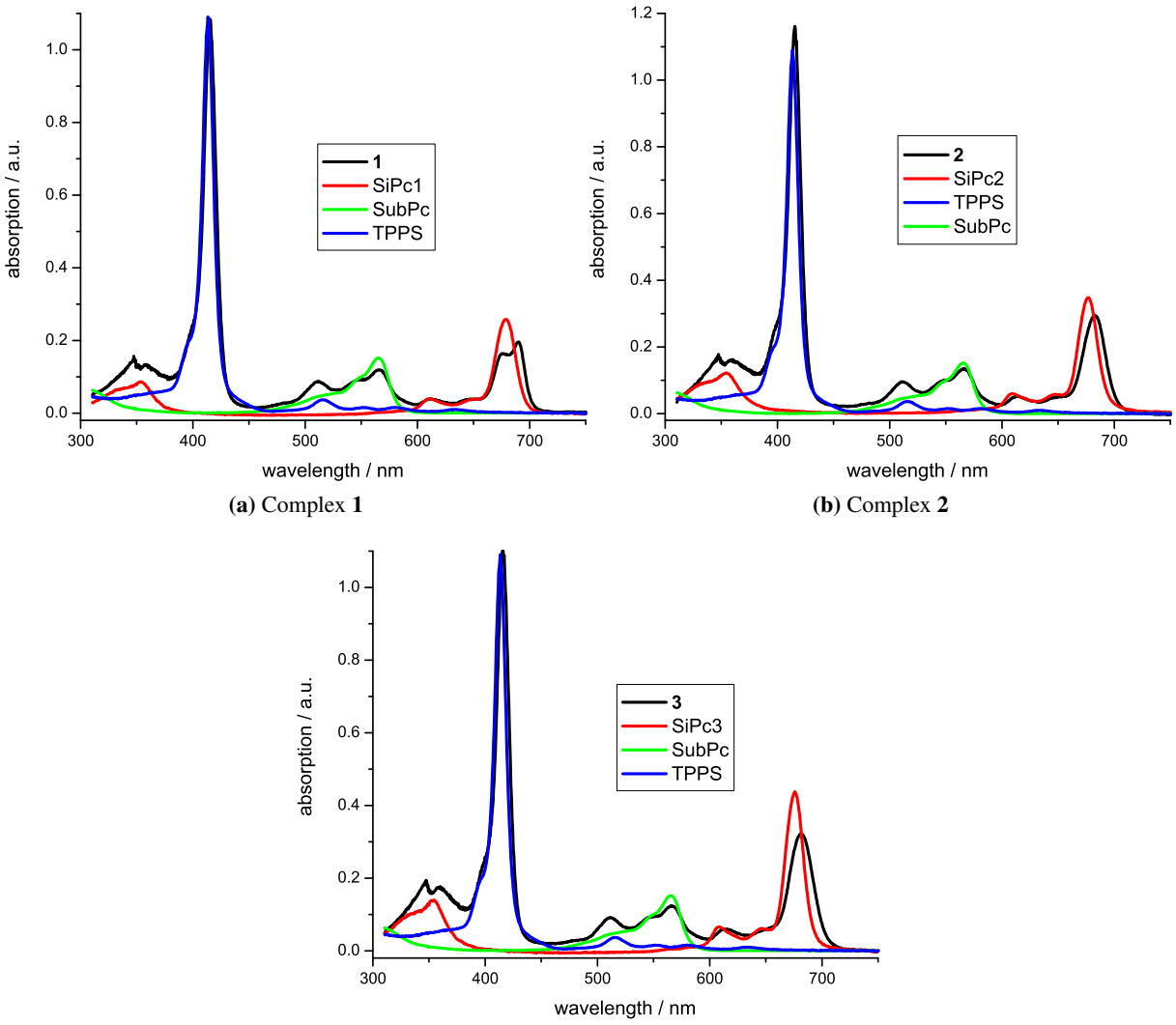

(a) Complex **1**

(b) Complex **2**

(c) Complex **3**

Figure 6.2: UV/Vis absorption spectra of SiPcs, SubPc, TPPS and their equimolar mixtures **1**, **2** and **3** in water. The concentration of the molecules was fixed at 2 μM for all the chromophores.

For mixture **1**, the Q-band of the SiPc moiety is split into two bands with maxima at 676.5 and 690.0 nm. Apparently, the two π-systems of TPPS and SiPc1 interact in the ground state as reported

in [77]. The ground-state interactions in the **2** and **3** mixtures are less pronounced, probably due to the larger separation between the SiPc core and the TPPS chromophore as a result of the enlarged spacer. The UV/Vis absorption spectra of mixtures **2** and **3** are similar. Spectral shifts to the red (within 230 cm^{-1}) and intensity losses of the absorption maxima in the mixture compared to their positions for monomeric compounds are observed for the Q-bands of the SiPc moiety. The spectral maximum of the SubPc-part remains unchanged, however, its intensity is slightly reduced. The maximum of the Por's Soret band at 413 nm undergoes a bathochromic shift of 150 cm^{-1} to 415.5 nm (table 6.1). All above mentioned effects indicate the formation of a self-assembled complex between SiPc and TPPS moieties [77, 125, 173].

Table 6.1: Fluorescence quantum yields and emission and absorption maxima of SiPcs, TPPS, SubPc as well as the supramolecular complexes **1**, **2** and **3**.

Compound	λ_{abs} **[nm]**	λ_{fl} **[nm]**	Φ_{fl}		
			SubPc-part excitation	**TPPS-part excitation**	**SiPc-part excitation**
SubPc	566	575	0.10	-	-
TPPS	413	643, 704	-	0.09	-
SiPc1	679	686	-	-	0.39
SiPc2	677	682	-	-	0.40
SiPc3	676	680	-	-	0.49
1	566[a] 415.5[b] 676.5[c] 690[c]	575[a] 645[b] 694[c,d]	0.006[a] 0.014[b] 0.006[c]	0.030[b] 0.014[c]	0.025[c]
2	566[a] 415.5[b] 683.5[c]	575[a] 645[b] 691[c]	0.011[a] 0.020[b] 0.027[c]	0.029[b] 0.16[c]	0.32[c]
3	566[a] 415.5[b] 682[c]	575[a] 645[b] 689[c]	0.020[a] 0.013[b] 0.010[c]	0.027[b] 0.10[c]	0.21[c]

[a] SubPc-part
[b] TPPS-part
[c] SiPc-part
[d] from DAF spectra (*vide infra*)

In order to obtain more information about the formed complexes, concentration-dependent investigations were carried out by UV/Vis absorption spectroscopy. The absorption spectra of SubPc+SiPc (both at a concentration of 2 μM) mixtures at different concentrations of TPPS are shown in figure 6.3.

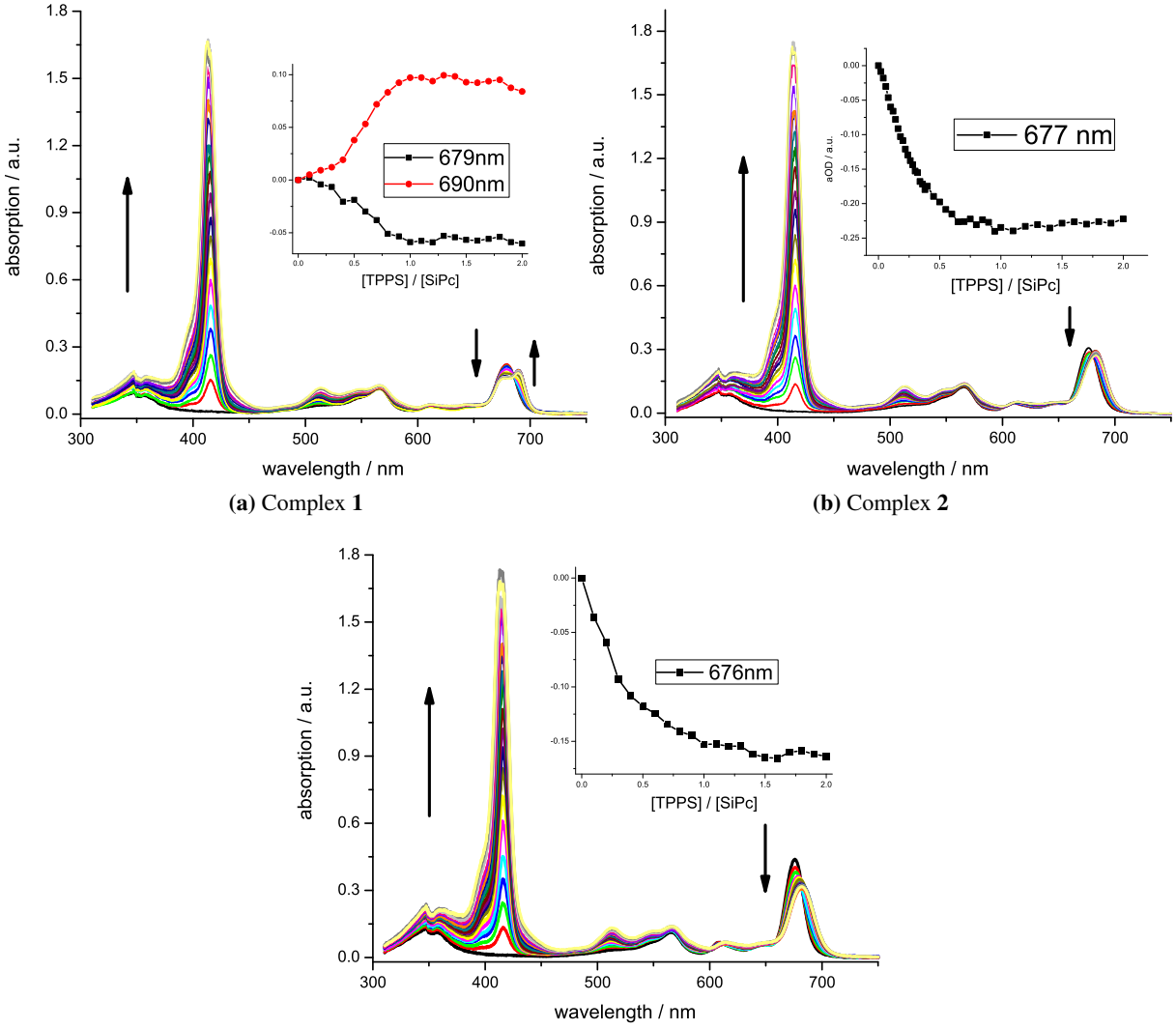

(a) Complex **1**

(b) Complex **2**

(c) Complex **3**

Figure 6.3: UV/Vis absorption spectra of the SubPc+SiPc mixtures (both at 2 μM) at different concentrations of TPPS. The concentration of TPPS was varied between 0 and 4 μM. The inset shows the change of optical density for the SiPc-part Q-bands at around 680.0 nm with rising concentration of TPPS.

As shown in figure 6.3, the Q-band of the SiPc moiety of **1** is gradually split into two bands upon addition of TPPS with an isobestic point at 685.5 nm. The Q-bands of SiPc2 and SiPc3 in the mixtures **2** and **3** shift to the red with increasing TPPS concentration, but no band splitting occurs. Furthermore, the intensity of these bands is lower compared to the corresponding free SiPc chromophores due to weak electronic coupling to the TPPS unit in the self-assembled complex. The above discussed spectral and intensity changes of the absorption spectra of the SiPc moieties come to a stop at an equimolar mixture of the three components. In addition, when adding an excess of TPPS to the mixture, i.e. more than one equivalent relative to the concentrations of SiPc and SubPc, the Soret band of free TPPS at 413 nm reappears. From these results the formation of a 1:1 complex between TPPS and SiPc compounds is affirmed. However, since the absorption of the SubPc-part shows neither intensity nor spectral shifts upon addition of TPPS, the formation of a SubPc-TPPS-SiPc complex is not evident from UV/VIS absorption results. Therefore, further investigations were carried out using the fluorescence technique.

6.1.2 Steady-state fluorescence

Since the absorption bands of SubPc, TPPS and SiPc chromophores are spectrally well-separated, the fluorescence properties of the mixtures could be determined upon selective excitation of each moiety. Figure 6.4 shows the steady-state fluorescence spectra of the 1:1:1 equimolar mixtures upon selective excitation of their parts. Regardless of which moiety is selectively excited, it is seen that the fluorescence of the SiPc-part of the complexes depends strongly on the linker between SiPc and CD.

The fluorescence quantum yields and emission wavelengths of highest intensity of the supramolecular complexes and their free components are also summarized in table 6.1.

Upon selective excitation of **2** at 615 nm (SiPc-part excitation) fluorescence of the Pc moiety is observed with an emission maximum at 691 nm which is 190 cm^{-1} shifted bathochromically compared to the reference SiPc2. The fluorescence intensity of the supramolecular complex **2** is slightly reduced, compared to the fluorescence of free SiPc2: the fluorescence quantum yield of **2** is 0.32, while for free SiPc2 the corresponding value is 0.40. For the complex **3** the fluorescence quenching is somewhat stronger. The fluorescence quantum yield of **3** was measured to be 0.21, whereas it is 0.49 for the reference SiPc3. The fluorescence intensity of the SiPc-part of **1** decreases dramatically in the presence of TPPS and SubPc. The emission quantum yield of **1** is solely 0.025 compared to 0.39 of free SiPc1.

Upon selective excitation of TPPS at 400 nm, for all complexes strong decrease of TPPS fluorescence and at the same time appearance of SiPc-part fluorescence are observed. This suggests that an EET occurs from the initially photo-excited TPPS to the SiPc moiety of the supramolecular complexes. The fluorescence quantum yield of TPPS was measured to be 0.030, 0.029 and 0.027 for the complexes **1**, **2** and **3**, respectively. The emission of the Por-part of the supramolecular complexes becomes more structured compared to the fluorescence spectrum of the reference TPPS, furthermore, a small bathochromic shift of 50 cm^{-1} is seen. The observations indicate that TPPS is entrapped in the CD nano-cavity [171]. The fluorescence quantum yield of the SiPc-part emission depends on the spacer between the CD unit and the SiPc core. Its value was determined to be 0.014, 0.16 and 0.10 for **1**, **2** and **3**, respectively (*cf.* table 6.1).

Upon selective excitation of the SubPc moiety at 532 nm complex fluorescence spectra are obtained (figure 6.4). The intensity of the SubPc-part fluorescence decreases substantially in the presence of TPPS and SiPc, its fluorescence quantum yield value is reduced from 0.10 (for free SubPc in aqueous solution)

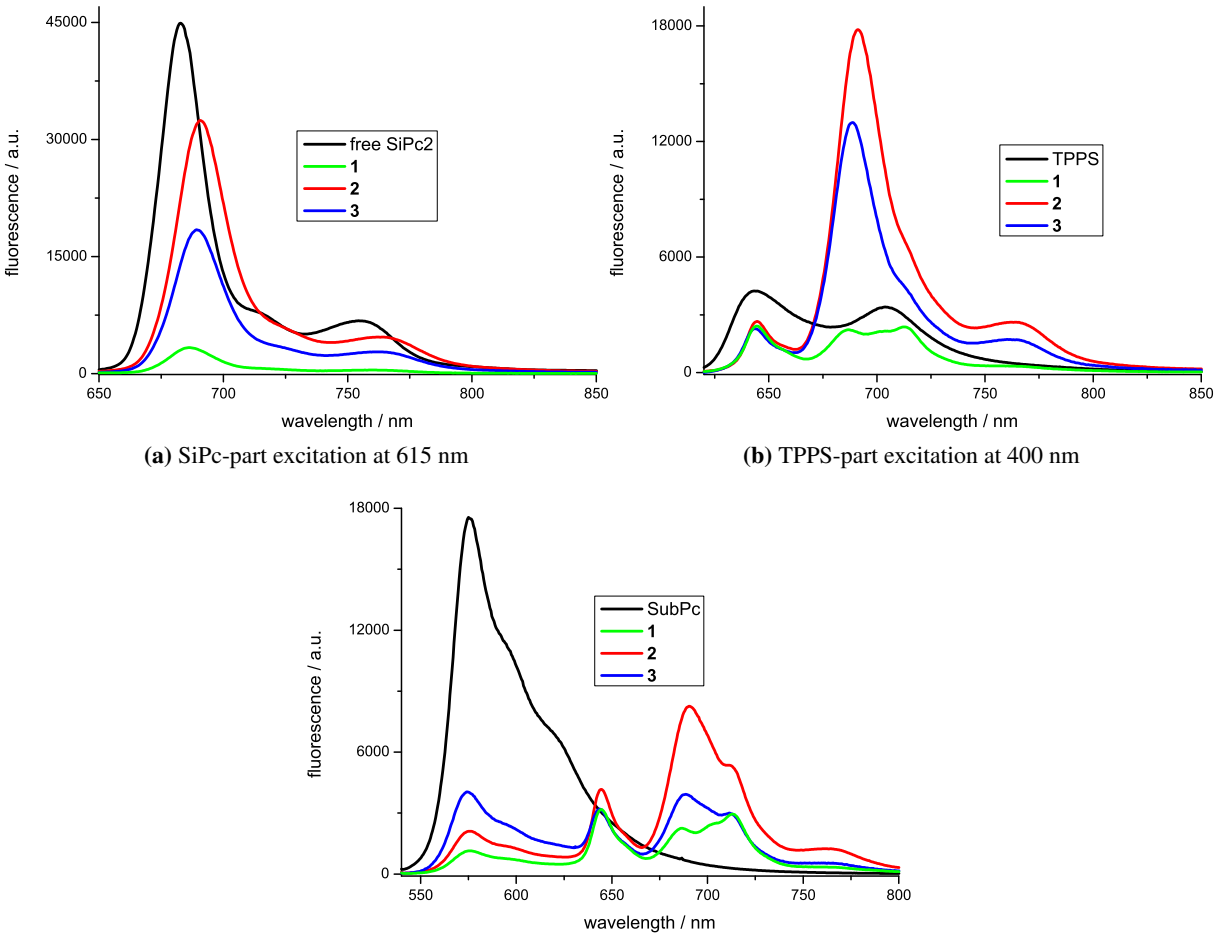

(a) SiPc-part excitation at 615 nm

(b) TPPS-part excitation at 400 nm

(c) SubPc-part excitation at 532 nm

Figure 6.4: Steady-state fluorescence spectra of the supramolecular complexes **1**-**3** and the reference compounds upon selective excitation of the SiPc- (a), TPPS- (b) and SubPc- (c) parts. The concentration of all components was fixed at 1 μM

to 0.020 (**3**) and down to 0.006 (**1**), see table 6.1. At the same time, fluorescence of the TPPS- and SiPc-part is observed. The results clearly show that EET takes place from the photo-excited SubPc to TPPS and SiPc moieties. The emission of the SiPc moiety upon excitation of SubPc is a strong evidence of the formation of a ternary host-guest-host complex. It should be mentioned that the fluorescence quantum yield of the SiPc-part of the supramolecular complexes is smaller compared to the values measured upon excitation of TPPS or SiPc moieties: for complexes **1**, **2** and **3** the SiPc-part fluorescence quantum yields amount to 0.006, 0.027 and 0.010, respectively. The same effect is observed for the TPPS fluorescence following SubPc-part excitation.

At this point it should be mentioned that besides SubPc, TPPS has slight absorption at 532 nm, too. It follows that the observed SiPc fluorescence may also be due to EET from the directly excited TPPS to SiPc in their binary complex without SubPc being involved [77]. To clarify the situation, a control measurement was carried out for equimolar mixtures of TPPS and SiPc. As shown in figure 6.5, fluorescence

of both TPPS and SiPc is significantly stronger for the mixtures containing all the three components compared with that for the mixtures containing only TPPS and SiPc. The results provide additional support for the formation of the ternary supramolecular complexes.

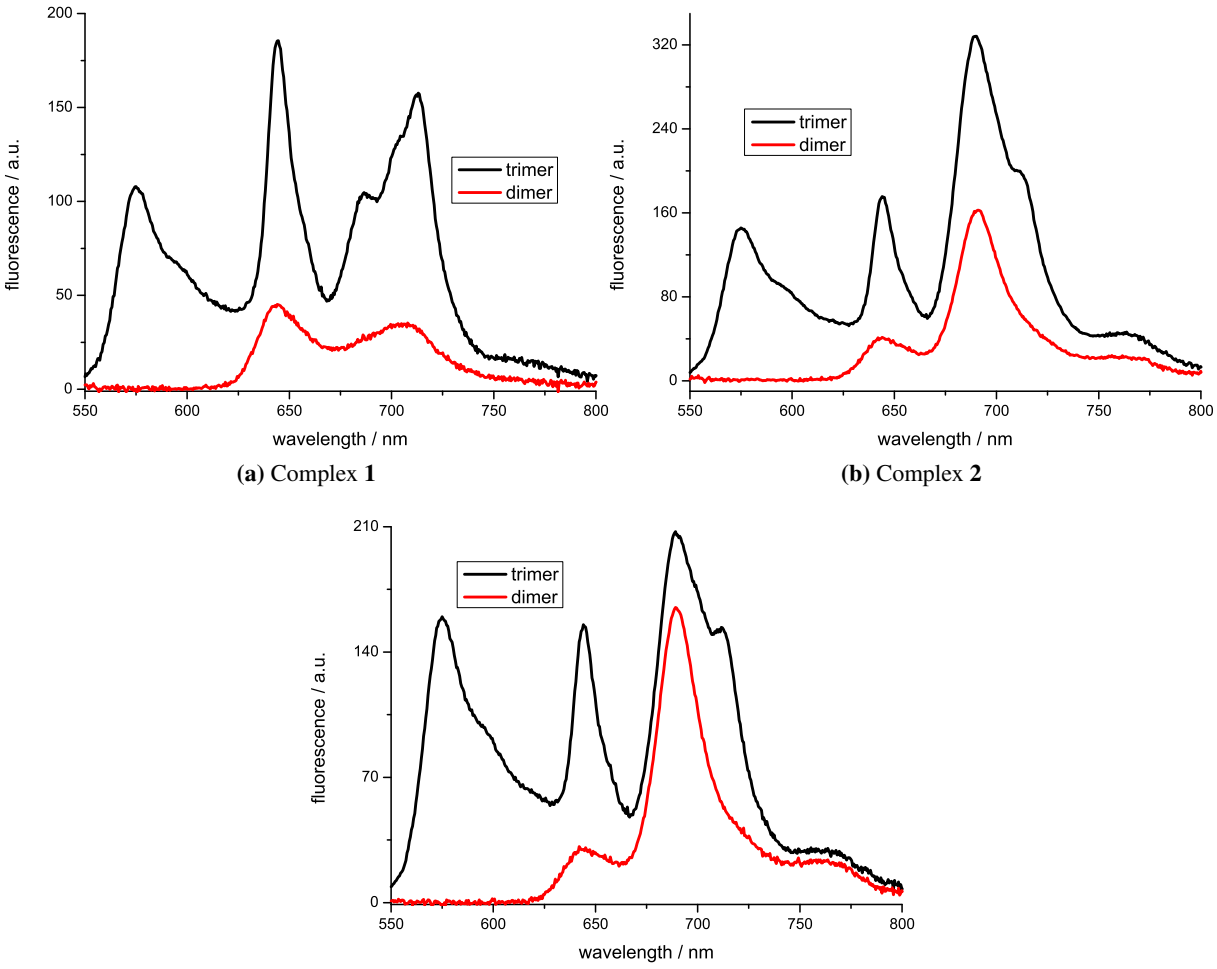

(a) Complex **1**

(b) Complex **2**

(c) Complex **3**

Figure 6.5: Fluorescence of **1** (a), **2** (b) and **3** (c) complexes upon excitation at 532 nm. The ternary complexes SubPc-TPPS-SiPc are shown in black, the binary complexes TPPS-SiPc in red. The concentration of the molecules was 1 μM.

6.1.3 Association constants

To support the formation of the supramolecular complexes, fluorescence titration experiments have been performed. From these experiments association constants can be determined (see page 99).

In figure 6.6 the change of the SiPc-part fluorescence of SubPc+SiPc mixtures is shown upon titration with TPPS following excitation of the SiPc-part. The concentration of SubPc and SiPc is fixed at 1 μM while the concentration of TPPS is varied from 0 μM to 2 μM.

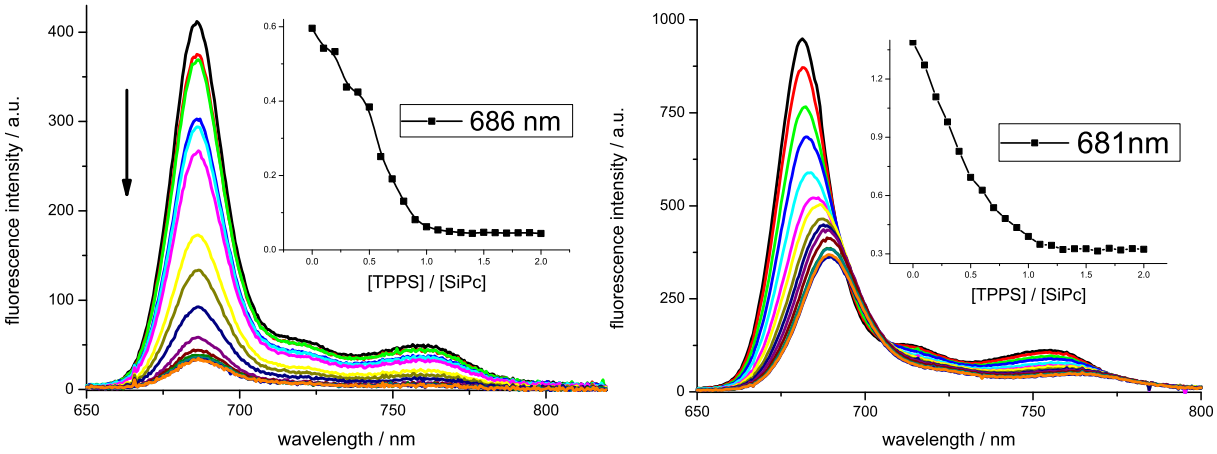

(a) Complex **1** **(b)** Complex **3**

Figure 6.6: Change of the fluorescence spectrum of a mixture of SubPc and SiPc1 (a) and SiPc3 (b) (both at 1 μM) upon addition of TPPS (up to 2 μM) in water. The SiPc-part was selectively excited at 615 nm. Insets: fluorescence intensity versus concentration of TPPS.

Notice that the fluorescence maximum at 686 nm of the SubPc-SiPc1 mixture decreases dramatically with rising TPPS concentration. The efficient quenching of SiPc1-part emission is clearly due to the short separation between the SiPc fluorophore and the entrapped TPPS quencher. The fluorescence maximum of SiPc3 is shifted bathochromically and its intensity drops as the concentration of TPPS increases. Similar results are obtained for complex **2** (see figure 8, appendix). When an equimolar (or higher) concentration of TPPS is added, the spectral position as well as the intensity of the fluorescence spectrum of the SiPc moiety of the supramolecular complexes remain constant. It is worth noting that the SiPc-part fluorescence intensities of complexes **2** and **3** remain quite high compared to that of **1**.

The change of fluorescence spectra of SubPc+SiPc2 and SubPc+SiPc3 mixtures upon addition of TPPS and upon selective excitation of TPPS at 400 nm is shown in figure 6.7. The corresponding spectra of **1** are shown in figure 9a (appendix).

The fluorescence intensity of the SiPc-part reaches its maximum at an equimolar concentration of SubPc, TPPS and SiPc. Interestingly, upon addition of an excess of TPPS, the fluorescence intensity gradually decreases. For the supramolecular complex **1** the same behaviour is observed.

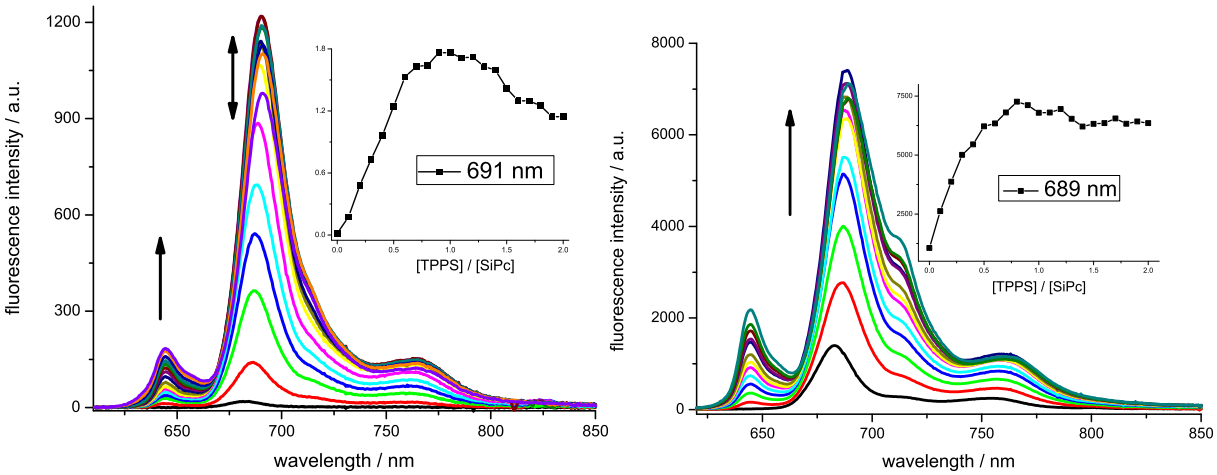

(a) Complex **2** **(b)** Complex **3**

Figure 6.7: Change of the fluorescence spectrum of a mixture of SubPc and SiPc2 (a) and SiPc3 (b) (both at 1 μM) upon addition of TPPS (up to 2 μM) in water. The TPPS-part was selectively excited at 400 nm. Insets: fluorescence intensity versus concentration of TPPS.

Figure 6.8 shows the changes in fluorescence spectra of 1:1 mixtures of SubPc+SiPc2 and SubPc+ SiPc3 at different concentrations of TPPS and upon excitation of the SubPc-part at 532 nm. The corresponding spectra of the SubPc+SiPc1 mixture are shown in figure 9b (appendix).

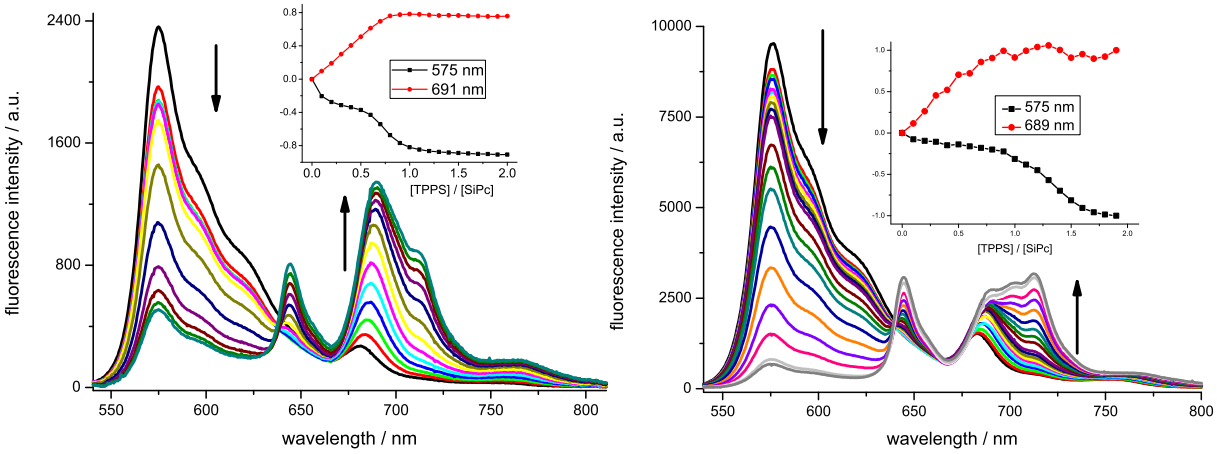

(a) Complex **2** **(b)** Complex **3**

Figure 6.8: Change of the fluorescence spectrum of a mixture of SubPc and SiPc2 (a) and SiPc3 (b) (both at 1 μM) upon titration of TPPS (from 0 μM up to 2 μM) in water. The SubPc-part was selectively excited at 532 nm. Insets: fluorescence intensity versus concentration of TPPS.

The SubPc-part fluorescence band at 575 nm decreases gradually with rising TPPS concentration, while concomitantly the intensity of the SiPc fluorescence increases. The fluorescence of SiPc reaches a plateau at the same concentration of TPPS and the fluorescence intensity of SubPc decreases until ap-

proximately one equivalent of TPPS is added. Since the concentrations of these chromophores (1-2 μM) were too low to facilitate EET between free chromophores in solution (*vide infra*), the results support the formation of a ternary host-guest-host complex for the three components, by which EET occurred from the initially excited SubPc to SiPc *via* TPPS.

Since several association equilibria are involved in ternary supramolecular complex formation, it is very difficult to carry out exact calculation of the association constants. However, some approximations could be done in order to demonstrate that the formation of a ternary complex is likely to occur. The fluorescence spectra of SubPc+SiPc mixtures upon titration with TPPS were analysed to determine the association constants K by using the Benesi-Hildebrand equation [174, 175, 176]:

$$\frac{I_0}{I_0 - I} = \frac{1}{AK}\frac{1}{[x]} + \frac{1}{A} \tag{6.1}$$

where $[x]$ stands for TPPS concentration, I_0 and I represent the fluorescence intensities of SubPc or SiPcs without and upon addition of TPPS, respectively, and A is a constant related to the difference in the emission quantum yield of the complexed and the uncomplexed moieties. The concentration of TPPS was kept low with respect to the concentrations of SubPc and SiPcs. When $\frac{I_0}{I_0-I}$ vs. $\frac{1}{[x]}$ was plotted, straight lines were obtained from which the different association constants K could be determined (e.g. for complex **2** see figure 10, appendix). The values of K are listed in table 6.2.

Table 6.2: Association constants K of the constituent parts of the complexes.

Complex	K [M^{-1}] ±10%		
	SubPc-TPPS	**TPPS-SiPc**	**SubPc-SiPc**
1	1.1×10^7	1.7×10^7	N.d.
2	1.5×10^6	1.8×10^5	7.3×10^5
3	7.6×10^6	8.5×10^6	8.1×10^6

For complexes **2** and **3** the following procedure was established. Upon excitation of the SubPc moiety, the fluorescence of the SubPc-part was monitored along with the addition of TPPS, from which the association constants that represent the complexation of SubPc with TPPS were calculated and the obtained values lie in the order of 10^6 M^{-1}. The association constants of SiPc with TPPS were determined by selective excitation of the TPPS moiety and monitoring the SiPc-part fluorescence. The values were in the order of 10^7 M^{-1} (for complex **2** it is slightly lower with 1.8×10^5 M^{-1}). The association constant of SubPc with SiPc was measured following excitation of SubPc and monitoring the SiPc fluorescence. The latter process is only possible in presence of TPPS and describes the formation of a ternary SubPc-TPPS-SiPc complex. The high values of approx. 10^6 M^{-1} show that this formation is very likely to occur.

For complex **1** due to the strong quenching of the SiPc-part fluorescence the association constant of SiPc with TPPS was obtained by excitation of SiPc and monitoring the SiPc fluorescence at different concentrations of TPPS. Its value is determined to 1.7×10^7 M^{-1}. The SubPc-TPPS association constant of 1.1×10^7 M^{-1} was determined as described above for complexes **2** and **3**. Since the SiPc fluorescence

is strongly quenched upon titration with TPPS, as expected very little rise of the SiPc-part fluorescence was observed following excitation of SubPc. Therefore, the stability constant of the association of SubPc and SiPc was not determined. However, since the association constants SubPc-SiPc for complexes **2** and **3** are large, it is expected that SubPc-SiPc1 features a high association probability, too.

For all association combinations SubPc-TPPS, TPPS-SiPc and SubPc-SiPc high values of K were found, indicating that complexes consisting of all the three molecules are formed in the mixture. The results may support the formation of a 1:1:1 SubPc-TPPS-SiPc complex. However, the results do not preclude the formation of other higher/lower aggregates.

6.1.4 Sequence of mixing the monomers

As mentioned in section 4.1.4, Kano et al. found that TPPS and CD form a very stable 1:2 inclusion complex in aqueous solution [125]. This 1:2 complexation of TPPS and CD has consequences for the formation of the SubPc-TPPS-SiPc complex. The SubPc moiety possesses one CD moiety, as a result, two SubPcs may undergo complexation with one TPPS molecule (see figure 6.9) [171].

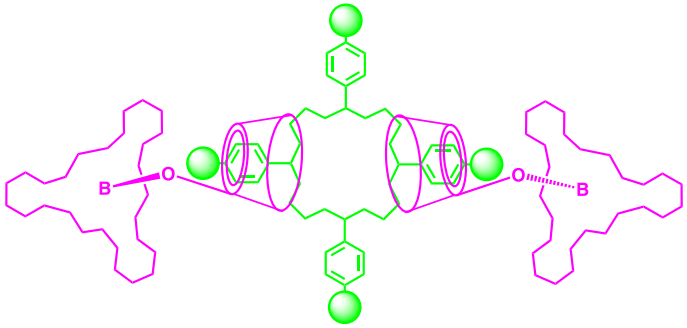

Figure 6.9: Schematic presentation of the 2:1 inclusion complex of SubPc (pink) and TPPS (green).

When TPPS is titrated to an aqueous solution containing SubPc, the compounds arrange in SubPc-TPPS-SubPc trimers. When more TPPS is added, the excess amount of TPPS is not able to undergo complexation with SubPc anymore, since the free, uncomplexed SubPc moieties have been consumed. When SiPc is added subsequently, the leftover, uncomplexed TPPS assembles to SiPc. Hence, the self-assembly of both SubPc-TPPS-SubPc and TPPS-SiPc complexes is successful, whereas the SubPc-TPPS-SiPc complex is not formed. Thus, the formation of ternary complexes consisting of SubPc, TPPS and SiPc is less likely when SubPc and TPPS are mixed together first. In the following, this mixing sequence is denoted as sequence A. Another option is to mix TPPS and SiPc first which is abbreviated to mixing sequence B. The SiPc compounds consist of two CD nano-cavities. Therefore, SiPc and TPPS arrange in 1:1 pairs [77]. At higher concentrations of TPPS and SiPc it is likely that head-to-tail polymeric structures like in figure 6.10 are formed since SiPc has two CD-association sites for TPPS. When SubPc is added hereafter, the TPPS-SiPc polymer prevents SubPc from forming inclusion complexes with TPPS.

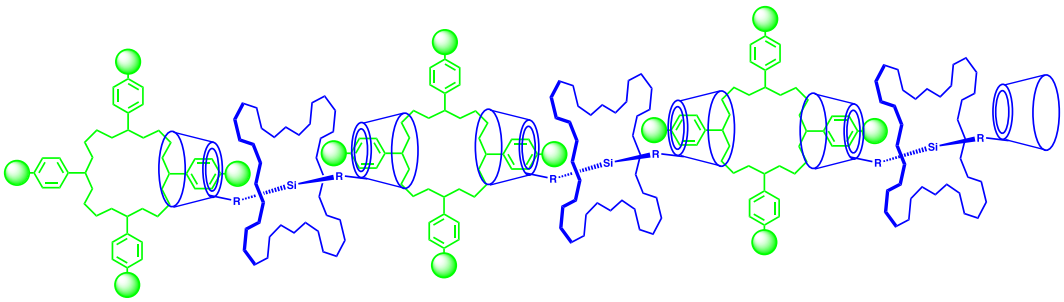

Figure 6.10: Head-to-tail polymeric structure of TPPS (green) and SiPc (blue).

The third way is to mix SubPc and SiPc first, subsequently, TPPS is added (sequence C). Since the association constants of SubPc-TPPS are somewhat greater than the association constants of TPPS-SiPc

(see table 6.2), the SubPc-TPPS association will proceed with a higher probability. After formation of SubPc-TPPS complexes, the uncomplexed tail of TPPS is encapsulated by the CD of SiPc, resulting in SubPc-TPPS-SiPc ternary complexes (figure 6.11). Sequence C is therefore expected to yield the highest amount of ternary SubPc-TPPS-SiPc complexes.

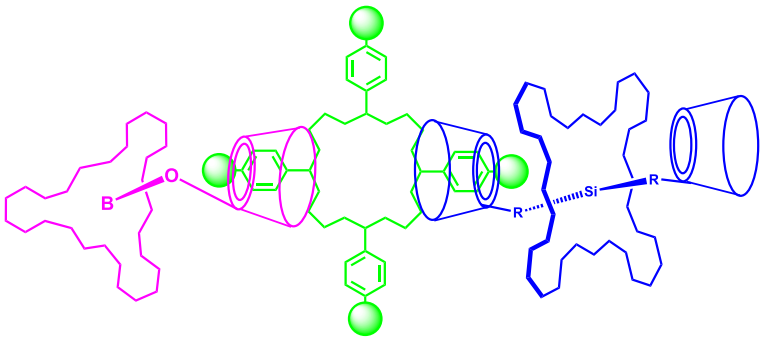

Figure 6.11: Supramolecular ternary complex of SubPc (pink), TPPS (green) and SiPc (blue).

For clarity, the different mixing sequences are summarized in table 6.3.

Table 6.3: Three different mixing sequences A, B and C.

Mixing sequence	Compounds mixed together first	Compound added subsequently
A	SubPc, TPPS	SiPc
B	TPPS, SiPc	SubPc
C	SubPc, SiPc	TPPS

Based on the aforementioned arguments, it is expected that the mixing sequence plays a role in complex formation. In order to investigate the effect of different mixing sequences, UV/Vis absorption and steady-state fluorescence experiments have been carried out. In figure 6.12 the UV/Vis spectra of equimolar SubPc+TPPS+SiPc mixtures are shown, for which the mixing sequence is varied.

It is seen that the UV/Vis absorption spectrum of the mixture prepared with sequence A appears to deviate from those prepared with sequences B and C. The splitting of the SiPc1 Q-band depends on the mixing sequence. For sequence A, the Q-band of the SiPc1 moiety is broadened, but the band is not split. On the contrary for sequences B and C, two distinct peaks at 677 and 690 nm appear. The intensity of the SiPc2 Q-band is smaller for sequences B and C, compared to sequence A. Apparently for both complexes, the interactions between TPPS and SiPc moieties are weaker for mixing sequence A.

The observed behaviour can readily be explained by the predictions presented above. For complex **1** a perturbation of the π-electron system of SiPc1 results in a splitting of the SiPc Q-band. The SubPc-TPPS-SubPc trimer hinders SiPc from binding to TPPS, thus the degree of complexed SiPc will be less and some amount of free SiPc remains in solution. Therefore, the SiPc Q-band of sequence A is a superposition of the Q-bands of free and complexed SiPc. Due to the relatively high amount of uncomplexed SiPc, mixing sequence A can be neglected for further discussion.

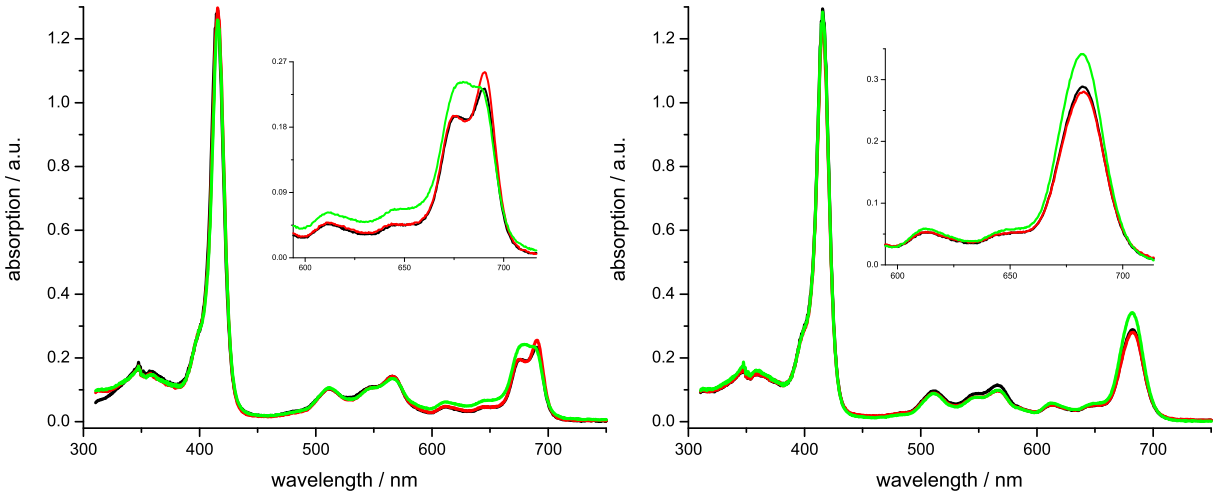

(a) Mixture **1** **(b)** Mixture **2**

Figure 6.12: UV/Vis absorption spectra of **1** (a) and **2** (b) mixtures at different mixing sequences of SiPc, SubPc and TPPS. The concentration of the molecules was 2 μM. Insets: SiPc-part Q-band absorption around 680 nm. Sequences A, B and C are depicted by the green, red and black graphs, respectively.

In UV/Vis absorption spectra the self-assembly between TPPS and SiPc moieties is visible due to the interactions between TPPS and SiPc that cause changes in absorbance. The SubPc-part of the UV/Vis absorption spectra is not affected upon complexation with TPPS. For this reason, the mixing sequence does not affect the UV/Vis absorption spectrum of SubPc.

Since the fluorescence quenching of SubPc is dependent on the complexation with TPPS, fluorescence experiments have been carried out to investigate the influence on the mixing sequence. Figure 6.13 shows the steady-state fluorescence spectra of the different mixing sequences upon excitation of SubPc at 532 nm.

As can be seen from figure 6.13, the fluorescence intensity of the SubPc moiety depends on the mixing sequence. For all mixtures, fluorescence quenching of SubPc is most effective for sequence C, followed by sequences B and A. Interestingly, the fluorescence behaviour of the TPPS and SiPc parts does not change significantly. Energy and electron transfer processes are responsible for the quenching of the first excited singlet state of the SubPc moiety [171]. These transfer processes can only take place when SubPc is in close proximity to TPPS and SiPc. From this it is concluded that the yield of formation of SubPc-TPPS-SiPc ternary complexes is the largest for mixing sequence C. In this way, TPPS is able to link SubPc and SiPc most effectively. It correlates well with the above-made considerations. All samples in this thesis have been prepared using this protocol.

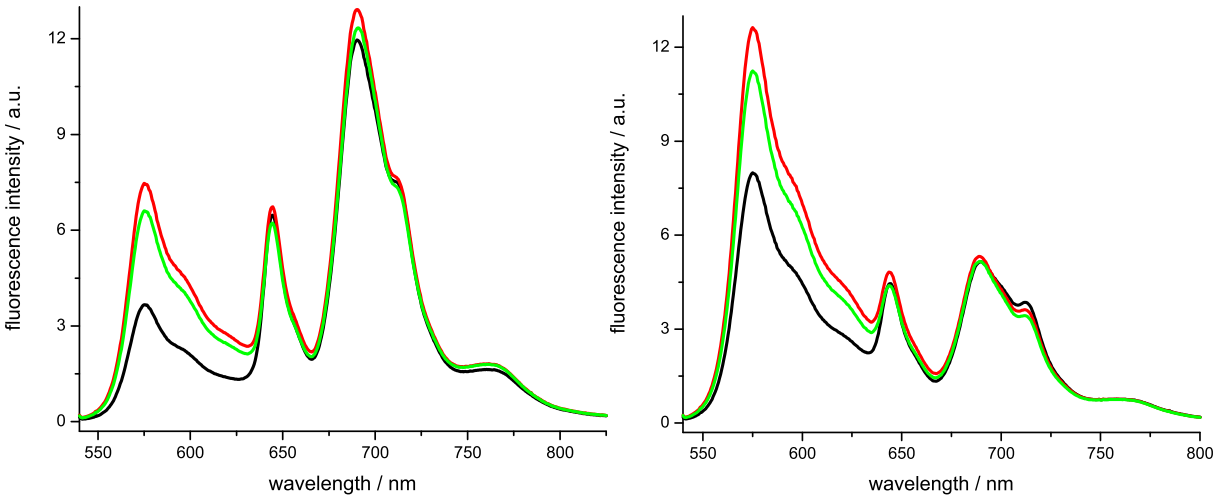

(a) Mixture **2** **(b)** Mixture **3**

Figure 6.13: Fluorescence spectra of **2** (a) and **3** (b) mixtures at different mixing sequences of SiPc, SubPc and TPPS upon selective excitation of SubPc at 532 nm. Sequences A, B and C are depicted by the green, red and black graphs, respectively. The concentration of the molecules was 1 μM.

In summary, the results obtained with steady-state UV/Vis and fluorescence experiments clearly show that a ternary complex between SubPc, TPPS and SiPc is formed. This is based on the following observations:

1. The fluorescence of SiPc in presence of SubPc and TPPS upon selective excitation of SubPc is indicative of EET from the initially excited SubPc to SiPc in its ground state. It provides evidence of the formation of a ternary SubPc-TPPS-SiPc supramolecular assembly, since the concentrations used (1 μM) are too small to facilitate EET between uncomplexed chromophores.

2. The large association constants demonstrate the spontaneous formation of SubPc-TPPS-SiPc complexes in aqueous solution.

3. The fact that the mixing sequence plays a role provides additional evidence of the formation of ternary complexes.

6.2 Excited-state dynamics of the self-assembled systems

To gain more insight into the transfer processes involved and the fate of the excited states after absorption of light, time-resolved experiments have been performed. The time-resolved experiments also corroborate the formation of host-guest-host supramolecular complexes. The efficiency of ternary complex formation can be determined by combining the results of steady-state and time-resolved experiments and will be estimated below (page 119).

6.2.1 Time-resolved fluorescence

The fluorescence decay of the supramolecular complexes as well as the corresponding reference compounds was measured upon selective excitation at the SubPc-, Por- or Pc-part using decay associated fluorescence (DAF) spectroscopy and TCSPC. The fluorescence lifetimes of the separate monomeric compounds were all found to be mono-exponential in aqueous solution. The fluorescence lifetimes of SubPc, TPPS and SiPcs were determined to be 2.05 ns, 9.9 ns and ∼5 ns, respectively, and are summarized in table 6.4.

Table 6.4: Fluorescence lifetimes of the supramolecular complexes and the reference compounds.

Compound	$\tau_{fl} \pm 0.02$ **[ns]**		
	SubPc-part	**TPPS-part**	**SiPc-part**
SubPc	2.05	-	-
TPPS	-	9.9	-
SiPc1	-	-	5.16
SiPc2	-	-	5.35
SiPc3	-	-	5.58
1	0.029 2.04	0.014 13.2	0.043 4.8
2	0.046 2.05	0.021 12.7	4.2
3	0.033 2.06	0.023 12.8	0.15 3.8

The DAF spectra of **2** upon selective excitation of SiPc, TPPS and SubPc are shown in figure 6.14.

Excitation of **2** at 620 nm (SiPc-part excitation) results in a mono-exponential fluorescence decay of 4.5 ns. This lifetime is somewhat reduced compared to the lifetime of reference SiPc2 of 5.35 ns. The spectral position as well as the shape of the DAF spectrum are similar to the corresponding steady-state fluorescence spectrum.

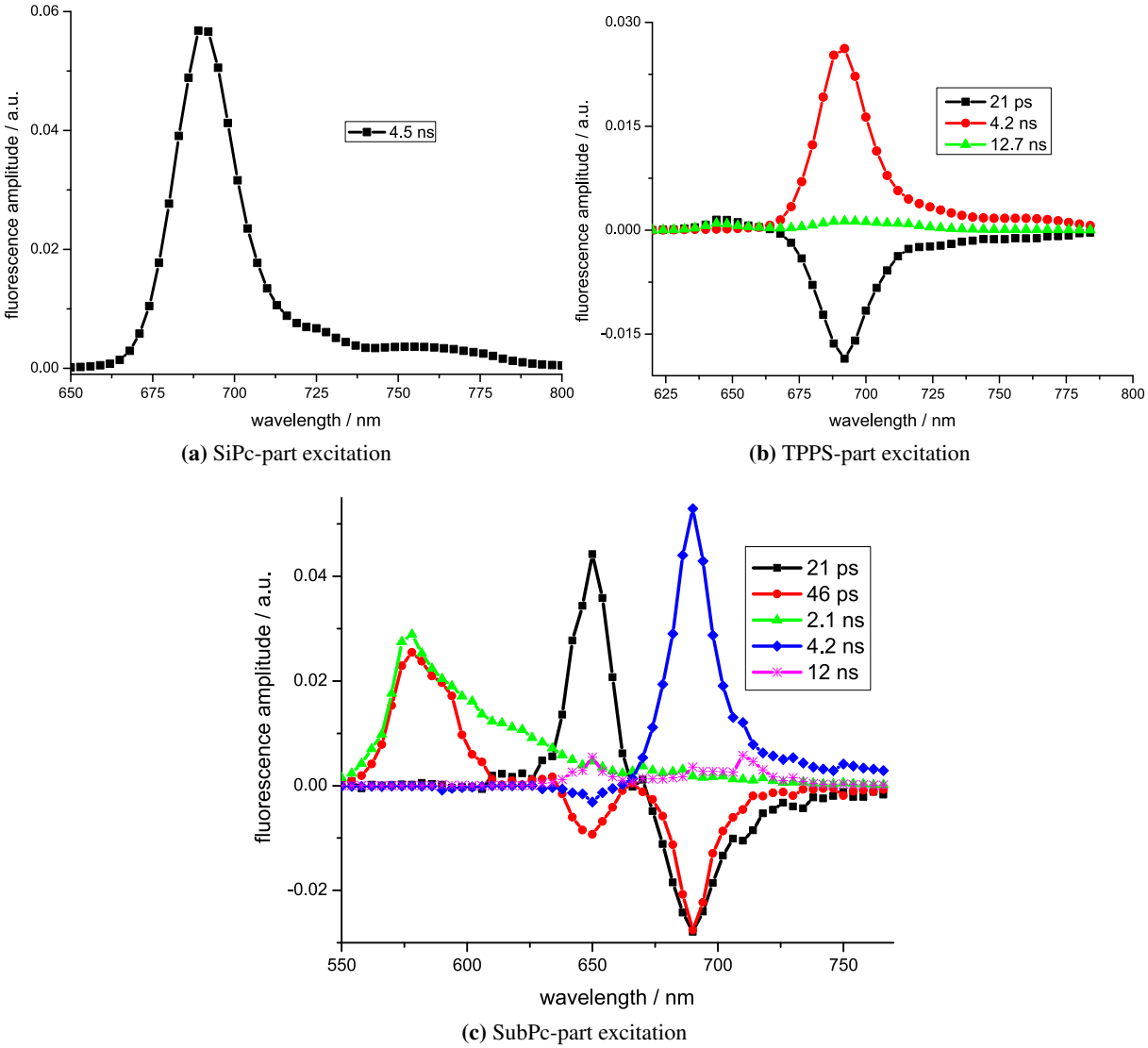

(a) SiPc-part excitation

(b) TPPS-part excitation

(c) SubPc-part excitation

Figure 6.14: DAF spectra of **2** upon excitation of SiPc at 620 nm (a), TPPS at 400 nm (b) and SuPc at 532 nm (c). The concentration of each component in the complex was 1 μM.

Following TPPS-part excitation of the same complex at 400 nm three lifetimes of 21 ps, 4.2 ns and 12.7 ns are obtained. The fast component has positive amplitude at TPPS emission, but becomes negative in the spectral region of SiPc-part fluorescence. This negative amplitude means a rise in fluorescence and therefore, it can be assigned to EET from the initially excited TPPS to the SiPc2 moiety in its ground state. The 4.2 ns and 12.7 ns lifetimes belong to the fluorescence of the SiPc-part and a small amount of free TPPS, respectively.

The analysis of the time-resolved fluorescence of complex **2** upon selective excitation of SubPc at 532 nm turned out to be delicate. The fluorescence kinetics of **2** are best described by a penta-exponential decay with decay times of 21 ps, 46 ps, 2.1 ns, 4.2 ns and 12 ns, see figure 6.14c. The latter two decay

components belong to the fluorescence of the SiPc-part and small amounts of free TPPS, respectively. The fluorescence decay of the SubPc-part has two components: a slow one (2.1 ns) that is similar to the fluorescence of free SubPc, and a fast decay of 46 ps. The latter has negative amplitude in the spectral regions of TPPS and SiPc emission and this fact supports the occurrence of EET in the supramolecular complex from the initially photo-excited SubPc to TPPS as well as SiPc moieties in the ground state. Furthermore, similar to the case of Por-part excitation, a fast decay component of 21 ps with positive amplitude in the region of TPPS fluorescence and negative amplitude at SiPc-part emission was resolved. This decay time could be associated to EET from the Por- to the Pc-part of the complex.

The DAF spectra of complexes **1** and **3** upon excitation of SiPc and TPPS are shown in figure 6.15.

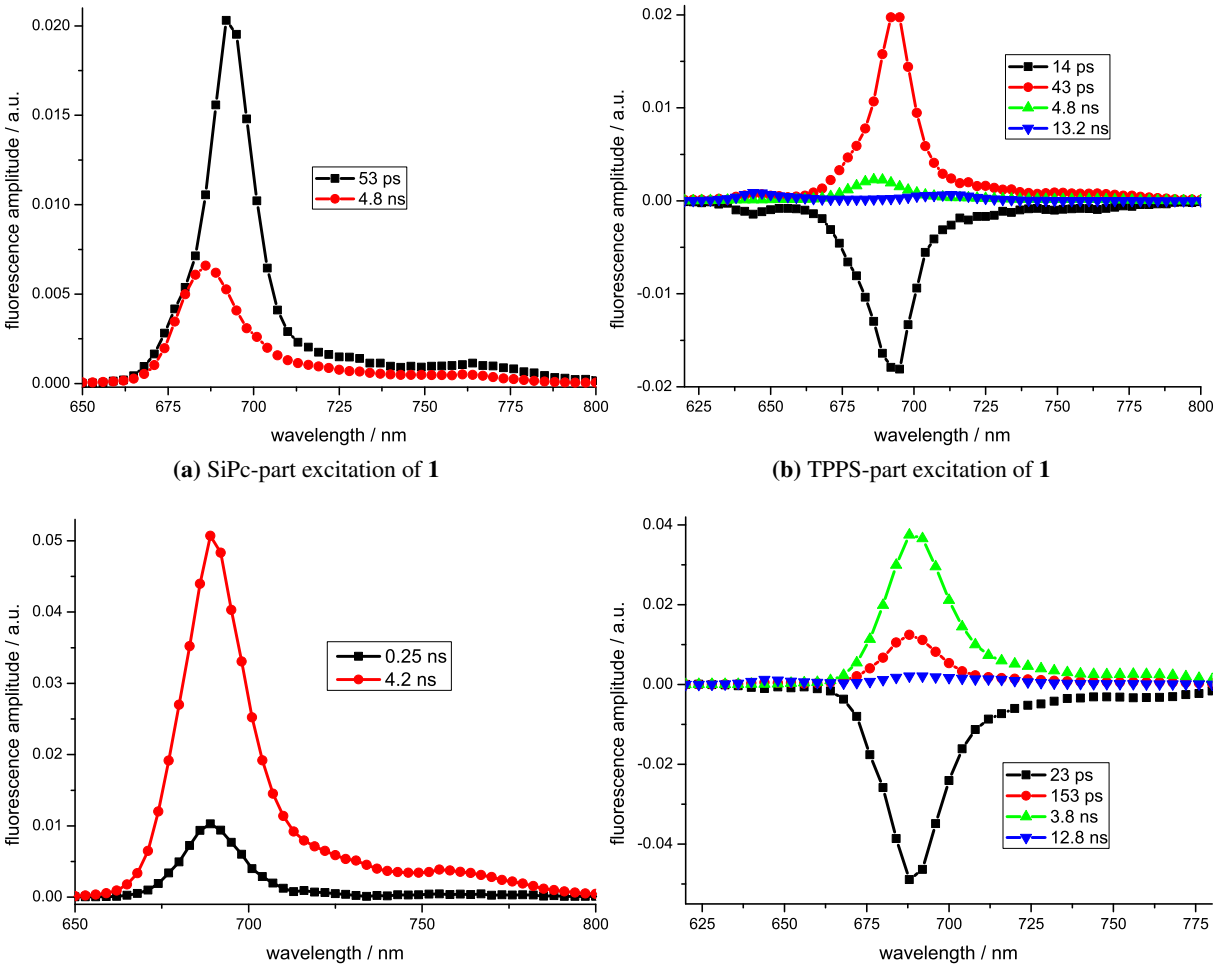

(a) SiPc-part excitation of **1**

(b) TPPS-part excitation of **1**

(c) SiPc-part excitation of **3**

(d) TPPS-part excitation of **3**

Figure 6.15: DAF spectra of the **1** (a,b) and **3** (c,d) complexes upon excitation of SiPc (a,c) and TPPS (b,d). The concentration of the components was 1 μM.

The time-resolved emission properties of the **1** and **3** complexes are more complicated than that of **2**. For both complexes the fluorescence of the SiPc-part decays bi-exponentially upon direct excitation of the SiPc moiety. For **1** a fast decay time of 53 ps and a slow decay time of 4.8 ns are observed. The emission decay of **3** occurs with 4.2 ns and 0.25 ns lifetimes. Note that the 3.8 ns decay time of **3** is somewhat reduced, compared with the fluorescence lifetime of 5.58 ns of free SiPc3. For **3** both the fast and slow components have a common maximum at 689 nm. Note that the fluorescence maximum of reference SiPc3 is at 680 nm. On the contrary, the fast component of **1** has its maximum at 694 nm, the slow one at 686 nm. At this point it is noted that the emission maximum of free SiPc1 lies at 686 nm, too (*cf.* table 6.1). For this reason, the long-lived component of **1** can be attributed to small amounts of uncomplexed SiPc1.

Selective excitation of TPPS at 400 nm results for both **1** and **3** in a tetra-exponential fluorescence decay. The following decay times were obtained for complex **1**: 14 ps, 43 ps, 4.8 ns and 13.2 ns. The latter decay time of 13.2 ns can be assigned to small amounts of free TPPS. The 14 ps component has strongly negative amplitude in the region of SiPc-emission and can therefore be attributed to energy transfer from TPPS to SiPc1. The shape of the remaining 43 ps and 4.8 ns components is typical for phthalocyanine emission spectra. Complex **3** behaved similarly showing a fast TPPS decay time with negative amplitude in the spectral region of SiPc-part emission, a slow 12.8 ns component that can be ascribed to free TPPS and two different SiPc lifetimes of 0.15 ns and 3.8 ns. Both lifetimes are shorter than the fluorescence decay time of 5.58 ns of reference SiPc3.

As shown above, an additional decay component that is addressed to the fluorescence of SiPc was resolved for the complexes **1** and **3** upon excitation of the Pc- or Por-part compared to the DAF spectra of complex **2**. It is expected that DAF of **1** and **3** upon excitation of the SubPc-part should have at least six components, thus making analysis very complicate. The calculated lifetimes as well as the amplitudes of the corresponding decay components could be error-prone. For this reason, the fluorescence decay of **1** and **3** was measured at fixed registration wavelength of 575 nm, where the emission spectrum of the SubPc moiety has its maximum. It is noted that contributions of SiPc as well as TPPS to the fluorescence signal at this detection wavelength are negligible. The decay of the SubPc-part fluorescence was fitted as a double exponential function and a fast decay time of 29 ps (**1**) and 33 ps (**3**) and a slow one of 2.05 ns (similar for both complexes) were resolved. The latter component has small amplitude and it could be assigned to a marginal amount of free SubPc in aqueous solution.

6.2.2 Transient absorption

The final part of the investigations focusses on TA measurements to confirm the aforementioned formation of ternary complexes and to investigate possible charge-separated states and triplet states.

As expected, the repopulation of the ground state of the monomeric references occurred mono-exponentially with recovery times that were consistent with their fluorescence lifetimes. The intersystem crossing quantum yields Φ_{ISC} of the free SiPc compounds were estimated to be 0.40, 0.38 and 0.40 for SiPc1, SiPc2 and SiPc3, respectively.

The recovery times of the SiPc bleaching signals, as well as the intersystem crossing quantum yields are summarized in table 6.5.

Table 6.5: SiPc ground state recovery times τ_{rec} and intersystem crossing quantum yields Φ_{ISC} of the SiPc-part.

Compound	$\boldsymbol{\tau_{rec}}$ **[ns]**	$\boldsymbol{\Phi_{ISC} \pm 0.03}$
SiPc1	5.2 ± 0.2	0.40
SiPc2	5.4 ± 0.2	0.38
SiPc3	5.5 ± 0.2	0.40
1	1.7 ± 0.1 0.100 ± 0.010	0.06
2	4.2 ± 0.3	0.27
3	3.8 ± 0.3 0.120 ± 0.010	0.10

The TA spectra of the supramolecular complex **1** following excitation of its parts are shown in figure 6.16.

Upon excitation of **1** at 615 nm, a strong bleaching signal at 692 nm which originates from the SiPc-part of the supramolecular complex, apparent from its spectral position and shape, is observed. The bleach reaches its minimum directly after excitation at 50 ps delay. As time progresses, the signal decreases and its minimum is shifted hypsochromically to 680 nm. The recovery of the SiPc ground state population obeys bi-exponential kinetics with 100 ± 10 ps and 1.7 ± 0.1 ns as time constants and both components have equal amplitudes. It is noted that these recovery times differ from the fluorescence lifetime of 43 ps as obtained with the TCSPC experiment. The spectra exhibit a transient feature, the maximum of which is located at 580 nm. This transient signature is not discernible for the reference SiPc1. The same characteristics were observed upon TPPS-part excitation at 420 nm. Following TPPS excitation the bleach at 692 nm minimizes at 80 ps delay, thus confirming the EET process from the initially excited TPPS to SiPc in its ground state. In addition, weak TPPS-part bleaching is observed at 515 nm.

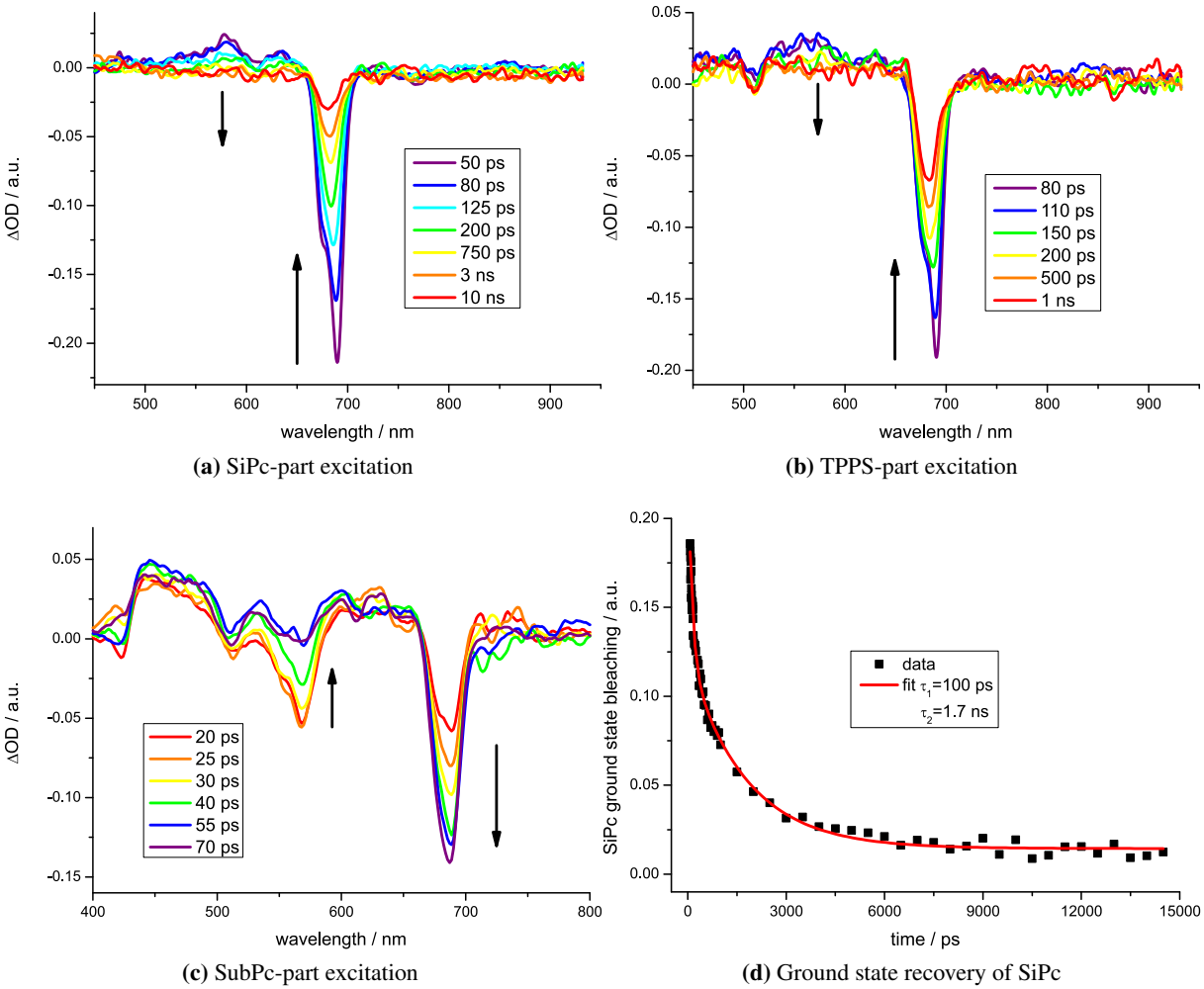

(a) SiPc-part excitation

(b) TPPS-part excitation

(c) SubPc-part excitation

(d) Ground state recovery of SiPc

Figure 6.16: TA spectra of complex **1** upon excitation of its parts at different delay times. The kinetics of the SiPc bleach is shown in (d). The concentration of each moiety was 10 μM.

Upon excitation of **1** at 550 nm (SubPc-part excitation), the TA spectra exhibit two distinct ΔOD features at 570 nm and at 690 nm. The former resembles SubPc-part absorption and the latter could be assigned to ground state bleaching of SiPc. The build-up of the ΔOD signal at 690 nm has the same rate as the decay of the SubPc ground state bleaching at 570 nm of 40 $\pm$ 10 ps, indicating that the quenching of SubPc leads to the subsequent depletion of the SiPc ground state population. This supports the sequential energy transfer processes from the photo-excited SubPc to SiPc in its ground state, obviously involving TPPS as mediator. The bleaching at 515 nm and transient absorption in the region 450-500 nm are typical ΔOD signals of TPPS.

Independent on the excitation wavelength ground state bleaching of the SiPc-part is still discernible at 15 ns delay after excitation, which is ascribed to the formation of the triplet state ^{3}SiPc*. The quantum yield of triplet state formation is rather small and its value is determined to be 0.06.

In figure 6.17, the TA spectra of complex **2** are shown.

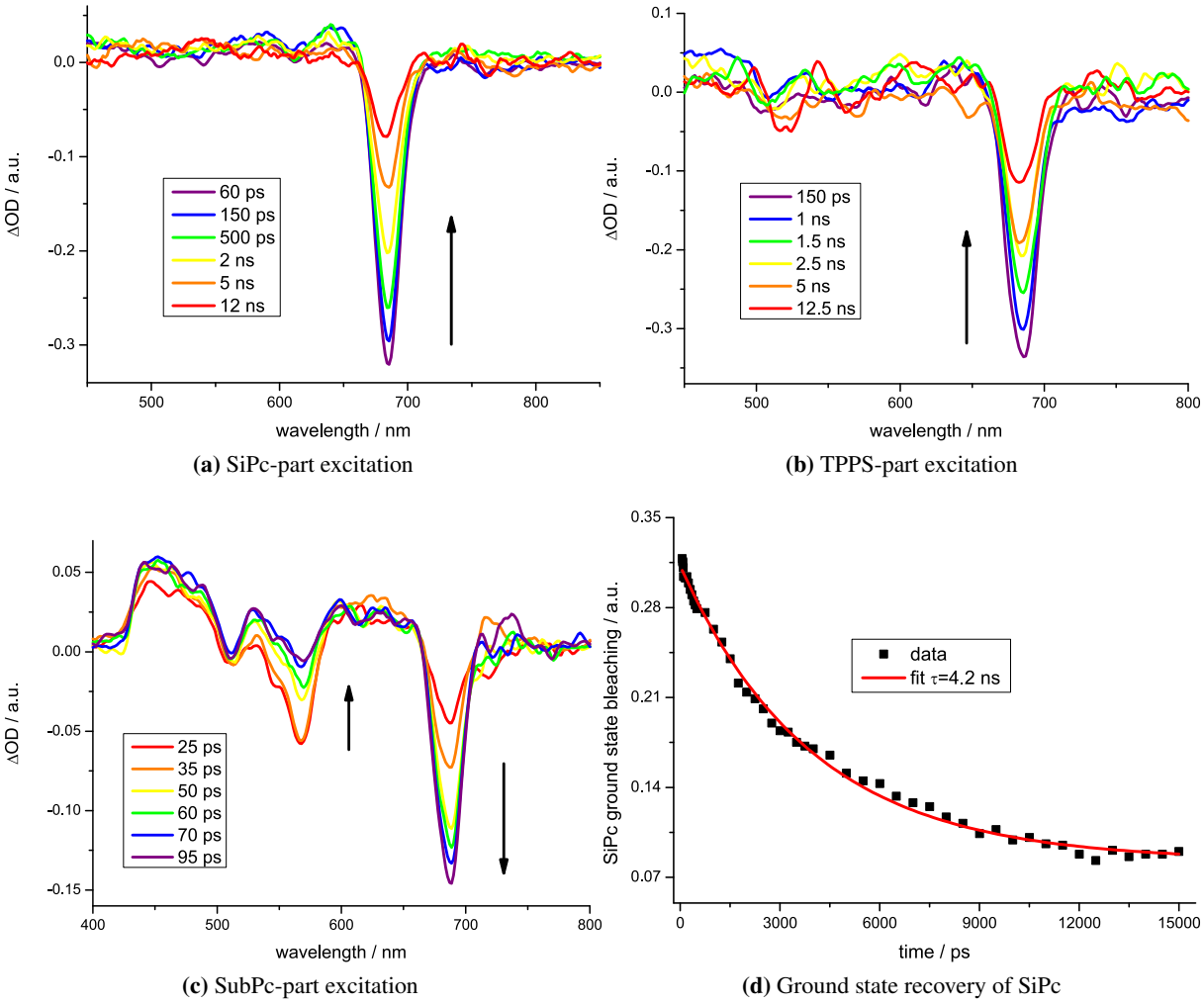

(a) SiPc-part excitation

(b) TPPS-part excitation

(c) SubPc-part excitation

(d) Ground state recovery of SiPc

Figure 6.17: TA spectra of **2** upon excitation of its parts at different delay times. The kinetics of the SiPc bleach is shown in (d). The concentration of each moiety was 10 μM.

Following SiPc-part excitation at 615 nm, strong bleaching is observed at 685 nm, which is addressed to the depletion of the SiPc-part ground state population. Except for small bathochromic shifts, the picosecond TA spectra of the supramolecular complex **2** are reminiscent of those of reference SiPc2.

Upon excitation of the Por-part at 420 nm a strong negative ΔOD signal at 685 nm that belongs to SiPc-part bleaching underlines the effective EET process from TPPS to SiPc. The TA spectra after excitation of TPPS are similar to the TA spectra following excitation of SiPc.

The TA spectra of **2** upon excitation of SubPc at 550 nm are shown in figure 6.17c. Two distinct ΔOD minima at 570 nm and 686 nm predominate the TA spectra. The former belongs to ground state bleaching of SubPc and the latter to ground state bleaching of SiPc. In addition, TPPS ground state bleaching at 515 nm and transient absorption at 450 nm are observed. The ΔOD signal of the SubPc-part

decreases with a time constant of 40 ± 10 ps, while at the same time the SiPc ΔOD signal increases. This means that the SubPc ground state is recovered and the SiPc ground state is depleted during the same time interval. Due to the fast deactivation of TPPS, the SiPc ground state depletion follows the recovery of the SubPc ground state.

When shedding light onto the excited state dynamics of complex **2**, it was found that the SiPc-part bleaching signal decays mono-exponentially with a characteristic time of 4.2 ± 0.3 ns. This decay is independent of the excitation wavelength; moreover, it is similar to the lifetime of the first excited singlet state of the SiPc moiety determined by time-resolved fluorescence experiments (*cf.* table 6.4).

Upon selective excitation of SiPc the ΔOD signal around 686 nm has its minimum directly after excitation at 60 ps, while upon TPPS-part excitation its minimum is reached at 80 ps. This 20 ps delay underlines the EET from TPPS to SiPc. The ΔOD signal of the SiPc-part at SubPc-part excitation minimizes at a delay time of 100 ps. From this, it follows that sequential hopping EET occurs from the photo-excited SubPc to TPPS and from TPPS to SiPc in its ground state. For complex **2** the value of Φ_{ISC} was obtained as 0.27.

The TA spectra of complex **3** are presented in figure 6.18.

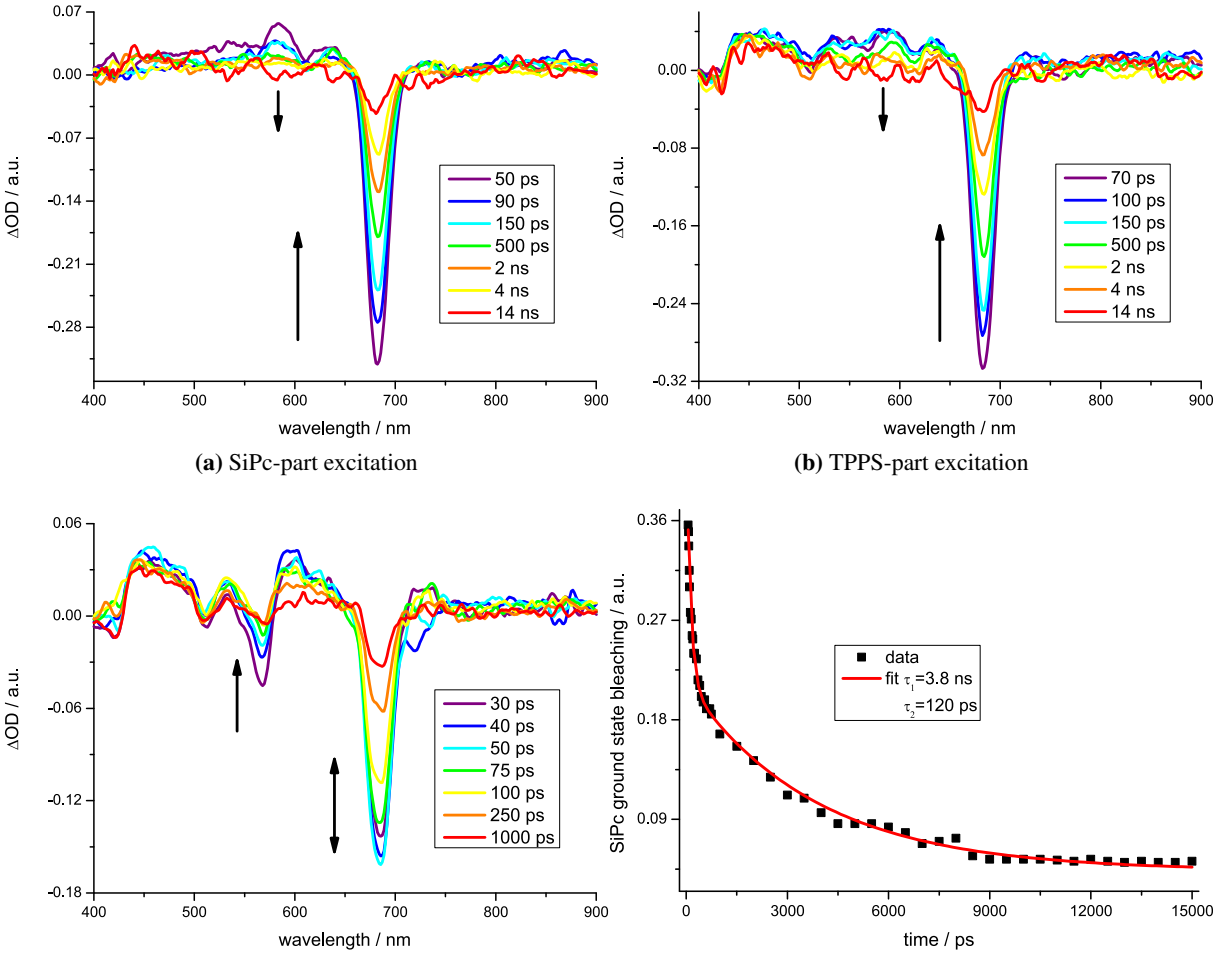

(a) SiPc-part excitation

(b) TPPS-part excitation

(c) SubPc-part excitation

(d) Ground state recovery of SiPc

Figure 6.18: TA spectra of **3** upon excitation of its parts at different delay times. The kinetics of the SiPc bleach is shown in (d). The concentration of each moiety was 10 μM.

For complex **3** similar spectral features were observed as for complex **1**. Following SiPc-, TPPS- and SubPc-part excitation the TA spectra of **3** show induced absorption at 580 nm and strong bleaching in the region where SiPc absorbs. The recovery of the SiPc ground state population occurred bi-exponentially with characteristic times of 120 $\pm$ 10 ps and 3.8 $\pm$ 0.2 ns, irrespective of the initially excited moiety. The amplitudes of these decay times were found to be equal to each other. It is noted that the 3.8 ns component is similar to the lifetime of the first excited singlet state of the SiPc-part obtained with the TCSPC experiment (table 6.4). Upon excitation of the SubPc unit at 550 nm the simultaneous decrease and increase of SubPc- and SiPc-part ground state depletion signals is observed as it occurs for complexes **1** and **2**. The decay of the SubPc ground state depletion was measured to be 40 $\pm$ 10 ps.

At 15 ns delay time still SiPc-part bleaching is observed and the ISC quantum yield of the SiPc moiety was found to be 0.10.

6.3 Discussion of the photophysical properties of the self-assembled systems

6.3.1 Excitation energy transfer

In previous work it was found that in a 2:1 SubPc-TPPS supramolecular complex efficient energy transfer follows excitation of the SubPc moiety [171]. Moreover, it has been shown that EET has high probability in 1:1 SiPc-TPPS host-guest complexes [77]. For this reason, it is reasonable to assume that EET plays an important role in the depopulation of the first excited singlet states of SubPc and TPPS moieties in the SubPc-TPPS-SiPc ternary complexes, too. This was firstly demonstrated for complex **2** in a recent study [151] and is outlined below in more detail for complexes **1**, **2** and **3**.

The assumption is supported by the appearance of TPPS and SiPc fluorescence after excitation of the SubPc moiety, - it is clear that energy is transferred from SubPc to TPPS and SiPc. Two mechanisms of EET that could be relevant under the described experimental conditions exist: FRET or Dexter exchange energy transfer. For the Dexter energy transfer mechanism an essential condition is the effective overlap of the relevant molecular orbitals of donor and acceptor molecules. The probability of an effective energy transfer falls rapidly with increasing distance between the participating molecules. In complexes **1**, **2** and **3** the CD nano-cavities prevent the molecules from stacking and therefore, the probability of close contact is nearly zero. For this reason, FRET is assumed to be the dominant EET mechanism.

The efficiency of FRET can be described by its Förster radius R_0 and the Förster radii of different donor-acceptor combinations are summarized in table 6.6. The spectral overlap between the donor's emission and the acceptor's absorption for the different donor-acceptor combinations is shown in figure 11 (appendix).

Table 6.6: Förster radii R_0 of different donor-acceptor combinations.

Donor-Acceptor	$\boldsymbol{R_0}$ **[Å]**
SubPc-TPPS	34
SubPc-SiPc1	19
SubPc-SiPc2	20
SubPc-SiPc3	19
TPPS-SiPc1	52
TPPS-SiPc2	52
TPPS-SiPc3	51

With equation 3.34 and the calculated values of R_0, the critical acceptor concentration can be calculated below which the efficiency of EET between two free, randomly distributed molecules in solution drops dramatically [65]. For the different energy donor-acceptor combinations A_0 varies from 3.2 mM (TPPS-SiPc) and 11 mM (SubPc-TPPS) to 65 mM (SubPc-SiPc). The concentrations used in fluorescence experiments did not exceed 2 μM, in TAS experiments the concentration of the chromophores was not higher than 10 μM. Hence, one can exclude the probability of EET between free molecules in

solution. It follows that the molecules have to be in close proximity. The EET from SubPc to SiPc is therefore strong evidence of the formation of a ternary supramolecular assembly. The sequential hopping transfer is nicely seen in the pump-probe experiments.

From table 6.1 it can be seen that the fluorescence quantum yield of the SiPc-part of the complexes depends on the initially excited moiety. E.g. for complex **2** the SiPc-part fluorescence quantum yields amount to 0.32, 0.16 and 0.027 following selective excitation of SiPc, TPPS and SubPc, respectively. Obviously, the sequential energy transfer processes do not proceed with unity quantum yields. As was reported in [171], EET from the photo-excited SubPc to TPPS occurs with a probability of 0.38. The EET process from the photo-excited TPPS to SiPc has a probability of around 0.5 [77], i.e. it is assumed that several relaxation pathways are introduced (electron transfer, enhanced internal conversion etc.) in the energy transfer pathway from SubPc to TPPS and subsequently to SiPc in the ternary supramolecular complexes. As a result, the fluorescence quantum yield of the SiPc-part following SubPc-part excitation is lower than in the case of direct excitation of the SiPc moiety. By comparing the experimental data obtained in the previous studies one can carry out estimations to calculate the efficiency of EET from SubPc to SiPc. The fluorescence quantum yield of SiPc in the host-guest-host complex at SubPc-part excitation $\Phi_{fl}^{Pc}(\text{SubPc})$ can be expressed as

$$\Phi_{fl}^{Pc}(\text{SubPc}) = \Phi_{EET}(\text{SubPc} \rightarrow \text{Por})\Phi_{EET}(\text{Por} \rightarrow \text{Pc})\Phi_{fl}^{Pc}(\text{Pc})\Psi \tag{6.2}$$

Here $\Phi_{EET}(\text{SubPc} \rightarrow \text{Por})$ and $\Phi_{EET}(\text{Por} \rightarrow \text{Pc})$ are the energy transfer probabilities from SubPc to TPPS and from TPPS to SiPc, respectively, $\Phi_{fl}^{Pc}(\text{Pc})$ is the fluorescence quantum yield of the SiPc-part of the complex upon excitation of SiPc and Ψ the probability of ternary complex formation. The latter has a value of 0.81 and 0.71 for complex **2** and **3**, respectively. The calculation of the probability Ψ is described below (see section 6.3.3). For the complexes **2** and **3** the calculated SiPc-part fluorescence quantum yields following SubPc-part excitation amount to 0.049 and 0.027, respectively. These values are somewhat higher than the fluorescence quantum yields of 0.027 and 0.010 obtained in the experiment. However, the calculated values lie in the same order of magnitude as the measured ones. It is expected that the EET efficiency can be increased by rational tuning of the system, e.g. by using dyes with higher fluorescence quantum yields.

6.3.2 Charge transfer

It was shown in [171] that electron transfer takes place in the 2:1 SubPc-TPPS supramolecular complex from the photo-excited SubPc-part to the TPPS moiety. This charge transfer is an uphill process when TPPS is initially excited and therefore, feasible only upon excitation of SubPc. On the other hand, in the TPPS-SiPc supramolecular dimer an electron is transferred from TPPS to SiPc, regardless of which moiety was initially excited [77]. The charge transfer probability is strongly dependent on the linker between Pc and CD moieties and it was shown that ET can only take place for the TPPS-SiPc1 and TPPS-SiPc3 complexes. Hence, it is postulated that the aforementioned electron transfer processes occur in the ternary complexes, too. Moreover, it stands to reason to assume that in the ternary complexes an electron is transferred from SubPc to SiPc.

To reveal whether photo-induced electron transfer is an exergonic process, the change in free enthalpy was calculated using the Rehm-Weller approach (equation 3.12). The redox potentials are taken from

table 3 (appendix), the energy of the first excited state can be calculated from the absorption and fluorescence maxima in table 6.1. The radii of the formed cations and anions were estimated from molecular modelling simulation [77, 171] and are 4.0 Å, 4.3 Å and 4.6 Å, for SubPc, TPPS and SiPc, respectively. The calculated values of ΔG_0 are summarized in table 6.7.

Table 6.7: Driving force ΔG_0 for different electron donor-acceptor pairs calculated with equation 3.12. $E_{0,0}$ denotes the energy of the first excited singlet state of the initially excited moiety (SubPc, TPPS or SiPc).

Cation-anion pair	$\Delta G_0 \pm 0.05$ **[eV]**		
	$E_{0,0}$**(SubPc)**	$E_{0,0}$**(TPPS)**	$E_{0,0}$**(SiPc)**
$SubPc^{\bullet+}$-$TPPS^{\bullet-}$	-0.20	0.03	
$TPPS^{\bullet+}$-$SiPc1^{\bullet-}$		-0.34	-0.22
$TPPS^{\bullet+}$-$SiPc2^{\bullet-}$		-0.40	-0.28
$TPPS^{\bullet+}$-$SiPc3^{\bullet-}$		-0.42	-0.30
$SubPc^{\bullet+}$-$SiPc1^{\bullet-}$	-0.64		-0.29
$SubPc^{\bullet+}$-$SiPc2^{\bullet-}$	-0.70		-0.35
$SubPc^{\bullet+}$-$SiPc3^{\bullet-}$	-0.72		-0.37

From table 6.7 it follows that in addition to the aforementioned ET reactions from SubPc to TPPS and from TPPS to SiPc, ET from SubPc to SiPc is thermodynamically favourable. Before going into details of the electron transfer from SubPc to SiPc, first the ET processes from SubPc to TPPS and from TPPS to SiPc are described.

Electron transfer from SubPc to TPPS

The ET from SubPc to TPPS readily explains the relatively small fluorescence quantum yields of the SiPc-part upon excitation of SubPc (see section 6.3.1). The electron transfer has a probability of 0.62, but it is feasible only upon excitation of the SubPc moiety. This fact is supported by the value of ΔG_0, *cf.* table 6.7, that is calculated to be negative for SubPc-part excitation (-0.20 eV), while for TPPS-part excitation its value is positive (0.03 eV). Estimation of the lifetime of the charge-separated species $SubPc^{\bullet+}$-$TPPS^{\bullet-}$-SiPc was difficult, since the lifetime of the first excited singlet state as found in time-resolved fluorescence experiments ($\sim$35 ps) is very similar to the characteristic recovery time of the SubPc ground state population of 40 ps as revealed in ps-TAS experiments. The $SubPc^{\bullet+}$ radical cation absorbs light at 620 nm [116]. Therefore, it would be possible to monitor the transient signature at 620 nm to obtain the lifetime of the charge-separated state. However, the transient absorption of $SubPc^{\bullet+}$ shows overlap with the ΔOD signals of the other species formed e.g. $TPPS^{*}$, $SiPc^{*}$ and $SiPc^{\bullet-}$ which absorb at 620 nm, too. Therefore, an upper bound of the charge recombination was estimated to be 40 ps.

Electron transfer from TPPS to SiPc

According to the negative values of ΔG_0 presented in table 6.7, electron transfer from TPPS to SiPc is a downhill process irrespective of the initially excited moiety (SiPc or TPPS) and SiPc used (SiPc1, SiPc2

or SiPc3). In the DAF spectra of complexes **1** and **3** fast SiPc-part fluorescence decay times have been resolved that do not occur for the corresponding free references. Moreover, in the ΔOD spectra of **1** and **3** complexes a transient absorption band is observed at 580 nm. This band is not seen in the transient absorption spectra of the monomeric references and therefore, the transient signature can be assigned to the $SiPc^{\bullet-}$ anion which absorbs light at the corresponding wavelength [15, 75, 76, 77, 90, 91, 92].

In accordance with the previously published data [77, 173], electron transfer from TPPS to SiPc is a feasible process for complex **1**. Due to the short linker between SiPc and CD, electron transfer takes place with high probability. The 43 ps DAF component of SiPc1 emission can be attributed to charge transfer from the photo-excited SiPc1 to TPPS, i.e. SubPc-TPPS-$SiPc1^{*}$ →SubPc-$TPPS^{\bullet+}$-$SiPc1^{\bullet-}$. In ps-TAS experiments the repopulation of the SiPc-part ground state occurs bi-exponentially with lifetimes of 100 ps and 1.7 ns, whereas the fluorescence lifetime of 43 ps obtained with DAF was not observed. The former decay time is similar to the 70 ps lifetime of the charge-separated state $TPPS^{\bullet+}$-$SiPc^{\bullet-}$ that is generated in the TPPS-SiPc1 supramolecular dimer [77]. The 100 ps component can therefore be attributed to charge recombination of SubPc-$TPPS^{\bullet+}$-$SiPc^{\bullet-}$ to the ground state. It is noted that the nature of the second decay component is more complicate and will be outlined below, see page 117.

Although thermodynamically favourable, electron transfer from TPPS to SiPc does not occur for **2**. It is well-known that the rate of electron transfer falls rapidly with increasing distance between electron donor and acceptor moieties [49, 51, 53, 54]. Apparently, the distance between Pc and Por moieties is too large due to the large spacer between SiPc and CD. Electron transfer cannot compete with other deactivation processes of the first excited singlet state of the SiPc moiety such as fluorescence. For this reason, the SiPc-part of **2** shows a relatively high fluorescence quantum yield and a fluorescence lifetime, that is typical for SiPcs.

Complex **3** exhibits charge transfer from TPPS to SiPc after photo-excitation in spite of the very long tetraethylene glycol linker between SiPc and CD. This may appear contradictory. However, due to its flexible nature and the strong dipole-dipole interaction between the oxyethylene units, it is likely that two stable conformations exist in aqueous solution [77]. The extended conformer is characterized by the slow decay of SiPc3 fluorescence (τ_{fl}=3.8 ns) and high fluorescence quantum yield. On the other hand, in the folded conformer the entrapped TPPS is able to come into close proximity to SiPc3 facilitating charge transfer. This results in fast depopulation of the first excited singlet state of SiPc and is expressed by the fluorescence lifetime of 150 ps. The lifetime of the charge-separated state was estimated to be 120 ps as found by ps-TAS experiments. The amplitudes of the SiPc ground state recovery times can be associated to the relative abundances of the folded and extended conformers, 0.5 each.

Electron transfer from SubPc to SiPc

As obtained from ps-TAS experiments, the SiPc-part ground state of complex **1** repopulates bi-exponentially with characteristic times of 100 ps and 1.7 ns (amplitudes of both components are 0.5). The ground state recovery of the SiPc-part of complex **3** occurs bi-exponentially with amplitudes of 0.5 for each component, too. However, the SiPc-part fluorescence is clearly observed for **3**, whereas for **1** the SiPc-part fluorescence is strongly quenched. Furthermore, the 1.7 ns component is observed neither in time-resolved fluorescence experiments nor for the ground state recovery of the TPPS-SiPc1 binary complex [77]. It is therefore assumed that the charge-separated state $SubPc^{\bullet+}$-TPPS-$SiPc^{\bullet-}$ is generated. This is supported by the driving force ΔG_0 (table 6.7), furthermore the energy of this state lies below the energies of the other charge-separated states $SubPc^{\bullet+}$-$TPPS^{\bullet-}$-SiPc and SubPc-$TPPS^{\bullet+}$-$SiPc^{\bullet-}$, see figure 6.19.

As a result, a sequential electron transfer from TPPS to SiPc and subsequently from SubPc to TPPS is thermodynamically favourable.

The 1.7 ns decay time is associated with the charge recombination to the ground state SubPc$^{\bullet+}$-TPPS-SiPc$^{\bullet-}$→SubPc-TPPS-SiPc. The difference in charge recombination rates of SubPc-TPPS$^{\bullet+}$-SiPc$^{\bullet-}$→SubPc-TPPS-SiPc (100 ps) and SubPc$^{\bullet+}$-TPPS$^{\bullet-}$-SiPc→SubPc-TPPS-SiPc (<40 ps) can be attributed to the increased distance between the charge-separated species. The separation between the radical cation and the radical anion is expected to be larger in SubPc$^{\bullet+}$-TPPS-SiPc$^{\bullet-}$ compared to that of SubPc-TPPS$^{\bullet+}$-SiPc$^{\bullet-}$ and SubPc$^{\bullet+}$-TPPS$^{\bullet-}$-SiPc. Therefore, charge recombination occurs with a slower rate for the former. The electron and energy transfer processes that occur in complex **1** are summarized in figure 6.19.

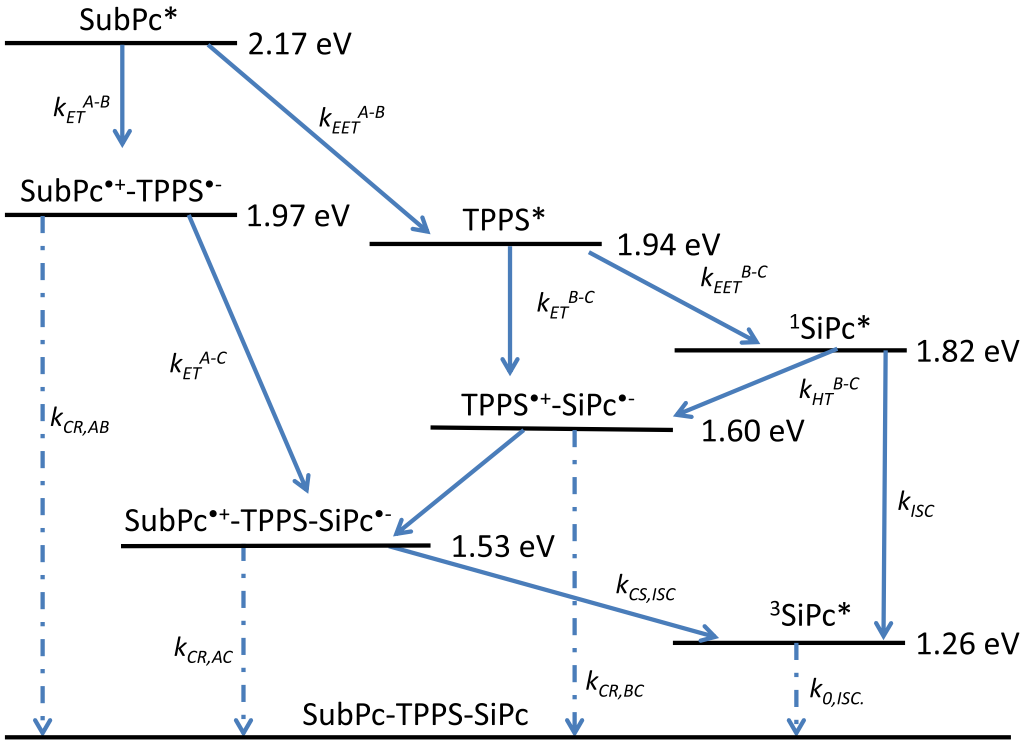

Figure 6.19: Main energy and electron transfer processes in the self-assembled ternary SubPc-TPPS-SiPc1 complex. For clarity, A, B and C denote SubPc, TPPS and SiPc, respectively.

It is clear that SubPc$^{\bullet+}$-TPPS-SiPc$^{\bullet-}$ can only be generated if electron transfer from TPPS to SiPc is feasible. Therefore, for complex **2** this transfer is not likely to occur due to the increased separation between electron donor and acceptor. For the folded conformer of complex **3** it is assumed that this charge transfer also takes place. However, its probability is expected to be small.

For complex **1** even at 15 ns delay after excitation ground state depletion of the SiPc moiety is observed in the TA spectra (see figure 6.16). The energy of the first excited triplet state of SiPc is 1.26 eV [85, 86, 87, 88], which is less than 1.53 eV (energy of SubPc$^{\bullet+}$-TPPS-SiPc$^{\bullet-}$, *cf.* figure 6.19). For this reason, it is reasonable to assume that the SiPc-part triplet state is generated. The relatively slow charge

recombination of 1.7 ns renders the charge recombination to the triplet state ^{3}SiPc* possible, which usually occurs within some nanoseconds [86].

6.3.3 Determination of the self-assembly efficiency

The fluorescence lifetime of the SiPc-part of **2** is slightly reduced compared to the decay time of monomeric SiPc2. It is caused by weak interactions between TPPS and SiPc2 in the self-assembled complex. As a matter of fact, one can carry out estimations as follows:

$$\Phi^x_{fl}(\text{complex}) = \Phi^x_{fl}(\text{free})\frac{\tau^x_{fl}(\text{complex})}{\tau^x_{fl}(\text{free})} \tag{6.3}$$

where Φ^x_{fl}(complex) is the calculated fluorescence quantum yield of the complexed moiety x, and Φ^x_{fl}(free) is the fluorescence quantum yield of free x, τ^x_{fl}(complex) and τ^x_{fl}(free) are fluorescence lifetimes of moiety x in the supramolecular complex and free in aqueous solution, respectively. With the values from tables 6.1 and 6.4, τ^x_{fl}(complex)=4.2 ns, τ^x_{fl}(free)=5.35 ns and Φ^x_{fl}(free)=0.40, the fluorescence quantum yield of complexed SiPc2 is estimated to be 0.31. This is in good agreement with the measured value of 0.32 obtained by steady-state fluorescence spectroscopy. A similar reduction was found for the intersystem crossing quantum yield: Φ_{ISC}=0.38 for free SiPc2, Φ_{ISC}=0.27 for **2**. This indicates enhanced probability of radiationless transitions from the excited singlet state to the ground state $S_1 \rightarrow S_0$, since both fluorescence and intersystem crossing are affected roughly in the same way. The same behaviour is observed for **3**: the ISC quantum yield and the fluorescence quantum yield of **3** are 0.10 and 0.21, respectively, compared to Φ_{ISC}=0.40 and Φ_{fl}=0.49 for reference SiPc3. This means that charge recombination SubPc-TPPS$^{\bullet+}$-SiPc3$^{\bullet-}$ $\rightarrow$ SubPc-TPPS-SiPc3 occurs without touching a triplet state, since Φ_{fl} and Φ_{ISC} are quenched similarly.

Combining the results obtained with steady-state and time-resolved fluorescence, one can estimate the degree of self-assembly. The measured fluorescence quantum yield is a superposition of the fluorescence quantum yields of free SiPc and complexed SiPc:

$$\Phi^x_{fl}(\text{measured}) = q \cdot \Phi^x_{fl}(\text{complex}) + (1-q)\Phi^x_{fl}(\text{free}) \tag{6.4}$$

where q is the ratio of complexation, x is the complexed moiety, Φ^x_{fl}(measured) is the measured fluorescence quantum yield and Φ^x_{fl}(free) is the fluorescence quantum yield of the uncomplexed moiety x. By using these equations with the corresponding values of the SiPc moieties, for **1** and **2** very high degrees of self-assembly have been found, 0.94 and 0.89 respectively. This means that 94% of all SiPc1 molecules and 89% of all SiPc2 molecules are incorporated in a supramolecular complex with TPPS. Hence, self-assembly is very efficient.

For **3** the estimation of Φ^{SiPc3}_{fl}(complex) is more complicated. Two conformers exist, whose time-resolved emission properties differ from each other. The lifetimes amount to 0.15 ns and 3.8 ns for the folded and extended conformers, respectively. Using equation 6.3, with Φ^{SiPc3}_{fl}(free)=0.49, τ^{SiPc3}_{fl}(free)= 5.58 ns, and τ^{SiPc3}_{fl}(complex)=3.8 ns, one obtains a fluorescence quantum yield Φ^{SiPc3}_{fl}(complex)=0.33. However, this does not take into account the electron transfer that is responsible for the reduced fluorescence lifetime of 0.15 ns. Assuming on the other hand that only electron transfer occurs, then the

fluorescence quantum yield calculated with equation 6.3 turns out to be Φ_{fl}^{SiPc3}(complex)=0.013. The measured fluorescence quantum yield is 0.21. Apparently, both processes compete with each other. For this reason, equation 6.3 is extended to

$$\Phi_{fl}^{x}(\text{complex}) = \Phi_{fl}^{x}(\text{free}) \left\{ r \cdot \frac{\tau_1}{\tau_{fl}^{x}(\text{free})} + (1-r) \frac{\tau_2}{\tau_{fl}^{x}(\text{free})} \right\} \tag{6.5}$$

where τ_1 is the fluorescence lifetime of the folded conformer, 0.15 ns, τ_2 is the fluorescence lifetime of the extended conformer, 3.8 ns, r is the percentage of molecules that are folded (and hence, generate the charge-separated state). The latter can be taken from the results obtained with ps-TAS experiments, r=0.5. This yields an overall complexation probability of 0.88 and correlates with the high degrees of complexation for complexes **1** and **2**.

The same calculations can be done for the other incorporated moiety SubPc. It follows that the SubPc-TPPS complexation is very efficient, too. The degrees of complexation of SubPc-TPPS vary from 0.81 (**3**), 0.91 (**2**) up to 0.95 (**1**). Since equimolar 1:1:1 mixtures were used for all measurements, the probabilities of the formation of ternary complexes can be calculated by multiplication of the SubPc-TPPS and TPPS-SiPc complexation probabilities. The resulting probabilities Ψ were determined to be 0.89, 0.81, and 0.71 for **1**, **2** and **3**, respectively. The large values suggest that the formation of ternary complexes proceeds with high probability.

6.4 Conclusions

In summary, for the first time the formation of ternary supramolecular complexes consisting of a silicon phthalocyanine, a porphyrin and a subphthalocyanine was shown. The components in the formed complexes are held in water through host-guest interactions. Moreover, the formation of these host-guest-host complexes is very efficient with complexation probabilities as high as 0.7-0.9. This complexation efficiency could be further optimized by choosing an appropriate sequence of mixing the monomers. The photophysical properties of the formed complexes are strongly dependent on the spacer between silicon phthalocyanine and CD.

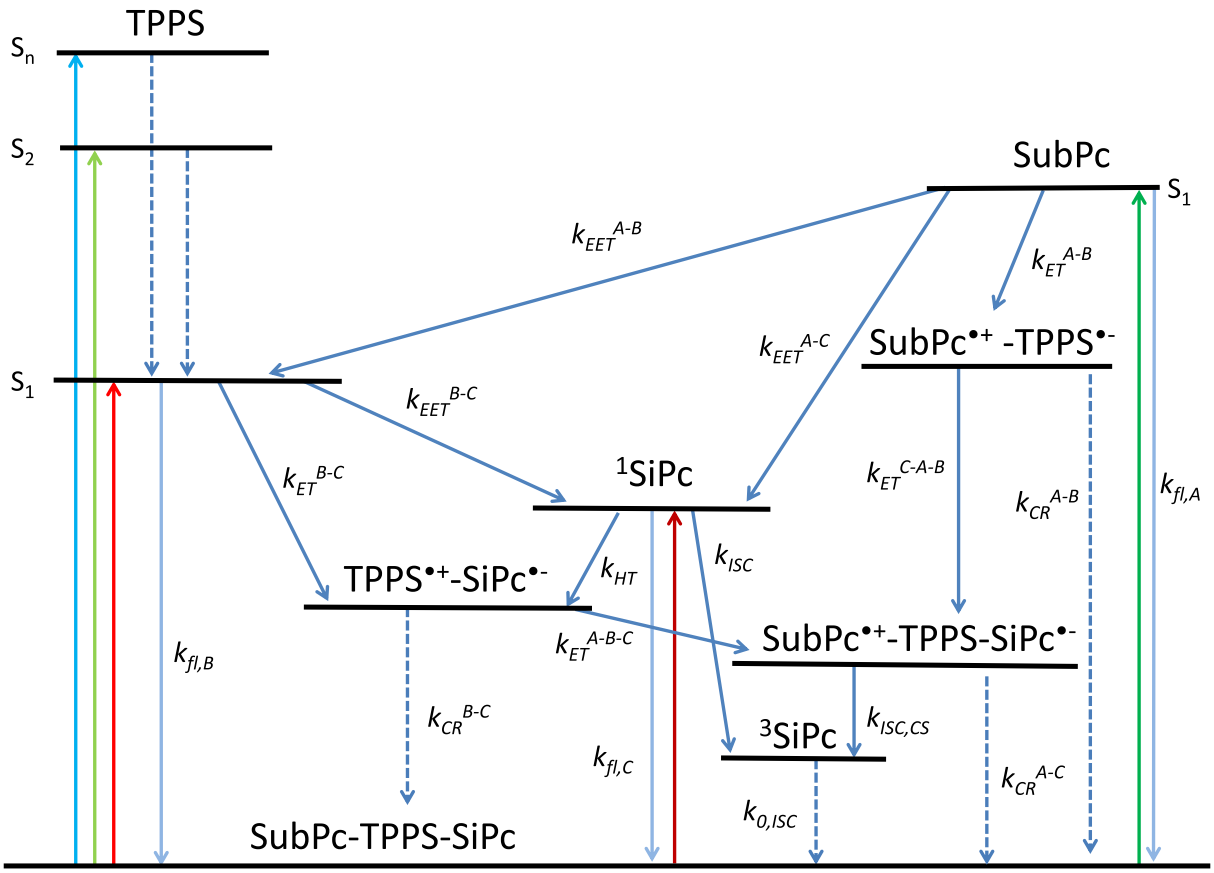

Figure 6.20: Scheme of energy levels of the supramolecular complex **1** and transitions between them. For clarity, A, B and C denote SubPc, TPPS and SiPc, respectively. The triplet levels of TPPS and SubPc are not shown.

All complexes turned out to be efficient light-harvesters. The complexes cover a broad spectrum in the UV/Vis that spans from 300 up to 700 nm with high extinction. Moreover, the excitation energy absorbed by the complex is funnelled to the SiPc core, irrespective of which constituent part was initially excited. Thereby TPPS acts as an energy transfer bridge enabling the transfer process from the photo-excited SubPc to SiPc in its ground state. Several electron transfer processes take place upon excitation of the

complexes. Following excitation of the SubPc unit in all complexes an electron transfer occurs from SubPc to TPPS. In addition, electron transfer from TPPS to SiPc may take place depending on the linker between CD and SiPc. Despite the fact that electron transfer is thermodynamically favourable for all SiPcs used, this electron transfer occurs only in **1** and **3**. For complex **1**, the short distance between TPPS and SiPc1 facilitates electron transfer from TPPS to SiPc1. Moreover, after an additional charge transfer step the SubPc$^{\bullet+}$-TPPS-SiPc$^{\bullet-}$ state is generated. In contrast, complex **2** lacks photo-induced electron transfer from TPPS to SiPc because of the large distance between electron donor and acceptor moieties. For complex **3** two stable conformers exist, a folded and an extended one with relative abundances of 0.5 each. As a result, electron transfer from TPPS to SiPc is a feasible process for the folded conformer, whereas in the extended conformer the energy dissipates *via* the regular deactivation channels of the SiPc unit. The lifetimes of the SubPc-TPPS$^{\bullet+}$-SiPc$^{\bullet-}$ charge-separated states were determined to be 100 and 120 ps for **1** and **3**, respectively. Due to the increased distance between donor and acceptor moieties, the charge recombination of SubPc$^{\bullet+}$-TPPS-SiPc$^{\bullet-}$ to the ground state in complex **1** occurs with a time constant of 1.7 ns. The photo-induced processes of complexes **1**, **2** and **3** are summarized in Jablonski-diagrams, see figures 6.20, 6.21a and 6.21b, respectively.

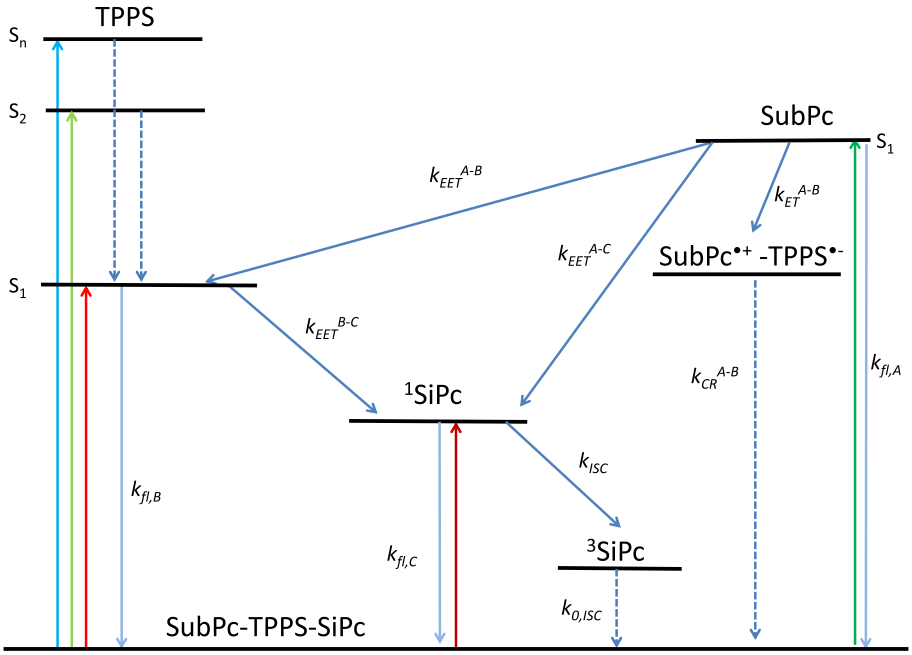

(a) complex **2**

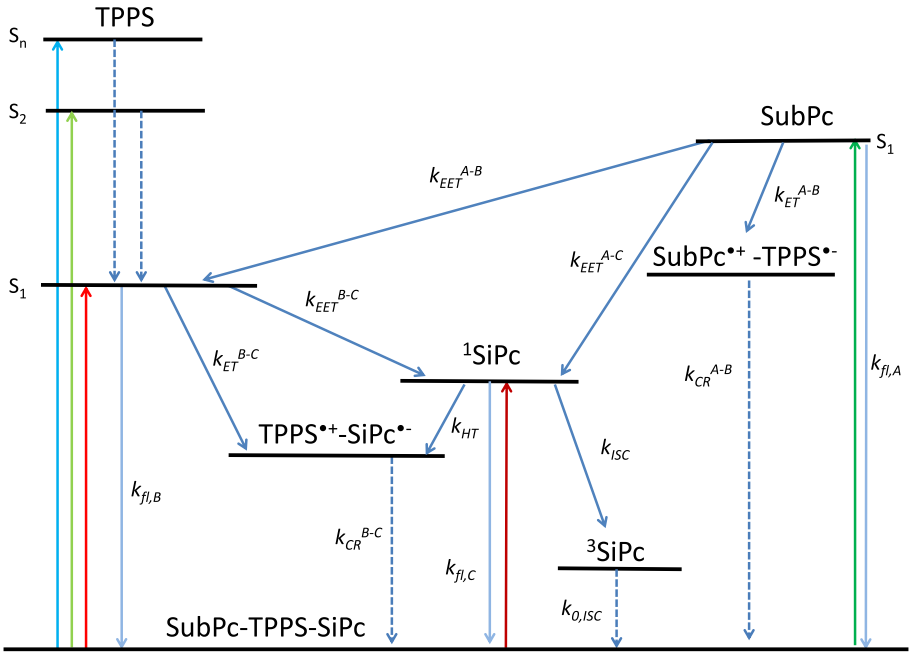

(b) complex **3**

Figure 6.21: Scheme of energy levels of the supramolecular complexes **2** (a) and **3** (b) and transitions between them. For clarity, A, B and C denote SubPc, TPPS and SiPc, respectively. The triplet levels of TPPS and SubPc are not shown.

7 Summary

The main objective of the present thesis was to conduct investigations of photo-induced energy and electron transfer processes in model compounds that are considered potentially appropriate for use in artificial photosynthesis. Two approaches have been used to construct the artificial photosynthetic systems, namely covalent and supramolecular approach. In both systems similar optically active molecules have been employed, particularly silicon-based phthalocyanines. A comparative study between the covalently-linked and self-assembled systems had been conducted. For these purposes, thorough spectroscopic measurements in the UV/Vis range had been performed on these conjugates. A combination of steady-state and time-resolved experiments allowed an identification and quantification of the photo-induced electron and energy transfer processes.

7.1 Covalently bound systems

The advantages of the covalently linked systems are the well-defined structures and robustness of the compounds. The covalently bound arrays exhibit accurate control of both the location and orientation of the chromophores. As a result, the energy and charge transfer processes occurred fast with high quantum yields. However, time-consuming syntheses that are necessary to optimize the conjugates illustrate the restriction that is imposed on covalently linked systems. Covalent syntheses become inefficient and costly as size and complexity of the systems increase.

The studied covalent arrays consisted of a BDP-SiPc-MSBDP triad as well as two reference triads $SiPc(BDP)_2$ and $SiPc(MSBDP)_2$. The photophysical behaviour of the triad was unravelled by comparing the triad with its references triads. It was shown that the triad combines the advantages of both reference triads and that the triad's photophysical properties supersede those of its references.

The triad covers a wide region of the UV/Vis spectrum from 300 to 700 nm with high extinction. After excitation of any part of the triad, the energy is transferred to the central SiPc moiety. Subsequently, the charge-separated state BDP-$SiPc^{\bullet -}$-$MSBDP^{\bullet +}$ is generated with nearly unity quantum yield, irrespective of the solvent used. The lifetime of the charge-separated state reaches its maximum of 1.7 ns in toluene and xylene. The electron and energy transfer processes involved in the triad are shown in figure 7.1.

The BDP-SiPc-MSBDP triad exhibits the best performance of all studied covalent systems with respect to light-harvesting and charge separation. It is a promising candidate for use in artificial photosynthesis and it should be investigated for application in dye sensitized solar cells.

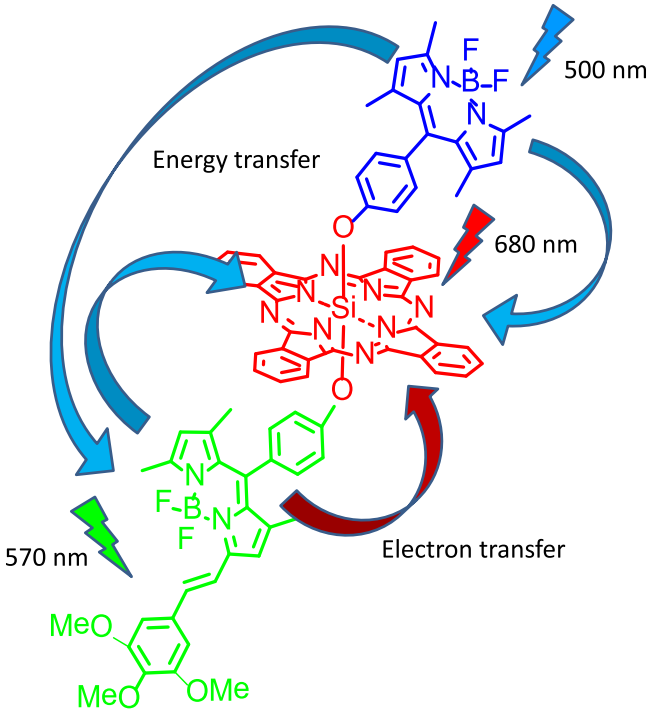

Figure 7.1: Transfer processes involved in the BDP-SiPc-MSBDP triad.

Based on these results a SiPc(BDP-MSBDP)$_2$ pentad was designed to take advantage of the properties of the Bodipy-SiPc triads. Owing to the doubled BDP and MSBDP moieties the pentad's UV/Vis absorption was expected to have much higher extinction than that of the BDP-SiPc-MSBDP triad. Furthermore, a sequential electron transfer from MSBDP to SiPc and from BDP to MSBDP was expected to take place. The increased distance between electron donor and acceptor moieties should slow down the charge recombination to the ground state.

Indeed, the light-harvesting function of the pentad outperforms that of the triads. After excitation of any part of the pentad, the absorbed energy is funnelled from the peripheral BDP and MSBDP moieties to the SiPc core. This process is followed by rapid charge transfer and the charge-separated state (BDP-MSBDP)$^{\bullet+}$-SiPc$^{\bullet-}$-MSBDP-BDP is generated with unity quantum yield. Due to the close proximity of the moieties, charge recombination to the ground state occurs with a lifetime that is faster than 25 ps. Unfortunately, this lifetime is much shorter than that of the reference SiPc(MSBDP)$_2$. No evidence was found for a sequential electron transfer that decelerates the charge recombination to the ground state. The pentad's photo-induced processes are summarized in figure 7.2.

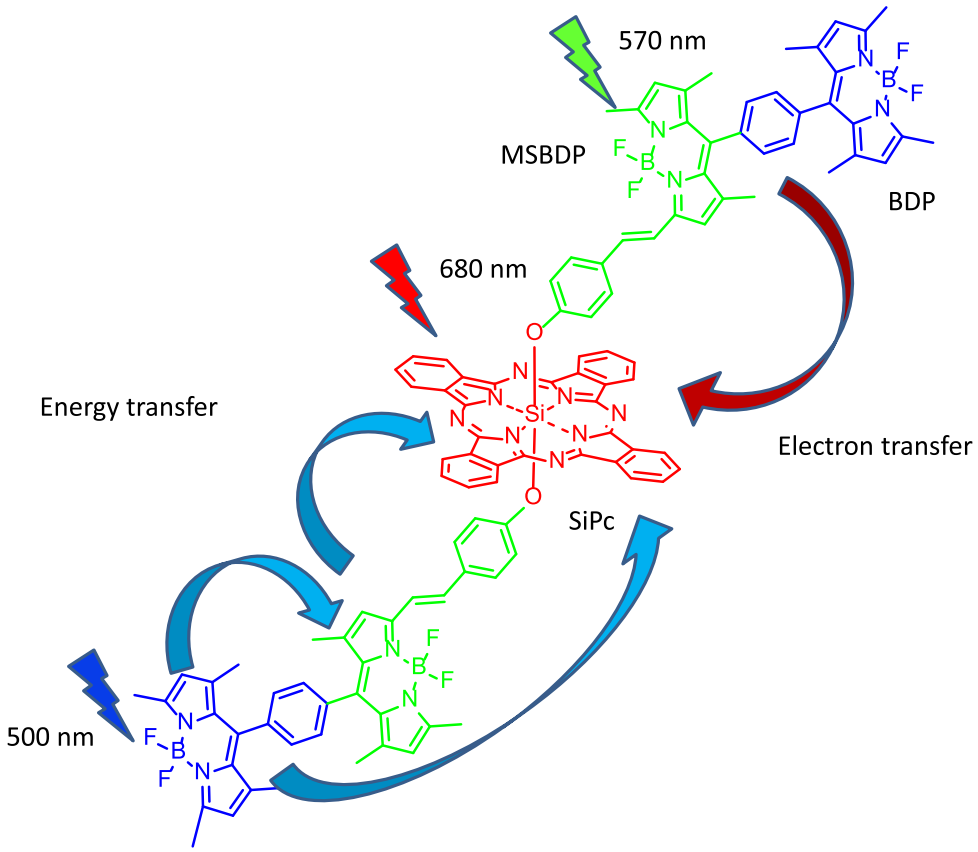

Figure 7.2: Electron and energy processes in the pentad.

In future work, the fast processes of the pentad should be investigated performing fluorescence and transient absorption experiments with femtosecond time resolution. It is noted that the pentad in its present form is not feasible for use in artificial photosynthesis. A modification of the pentad's structure is required in order to optimize the system with respect to the lifetime of the charge-separated state.

7.2 Self-assembled systems

Due to its easy synthesis and its resemblance to nature supramolecular chemistry provides a facile means to assemble complex molecular systems from small building blocks. The use of molecular recognition offers the great promise for the assembly of sophisticated architectures which would not be accessible by the covalent strategy. Moreover, once the molecular building blocks have been synthesized, they can be combined or exchanged to compose new systems without having to resynthesize the whole system.

The self-assembly process is governed by the hydrophobic interactions between a cyclodextrin (CD) and a tetrasulfonated tetraphenyl porphyrin (TPPS) in aqueous solution. The supramolecular architectures consist of a CD conjugated subphthalocyanine (SubPc), a TPPS and a silicon(IV) phthalocyanine (SiPc). The latter was covalently linked to two CDs *via* three different spacers. Depending on the length of the spacer between SiPc and CD the complexes are called **1**, **2** and **3**.

The preparation of the samples was straightforward. To obtain the supramolecular complexes the components were dissolved in aqueous solution and mixed subsequently. For the first time, it was shown that a supramolecular ternary complex consisting of SiPc, TPPS and SubPc can be formed. Not only did we demonstrate the successful self-assembly of a ternary complex, but we also showed that the formation of this ternary complex is very efficient, with probabilities in the order of 0.7-0.9.

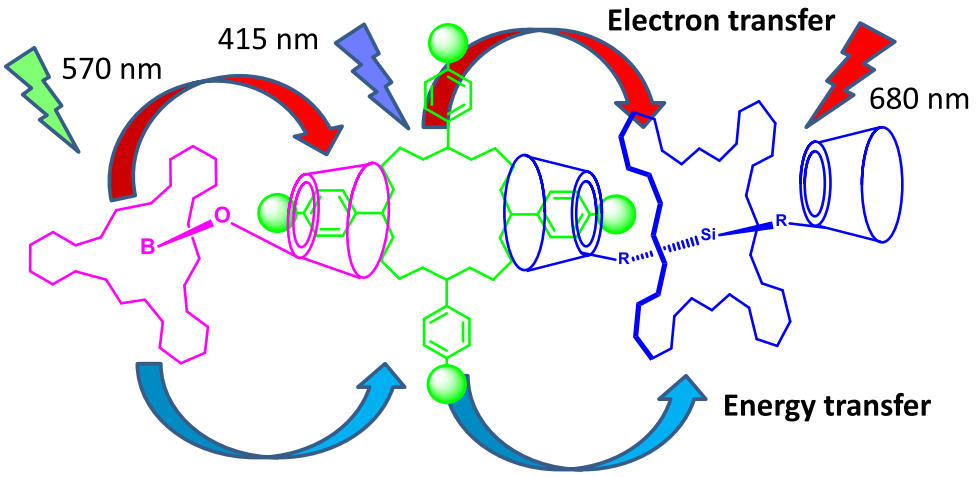

Figure 7.3: Sequential energy and electron transfer processes in the self-assembled ternary SubPc-TPPS-SiPc1 complex.

The formed ternary complexes capture a large part of the sunlight that includes wavelengths in the range of 300-700 nm. After excitation of the SubPc-part of the complexes, the energy is transferred to the SiPc-part. TPPS acts as an excitational bridge, enabling the transfer process from the photo-excited SubPc to SiPc. In addition, upon excitation of SubPc all complexes exhibit electron transfer from SubPc to TPPS. Moreover, when the SiPc or TPPS moieties are excited, an electron transfer from TPPS to SiPc may occur. In spite of the fact that charge transfer is thermodynamically favourable for all SiPcs employed, for steric reasons, electron transfer from TPPS to SiPc takes place in complexes **1** and **3** only. Moreover, in complex **1** a sequential electron transfer takes place resulting in the $SubPc^{\bullet+}$-TPPS-$SiPc^{\bullet-}$ charge-separated species. It was found that complex **3** can exist in two stable conformations, with relative abundances of 0.5 each. The folded conformer is able to generate the charge-separated

state SubPc-TPPS$^{\bullet+}$-SiPc$^{\bullet-}$ effectively. The lifetimes of the charge-separated species SubPc-TPPS$^{\bullet+}$-SiPc$^{\bullet-}$ of complexes **1** and **3**, as determined by means of pump-probe experiments, are 100 and 120 ps, respectively. Owing to the increased separation between donor and acceptor moieties, for complex **1** the lifetime of SubPc$^{\bullet+}$-TPPS-SiPc$^{\bullet-}$ is prolonged and its value was determined to be 1.7 ns. The sequential photo-induced energy and electron transfer processes of complex **1** are summarized in figure 7.3.

Due to the facile synthetic route and the long charge recombination time of 1.7 ns in aqueous solution, complex **1** should be investigated for use in dye sensitized solar cells. However, the energy transfer efficiency from SubPc to TPPS and SiPc should be further optimized.

Two self-assembled binary complexes, SubPc-TPPS-SubPc and TPPS-SiPc, were integrated into a new ternary supramolecular complex, namely SubPc-TPPS-SiPc, thereby creating synergistic effects with respect to light-harvesting and charge separation. For optimization of the system, the SiPcs could be effortlessly exchanged. Although the ternary complex SubPc-TPPS-SiPc was built upon hydrophobic interactions, its accuracy of controlling the location of the dyes can compete with that of the covalent approach owing to the very strong association ability of both SubPc(CD) and SiPc$(CD)_2$ to TPPS. It is therefore expected that supramolecular chemistry will play an important role in realizing artificial photosynthesis.

In future work, a construction kit for artificial photosynthesis based on CD-linked dyes and TPPS is conceivable. Recently, in the group of Prof. Dr. Ng a novel azaBodipy has been synthesized that is covalently linked to two CDs. Preliminary results show that azaBodipy$(CD)_2$ forms a stable complex with TPPS and ZnTPPS in aqueous solution. First own spectroscopic results have been obtained which reveal both energy and electron processes in the azaBodipy-TPPS self-assembled complexes [177]. The aforementioned CD equipped dyes could be exchanged with each other. In addition, TPPS may also be substituted by another chromophore. It should be also possible to use several supramolecular strategies within one system.

7.3 Concluding remarks

The development of artificial photosynthetic model systems containing both a light-harvesting entity and a reaction centre remains a challenging task in the field of synthetic chemistry as well as photophysics. The present thesis makes a contribution to the development of such systems and it provides a stimulus for further research.

8 Zusammenfassung

Der Gegenstand der vorliegenden Arbeit ist die Untersuchung von photoinduzierten Energie- und Elektronentransferprozessen in Modellsystemen, die als potentiell geeignet für eine Nutzung in der artifiziellen Photosynthese angesehen werden. Entsprechend den beiden wesentlichen Zugängen zur Architektur artifizieller Photosynthese-Systeme wurden vergleichend kovalente und sich selbst organisierende Systeme untersucht. In beiden Zugängen wurden als optisch aktive Moleküle ähnliche chemische Komponenten eingesetzt, insbesondere Phthalocyanine mit einem Silizium-Zentralatom. Durch eine Kombination von stationären und zeitaufgelösten optisch-spektroskopischen Methoden konnten die lichtinduzierten Elektronen- und Energietransferprozesse identifiziert und quantifiziert werden.

8.1 Kovalent gebundene Systeme

Die Vorteile von kovalent gebundenen Systemen sind die wohl definierten Strukturen und die Robustheit der Verbindungen. Mittels kovalenter Synthese ist eine präzise Kontrolle der Orientierung und Lage der Chromophore möglich. Dies resultiert in sehr schnellen Energie- und Ladungstransferprozessen mit entsprechend hohen Quantenausbeuten. Allerdings sind zeitaufwendige Synthesen notwendig, um die Verbindungen zu optimieren. Dies verdeutlicht die Einschränkungen, denen kovalent gebundene Moleküle unterliegen. Kovalente Synthesen werden mit wachsender Größe und Komplexität der Verbindungen ineffizient und arbeitsaufwendig.

Als kovalent gebundene Systeme wurden in der vorliegenden Arbeit eine BDP-SiPc-MSBDP Triade sowie die Referenztriaden SiPc$(BDP)_2$ und SiPc$(MSBDP)_2$ vollständig photophysikalisch charakterisiert. Es wurde gezeigt, dass die Triade die vorteilhaften Charakteristika der beiden Referenztriaden kombiniert und dass ihre photophysikalischen Eigenschaften die der Referenzen übertreffen.

Die Triade deckt ein breites Spektrum von 300 bis 700 nm mit hoher Extinktion ab. Nach Anregung von BDP oder MSBDP wird die absorbierte Energie zum zentralen SiPc Molekül transferiert. Hiernach wird der ladungsgetrennte Zustand BDP-SiPc$^{\bullet -}$-MSBDP$^{\bullet +}$ mit einer Quantenausbeute von nahezu eins, unabhängig vom verwendeten Lösungsmittel, generiert. Die Lebensdauer des ladungsgetrennten Zustandes erreicht mit 1,7 ns in Toluol und Xylol ihr Maximum. Die photoinduzierten Energie- und Ladungstransfer-Prozesse der Triade sind in Abbildung 8.1 zusammengefasst.

Die BDP-SiPc-MSBDP Triade weist in Bezug auf Lichtsammeleffizienz und Ladungstrennung die besten Eigenschaften der untersuchten kovalent gebundenen Systeme auf. Die Triade ist ein vielversprechender Kandidat für den Einsatz in artifizieller Photosynthese und sollte auf ihre Funktionsfähigkeit in Grätzelzellen untersucht werden.

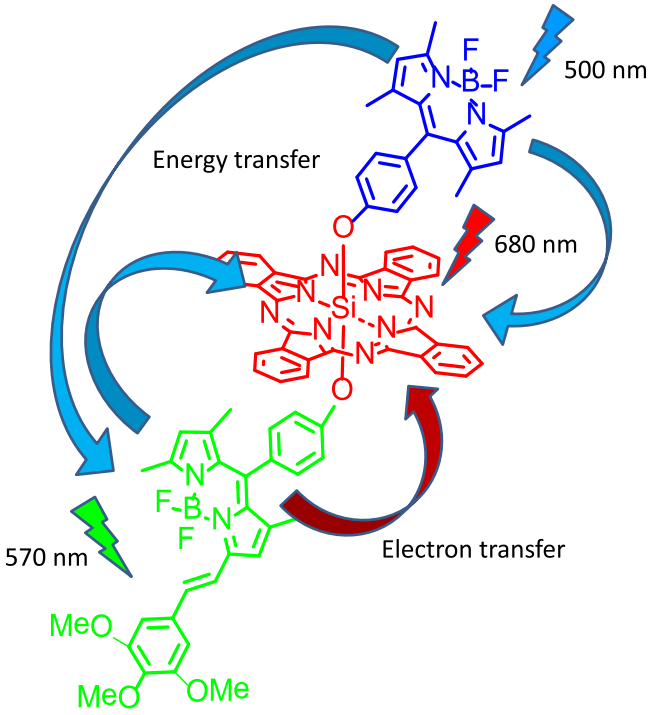

Figure 8.1: Energie- und Ladungstransfer-Prozesse in der Triade.

Basierend auf diesen Ergebnissen wurde eine SiPc(BDP-MSBDP)$_2$ Pentade konzipiert, um die vorteilhaften Eigenschaften der Bodipy-SiPc Triaden zu kombinieren. Wegen der doppelten Anzahl von BDP und MSBDP Einheiten wurde eine weitere Erhöhung der Extinktion gegenüber der BDP-SiPc-MSBDP Triade erwartet. Des Weiteren wäre ein sequenzieller Elektronentransfer von MSBDP zu SiPc und von BDP zu MSBDP möglich. Der vergrößerte Abstand zwischen Elektrondonor und -akzeptor sollte die Ladungsrekombination in den Grundzustand verzögern.

Tatsächlich übersteigt die Lichtsammeleffizienz der Pentade die der untersuchten Triaden. Nach Anregung eines Teils der Pentade wird die absorbierte Energie von den peripheren BDP und MSBDP Gruppen zum SiPc Kern geleitet. Diesem Prozess folgt ein schneller Ladungstransfer und der ladungsgetrennte Zustand (BDP-MSBDP)$^{\bullet+}$-SiPc$^{\bullet-}$-MSBDP-BDP wird mit fast hundertprozentiger Wahrscheinlichkeit generiert. Aufgrund des geringen Abstandes der Chromophore erfolgt die Ladungsrekombination zum Grundzustand mit einer Zeitkonstante kleiner als 25 ps. Leider ist diese Lebensdauer viel kürzer als die der Referenz SiPc(MSBDP)$_2$. Ein Hinweis auf einen sequenziellen Elektronentransfer, der die Ladungsrekombination verlangsamt, wurde nicht gefunden. Die photoinduzierten Energie- und Ladungstransfer-Prozesse der Pentade sind in Abbildung 8.2 zusammengefasst.

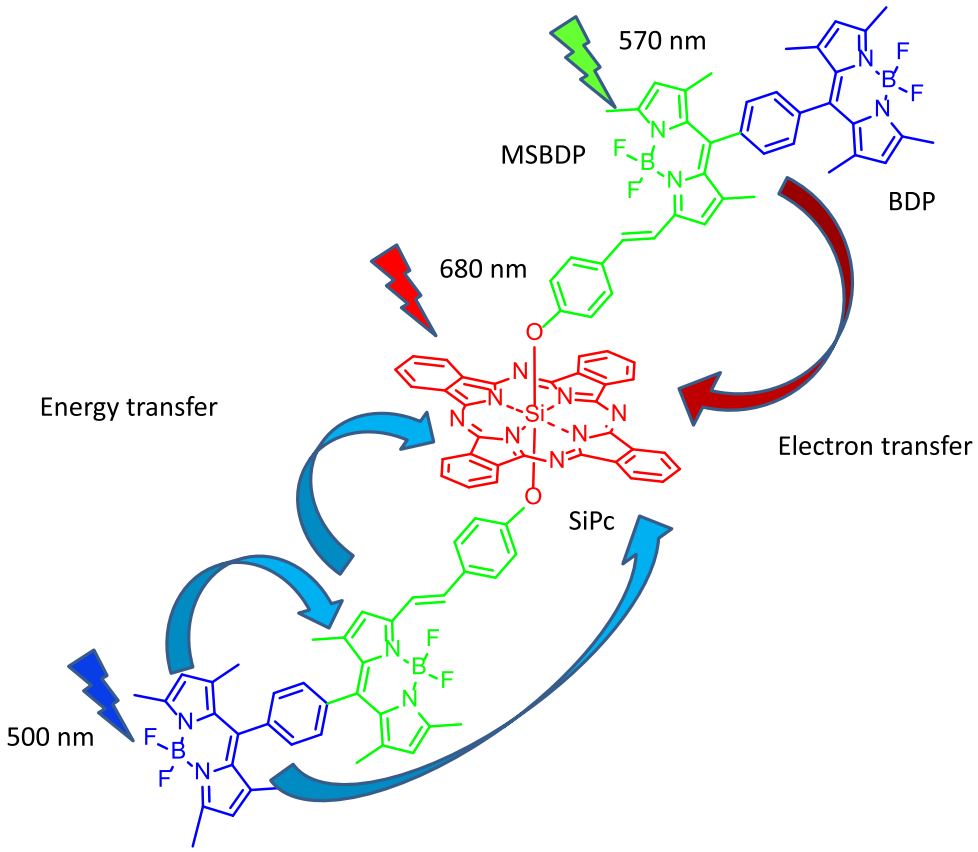

Figure 8.2: Energie- und Ladungstransfer-Prozesse in der Pentade.

In künftigen Arbeiten sollten die schnellen Prozesse der Pentade mittels Fluoreszenz und transienter Absorption mit Auflösung im Femtosekundenbereich untersucht werden. Es wird an dieser Stelle darauf hingewiesen, dass die Pentade in ihrer derzeitigen Form unbrauchbar für den Einsatz in künstlicher Photosynthese ist. Eine Modifikation ihrer Struktur ist notwendig, um das System in Bezug auf die Lebensdauer des ladungsseparierten Zustandes zu optimieren.

8.2 Selbst-assemblierte Systeme

Die supramolekulare Chemie zeichnet sich durch einfache Synthesen aus. Durch die Nutzung von Mechanismen der Selbstorganisation können Systeme erhalten werden, die den komplexen Strukturen in der Natur ähneln. Damit ist sie ein wirksames Mittel, um komplexe molekulare Systeme aus kleinen Bausteinen aufzubauen. Durch die Verwendung von molekularer Erkennung können ausgeklügelte molekulare Netzwerke hergestellt werden, die nicht mittels kovalenter Synthese zugänglich sind. Außerdem können die molekularen Einheiten kombiniert und ausgetauscht werden um neuartige Systeme zu konstruieren. So muss bei der Modifizierung der Eigenschaften nicht das gesamte System neu synthetisiert werden.

Die Selbstorganisation wurde durch die hydrophoben Wechselwirkungen zwischen einem Cyclodextrin (CD) und einem Porphyrin (TPPS) in wässriger Lösung vermittelt. Die supramolekularen Komplexe bestanden aus einem CD-konjugierten Subphthalocyanin (SubPc), dem TPPS und aus einem Silizium(IV)-Phthalocyanin (SiPc). Letzteres wurde an zwei CDs kovalent gebunden. Es wurden drei verschiedene SiPcs untersucht, die sich durch eine unterschiedliche Kettenlänge zwischen dem SiPc und dem CD auszeichnen.

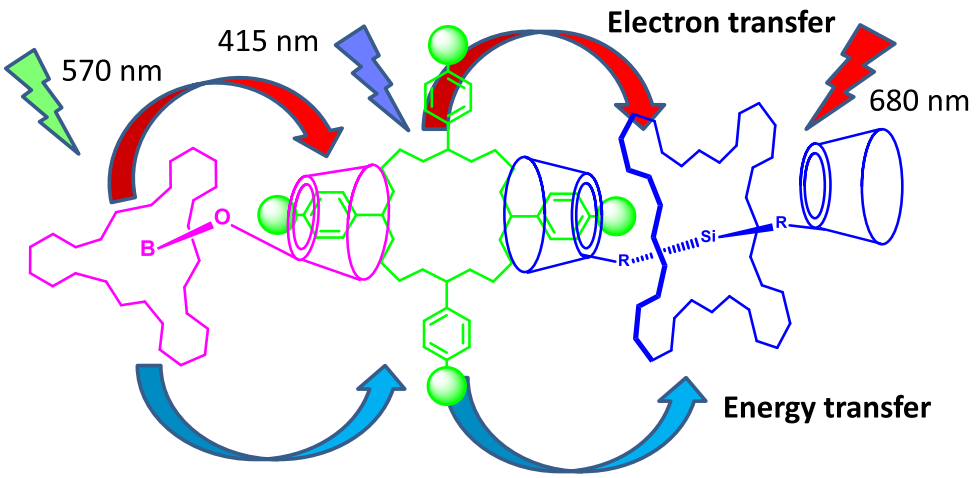

Figure 8.3: Sequenzielle Energie- und Ladungstransfer-Prozesse im supramolekularen Komplex SubPc-TPPS-SiPc1.

Erstmals wurde in dieser Arbeit gezeigt, dass sich in wässriger Lösung ein supramolekularer Komplex bestehend aus den drei genannten Farbstoffen bilden kann. Es konnte nicht nur die erfolgreiche Herstellung, sondern auch die effiziente Komplexbildung mit Wahrscheinlichkeiten in der Größenordnung 70 bis 90% demonstriert werden.

Die gebildeten Komplexe absorbieren einen großen Teil des Sonnenlichtspektrums im Bereich 300-700 nm. Nach Anregung des SubPc-Teils wird die Energie zum SiPc-Teil transferiert. TPPS spielt die Rolle einer energetischen Brücke und ermöglicht den Transfer vom anfänglich angeregten SubPc zu SiPc. Außerdem findet nach selektiver Anregung von SubPc ein Elektronentransfer von SubPc zu TPPS statt. Wenn SiPc oder TPPS angeregt werden, kann ein Elektron von TPPS zu SiPc transferiert werden. Der photoinduzierte Ladungstransfer ist für alle verwendeten SiPcs thermodynamisch möglich,

findet jedoch aus sterischen Gründen nur in den Komplexen **1** mit der kürzesten und **3** mit der längsten Kette statt. Darüber hinaus findet in Komplex **1** ein sequenzieller Elektronentransfer statt, der zur Entstehung des ladungsseparierten Zustandes SubPc$^{\bullet+}$-TPPS-SiPc$^{\bullet-}$ führt. Komplex **3** liegt in zwei stabilen Konformationen mit einer relativen Häufigkeit von jeweils 0,5 vor. Im gefalteten Konformer wird über photoinduzierten Ladungstransfer der Zustand SubPc-TPPS$^{\bullet+}$-SiPc$^{\bullet-}$ generiert. Die Lebensdauer der ladungsgetrennten Zustände SubPc-TPPS$^{\bullet+}$-SiPc$^{\bullet-}$ der Komplexe **1** und **3** wurde mittels transienter Absorptionsmessungen im Pikosekundenbereich zu 100 beziehungsweise 120 ps bestimmt. Dank des größeren Abstandes zwischen Donor und Akzeptor ist der ladungsgetrennte Zustand SubPc$^{\bullet+}$-TPPS-SiPc$^{\bullet-}$ langlebiger und die Ladungsrekombination erfolgt mit einer Zeitkonstante von 1,7 ns. Aufgrund der relativ einfachen Synthese und der langen Ladungsrekombinationszeit von 1,7 ns in einem polaren Medium sollte Komplex **1** für den Einsatz in Grätzelzellen untersucht werden. Allerdings sollte die Energietransfereffizienz von SubPc zu TPPS und SiPc weiter gesteigert werden.

Somit wurden zwei selbst-assemblierte Systeme, SubPc-TPPS-SubPc und TPPS-SiPc, in ein neues System integriert, nämlich SubPc-TPPS-SiPc. Hierdurch wurde in Bezug auf Lichtsammeleffizienz und Ladungstrennung Synergie geschaffen. Außerdem konnten verschiedene SiPcs für die Optimierung des Systems mühelos ausgetauscht werden. Der Komplex SubPc-TPPS-SiPc assembliert durch Vermittlung hydrophober Wechselwirkungen. Dennoch liegt eine kontrollierte Anordnung der Chromophore vor und kann aufgrund der sehr hohen Stabilitätskonstanten von SubPc(CD) und SiPc$(CD)_2$ mit TPPS als vergleichbar mit den kovalent gebundenen Systemen angesehen werden. Diese Ergebnisse illustrieren die bereits vielfach geäußerte Erwartung, dass der supramolekulare Ansatz in Zukunft eine wichtige Rolle in der künstlichen Photosynthese spielen wird.

Künftig könnte ein Baukasten für artifizielle Photosynthesesysteme, der auf verschiedenen CD-gebundenen Farbstoffen basiert, realisiert werden. Unlängst wurde in der Gruppe von Prof. Dr. Ng ein neuartiges azaBodipy synthetisiert, das kovalent an zwei CD-Gruppen gebunden ist. Vorläufige Ergebnisse zeigen, dass das azaBodipy$(CD)_2$ in wässriger Lösung mit TPPS und ZnTPPS einen stabilen Komplex bildet. Erste eigene orientierende spektroskopische Untersuchungen an diesen Komplexen haben gezeigt, dass sowohl lichtinduzierter Energie- wie auch Elektronentransfer stattfinden. Die oben genannten Farbstoffe können untereinander ausgetauscht werden und auch das TPPS kann durch ein anderes Chromophor ersetzt werden. Ebenso sind verschiedene supramolekulare Strategien, die innerhalb eines Systems miteinander kombiniert werden könnten, denkbar.

8.3 Schlussbemerkung

Die Entwicklung von artifiziellen Photosynthese-Systemen, die eine Lichtsammeleinheit und ein Reaktionszentrum besitzen, stellt eine Herausforderung für die Forschung auf dem Gebiet der synthetischen Chemie sowie der Photophysik dar. Die gegenwärtig vorliegende Arbeit leistet einen Beitrag zur Entwicklung solcher Systeme und bietet Ansätze für die weitere Forschung.

Appendix

Table 1: Dielectric constants ε_S of the solvents used at ambient temperature.

Solvent	$\boldsymbol{\varepsilon_S}$
toluene	2.4
xylene	2.4
chloroform	4.8
THF	7.5
DCM	8.9
acetonitrile	36.6
DMF	38.3
water	80.1

Table 2: Electrochemical properties of BDP, MSBDP and SiPc as taken from [92, 148]. All values presented are given in [V]. The SiPc$(BDP)_2$, SiPc$(MSBDP)_2$ and BDP-SiPc-MSBDP triads as well as the BDP-MSBDP dyad and SiPc$(BDP\text{-}MSBDP)_2$ pentad had limited solubility in DMF, therefore, their electrochemical data have not been determined.

Compound	$\boldsymbol{E_{pc}}$	$\boldsymbol{E_{1/2}}$ **(red 1)**
BDP	1.05	-1.21
MSBDP	0.88	-1.05
SiPc	1.06	-0.57

Table 3: Electrochemical data of SubPc, TPPS, SiPc1, SiPc2 and SiPc3 as taken from [77, 171]. All values are given in [V].

Compound	$\boldsymbol{E_{pc}}$	$\boldsymbol{E_{1/2}}$**(red 1)**	$\boldsymbol{E_{1/2}}$ **(red 2)**
SubPc	0.86	-1.09	
TPPS	0.93	-1.15	-1.57
SiPc1	0.97	-0.71	-1.31
SiPc2	1.05	-0.65	-1.21
SiPc3	0.96	-0.63	-1.19

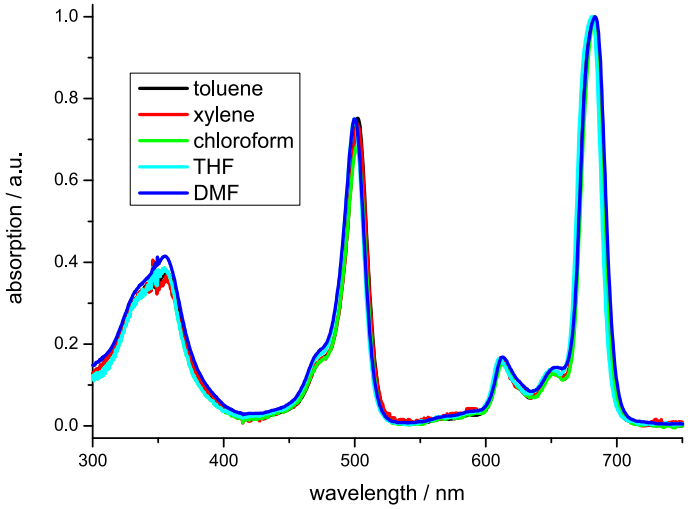

(a) SiPc(BDP)$_2$

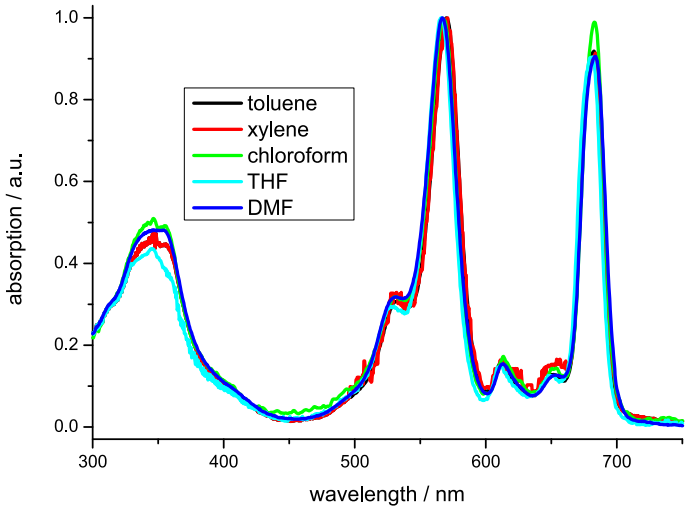

(b) SiPc(MSBDP)$_2$

Figure 4: UV/Vis absorption spectra of the triads SiPc(BDP)$_2$ (a) and SiPc(MSBDP)$_2$ (b) dissolved in toluene, xylene, chloroform, THF and DMF.

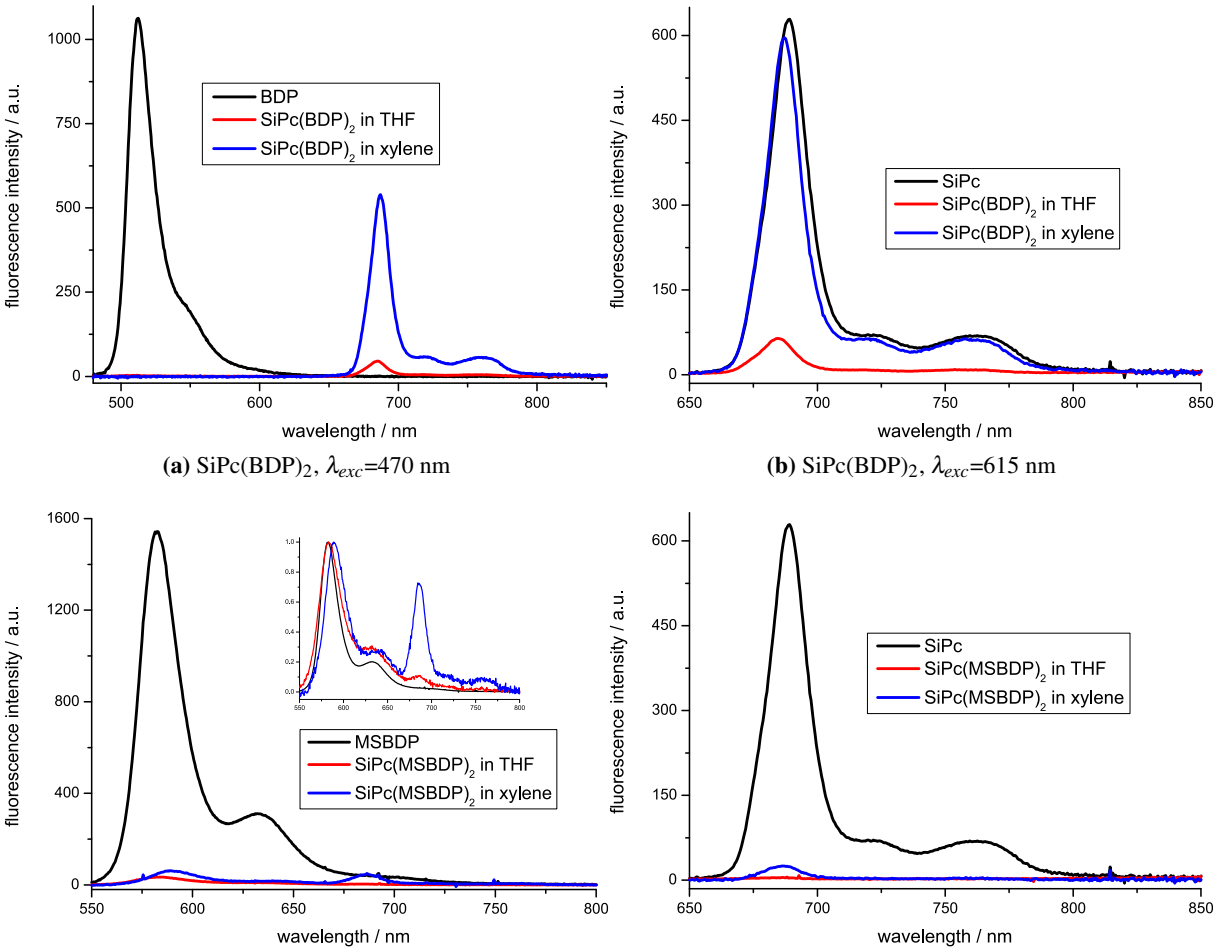

(a) SiPc(BDP)$_2$, λ_{exc}=470 nm

(b) SiPc(BDP)$_2$, λ_{exc}=615 nm

(c) SiPc(MSBDP)$_2$, λ_{exc}=532 nm

(d) SiPc(MSBDP)$_2$, λ_{exc}=615 nm

Figure 5: Steady-state fluorescence spectra of SiPc(BDP)$_2$, SiPc(MSBDP)$_2$ and their references dissolved in xylene and THF following excitation of their parts.

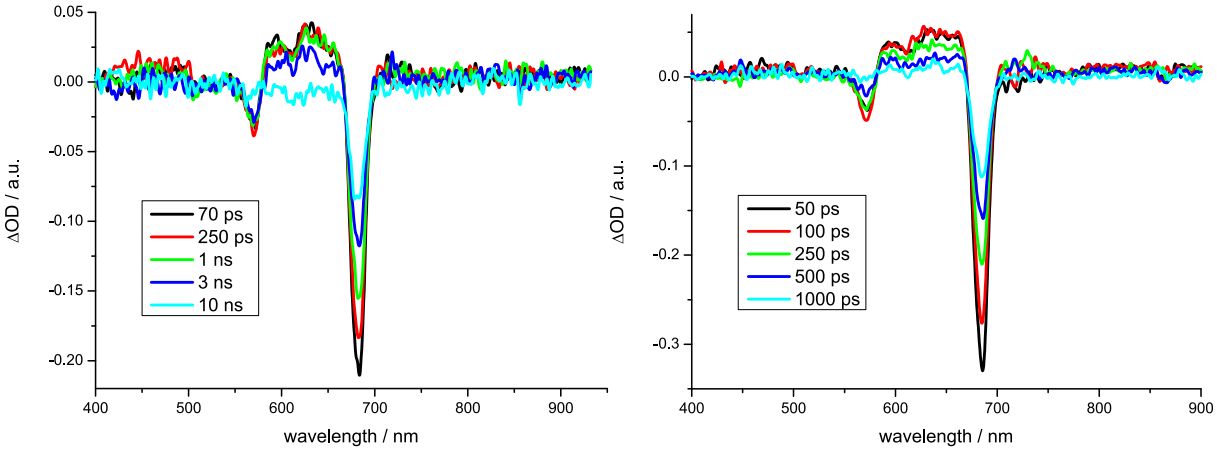

(a) Xylene, BDP-part excitation

(b) Chloroform, SiPc-part excitation

Figure 6: ΔOD spectra of BDP-SiPc-MSBDP dissolved in xylene upon excitation of BDP (a) and dissolved in chloroform upon excitation SiPc (b) at different delay times.

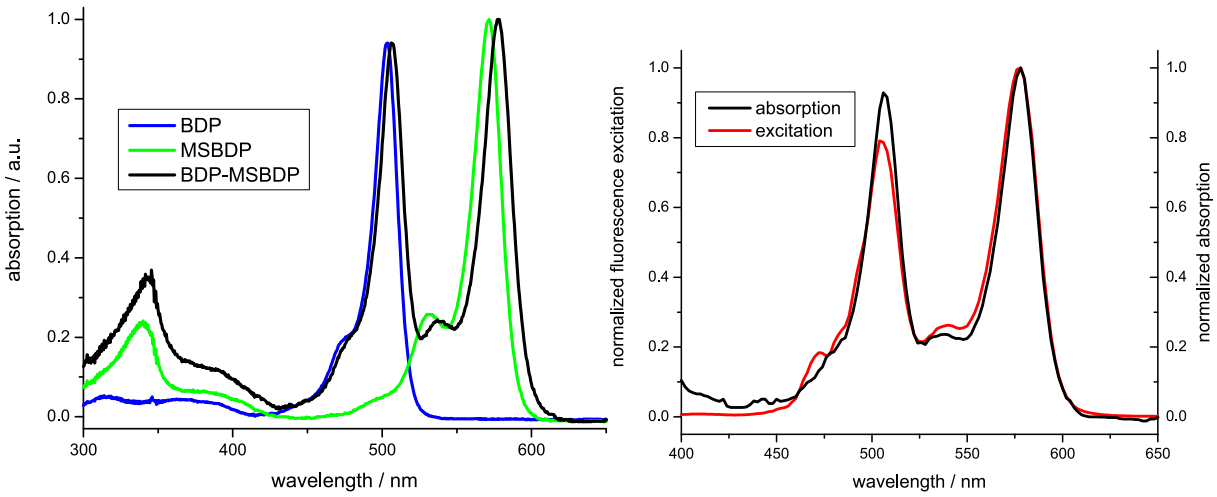

(a) UV/Vis spectra

(b) Fluorescence excitation spectrum

Figure 7: UV/Vis absorption (a) and fluorescence excitation spectra (b) of the BDP-MSBDP dyad dissolved in toluene.

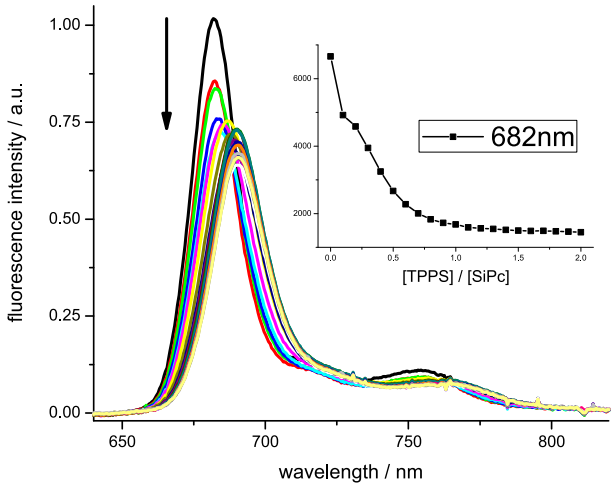

Figure 8: Change in fluorescence spectrum of a mixture of SubPc and SiPc2 (both at 1 μM) upon addition of TPPS (up to 2 μM) in water. The SiPc-part was selectively excited at 615 nm. Insets: fluorescence intensity versus concentration of TPPS.

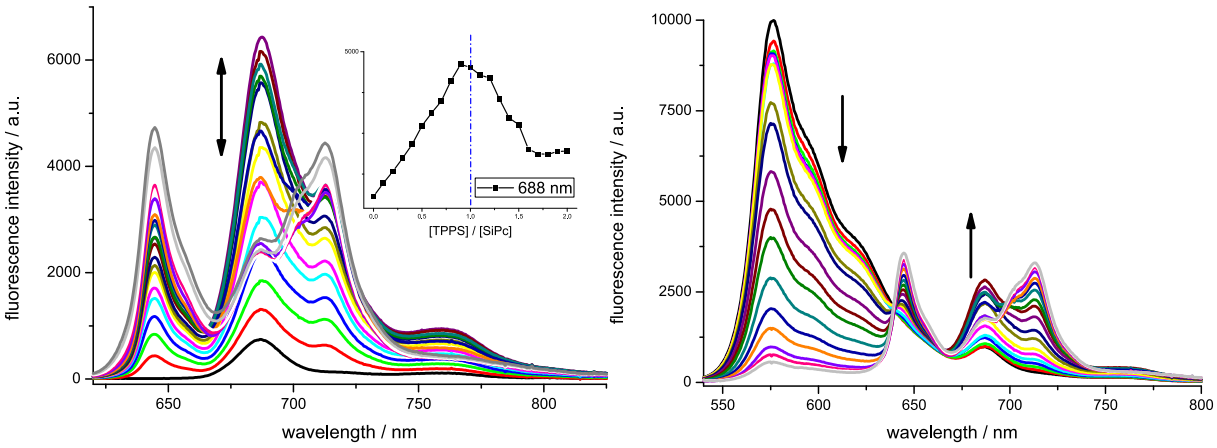

(a) TPPS-part excitation **(b)** SubPc-part excitation

Figure 9: Change in fluorescence spectrum of a mixture of SubPc and SiPc1 (both at 1 μM) upon addition of TPPS (up to 2 μM) in water. The TPPS- and SubPc-part were selectively excited at 400 and 532 nm, respectively. Inset in (a): fluorescence intensity versus concentration of TPPS.

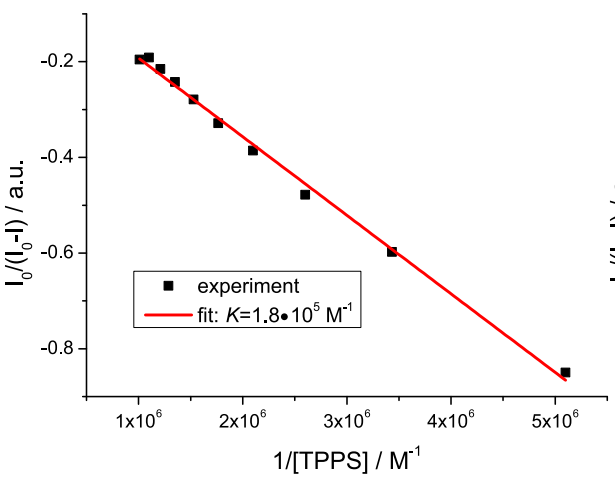

(a) SiPc2 fluorescence upon excitation of TPPS

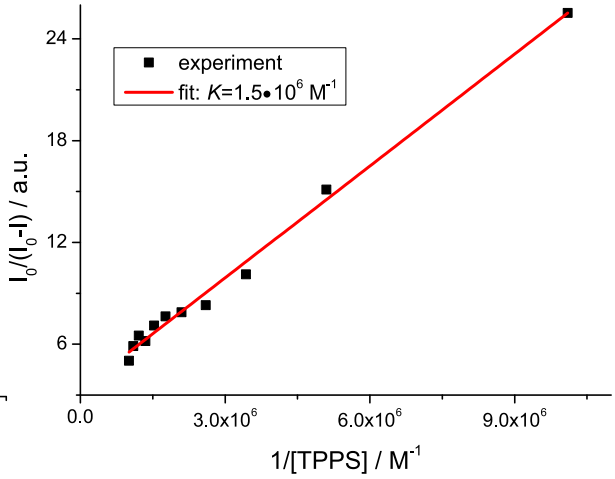

(b) SubPc fluorescence upon excitation of SubPc

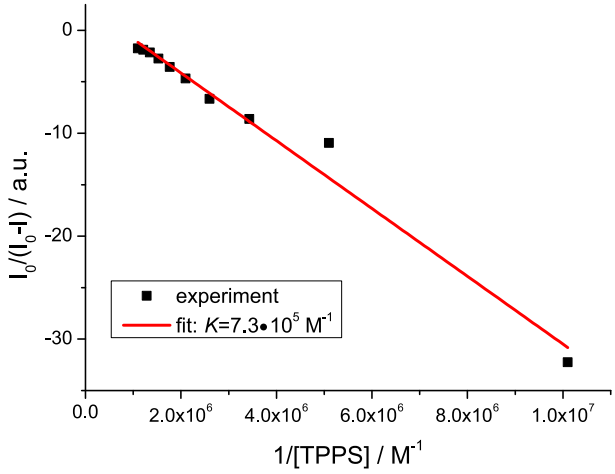

(c) SiPc2 fluorescence upon excitation of SubPc

Figure 10: Plot of $I_0/(I_0\text{-}I)$ vs. 1/[TPPS]. The concentrations of both SubPc and SiPc2 were 5 μM, subsequently, the mixture was titrated with TPPS. The slope of the linear regression determines the reciprocal value of the association constant *K*.

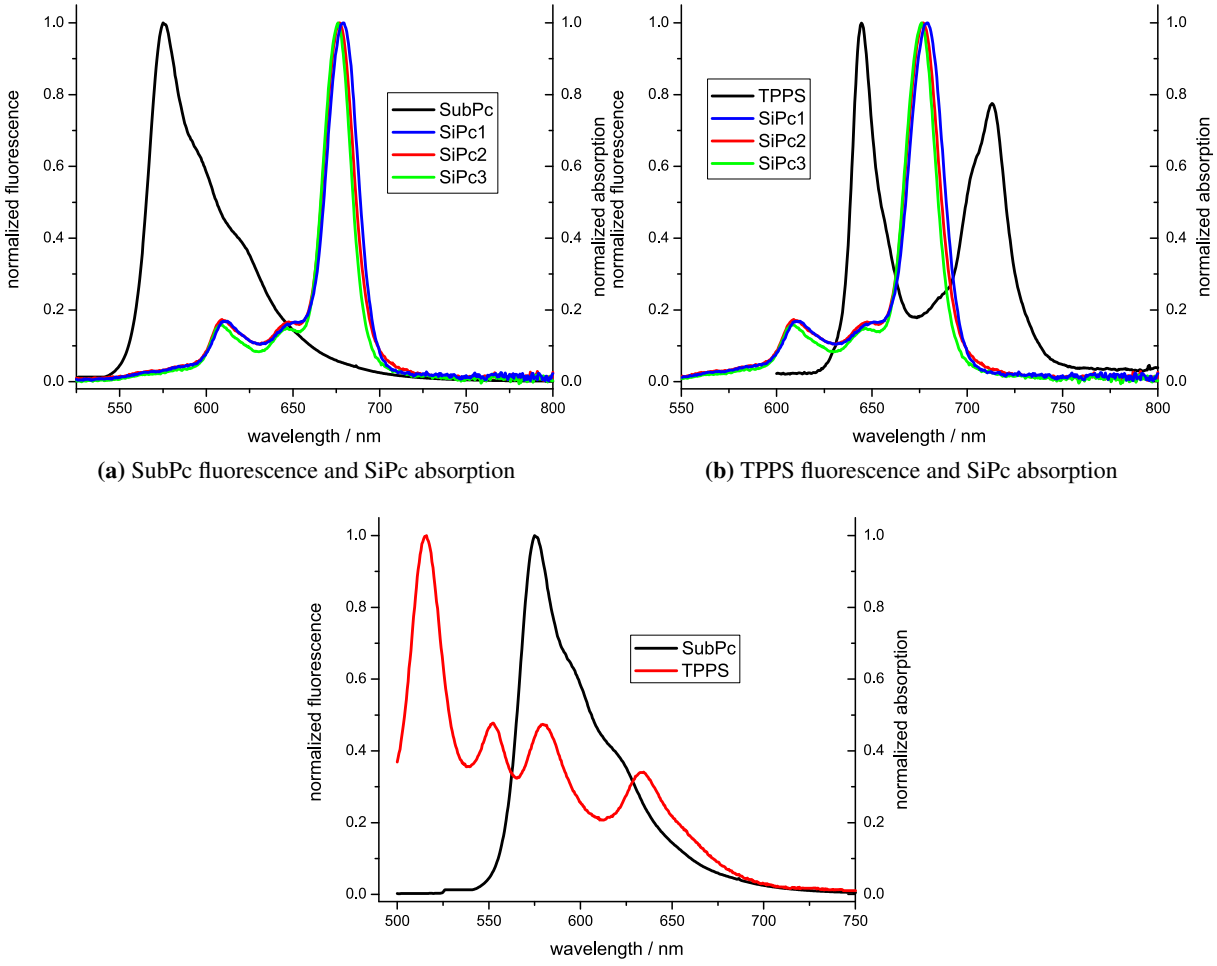

(a) SubPc fluorescence and SiPc absorption

(b) TPPS fluorescence and SiPc absorption

(c) SubPc fluorescence and TPPS absorption

Figure 11: Spectral overlap between donor fluorescence and acceptor absorption for different donor-acceptor combinations within the supramolecular complexes.

Publications and conference contributions

R. MENTING, D. K. P. NG, B. RÖDER AND E. A. ERMILOV, Sequential energy and charge transfer processes in mixed host-guest complexes consisting of subphthalocyanine, porphyrin and phthalocyanine chromophores, *Phys. Chem. Chem. Phys.*, **14**, 14573-14584 (2012)

R. MENTING, J. T. F. LAU, H. XU, D. K. P. NG, B. RÖDER AND E. A. ERMILOV, Formation and photoinduced processes of a self-assembled subphthalocyanine-porphyrin-phthalocyanine supramolecular complex, *Chem. Comm.*, **48**, 4597-4599 (2012)

E. A. ERMILOV, R. MENTING, J. T. F. LAU, X. LENG, B. RÖDER AND D. K. P. NG, Switching the photoinduced processes in host-guest complexes of β-cyclodextrin-substituted silicon(IV) phthalocyanines and a tetrasulfonated porphyrin, *Phys. Chem. Chem. Phys.*, **13**, 17633-17641 (2011)

T. BORNHÜTTER, R. FENGER, R. MENTING, V. MAY, K. RADEMANN AND B. RÖDER, Gold Nanoparticle Based Enhancement of Singlet Oxygen Luminescence in Aqueous Environment, *Nano Lett.*, in preparation (2012)

S. WENJING, R. MENTING, E. A. ERMILOV, G. P. C. LO, B. RÖDER AND D. K. P. NG, Supermolecular Arrays by AzaBodipy-bridged Bis(permethyl-β-cyclodextrin)s with Porphyrins in Aqueous Media, *Chem. Comm.*, in preparation (2012)

R. MENTING, J.-Y. LIU, Y. HUANG, D. K. P. NG, B. RÖDER AND E. A. ERMILOV, Photoinduced Energy and Charge Transfer in a Novel Bodipy - mono-styril Bodipy Dyad, *Inorg. Chem.*, in preparation (2012)

R. MENTING, J.-Y. LIU, Y. HUANG, D. K. P. NG, B. RÖDER, AND E. A. ERMILOV, Panchromatic light-harvesting and charge separation in a novel Bodipy-silicon-phthalocyanine-Bodipy triad, Seventh International Conference on Porphyrins and Phthalocyanines (ICPP), Jeju, Korea (2012), poster presentation

R. MENTING, J. T. F. LAU, X. LENG, J.-Y. LIU, Y.-S. HUANG, H. XU, D. K. P. NG, B. RÖDER, E. A. ERMILOV, Phthalocyanine based covalently bound and self-assembly nanosystems for efficient light-harvesting and charge-separation, Artificial Photosynthesis, Post Faraday Meeting, Edinburgh, UK (2011), oral Presentation

R. MENTING, J. T. F. LAU, H. XU, D. K. P. NG, B. RÖDER, E. A. ERMILOV, A supramolecular approach on artificial photosynthesis using host-guest porphyrin-phthalocyanine self-assemblies, Faraday

Discussion 155: Artificial Photosynthesis, Edinburgh, UK (2011), poster presentation

R. MENTING, J.-Y. LIU, Y. HUANG, D. K. P. NG, E. A. ERMILOV AND B. RÖDER, Electron- and energy transfer in a novel Bodipy-Bodipy-silicon-phthalocyanine pentad, Faraday Discussion 155: Artificial Photosynthesis, Edinburgh, UK (2011), poster presentation

E. A. ERMILOV, R. MENTING, J.-Y. LIU, Y. HUANG, D. K. P. NG AND B. RÖDER, Phthalocyanine-Based Nanosystems for Efficient Light-Harvesting and Charge-Separation, International Symposia on Advancing the Chemical Sciences - Challenges in Renewable Energy (ISACS 4), Boston, USA (2011), poster presentation

R. MENTING, J.-Y. LIU, Y. HUANG, D. K. P. NG, E. ERMILOV AND B. RÖDER, Bodipy-Phthalocyanine based nanosystems for efficient light-harvesting and charge separation, Tetra Pyrrol Discussion Group (TPDG), Berlin, Germany (2010), oral presentation

R. MENTING, E. A. ERMILOV, J. T. F. LAU, H. XU, D. K. P. NG AND B. RÖDER, Host-guest porphyrin-phthalocyanine self-assembled supramolecules as artificial photosynthetic system, Frühjahrestagung der Deutschen Physikalischen Gesellschaft, Hamburg, Germany (2009), oral presentation

R. MENTING, Lichtinduzierter Energie- und Elektronentransfer in komplexen Bausteinen für artifizielle Photosynthesesysteme, Diploma Thesis, Humboldt Universität zu Berlin, Germany (2010)

Acknowledgements

Ich danke Frau **Prof. Dr. Beate Röder** für die Möglichkeit in der AG Photobiophysik meine Dissertation anzufertigen. Außerdem danke ich ihr für die guten Gespräche und die großzügige Unterstützung, die ich während der ganzen Zeit erhalten habe.

Ein besonderer Dank geht an **Dr. Eugeny Ermilov** für seine intensive Betreuung und die zahlreichen Diskussionen.

Für die Synthese der Moleküle möchte ich mich bei **Prof. Dr. Dennis Ng** und seiner Arbeitsgruppe bedanken.

Prof. Dr. Christian Brückner und **Prof. Dr. Oliver Benson** danke ich für die Bereitschaft, meine Dissertation zu begutachten.

Der **Deutschen Forschungsgemeinschaft** danke ich für die finanzielle Förderung.

Dr. Norbert Jux danke ich für die großzügige finanzielle Unterstützung.

Bei **Dr. Jörg Biermann** möchte ich mich für die guten Ratschläge und Tipps bedanken.

Lutz Jäger für das gute Fleisch, die netten Gespräche und die Hilfe im Chemielabor.

Dr. Steffen Hackbarth und **Dr. Ronald Steffen** für ihre Unterstützung im Labor und die interessanten Diskussionen.

Sebastian Jungwirth für seine Hilfe im TCSPC Labor und seine Kompetenz in Sachen Kochen.

Tobias Bornhütter, weil er immer gute Laune hat.

Dr. Annegret Preuß, **Jan Schlothauer**, **Jörg Megow**, **Torsten Wendav** und **Jens Föhlinger** für die gute Stimmung und die geleisteten Hilfen.

Bei der gesamten **AG Photobiophysik** möchte ich mich für die gute Atmosphäre und hilfsbereitschaft bedanken.

Yori Manzke für die vielen Korrekturen meiner Arbeit, die gute Zeit außerhalb der Uni und seine Vorliebe für Whisky.

Acknowledgements

Alonso M. Acuña für die lustige Zeit in und außerhalb der Uni und den Kaffee auf dem Weg zur Uni.

Maurice Mersinger, weil er ein großer Freund ist und als Mitbewohner eine Menge Physik dulden musste.

Dr. Gemma Kuijpers und **Matthew Watson** für die vielen Korrekturvorschläge meiner Arbeit.

Bei meinen Eltern **Martha Roelofs**, **Erik van Houten**, **Eric Menting** und **Michaela Menting** und meinem Bruder **Remco Menting**, die mich seit Jahren bedingungslos unterstützen.

Zu guter Letzt möchte ich mich bei meiner Freundin **Ines Brockhoff** bedanken, weil sie immer für mich da ist und mir unglaublich viel geholfen hat, während ich die Doktorarbeit angefertigt habe. Bei meinem Sohn **Noah Maarten** möchte ich mich bedanken, weil er das ruhigste Baby der Welt ist.

Bibliography

[1] Giacomo Ciamician. The photochemistry of the future. *Science*, 36:385–394, 1912.

[2] Leif Hammarström and Michael R. Wasielewski. Biomimetic approaches to artificial photosynthesis. *Energy Environ. Sci.*, 4:2339–2339, 2011.

[3] Magnus Falkenström, Olof Johansson, and Leif Hammarström. Light-induced charge separation in ruthenium based triads - new variations on an old theme. *Inorg. Chim. Acta*, 360:741–750, 2007.

[4] Michael R. Wasielewski. Photoinduced electron transfer in supramolecular systems for artificial photosynthesis. *Chem. Rev.*, 92:435–461, 1992.

[5] Devens Gust and Thomas A. Moore. Mimicking photosynthesis. *Science*, 244:35–41, 1989.

[6] Thomas J. Meyer. Chemical approaches to artificial photosynthesis. *Acc. Chem. Res.*, 22:163–170, 1989.

[7] Devens Gust, Thomas A. Moore, and Ana L. Moore. Realizing artificial photosynthesis. *Faraday Discuss.*, 155:9–26, 2012.

[8] Xin-Guang Zhu, Stephen P Long, and Donald R Ort. What is the maximum efficiency with which photosynthesis can convert solar energy into biomass? *Curr. Opin. Biotech.*, 19:153–159, 2008.

[9] Graham R. Fleming, Gabriela S. Schlau-Cohen, Kapil Amarnath, and Julia Zaks. Design principles of photosynthetic light-harvesting. *Faraday Discuss.*, 155:27–41, 2012.

[10] Devens Gust, Thomas A. Moore, and Ana L. Moore. Solar fuels via artificial photosynthesis. *Acc. Chem. Res.*, 42(12):1890–1898, 2009. PMID: 19902921.

[11] J. Barber and B. Anderson. Revealing the blueprint of photosynthesis. *Nature*, 370:31–34, 1994.

[12] Bernhard Loll, Jan Kern, Wolfram Saenger, Athina Zouni, and Jacek Biesiadka. Towards complete cofactor arrangement in the 3.0Å resolution structure of photosystem ii. *Nature*, 438:1040–1044, 2005.

[13] Kristina N. Ferreira, Tina M. Iverson, Karim Maghlaoui, James Barber, and So Iwata. Architecture of the photosynthetic oxygen-evolving center. *Science*, 303:1831–1838, 2004.

[14] James Barber. Photosynthetic energy conversion: natural and artificial. *Chem. Soc. Rev.*, 38: 185–196, 2009.

[15] Gerdenis Kodis, Christian Herrero, Rodrigo Palacios, Ernesto Mari o Ochoa, Stephanie Gould, Linda de la Garza, Rienk van Grondelle, Devens Gust, Thomas A. Moore, Ana L. Moore, , and John T. M. Kennis. Light harvesting and photoprotective functions of carotenoids in compact artificial photosynthetic antenna designs. *J. Phys. Chem. B*, 108:414–425, 2004.

[16] Gerdenis Kodis, Paul A. Liddell, Ana L. Moore, Thomas A. Moore, and Devens Gust. Synthesis and photochemistry of a carotene-porphyrin-fullerene model photosynthetic reaction center. *J. Phys. Org. Chem.*, 17:724–734, 2004.

[17] Olaf Korth, Arno Wiehe, Harry Kurreck, and Beate Röder. Photoinduced intramolecular electron transfer in covalently linked porphyrin-triptycene-(bis)quinone diads and triads. *Chem. Phys.*, 246:363–372, 1999.

[18] Stephen D. Straight, Gerdenis Kodis, Yuichi Terazono, Michael Hambourger, Thomas A. Moore, Ana L. Moore, and Devens Gust. Self-regulation of photoinduced electron transfer by a molecular nonlinear transducer. *Nature Nanotech.*, 3:280–283, 2008.

[19] Nancy E. Holt, Donatas Zigmantas, Leonas Valkunas, Xiao-Ping Li, Krishna K. Niyogi, and Graham R. Fleming. Carotenoid cation formation and the regulation of photosynthetic light harvesting. *Science*, 307:433–436, 2005.

[20] Bo Albinsson and Jerker Mårtensson. Excitation energy transfer in donor-bridge-acceptor systems. *Phys. Chem. Chem. Phys.*, 12:7338–7351, 2010.

[21] Anthony Harriman, Laura Mallon, and Raymond Ziessel. Energy flow in a purpose-built cascade molecule bearing three distinct chromophores attached to the terminal acceptor. *Chem. Eur. J.*, 14:11461–11473, 2008.

[22] Giovanni Bottari, Gema de la Torre, Dirk M. Guldi, and Tomás Torres. Covalent and non-covalent phthalocyanine carbon nanostructure systems: Synthesis, photoinduced electron transfer, and application to molecular photovoltaics. *Chem. Rev.*, 110(11):6768–6816, 2010.

[23] Yuichi Terazono, Gerdenis Kodis, Kul Bhushan, Julia Zaks, Christopher Madden, Ana L. Moore, Thomas A. Moore, Graham R. Fleming, and Devens Gust. Mimicking the role of the antenna in photosynthetic photoprotection. *J. Am. Chem. Soc.*, 133:2916–2922, 2011.

[24] Raymond Ziessel and Anthony Harriman. Artificial light-harvesting antennae: electronic energy transfer by way of molecular funnels. *Chem. Comm.*, 47:611–631, 2011.

[25] Yutaka Amao, Naho Shuto, Kana Furuno, Asami Obata, Yoshiko Fuchino, Keiko Uemura, Tsutomu Kajino, Takeshi Sekito, Satoshi Iwai, Yasushi Miyamotod, and Masatoshi Matsuda. Artificial leaf device for solar fuel production. *Faraday Discuss.*, 155:289–296, 2012.

[26] Yusuke Tamaki, Katsuhiro Watanabe, Kazuhide Koike, Haruo Inoue, Tatsuki Morimotoa, and Osamu Ishitani. Development of highly efficient supramolecular CO_2 reduction photocatalysts with high turnover frequency and durability. *Faraday Discuss.*, 155:115–127, 2012.

[27] Naoki Aratani, Dongho Kim, and Atsuhiro Osuka. Discrete cyclic porphyrin arrays as artificial light-harvesting antenna. *Acc. Chem. Res.*, 42(12):1922–1934, 2009.

[28] Susanne Karlsson, Julien Boixel, Yann Pellegrin, Errol Blart, Hans-Christian Becker, Fabrice Odobel, and Leif Hammarström. Accumulative electron transfer: Multiple charge separation in artificial photosynthesis. *Faraday Discuss.*, 155:233–252, 2012.

[29] Anders Hagfeldt and Michael Grätzel. Molecular photovoltaics. *Acc. Chem. Res.*, 33:269–277, 2000.

[30] Michael Grätzel. Dye-sensitized solar cells. *J. Photochem. Photobiol. C*, 4:145–153, 2003.

[31] Michael Grätzel. Conversion of sunlight to electric power by nanocrystalline dye-sensitized solar cells. *J. Photochem. Photobiol. A*, 164:3–14, 2004.

[32] Michael Grätzel. Solar energy conversion by dye-sensitized photovoltaic cells. *Inorg. Chem.*, 44: 6841–6851, 2005.

[33] Md. K. Nazeeruddin, Etienne Baranoff, and Michael Grätzel. Dye-sensitized solar cells: A brief overview. *Sol. Energy*, 85:1172–1178, 2011.

[34] Anders Hagfeldt, Gerrit Boschloo, Licheng Sun, Lars Kloo, and Henrik Pettersson. Dye-sensitized solar cells. *Chem. Rev.*, 110(11):6595–6663, 2010.

[35] Helmut Tributsch. Dye sensitization solar cells: a critical assessment of the learning curve. *Coord. Chem. Rev.*, 248:1511–1530, 2004.

[36] M. Victoria Martínez-Díaz, Gema de la Torre, , and Tomás Torres. Lighting porphyrins and phthalocyanines for molecular photovoltaics. *Chem. Comm.*, 46:7090–7108, 2010.

[37] Brian O'Regan and Michael Grätzel. A low-cost, high-efficiency solar cell based on dye-sensitized colloidal TiO_2 films. *Nature*, 353:737–740, 1991.

[38] Aswani Yella, Hsuan-Wei Lee, Hoi Nok Tsao, Chenyi Yi, Aravind Kumar Chandiran, Md.Khaja Nazeeruddin, Eric Wei-Guang Diau, Chen-Yu Yeh, Shaik M Zakeeruddin, and Michael Grätzel. Porphyrin-sensitized solar cells with cobalt (II/III)-based redox electrolyte exceed 12 percent efficiency. *Science*, 334:629–634, 2011.

[39] D.L. Staebler and C.R. Wronski. Optically induced conductivity changes in dischargeproduced hydrogenated amorphous silicon. *J. Appl. Phys.*, 51:3262–3268, 1980.

[40] J. Emsley. *Nature's Building Blocks: An A-Z Guide to the Elements*. Oxford University Press, 2003.

[41] Hans Wedepohl. The composition of the continental crust. *Geochim. et Cosmochim. Ac.*, 59: 1217–1232, 1995.

[42] Rudolph A. Marcus. On the theory of oxidation-reduction reactions involving electron transfer I. *J. Chem. Phys.*, 24:966–978, 1956.

[43] Rudolph A. Marcus. Electron transfer reactions in chemistry: Theory and experiment. *Angew. Chem. Intl. Ed.*, 32:1111–1121, 1993.

[44] Ian R. Gould, Ralph H. Young, Roger E. Moody, and Samir Farid. Contact and solvent-separated geminate radical ion pairs in electron-transfer photochemistry. *J. Phys. Chem.*, 95:2068–2080, 1991.

[45] Ian R. Gould, Deniz Ege, Jacques E. Maser, and Samir Farid. Efficiencies of photoinduced electron-transfer reactions: Role of the marcus inverted region in return electron transfer within geminate radical-ion pairs. *J. Am. Chem. Soc.*, 112:4290–4301, 1990.

[46] James R. Bolton and Mary D. Archer. *Electron Transfer in Inorganic, Organic, and Biological Systems*, volume 228 of *Advances in Chemistry Series*. The American Chemical Society, 1991.

[47] W. Ebeling and I. Sokolov. *Statistical Thermodynamics and Stochastic Theory of Nonequilibrium Systems*. World Scientific, Singapore, 2005.

[48] Volkhard May and Oliver Kühn. *Charge And Energy Transfer Dynamics In Molecular Systems*. Wiley-VCH, 2011.

[49] Paul F. Barbara, Thomas J. Meyer, and Mark A. Ratner. Contemporary issues in electron transfer research. *J. Phys. Chem.*, 100:13148–13168, 1996.

[50] J. R. Miller, L. T. Calcaterra, and G. L. Closs. Intramolecular long-distance electron transfer in radical anions. the effects of free energy and solvent on the reaction rates. *J. Am. Chem. Soc.*, 106: 3047–3049, 1984.

[51] Gerhard L. Closs and John R. Miller. Intramolecular long-distance electron transfer in organic molecules. *Science*, 240:440–447, 1988.

[52] Christopher C. Moser and P. Leslie Dutton. Engineering protein structure for electron transfer function in photosynthetic reaction centers. *Biochim. Biophys. Acta*, 1101:171–176, 1992.

[53] George J. Kavarnos and Nicholas J. Turro. Photosensitization by reversible electron transfer: Theories, experimental evidence, and examples. *Chem. Rev.*, 86:401–449, 1986.

[54] Norman Sutin. *Electron Transfer in Inorganic, Organic, and Biological Systems*, volume 228 of *Advances in Chemistry Series*. The American Chemical Society, 1991.

[55] D. Rehm and A. Weller. Kinetik und Mechanismus der Elektronübertragung bei der Fluoreszenzlöschung in Acetonitril. *Ber. Bunsen-Ges. Phys. Chem.*, 73:834–839, 1969.

[56] D. Rehm and A. Weller. Kinetics of fluorescence quenching by electron and hydrogen-atom transfer. *Isr. J. Chem.*, 8:259–271, 1970.

[57] A. Weller. Photoinduced electron transfer in solution: Exciplex and radical ion pair formation, free enthalpies and their solvent dependence. *Z. Phys. Chem.*, 133:93–98, 1982.

[58] William T. Simpson and Don L. Peterson. Coupling strength for resonance force transfer of electronic energy in van der waals solids. *J. Chem. Phys.*, 26:588–593, 1957.

[59] M. Kasha, H.R. Rawls, and M. Ashraf El-Bayoumi. The exciton model in molecular spectroscopy. *Pure Appl. Chem.*, 11:371–392, 1965.

[60] Beate Röder. *Einführung in die Molekulare Photobiophysik*. Teubner Verlag, 1999.

[61] Th. Förster. Energiewanderung und Fluoreszenz. *Naturwiss.*, 2:166–175, 1946.

[62] T. Förster. Zwischenmolekulare Energiewanderung und Fluoreszenz. *Ann. Phys.*, 2:55–75, 1948.

[63] Th. Förster. Transfer mechanisms of electronic excitation. *Discuss. Faraday Soc.*, 27:7–17, 1959.

[64] D. L. Dexter. A theory of sensitized luminescence in solids. *J. Chem. Phys.*, 21:836–850, 1953.

[65] Joseph R. Lakowicz. *Principles of Fluorescence Spectroscopy*. Springer, Berlin, 2006.

[66] A. Braun and J. Tcherniac. Über die Produkte der Einwirkung von Acetanhydid auf Phthalamid. *Ber. Deut. Chem. Ges.*, 40:2709–2714, 1907.

[67] Martin Gouterman. Study of the effects of substitution on the absorption spectra of porphin. *J. Chem. Phys.*, 30:1139–1161, 1959.

[68] Martin Gouterman. Spectra of porphyrins. *J. Mol. Spectrosc.*, 6:138–163, 1961.

[69] Martin Gouterman, Georges H. Wagnière, and Lawrence C. Snyder. Spectra of porphyrins - part II four orbital model. *J. Mol. Spectrosc.*, 11:108–127, 1963.

[70] Lawrence Edwards and Martin Gouterman. Porphyrins XV. vapor absorption spectra ans stability: Phthalocyanines. *J. Mol. Spectrosc.*, 33:292–310, 1970.

[71] John R. Platt. Classification and assignments of ultraviolet spectra of conjugated organic molecules. *J. Opt. Soc. Am.*, 43:252–257, 1953.

[72] M. Gouterman. *Physical Chemistry in The Porphyrins, Bd. 3*. Academic Press: New York, 1978.

[73] T. H. Tran-Thi, C. Desforge, and C. Thiec. Singlet-singlet and triplet-triplet intramolecular transfer processes in a covalently linked porphyrin-phthalocyanine heterodimer. *J. Phys. Chem.*, 93:1226–1233, 1989.

[74] Pui-Chi Lo, Xuebing Leng, and Dennis K.P. Ng. Hetero-arrays or porphyrins and phthalocyanines. *Coord. Chem. Rev.*, 251:2334–2353, 2007.

[75] Sebastian Tannert, Eugeny A. Ermilov, Jörn Oliver Vogel, Michael T.M. Choi, Dennis K.P. Ng, and Beate Röder. The influence of solvent polarity and metalation on energy and electron transfer in porphyrin-phthalocyanine heterotrimers. *J. Phys. Chem. B*, 111:8053–8062, 2007.

[76] Eugeny A. Ermilov, Sebastian Tannert, Thomas Werncke, Michael T.M. Choi, Dennis K.P. Ng, and Beate Röder. Photoinduced electron and energy transfer in a new porphyrin-phthalocyanine triad. *Chem. Phys.*, 328:428–437, 2006.

[77] Eugeny A. Ermilov, Roel Menting, Janet T. F. Lau, Xuebing Leng, Beate Röder, and Dennis K. P. Ng. Switching the photoinduced processes in host-guest complexes of β-cyclodextrin-substituted silicon(IV) phthalocyanines and a tetrasulfonated porphyrin. *Phys. Chem. Chem. Phys.*, 13:17633–17641, 2011.

[78] Hiroshi Imahori, Tomokazu Umeyama, and Seigo Ito. Large π-aromatic molecules as potential sensitizers for highly efficient dye-sensitized solar cells. *Acc. Chem. Res.*, 42:1809–1818, 2009.

[79] P.-C. Lo, S. Wang, A. Zeug, M. Meyer, B. Röder, and D. K. P. Ng. Preparation and photophysical properties of halogenated silicon(IV) phthalocyanines substituted axially with poly(ethylene glycol) chains. *Tetrahedron Lett.*, 44:1967–1970, 2003.

[80] Neil B. McKeown. Phthalocyanine-containing polymers. *J. Mater. Chem.*, 10:1979–1995, 2000.

[81] Christopher Farren, Christian A. Christensen, Simon FitzGerald, Martin R. Bryce, and Andrew Beeby. Synthesis of novel phthalocyanine-tetrathiafulvalene hybrids; intramolecular fluorescence quenching related to molecular geometry. *J. Org. Chem.*, 67:9130–9139, 2002.

[82] Mohamed E. El-Khouly, Eui Su Kang, Kwang-Yol Kay, Chan Soo Choi, Yasuyuki Aaraki, and Osamu Ito. Silicon-phthalocyanine-cored fullerene dendrimers: Synthesis and prolonged charge-separated states with dendrimer generations. *Chem. Eur. J.*, 13:2854–2863, 2007.

[83] José L. Rodríguez-Redondo, Angela Sastre-Santos, Fernando Fernández-Lázaro, Dilcelli Soares, Gianluca C. Azzellini, Bevan Elliott, and Luis Echegoyen. Phthalocyanine-modulated isomerization behaviour of an azo-based photoswitch. *Chem. Comm*, 12:1265–1267, 2006.

[84] Jack Silver, Jose L. Sosa-Sanchez, and Christopher S. Frampton. Structure, electrochemistry, and properties of bis(ferrocenecarboxylato)-(phthalocyaninato)-silicon(IV) and its implications for $(Si(Pc)O)_n$ polymer chemistry. *Inorg. Chem.*, 37:411–417, 1998.

[85] Luis Martín-Gomis, Kei Ohkubo, Fernando Fernández-Lázaro, Shunichi Fukuzumi, and Angela Sastre-Santos. Synthesis and photophysical studies of a new nonaggregated C_{60}-silicon phthalocyanine-C_{60} triad. *Org. Lett.*, 9:3441–3444, 2007.

[86] Luis Martín-Gomis, Kei Ohkubo, Fernando Fernández-Lázaro, Shunichi Fukuzumi, and Angela Sastre-Santos. Adiabatic photoinduced electron transfer and back electron transfer in a series of axially substituted silicon phthalocyanine triads. *J. Phys. Chem. C*, 112:17694–17701, 2008.

[87] Luis Martín-Gomis, Kei Ohkubo, Fernando Fernández-Lázaro, Shunichi Fukuzumi, and Angela Sastre-Santos. Multistep electron transfer systems based on silicon phthalocyanine, [60]fullerene and trinitrofluorenone. *Chem. Comm.*, 46:3944–3946, 2010.

[88] F. Javier Céspedes-Guirao, Luis Martín-Gomis, Kei Ohkubo, Shunichi Fukuzumi, Fernando Fernández-Lázaro, and Angela Sastre-Santos. Synthesis and photophysics of silicon phthalocyanine-perylenebisimide triads connected through rigid and flexible bridges. *Chem. Eur. J.*, 17:9153–9163, 2011.

[89] Zhixin Zhao, Andrew N. Cammidge, and Michael J. Cook. Towards black chromophores: μ-oxo linked phthalocyanine-porphyrin dyads and phthalocyanine-subphthalocyanine dyad and triad arrays. *Chem. Comm.*, 48:7530–7532, 2009.

[90] V. N. Myakov, V. A. Kuropatov, and T. I. Lopatina. Synthesis and some reactions of silicon phthalocyanine anions. *Russ. J. Coord. Chem.*, 35:193–196, 2009.

[91] V. N. Myakov, M. A. Lopatin, T. I. Lopatina, and V. I. Faerman. Some donor-acceptor complexes of silicon phthalocyanine dianions. *Russ. J. Gen. Chem.*, 80:1547–1553, 2010.

[92] Eugeny A. Ermilov, Jian-Yong Liu, Dennis K. P. Ng, and Beate Röder. Spectroscopic study of electron and energy transfer in novel silicon phthalocyanine-boron dipyrromethene triads. *Phys. Chem. Chem. Phys.*, 11:6430–6440, 2009.

[93] Alfred Treibs and Franz-Heinrich Kreuzer. Difluorboryl-Komplexe von Di- und Tripyrrylmethenen. *Justus Liebigs Ann. Chem.*, 718:208–223, 1968.

[94] Aurore Loudet and Kevin Burgess. Bodipy dyes and their derivatives: Syntheses and spectroscopic properties. *Chem. Rev.*, 107:4891–4932, 2007.

[95] Noël Boens, Volker Leen, and Wim Dehaen. Fluorescent indicators based on Bodipy. *Chem. Soc. Rev.*, 41:1130–1172, 2012.

[96] Gilles Ulrich, Raymond Ziessel, and Anthony Harriman. The chemistry of fluorescent Bodipy dyes: Versatility unsurpassed. *Angew. Chem. Int. Ed.*, 47:1184–1201, 2008.

[97] Jan Karolin, Lennart B.-A. Johansson, Leif Strandberg, and Tor Ny. Fluorescence and absorption spectroscopic properties of dipyrrometheneboron difluoride (Bodipy) derivatives in liquids, lipid membranes, and proteins. *J. Am. Chem. Soc.*, 116:7801–7806, 1994.

[98] *Molecular Probes: The Handbook, http://www.probes.com/handbook*. Invitrogen (online), 2012.

[99] Andrew C. Benniston and Graeme Copley. Lighting the way ahead with boron dipyrromethene (Bodipy) dyes. *Org. Lett.*, 11:4124–4131, 2009.

[100] Shuichi Suzuki, Masatoshi Kozaki, Koichi Nozaki, and Keiji Okada. Recent progress in controlling photophysical processes of donor-acceptor arrays involving perylene diimides and boron-dipyrromethenes. *J. Photochem. Photobiol. C*, 12:269–292, 2011.

[101] Anthony Harriman, James P. Rostron, Michèle Cesario, Gilles Ulrich, and Raymond Ziessel. Electron transfer in self-assembled orthogonal structures. *J. Phys. Chem. A*, 110:7994–8002, 2006.

[102] Shigeki Hattori, Kei Ohkubo, Yasuteru Urano, Hisato Sunahara, Tetsuo Nagano, Yuji Wada, Nikolai V. Tkachenko, Helge Lemmetyinen, and Shunichi Fukuzumi. Charge separation in a non-fluorescent donor-acceptor dyad derived from boron dipyrromethene dye, leading to photocurrent generation. *J. Phys. Chem. B*, 109:15368–15375, 2005.

[103] Guillaume Duvanel, Natalie Banerji, and Eric Vauthey. Excited-state dynamics of donor-acceptor bridged systems containing a boron-dipyrromethene chromophore: Interplay between charge separation and reorientational motion. *J. Phys. Chem. A*, 111:5361–5369, 2007.

[104] Safacan Kolemen, Altan Bozdemir, Yusuf Cakmak, Gokhan Barin, Sule Erten-Ela, Magdalena Marszalek, Jun-Ho Yum, Shaik M. Zakeeruddin, Mohammad K. Nazeeruddin, Michael Grätzel, and Engin U. Akkaya. Optimization of distyryl-Bodipy chromophores for efficient panchromatic sensitization in dye sensitized solar cells. *Chem. Sci.*, 2:949–954, 2011.

[105] BongSoo Kim, Biwu Ma, Venkat R. Donuru, Haiying Liu, and Jean M. J. Fréchet. Bodipy-backboned polymers as electron donor in bulk heterojunction solar cells. *Chem. Comm.*, 46: 4148–4150, 2010.

[106] A. Meller and A. 0ssko. Phthalocyaninartige Bor-Komplexe. *Monatsh. Chem.*, 103:150–155, 1972.

[107] Christian G. Claessens, David Gonzalez-Rodriguez, and Tomas Torres. Subphthalocyanines: Singular nonplanar aromatic compounds-synthesis, reactivity, and physical properties. *Chem. Rev.*, 102:835–853, 2002.

[108] Christian G. Claessens, David González-Rodríguez, Rodrigo S. Iglesias, and Tomás Torres. Convex-convex and concave-convex interactions between C_{60} and non-planar aromatic subphthalocyanine macrocycle in both covalent and supramolecular arrays. *Compt. Rend. Chim.*, 9: 1094–1099, 2006.

[109] Hu Xu and Dennis K. P. Ng. Construction of subphthalocyanine-porphyrin and subphthalocyanine-phthalocyanine heterodyads through axial coordination. *Inorg. Chem.*, 47: 7921–7927, 2008.

[110] Christian Litwinski, Ines Corral, Eugeny A. Ermilov, Sebastian Tannert, Dmitri Fix, Sergey Makarov, Olga Suvorova, Leticia Gonzalez, Dieter Wöhrle, and Beate Röder. Annulated dinuclear metal-free and zn(II) phthalocyanines: Photophysical studies and quantum mechanical calculations. *J. Phys. Chem. B*, 112:8466–8476, 2008.

[111] Raymond Ziessel, Gilles Ulrich, Kristopher J. Elliott, and Anthony Harriman. Electronic energy transfer in molecular dyads built around boron-ethyne-substituted subphthalocyanines. *Chem. Eur. J.*, 15:4980–4984, 2009.

[112] Jian-Yong Liu, Hoi-Sze Yeungj, Wei Xu, Xiyou Li, and Dennis K. P. Ng. Highly efficient energy transfer in subphthalocyanine-Bodipy conjugates. *Org. Lett.*, 10:5421–5424, 2008.

[113] Pavlo V. Solntsev, Katelynn L. Spurgin, Jared R. Sabin, Ahmed A. Heikal, and Victor N. Nemykin. Photoinduced charge transfer in short-distance ferrocenylsubphthalocyanine dyads. *Inorg. Chem.*, 51:6537–6547, 2012.

[114] David González-Rodríguez, Christian G. Claessens, Tomas Torres, Shenggao Liu, Luis Echegoyen, Nuria Vila, and Santi Nonell. Tuning photoinduced energy- and electron-transfer events in subphthalocyanine-phthalocyanine dyads. *Chem. Eur. J.*, 11:3881–3893, 2005.

[115] Rachael A. Kipp, Jerald A. Simon, Matthew Beggs, Harry E. Ensley, and Russell H. Schmehl. Photophysical and photochemical investigation of a dodecafluorosubphthalocyanine derivative. *J. Phys. Chem. A*, 102:5659–5664, 1998.

[116] David González-Rodríguez, Tomás Torres, Dirk M. Guldi, José Rivera, Maria Ángeles Herranz, and Luis Echegoyen. Subphthalocyanines: Tuneable molecular scaffolds for intramolecular electron and energy transfer processes. *J. Am. Chem. Soc.*, 126:6301–6313, 2004.

[117] A. Villiers. *Compt. Rend. Chim.*, 112:536–538, 1891.

[118] József Szejtli. Introduction and general overview of cyclodextrin chemistry. *Chem. Rev.*, 98: 1743–1753, 1998.

[119] Yu Liu and Yong Chen. Cooperative binding and multiple recognition by bridged bis(β-cyclodextrin)s with functional linkers. *Acc. Chem. Res.*, 39:681–691, 2006.

[120] Mikhail V. Rekharsky and Yoshihisa Inoue. Complexation thermodynamics of cyclodextrins. *Chem. Rev.*, 98:1875–1917, 1998.

[121] Gerhard Wenz, Bao-Hang Han, and Axel Müller. Cyclodextrin rotaxanes and polyrotaxanes. *Chem. Rev.*, 106:782–817, 2006.

[122] Abderrazzak Douhal. Ultrafast guest dynamics in cyclodextrin nanocavities. *Chem. Rev.*, 104: 1955–1976, 2004.

[123] John S. Manka and David S. Lawrence. Template-driven self-assembly of a porphyrin-containing supramolecular complex. *J. Am. Chem. Soc.*, 112:2440–2442, 1990.

[124] Josep M. Ribó, Joan-Anton Farrera, Maria Luz Valero, and Albert Virgili. Self-assembly of cyclodextrins with meso-tetrakis(4-sulfonatophenyl)porphyrin in aqueous solution. *Tetrahon*, 51: 3705–3712, 1995.

[125] Koji Kano, Ryuhei Nishiyabu, Takuji Asada, and Yasuhisa Kuroda. Static and dynamic behavior of 2:1 inclusion complexes of cyclodextrins and charged porphyrins in aqueous organic media. *J. Am. Chem. Soc.*, 124:9937–9944, 2002.

[126] Werner Schmidt. *Optische Spektroskopie. Eine Einführung für Naturwissenschaftler und Techniker*. Wiley-VCH, 1994.

[127] J.N. Demas and G.A. Crosby. The measurement of photoluminescence quantum yields. *J. Phys*, 75:991–1024, 1971.

[128] Alun T. Rhys Williams and Stephen A. Winfield. Relative fluorescence quantum yields using a computer-controlled luminescence spectrometer. *Analyst*, 108:1067–1071, 1983.

[129] R. F. Kubin and A. N. Fletcher. Fluorescence quantum yields of some rhodamine dyes. *J. Lumin.*, 27:455–462, 1982.

[130] Douglas Magde, Roger Wong, and Paul G. Seybold. Fluorescence quantum yields and their relation to lifetimes of rhodamine 6G and fluorescein in nine solvents: Improved absolute standards for quantum yields. *Photochem. Photobiol.*, 75:327–334, 2002.

[131] R. Sens. *Strahlungslose Desaktivierung in Xanthen-, Oxazin- und Carbazinfarbstoffen*. PhD thesis, University of Siegen, 1984.

[132] Paul G. Seybold and Martin Gouterman. Fluorescence spectra and quantum yields. *J. Mol. Spectrosc.*, 31:1–13, 1969.

[133] J. R. Knutson, D. G. Walbridge, and L. Brand. Decay associated fluorescence spectra and the heterogeneous emission of alcohol dehydrogenase. *Biochem.*, 21:4671–4679, 1982.

[134] Christian Litwinski. *Elektronische Eigenschaften von oligonuklearen Phthalocyaninen*. PhD thesis, Humboldt Universität zu Berlin, 2008.

[135] Wolfgang Becker. *Advanced Time-Correlated Single Photon Counting Techniques*. Springer, Berlin, 2005.

[136] André Zeug. *Beiträge zur Weiterentwicklung der Transienten Absorptionsspektroskopie zur experimentellen Untersuchung ausgewählter Tetrapyrrole*. PhD thesis, Humboldt Universität zu Berlin, 2002.

[137] Ilja Rückmann, Andre Zeug, Ralph Herter, and Beate Röder. On the influence of higher excited states on the ISC quantum yield of octa-α-alkyloxy-substituted Zn-phthalocyanine molecules studied by non-linear absorption. *Photochem. Photobiol.*, 66:576–584, 1997.

[138] Eugeny Ermilov. Photophysics: Optical characterisation of molecules and polymers. Lecture at the Humboldt Universität zu Berlin, 2008.

[139] H. E. Lessing and A. v. Jena. *Laser Handbook Vol.3*. North-Holland, 1979.

[140] Jian-Yong Liu, Mohamed E. El-Khouly, Shunichi Fukuzumi, and Dennis K.P. Ng. Photoinduced electron transfer in a distyryl Bodipy-fullerene dyad. *Chem. Asian J.*, 6:174–179, 2011.

[141] Theodore Lazarides, Georgios Charalambidis, Alexandra Vuillamy, Marius Réglier, Emmanuel Klontzas, Georgios Froudakis, Susanne Kuhri, Dirk M. Guldi, and Athanassios G. Coutsolelos. Promising fast energy transfer system via an easy synthesis: Bodipy-porphyrin dyads connected via a cyanuric chloride bridge, their synthesis, and electrochemical and photophysical investigations. *Inorg. Chem.*, 50:8926–8936, 2011.

[142] Alexander B. Nepomnyashchii, Martin Bröring, Johannes Ahrens, and Allen J. Bard. Synthesis, photophysical, electrochemical, and electrogenerated chemiluminescence studies. multiple sequential electron transfers in Bodipy monomers, dimers, trimers, and polymer. *J. Am. Chem. Soc.*, 133:8633–8645, 2011.

[143] Chang Yeon Lee, Omar K. Farha, Bong Jin Hong, Amy A. Sarjeant, SonBinh T. Nguyen, and Joseph T. Hupp. Light-harvesting metal-organic frameworks (MOFs): Efficient strut-to-strut energy transfer in Bodipy and porphyrin-based MOFs. *J. Am. Chem. Soc.*, 133:15858–15861, 2011.

[144] Ana M. V. M. Pereira, Ana R. M. Soares, Anita Hausmann, Maria G. P. M. S. Neves, Augusto C. Tomé, Artur M. S. Silva, José A. S. Cavaleiro, Dirk M. Guldi, and Tomás Torres. Distorted fused porphyrin-phthalocyanine conjugates: synthesis and photophysics of supramolecular assembled systems with a pyridylfullerene. *Phys. Chem. Chem. Phys.*, 13:11858–11863, 2011.

[145] Maligaspe, Kumpulainen, Subbaiyan, Zandler, Lemmetyinen, Tkachenko, and D'Souza. Electronic energy harvesting multi Bodipy-zinc porphyrin dyads accommodating fullerene as photosynthetic composite of antenna reaction center. *Phys. Chem. Chem. Phys.*, 12:7434–7444, 2010.

[146] Gema de la Torre, Christian G. Claessens, and Tomás Torres. Phthalocyanines: old dyes, new materials. putting color in nanotechnology. *Chem. Comm.*, 20:2000–2015, 2007.

[147] Yannick Rio, Wolfgang Seitz, Andreas Gouloumis, Purificacion, Vazquez, Jonathan L. Sessler, Dirk M. Guldi, and Tomas Torres. A panchromatic supramolecular fullerene-based donor-acceptor assembly derived from a peripherally substituted Bodipy-zinc phthalocyanine dyad. *Chem. Eur. J.*, 16:1929–1940, 2010.

[148] Jian-Yong Liu, Eugeny A. Ermilov, Beate Röder, and Dennis K. P. Ng. Switching the photoinduced energy and electron-transfer processes in Bodipy-phthalocyanine conjugates. *Chem. Comm.*, 12:1517–1519, 2009.

[149] Zeynep Dost, Serdar Atilgan, and Engin U. Akkaya. Distyryl-boradiazaindacenes: facile synthesis of novel near ir emitting fluorophores. *Tetrahedron*, 62:8484–8488, 2006.

[150] Roel Menting. Lichtinduzierter energie- und elektronentransfer in komplexen bausteinen für artifizielle photosynthesesysteme. Master's thesis, Humboldt Universität zu Berlin, 2010.

[151] Roel Menting, Janet T. F. Lau, Hu Xu, Dennis K. P. Ng, Beate Röder, and Eugeny A. Ermilov. Formation and photoinduced processes of a self-assembled subphthalocyanine-porphyrin-phthalocyanine supramolecular complex. *Chem. Comm.*, 48:4597–4599, 2012.

[152] H. Heitele, P. Finckh., S. Weeren, F. Pöllinger, and M.E. Michel-Beyerle. Solvent polarity effects on intramolecular electron transfer. 1. energetic aspects. *J. Phys. Chem.*, 93:5173–5179, 1989.

[153] H. Heitele, F. Pöllinger, T. Häberle, M. E. Michel-Beyerle, and H. A. Staab. Energy gap and temperature dependence of photoinduced electron transfer in porphyrin-quinone cyclophanes. *J. Phys. Chem.*, 98:7402–7410, 1994.

[154] P. Toele, H. Zhang, C. Trieflinger, J. Daub, and M. Glasbeek. Femtosecond fluorescence upconversion study of a boron dipyrromethene dye in solution. *Chem. Phys. Lett.*, 368:66–75, 2003.

[155] H. J. Marrinan and N. Sheppard. Relative intensities of the raman lines of carbon tetrachloride, chloroform and methylene chloride. *J. Opt. Soc. Am.*, 44:815–819, 1954.

[156] Heli Lehtivuori, Tatu Kumpulainen, Matti Hietala, Alexander Efimov, Helge Lemmetyinen, Aiko Kira, Hiroshi Imahori, and Nikolai V. Tkachenko. Photodynamics of charge separation and recombination in solid alternating films of phthalocyanine or phthalocyanine-fullerene dyad and perylene dicarboximide. *J. Phys. Chem. C*, 113:1984–1992, 2009.

[157] Michael R. Wasielewski. Self-assembly strategies for integrating light harvesting and charge separation in artificial photosynthetic systems. *Acc. Chem. Res.*, 42(12):1910–1921, 2009.

[158] Shin-Ichiro Sakurai, Jetsuda Areephong, Leonardo Bertone, Nai-Ti Lin, Naomi Sakai, and Stefan Matile. Toward polymerized artificial photosystems with supramolecular n/p-heterojunctions and antiparallel redox gradients. *Energy Environ. Sci.*, 4:2409–2416, 2011.

[159] Yoshiaki Kobuke. Artificial light-harvesting systems by use of metal coordination. *Eur. J. Inorg. Chem.*, 12:2333–2351, 2006.

[160] Yusuke Kuramochi, Atula S. D. Sandanayaka, Akiharu Satake, Yasuyuki Araki, Kazuya Ogawa, Osamu Ito, and Yoshiaki Kobuke. Energy transfer followed by electron transfer in a porphyrin macrocycle and central acceptor ligand: A model for a photosynthetic composite of the light-harvesting complex and reaction center. *Chem. Eur. J.*, 15:2317–2327, 2009.

[161] Shunichi Fukuzumi, Kenji Saito, Kei Ohkubo, Vincent Troiani, Hongjin Qiu, Suresh Gadde, Francis D'Souza, and Nathalie Solladié. Multiple photosynthetic reaction centres using zinc porphyrinic oligopeptide-fulleropyrrolidine supramolecular complexes. *Phys. Chem. Chem. Phys.*, 13:17019–17022, 2011.

[162] Dirk M. Guldi, Andreas Gouloumis, Purificación Vázquez, Tomás Torres, Vasilios Georgakilas, and Maurizio Prato. Nanoscale organization of a phthalocyanine-fullerene system: Remarkable stabilization of charges in photoactive 1-D nanotubules. *J. Am. Chem. Soc.*, 127:5811–5813, 2005.

[163] Francis D'Souza, Anu N. Amin, Mohamed E. El-Khouly, Navaneetha K. Subbaiyan, Melvin E. Zandler, and Shunichi Fukuzumi. Control over photoinduced energy and electron transfer in supramolecular polyads of covalently linked azaBodipy-bisporphyrin 'molecular clip' hosting fullerene. *J. Am. Chem. Soc.*, 134:654–664, 2012.

[164] Francis D'Souza and Osamu Ito. Photoinduced electron transfer in supramolecular systems of fullerenes functionalized with ligands capable of binding to zinc porphyrins and zinc phthalocyanines. *Coord. Chem. Rev.*, 249:1410–1422, 2005.

[165] Hiroshi Imahori, Tomokazu Umeyama, Kei Kurotobi, and Yuta Takano. Self-assembling porphyrins and phthalocyanines for photoinduced charge separation and charge transport. *Chem. Comm.*, 48:4032–4045, 2012.

[166] Wei Deng, Takeshi Onji, Hiroyasu Yamaguchi, Noriaki Ikedab, and Akira Harada. Competitive photoinduced electron transfer by the complex formation of porphyrin with cyclodextrin bearing viologen. *Chem. Comm.*, 42:4212–4214, 2006.

[167] Ying-Ming Zhang, Yong Chen, Rui-Jie Zhuang, and Yu Liu. Supramolecular architecture of tetrathiafulvalene-bridged bis(β-cyclodextrin) with porphyrin and its electron transfer behaviors. *Photochem. Photobiol. Sci.*, 10:1393–1398, 2011.

[168] Ke-Rang Wang, Dong-Sheng Guo, Bang-Ping Jiang, and Yu Liu. Excitonic coupling interactions in the self-assembly of perylene-bridged bis(β-cyclodextrin)s and porphyrin. *Chem. Comm.*, 48: 3644–3646, 2012.

[169] Ying-Ming Zhang, Yong Chen, Yang Yang, Peng Liu, and Yu Liu. Supramolecular architectures by fullerene-bridged bis(permethyl-β- cyclodextrin)s with porphyrins. *Chem. Eur. J.*, 15:11333–11340, 2009.

[170] Zhuo-Yi Gu, Dong-Sheng Guo, Mo Sun, and Yu Liu. Effective enlargement of fluorescence resonance energy transfer of poly-porphyrin mediated by β-cyclodextrin dimers. *J. Org. Chem.*, 75:3600–3607, 2010.

[171] Hu Xu, Eugeny A. Ermilov, Beate Röder, and Dennis K. P. Ng. Formation and energy transfer property of a subphthalocyanine-porphyrin complex held by host-guest interactions. *Phys. Chem. Chem. Phys.*, 12:7366–7370, 2010.

[172] Janet T. F. Lau, Pui-Chi Lo, Wing-Ping Fong, and Dennis K. P. Ng. Preparation and photodynamic activities of silicon(IV) phthalocyanines substituted with permethylated β-cyclodextrins. *Chem. Eur. J.*, 17:7569–7577, 2011.

[173] Xuebing Leng, Chi-Fung Choi, Pui-Chi Lo, and Dennis K. P. Ng. Assembling a mixed phthalocyanine-porphyrin array in aqueous media through host-guest interactions. *Org. Lett.*, 9:231–234, 2007.

[174] H.A. Benesi and J.H. Hildebrand. A spectrophotometric investigation of the interaction of iodine with aromatic hydrocarbons. *J. Am. Chem. Soc.*, 71:2703–2707, 1949.

[175] Yoshihisa Inoue, Keiko Yamamoto, Takehiko Wada, Simon Everitt, Xing-Ming Gao, Zhi-Jie Hou, Lin-Hui Tong, Shao-Kai Jiang, and Hou-Ming Wu. Inclusion complexation of (cyclo)alkanes and (cyclo)alkanols with 6-*O*-modified cyclodextrins. *J. Chem. Soc.*, Perkin Trans. 2:1807–1816, 1998.

[176] Kenta Adachi and Hitoshi Watarai. Site-selective formation of optically active inclusion complexes of alkoxo-subphthalocyanines with β-cyclodextrin at the toluene/water interface. *Chem. Eur. J.*, 12:4249–4260, 2006.

[177] Shi Wenjing, Roel Menting, Eugeny A. Ermilov, Beate Röder, Gigi P. C. Lo, and Dennis K. P. Ng. Supermolecular arrays by azaBodipy-bridged bis(permethyl-β-cyclodextrin)s with porphyrins in aqueous media. *Chem. Comm.*, page in preparation, 2012.

List of Figures

List of Tables

Selbständigkeitserklärung

Ich erkläre, dass ich die vorliegende Arbeit selbständig und nur unter Verwendung der angegebenen Literatur und Hilfsmittel angefertigt habe.

Berlin, den 26.07.2012 Raoul Merijn Menting